Triaging of mammalian cofactor-free flavoproteins by the protein quality control machinery

Dissertation
zur Erlangung des Doktorgrades
der Naturwissenschaften

vorgelegt beim Fachbereich
Biochemie, Chemie und Pharmazie (FB14)
der Johann Wolfgang Goethe-Universität
in Frankfurt am Main

von
Adrián Martínez Limón
aus Barcelona, Spanien

Frankfurt 2019
(D30)

vom Fachbereich Biochemie, Chemie und Pharmazie (FB14)
der Johann Wolfgang Goethe-Universität als Dissertation angenommen.

Dekan: Prof. Dr. Clemens Glaubitz

Gutachter: Dr. Martin Vabulas
Prof. Dr. Volker Dötsch

Datum der Disputation: 21.10.2019

ABSTRACT

Protein quality control (PQC) machinery is in charge of ensuring protein homeostasis in the cell, i.e. proteostasis. Chaperones assist polypeptides throughout their maturation until functionality is achieved. This process might be disrupted in the presence of mutations or external damaging agents that affect the folding and stability of proteins. In this case, proteins can be efficiently recognized and targeted for degradation in a controlled manner. Ubiquitylation refers to the covalent attachment of one or more ubiquitin moieties to faulty proteins, thus triggering their degradation by the 26S proteasome.

More than 30% of proteins need cofactor molecules. Lack of cofactors renders proteins non-functional. We wanted to understand how the PQC deals with wild-type proteins in the absence of their cofactors. Several studies have indicated the importance of the riboflavin-derived cofactor FAD in the stability of individual flavoproteins, and hence we assumed that loss of flavin should mediate a targeted degradation of this group of proteins. Indeed, our mass spectrometry experiments showed that flavoproteome levels decreased under riboflavin starvation. The oxidoreductase NQO1 was used as a model enzyme to further investigate the mechanism of flavoproteome targeting by the PQC. We showed that cofactor loading determines ubiquitylation of NQO1 by the co-chaperone CHIP, both *in vivo* and *in vitro*. Furthermore, subtle changes in the C-terminus of NQO1 in the absence of FAD seemed to be crucial for this recognition event. ApoNQO1 interactome differed from holoNQO1. Chaperones and degradation factors were enriched on NQO1 upon cofactor withdrawal, probably to support maturation and prevent aggregation of the enzyme.

Loss of protein folding and stability, even to a small extent, can enhance the aggregating behavior of proteins. Proper loading with FAD reduced the co-aggregation of NQO1 with $A\beta_{1\text{-}42}$ peptide. We assumed that the flavoproteome might represent aggregating-prone species under riboflavin deprivation. Supportingly, reversible apoNQO1 aggregates were observed *in vivo* in the absence of cofactor. General amyloidogenesis *in vivo* also increased under these conditions, apparently as a result of flavoproteome destabilization. In this context, we think that our data might have important implications considering the onset and development of conformational diseases.

This work has shed some light on the therapeutic implications of riboflavin deficiency as well. The sensitivity of melanoma cells towards the alkylating agent methyl methanesulfonate (MMS) increased under riboflavin starvation. Subsequent analyses indicated that a complex metabolic reorganization, mostly affecting proliferation and energy metabolism, occurs in response to starvation. What we suggest to call “flavoaddiction” can be understood as the dependence of melanoma cells on the flavoproteome structural and functional intactness to survive chemotherapy. Understanding this cellular reprogramming in detail might reveal new possibilities for future therapies.

SUMMARY

Protein folding and maturation is an intricate process that needs constant supervision by the protein quality control (PQC) system. Molecular chaperones comprise a large family of maturation-assisting factors that guide polypeptides throughout this process. Diverse sources of protein damage like mutations or chemical agents might hinder folding and eventually prevent proteins from reaching the final functional state. In these cases the 26S proteasome, in combination with molecular chaperones is able to selectively degrade these faulty proteins. To this end, several ubiquitin molecules are usually attached to proteins, a modification that works as a degradation signal. Despite the many strategies that the PQC has evolved to distinguish between "normal" and "defective" proteins, the crowded cellular environment and the heterogeneity of the proteome make the protein triaging a challenging task.

Cofactor shortage results in the malfunctioning of the respective proteins. Vitamin B2 (riboflavin) cannot be stored in the cell and thus needs to be constantly acquired through the diet. Flavoproteins constitute a group of ca. 100 enzymes that use riboflavin-derived flavin mononucleotide (FMN) and flavin adenine dinucleotide (FAD) molecules as cofactors. Previous studies have found that the stability of several flavoenzymes is compromised under cofactor loss. Patients suffering from metabolic diseases affecting the catabolism of fatty acids have been shown to improve their conditions by the increased supplementation of vitamin B2. Biochemical studies indicate that the improvement probably comes as a result of the stabilization of key flavoproteins causing these disorders. Here, we wanted to investigate in detail the relationship between the PQC and flavin-free proteins. We assumed that subtle structural changes might be sufficient for selective targeting of apoproteins for degradation.

NAD(P)H:quinone oxidoreductase 1 (NQO1) could be used in this study by comparing it to its mutant, NQO1 P187S. The protein levels of the mutant are reduced *in vivo*. Biophysical analyses of the mutant have reported low affinity for FAD and increased flexibility of some regions, especially the C-terminal tail. Furthermore, CHIP was shown to bind NQO1 mutant more avidly than wild-type. We set out to investigate the role of FAD loading for the stability of NQO1, seeking a better understanding of the mechanisms that the PQC employs to deal with apoproteins.

Unstable proteins or proteins with structural defects are more prone to aggregate. There is a pressing need for understanding aggregation-driving processes, given the role they play during the development of neurodegenerative diseases. This work aimed to investigate the aggregating predisposition of flavin-deficient flavoproteins.

Enlarging the burden of defective proteins might have severe consequences for the cell, which has to sacrifice some of its folding and degradation capacity to deal with proteome destabilization. The relevance of flavoproteins in many aspects of the biology of the cell, especially in processes that require oxidation/reduction power, suggests cellular toxicity under vitamin B2 deficiency. New cellular vulnerabilities might appear when both stability and functionality of the flavoproteome are compromised. Among the aims of this work was to study the exposed liabilities of cells under riboflavin starvation to open novel therapeutic possibilities to target tumor cells.

Initial mass spectrometry experiments showed that the flavoproteome was degraded under riboflavin-deficient conditions. A major fraction of proteins were rescued from degradation by using the 26S proteasome inhibitor MG132. The effect was stronger with longer starvation. Immunoblotting supported the mass spectrometry results by showing a decrease of wild-type NQO1 protein levels in the absence of vitamin B2 and a rescuing effect was observed upon MG132 treatment. *In vivo* degradation of apoNQO1 correlated with the presence of the E3 ligase CHIP. Ubiquitylation assay was carried out *in vitro* using recombinant wild-type holoNQO1, apoNQO1, and mutant NQO1 proteins. Here we found that cofactor-free enzymes were more susceptible for ubiquitylation.

To understand the mechanism by which CHIP recognizes apo- and mutant NQO1, we investigated the behavior of the NQO1 C-terminal tail. Earlier studies had underscored the flexibility of this region. We found that the C-terminus became more susceptible to hydrolysis by trypsin when NQO1 had no FAD. Dicoumarol is a potent inhibitor of NQO1 that occupies the binding site of NADH, right next to the FAD pocket. Its binding to the enzyme is known to partially stabilize the C-terminal tail. An *in vitro* ubiquitylation experiment showed that dicoumarol can help apoNQO1 escape form CHIP recognition. Partial recovery of NQO1 protein levels *in vivo* was also observed when melanoma cells under riboflavin starvation were treated with dicoumarol. Finally, engineered NQO1 proteins without the last 50 amino acids were purified. As expected, CHIP hardly ubiquitylated these tail-free proteins. CHIP could not ubiquitylate NQO2 either, an NQO1 paralog without C-terminus.

We wondered whether small changes at the structure level would enhance the propensity of NQO1 to aggregate. Indeed, computational analysis revealed that the C-terminal tail of NQO1 has a mild potential for aggregation. We tested our hypothesis by incubating NQO1 proteins with $A\beta_{1-42}$ peptide *in vitro*. This short peptide accumulates in the brain of Alzheimer's disease patients and causes severe cellular damage. We found that apo- and mutant NQO1 bound with higher affinity to $A\beta_{1-42}$. Interestingly, tail-free NQO1 proteins significantly lost this co-aggregation behavior. Next, we succeeded in detecting NQO1 aggregation *in vivo*. BN-PAGE showed apoNQO1 forming aggregates in the absence of $A\beta_{1-42}$ in melanoma cells. Addition of FAD to lysates before sample separation by BN-PAGE disaggregated NQO1 completely. This result implies that, under our experimental conditions, high molecular weight NQO1 species populated a semi-native structure that can be fully disassembled by the presence of the cofactor. This prompted us to study in detail holo- and apoNQO1 interactomes. To this end, NQO1 pull-down followed by mass spectrometry analysis was carried out. Under riboflavin deficiency, a number of different chaperones were found to bind NQO1. To a lesser extent degradation factors were found as well among the enriched interactors. By inhibiting HSP70 (one of the most enriched chaperones), apoNQO1 aggregation increased markedly. Another series of experiments showed that the amyloidogenesis of $A\beta_{1-42}$ was exacerbated *in vivo* under riboflavin deprivation, indicating a general increase in aggregation.

Activation of chemotherapeutic Mitomycin C is NQO1-dependent. Accordingly, the activity of this DNA-crosslinking agent was strongly diminished in the absence of vitamin B2. Conversely, the chemotherapy with methyl methanesulfonate (MMS) was selectively more efficient against starved cells. This observation was truly unexpected since MMS does not require any transformation to reach its maximal activity. These results implied that a complex cell biochemical reorganization occurs as a consequence of riboflavin deficiency. Such changes could explain why starved cells respond differently to MMS. AMP-activated protein kinase (AMPK) is the central sensor molecule that controls metabolic reorganization in response to nutrient starvation. We found that phosphorylated AMPK levels slightly increased after prolonged riboflavin starvation. This finding indicates to the molecular adaptation during vitamin B2 deficiency.

GO enrichment analysis of the proteomics results revealed that specific changes occurred after 3 days incubation of cells in medium without riboflavin. More specifically, 88 proteins

increased while 162 decreased under these conditions. Among the enriched group several glycolytic enzymes were found. Lysosomal activity seemed to have risen as well. The levels of enzymes involved in the processing of complex carbohydrates increased. Thus, melanoma cells developed a senescent-like phenotype under riboflavin starvation. Fittingly, β-galactosidase activity increased more than 2-fold and cell size increased by ca. 2.5 times.

There were three main functional clusters of proteins that were reduced after 3 days incubation without riboflavin: oxidative phosphorylation, cell cycle, and sterol synthesis. 24 proteins involved in the ATP production in mitochondria markedly decreased. Among them, 21 belong to the NADH dehydrogenase complex (also known as complex I). We investigated the functional consequences of this result by high resolution respirometry. Cellular respiration was severely affected under riboflavin starvation. More detailed analysis revealed that complex I activity was almost completely abolished under these conditions, as expected from the proteomics data.

More than 60 cell cycle-related proteins decreased in the absence of riboflavin. Compared to the rest, this group was particularly heterogeneous since it encompassed proteins involved in cell cycle signaling events, DNA replication and repair, and chromosome organization. Biochemical and cellular analyses verified that riboflavin deficiency inhibited cell proliferation.

The last cluster of reduced proteins included 9 enzymes from sterol biosynthetic pathway, also known as mevalonate pathway. Cholesterol is one of the main products of this pathway. Cholesterol levels were reduced by ca. 30% in cells under riboflavin starvation.

One of the main objectives of proteomics and biochemical analyses was to elucidate the molecular mechanism of increased MMS vulnerability under vitamin B2 starvation. Interestingly, non-proliferating melanoma cells under serum withdrawal were more sensitive to MMS as well. Hence, cell cycle stop could promote the appearance of such sensitivity. The phosphorylation levels of AKT, one of the main cellular pro-survival factors, were also analyzed upon MMS treatment. Specific phosphorylation at the S473 site was partially inefficient under riboflavin starvation.

In conclusion, the stability of the flavoproteome was found to be tightly linked to the levels of riboflavin. Small structural changes caused by the lack of cofactor might serve as defective signals that flavin-free proteins expose to the PQC. NQO1 serves as an example thereof. ApoNQO1 could still acquire a native-like conformation, but the C-terminal tail of the

enzyme gained flexibility without FAD, which became crucial for NQO1 recognition by the E3 ligase CHIP. Chaperones could also detect apoNQO1 *in vivo*. This interaction might provide apoNQO1 some aid for structural maturation while preventing its aggregation. Amyloidogenesis increased under riboflavin-deficient conditions. These results are especially important in regard to neurodegeneration. We believe that the stability of apoproteins should be carefully addressed in the context of aggregating diseases. Finally, vitamin B2 deprivation forced melanoma cells to adapt. In general terms, the adaptation mechanism involved inhibiting proliferation and switching from a respiratory-based to a fermentation-based metabolism. We observed increased vulnerability of cells to MMS upon the adaptation. This phenomenon might be a consequence of cell cycle block, although impairment of AKT activation under starvation conditions could also be involved. Overall, this work highlighted the therapeutic implications of riboflavin in two different contexts, i.e. as a folding agent that works as pharmacological chaperones and by creating cellular vulnerabilities for anti-cancer treatment.

ZUSAMMENFASSUNG

Proteinfaltung und Prozessierung ist ein komplexer Prozess, der der konstanten Überwachung durch das Protein-Qualitätskontroll-System (PQS) bedarf. Molekulare Chaperone sind eine große Familie von Proteinen, die neu-synthetisierte Polypeptidketten durch den Prozess der Faltung und Funktionalisierung begleiten. Verschiedene Faktoren, wie Mutationen oder chemische Agenzien können die korrekte Faltung von Proteinen beeinträchtigen und unter Umständen die Entstehung eines funktionalen Proteins verhindern. In diesem Fall ist das 26S Proteasom zusammen mit molekularen Chaperonen in der Lage diese fehlgefalteten Proteine selektiv abzubauen. Um den Abbau einzuleiten wird das Zielprotein mit mehreren Ubiquitinmolekülen modifiziert, welche als Signal für den Abbau fungieren. Trotz der zahlreichen Strategien des PQS defekte Proteine von nativen zu unterscheiden, ist dieser Prozess aufgrund der hohen Konzentration von Proteinen in der Zelle und der Heterogenität des Proteoms fehleranfällig.

Die Abwesenheit von Cofaktoren resultiert häufig in der Fehlfunktion der entsprechenden Proteine. Vitamin B2 (Riboflavin) kann nicht in der Zelle gespeichert werden und muss deshalb kontinuierlich mit der Nahrung aufgenommen werden. Flavoproteine bilden eine Gruppe von ca. 100 Enzymen, die die Riboflavinderivate Flavinmononukleotid (FMN) und Flavinadenindinukleotid (FAD) als Cofaktoren benötigen. Frühere Studien haben gezeigt, dass die Struktur einiger Flavoproteine von der Anwesenheit der Cofaktoren abhängig ist. Das Befinden von Patienten, die unter einer Beeinträchtigung des Fettsäurestoffwechsels leiden, konnte durch erhöhte Zugabe von Vitamin B2 verbessert werden. Biochemische Studien weisen darauf hin, dass die Verbesserung vermutlich durch eine Stabilisierung von wichtigen Flavoproteinen, die ursächlich am Krankheitsbild beteiligt sind, hervorgerufen wird. In dieser Arbeit wollten wir die Beziehung zwischen dem PQS, besonders der Ubiquitinligase CHIP, und flavin-freien Proteinen untersuchen. Wir nahmen an, dass kleinste Änderungen in der Struktur dieser Apoproteine ausreichen, um diese selektiv abzubauen.

Wildtyp NAD(P)H:quinon oxidoreduktasen 1 (NQO1) konnte für die Untersuchung dieser Hypothese mit einer Mutante NQO1 P187S verglichen werden. Die Expressionslevels des Mutanten sind *in vivo* im Vergleich zum Wildtypprotein reduziert. Biophysikalische Untersuchungen konnten eine reduzierte Affinität des Mutanten für FAD und eine erhöhte

strukturelle Flexibilität in einigen Regionen des Proteins, besonders im C-Terminus, zeigen. Desweiteren konnte gezeigt werden, dass CHIP die NQO1 Mutante stärker bindet als das Wildtypprotein. Wir untersuchten welchen Einfluss die Bindung von FAD auf die Stabilität von NQO1 hat und welche Mechanismen das PQS in der Prozessierung von Apoproteinen nutzt.

Instabile Proteine oder solche mit strukturellen Defekten aggregieren leichter, weshalb es von besonderer Wichtigkeit ist, Aggregationsprozesse zu verstehen, besonders in Hinblick auf deren Rolle in der Entstehung von neurodegenerativen Erkrankungen. Diese Arbeit untersuchte die Prädisposition zur Aggregation von Flavoproteinen ohne gebundenen Cofaktor.

Eine Anhäufung von defekten Proteinen kann schwerwiegende Konsequenzen für die Zelle haben, die mit einem Teil ihrer Faltungs- und Abbaukapazitäten die Destabilisierung des Proteoms ausgleichen muss. Die Beteiligung von Flavoproteinen in essenziellen Prozessen der Zellbiologie, besonders solchen, die mit Oxidation/Reduktion verbunden sind, legt nahe, dass ein Vitamin B2 Mangel toxische Effekte auf die Zelle haben kann. Neue Schwachstellen können in der Zelle auftreten, wenn Funktionalität und Stabilität des Flavoproteoms beeinträchtigt sind. Eines der Ziele dieser Arbeit war es diese Schwachstellen unter Riboflavinmangel zu untersuchen und neue Möglichkeiten zur gezielten Tumortherapie aufzuzeigen.

Massenspektrometrische Analysen zeigten, dass das Flavoproteom unter Riboflavinmangel abgebaut wird. Ein Großteil der Proteine konnte durch Behandlung mit dem Proteasominhibitor MG132 vor dem Abbau geschützt werden. Der Effekt war desto stärker, je länger die Behandlung unter Riboflavinmangel war. Immunoblotting unterstützte die Ergebnisse der Massenspektrometrie, da es eine Abnahme der Proteinlevel von NQO1 Wildtyp unter Riboflavinmangel zeigte und dieser Effekt durch Behandlung mit MG132 negiert werden konnte.

In vivo Abbau von apoNQO1 korrelierte mit der Anwesenheit der E3 Ligase CHIP. Ubiquitinierungsassays mit rekombinantem holoNQO1, apoNQO1 und NQO1 P187S wurden *in vitro* durchgeführt. Hier entdeckten wir, dass cofaktor-freie Enzyme stärker ubiquitiniert wurden.

Um den Mechanismus zu verstehen, wie CHIP apoNQO1 und die NQO1 Mutante erkennt, untersuchten wir die Beteiligung des C-terminalen Endes von NQO1. Frühere Studien hatten

eine besondere Flexibilität dieser Region aufgedeckt. Wir konnten zeigen, dass der C-terminale Abschnitt von NQO1 leichter von Trypsin hydrolysiert wurde, wenn NQO1 kein FAD gebunden hatte.

Dicoumarol ist ein potenter Inhibitor von NQO1, der die Bindungsstelle für NADH blockiert, die direkt neben der Bindungsstelle für FAD liegt. Es konnte gezeigt werde, dass die Bindung des Inhibitors den C-terminalen Abschnitt partiell stabilisiert. In einem *in vitro* Ubiquitinierungsassay konnte gezeigt werden, dass durch Zugabe von Dicoumarol die Ubiquitinierung von apoNQO1 durch CHIP reduziert wurde. Die *in vivo* Behandlung mit Dicoumarol zeigte einen reduzierten Abbau von NQO1 in Melanomzellen unter Riboflavinentzug. Außerdem wurde eine Proteinvariante von NQO1 ohne den C-terminalen Abschnitt rekombinant erstellt und produziert. Als erwartet war CHIP kaum in der Lage diese Variante von NQO1 zu ubiquitinieren. NQO2, ein Paralog von NOQ1, dem der C-terminale Abschnitt von NOQ1 fehlt, konnte ebenfalls nicht von CHIP ubiquitiniert werden.

Wir vermuteten, dass kleine strukturelle Änderungen in NQO1 die Wahrscheinlichkeit erhöhen, dass das Protein aggregiert. Tatsächlich zeigten computergestützte Analysen, dass der C-terminale Abschnitt von NQO1 ein erhöhtes Aggregationspotenzial hat. Wir untersuchten unsere Hypothese, indem wir NQO1 mit $A\beta_{1-42}$ Peptid *in vitro* inkubierten. Dieses kurze Peptid akkumuliert in Neuronen von Alzheimerpatienten und verursacht dort erheblichen Schaden. Wir konnten feststellen, dass apoNQO1 und die NQO1 Mutante $A\beta_{1-42}$ Peptide stärker bindet. Interessanterweise zeigten NQO1 Proteine ohne den C-terminalen Teil diese Coaggregation nicht.

Es gelang uns außerdem NQO1 Aggregation *in vivo* nachzuweisen. Die Bildung von apoNQO1 Aggregaten auch in Abwesenheit von $A\beta_{1-42}$ konnte mittels BN-PAGE in Melanomzellen gezeigt werden. Die Zugabe von FAD zu den Zelllysaten vor der Auftrennung mittels BN-PAGE löste die NQO1 Aggregate vollständig auf. Diese Ergebnisse implizieren, dass unter unseren experimentellen Bedingungen NQO1 nicht-native, hochmolekulare Spezies bildet, die durch Cofaktorzugabe disassembliert werden können. Daraufhin untersuchten wir detailliert das Interaktom von holo- und apoNQO1. Zu diesem Zweck wurden NQO1 pull-downs mit nachfolgender massenspektrometrischer Analyse durchgeführt. In Abwesenheit von Riboflavin konnte eine Reihe von Chaperonen in Assoziation mit NQO1 identifiziert werden. In geringerem Maße konnten auch Abbaufaktoren unter den angereicherten Interaktoren gefunden werden.

Durch die Inhibition von HSP70 (eines der am meisten angereicherten Chaperone) erhöhte sich die Aggregation von apoNQO1 deutlich. Eine weitere Experimentreihe zeigte, dass auch die Amyloidogenese von $A\beta_{1-42}$ unter Riboflavinentzug *in vivo* verschärft auftrat, was auf eine generell erhöhte Aggregation hindeutet.

Die Biotransformation und Aktivierung des Chemotherapeutika Mitomycin C ist NQO1-abhängig. Folglich war die Aktivität dieses DNA-vernetzenden Agens in der Abwesenheit von Vitamin B2 deutlich reduziert. Im Gegensatz dazu war die Chemotherapie mit Methylmethansulfonat (MMS) selektiv effizienter bei Zellen unter Riboflavinentzug. Dieser Effekt war unerwartet, da MMS keine Biotransformation oder Aktivierung für seine maximale Wirksamkeit benötigt. Dieser Ergebnisse legen nahe, dass komplexe zellbiologische Umstrukturierungen als Reaktion auf Riboflavinentzug stattfinden. Solche komplexen Veränderungen könnten erklären, warum vitamin-defiziente Zellen anders auf MMS reagieren. AMP-activated protein kinase (AMPK) ist das zentrale Sensormolekül, dass metabolische Veränderungen als Reaktion auf Nährstoffmangel kontrolliert. Wir konnten feststellen, dass sich die Menge an phosphorylierter AMPK in Zellen durch langen Riboflavinentzug leicht erhöhte. Dieses Ergebnis impliziert eine molekulare Adaption während eines Vitamin B2 Mangels.

GO Enrichment Analysen der gemessenen Proteomdaten zeigten spezifische Änderungen nach dreitägiger Inkubation in Wachstumsmedium ohne Riboflavin. Insgesamt wurden unter diesen Bedingungen 88 Proteine angereichert, während bei 162 Proteine eine Abnahme festgestellt werden konnte. Unter den angereicherten Proteinen fanden sich einige glykolytische Enzyme. Außerdem schien die lysosomale Aktivität erhöht. Die Menge an Enzymen, die in der Verarbeitung von komplexen Kohlenhydraten involviert ist, war ebenfalls erhöht. Folglich entwickeln Melanomzellen einen seneszenz-ähnlichen Phänotyp unter Riboflavinentzug. Passend dazu zeigte β-Galaktosidase eine mehr als 2-fach erhöhte Aktivität und die Zellen wurden ungefähr 2.5-fach größer.

Es gab drei funktionale Cluster von Proteinen, deren Vorkommen durch dreitägigen Riboflavinentzug signifikant reduziert wurde: Oxidative Phosphorylierung, Zellzyklus und Sterolsynthese. 24 Proteine, die in ATP Produktion involviert sind, waren ebenfalls deutlich reduziert. 21 davon gehören zum NADH Dehydrogenasekomplex (auch bekannt als Komplex I). Wir untersuchten die funktionalen Konsequenzen dieser Ergebnisse mit hochauflösender Respirometrie. Die zelluläre Respiration wurde durch Riboflavinentzug schwerwiegend

beeinflusst. Detailliertere Analysen zeigten, dass unter diesen Bedingungen Komplex I fast keine Aktivität mehr zeigte. Dies war auf Grundlage der Proteomdaten zu erwarten.
Mehr als 60 Proteine, die an der Kontrolle des Zellzyklus beteiligt sind, waren in Abwesenheit von Riboflavin reduziert. Verglichen mit den anderen Clustern, diese Gruppe war besonders heterogen, da sie Proteine enthielt, die in der Signalkaskade des Zellzyklus, der DNA Replikation und Reparatur und chromosomaler Organisation beteiligt sind. Biochemische und zelluläre Analysen bestätigten, dass der Riboflavinentzug die Zellproliferation inhibierte.
Das letzte Cluster von Proteinen enthielt 9 Enzyme der Sterolbiosynthese, auch bekannt als Mevalonatweg. Cholesterol ist eines der Hauptprodukte des Mevalonatwegs und war folglich in Zellkulturen ohne Riboflavin um 30% reduziert.
Eines der Hauptziele unseren Analysen war es, den molekularen Mechanismus der erhöhten MMS-Sensitivität unter Vitamin B2 Entzug aufzuklären. Interessanterweise waren sich nicht teilende Melanomzelle, die ohne Serum kultiviert wurden, ebenfalls anfälliger gegenüber der Behandlung mit MMS. Folglich könnte eine Arretierung des Zellzyklus die Ursache für die erhöhte Sensitivität sein. Die Phosphorylierung von AKT Kinase, einem der wichtigsten Faktoren für das Überleben von Säugerzellen, wurde ebenfalls unter MMS Behandlung untersucht. Die spezifische Phosphorylierung von AKT an S473 war teilweise beeinträchtigt in Abwesenheit von Riboflavin.
Zusammenfassend, es konnte gezeigt werden, dass die Stabilität des Flavoproteoms eng mit der Verfügbarkeit von Riboflavin verknüpft ist. Kleine strukturelle Änderungen, die durch die Abwesenheit des Cofaktors ausgelöst werden, können als Signal dienen, wodurch die flavin-freien Proteine vom PQS erkannt werden. Erkennung von apoNQO1 ist ein Beispiel für einen solchen Mechanismus. ApoNQO1 zeigte eine nahezu native Struktur. Nur im C-terminalen Abschnitt konnte erhöhte Flexibilität in er Abwesenheit von FAD festgestellt werden. Es zeigte sich, dass diese Änderung essentiell für die Detektion von apoNQO1 durch die E3-Ligase CHIP war. Desweiteren konnten Chaperone apoNQO1 *in vivo* spezifisch binden. Diese Interaktion könnte apoNQO1 bis zur Bindung von FAD stabilisieren und eine Aggregation verhindern. Amyloidogenese war in Abwesenheit von Riboflavin erhöht. Diese Ergebnisse sind besonders wichtig im Hinblick auf Neurodegeneration. Wir sind überzeugt, dass die Stabilität von Apoproteinen im Kontext aggreationsbezogener Krankheiten sorgfältig berücksichtigt werden sollte. Ferner, der Vitamin B2 Entzug zwang Melanomzellen zur

Anpassung. Generell umfasste die Adaption eine Inhibition der Proliferation und eine Umstellung von einem respiration-fokussiertem Stoffwechsel zu einem fermentation-fokussiertem Stoffwechsel. Wir beobachteten, dass diese Adaption eine erhöhte Sensitivität gegenüber MMS zur Folge hatte. Dieses Phänomen könnte auf eine Störung des Zellzyklus zurückzuführen sein, wobei auch die reduzierte Aktivität von AKT Kinase involviert sein könnte.

Diese Arbeit hat die therapeutischen Implikationen von Riboflavin in zwei unterschiedlichen Zusammenhängen hervorgehoben, nämlich in Proteinfaltung und Amyloidogenese als notwendiges Agens, dass als pharmakologisches Chaperon agiert, und in Stoffwechsel, indem sein Fehlen zelluläre Schwachstellen erzeugt, die zur Behandlung von Krebs eingesetzt werden können.

ACKNOWLEDGMENTS

I want to express my most sincere appreciation to Dr. Martin Vabulas for giving me the opportunity to join his research group in Frankfurt to do my PhD. He has become a mentoring figure for me during this journey. My value as a scientist would not be the same without his teachings. His encouraging and positive attitude has always helped me to find the strength and motivation needed to overcome the most challenging situations. For these reasons I am especially grateful to him. I would like to thank Dr. Giulia Calloni for taking care of processing and analyzing mass spectrometry samples. The development of this project has truly benefited from her invaluable work.

I am grateful to our partner collaborator Dr. Ilka Witig. Her expertise and scientific support have been a major contribution to our studies. I want to thank her as well for allowing me to work for a month in her laboratory. In this regard, I want to thank Dr. Juliana Heider for teaching me how to carry out the respirometry measurements. I really appreciate the scientific and technical expertise I acquired during this time.

I want to thank Dr. Masato Akutsu for introducing me to the preparation and processing of protein crystals and to Prof. Dr. Achilleas Frangakis, Dr. Margot Frangakis, and Dr. Anja Seybert for the TEM training.

I am especially thankful to all my colleagues Dr. Tobias Schuster, Marion Alriquet, Wei-Han Lang, Yannick Kopp, and Haotian Wang, with whom I shared several years of my life. I thank them all their support, insights and stimulating discussions that have helped me at the scientific and personal level.

I want to thank my girlfriend Inés for all the time and dedication she has put on guiding me along this path. I truly appreciate the encouraging and kind words from my family and friends in Barcelona.

TABLE OF CONTENT

ADDITIONAL INDEXES

List of figures

List of tables

Abbreviations

17-AAG	17-N-allylamino-17-demethoxygeldanamycin
ADP	Adenosine diphosphate
AMP	Adenosine monophosphate
ANOVA	Analysis of variance
ANS	8-Anilino-1-naphtalensulfonic acid
ATP	Adenosine triphosphate
BN-PAGE	Blue native-polyacrylamide gel electrophoresis
BrdU	Bromodeoxyuridine
BSA	Bovine serum albumin
CI	Mitochondrial complex I
CII	Mitochondrial complex II
CD	Circular dichroism
cDNA	Complementary DNA
CHX	Cycloheximide
CoA	Coenzyme A
DAPI	4', 6-diamidino-2-phenylindole
DIC	Differential interference contrast
DMEM	Dulbecco's Modified Eagle Medium
DMSO	Dimethyl sulfoxide
dNTP	Deoxyribose nucleoside triphosphate
DNA	Deoxyribonucleic acid
DTT	Dithiothreitol
ECL	Enhanced chemiluminescence
E.coli	*Escherichia coli*
EDTA	Ethylendiamintetraacetic acid
EGFP	Enhanced green fluorescent protein
ER	Endoplasmic reticulum
ETS	Electron transfer system
FAD	Flavin adenine dinucleotide
FDR	False-discovery rate
FIN56	N^2,N^7-dicyclohexyl-9-(hydroxyimino)-9H-fluorene-2,7-disulfonamide
FMN	Flavin mononucleotide

G418	Geneticin
GAPDH	Glyceraldehyde 3-phosphate dehydrogenase
GO	Gene onthology
HCD	Higher-energy collisional dissociation
HRP	Horseradish peroxidase
IPTG	Isopropyl β-D-1-thiogalactopyranoside
KO	Knockout
LB	Lysogeny broth
LC-MS/MS	Liquid chromatography-tandem mass spectrometry
LFQ	Label-free quantification
MMS	Methyl methanesulfonate
M. musculus	*Mus musculus*
mRNA	Messenger RNA
NAD(P)H	Nicotinamide adenine dinucleotide (phosphate)
ns	Not significant
PI	Propidium iodide
PQC	Protein quality control
RMSD	Relative mean square deviation
ROS	Reactive oxygen species
ROX	Residual oxygen consumption
rpm	Revolutions per minute
SD	Standard deviation
SDS-PAGE	Sodium dodecyl sulphate-polyacrylamide gel electrophoresis
TBS	Tris-buffered saline
TCA	Tricarboxylic acid cycle
Tm	Melting temperature
X-gal	5-Bromo-4-chloro-3-indolyl-β-D-galactopyranoside

1 INTRODUCTION

1.1 Protein folding and aggregation

After translation, polypeptides must undergo an intricate folding process in order to acquire a final and functional 3D conformation. Funnel-like thermodynamic models were suggested in the 80s to represent such events. These classical illustrations depict extended polypeptides populating a vast free energy landscape where chains undergo different conformational changes in the search of more stable structures (Figure 1). Energy gradient favors intramolecular interactions that ultimately lead to the native form of the protein, normally illustrated as low free energy valleys of high stability in the funnel-like folding map (1). However, folding is still the most critical event during the whole maturation process of a protein, which also includes post-translational modification and transport within and outside of the cell. The competition between intramolecular and intermolecular interactions can

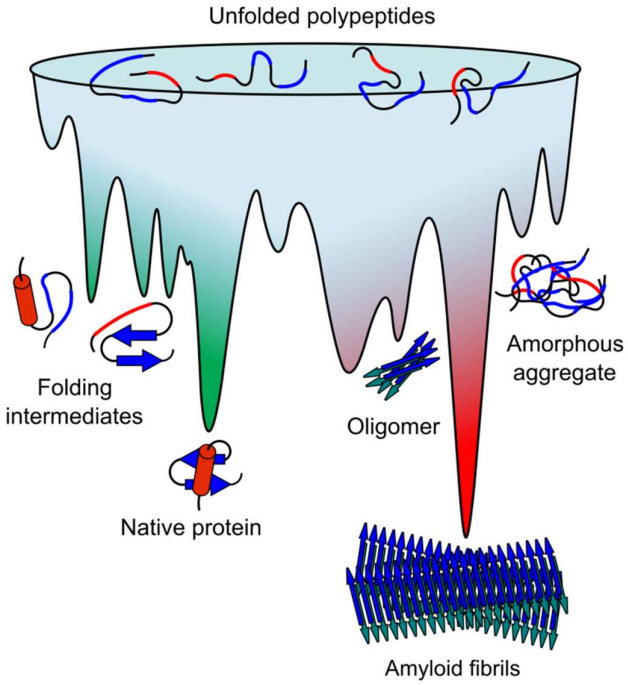

Figure 1. The protein folding model. Schematic representation of the protein folding process is shown. Intermolecular contacts (green area) favor correct folding of the polypeptide chain. Formation of folding intermediates finally leads to native structure. Aberrant interactions (red area) with other chains promote the formation of aberrant species which are potentially toxic.

account for the failure of polypeptides to acquire their correct structure. The desired functionality of the protein is actually at risk due to this competition. The appearance of aberrant and non-native conformational structures, known as aggregates or amyloids (Figure 1, red area of the funnel) depends on abnormal interactions among different protein molecules that have not yet achieved their native conformation (2). This may ultimately lead to the formation of amyloid fibrils, a group of extremely stable arrangement of proteins, all sharing a common structural pattern. This structure is formed by a continuous alignment of cross-β-strands running perpendicular to the orientation of the fiber axis and whose stability is mostly sustained by hydrogen bonds oriented in parallel to the direction of this axis (3). Overall, a competition between folding and aggregation exists as a result of the balance between native molecular interactions and dysfunctional or aberrant ones (4,5). Other factors like mutations, heat and oxidative stress can also disturb protein folding and push the equilibrium towards aggregation (6). Human disorders arise when an unusually large amount of misfolded species accumulate in the cell. These are also known as "conformational diseases". The resulting aggregates can accumulate extracellularly as well as intracellularly in the form of inclusions bodies or plaques (7). The aggregate terminology refers to a wide variety of heterogeneous structures, from highly ordered fibrils to less ordered amorphous conformations that may differ in their biophysical and biochemical properties. Several pathologies may arise from protein accumulation in any part of the body, but aggregation-related diseases affecting the central nervous system, known as neurodegenerative diseases, are the most commonly studied ones and altogether entail one of the alarming worldwide health problems nowadays. Some examples include Alzheimer's disease, Huntington's disease, Parkinson's disease or prion diseases, which are caused by aggregation of β-amyloid peptide (Aβ) and tau, huntingtin, α-synuclein, and prions, respectively (8).

1.2 The protein quality control system

1.2.1 Molecular chaperones

Protein concentration in eukaryotic cells range from 50 to 200 mg/ml (9). Understanding how billions of polypeptides are translated and successfully reach their native state in such a crowded environment escaping aggregation is still not clear. To ensure that the whole proteome is appropriately guided through the processes of synthesis, folding, assembling, trafficking, import/export, and modification as well as maintenance, nature evolved a protein quality control (PQC) machinery that ensures protein homeostasis (proteostasis) (6). In

mammalian cells, approximately 1400 proteins work together for this purpose (10). Among these, molecular chaperones together with many regulatory factors form a big heterogeneous network which assist other proteins until their maturation process is completed (11). Referring to the funnel-like representation of the folding process, chaperones can modulate the free energy landscape of protein folding by binding extended polypeptides and folding intermediate species. Hence, formation of native structures is stimulated while intermolecular interactions are highly restricted. Two separated degradation machineries, namely ubiquitin-proteasome system (6) and autophagy (12), are in charge of eliminating irreversibly misfolded and aggregated proteins. Molecular chaperones consist of a group of ca. 200 proteins that are found in all organisms (10). These proteins are also commonly referred to as heat-shock proteins (HSPs) since several stress conditions affecting correct protein folding increase the expression levels of some members. Chaperones are classified in different families according to their molecular weight: HSP100, HSP90, HSP70, HSP60 chaperonins, HSP40 and small HSPs (11). The activity of chaperones extends to almost every aspect of any protein's life,

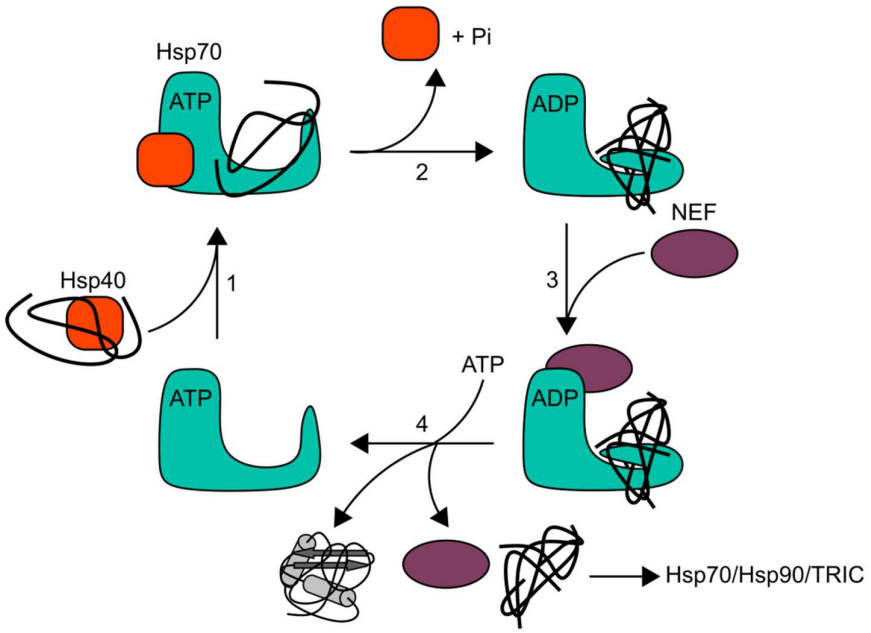

Figure 2. The HSP7 folding cycle. HSP70 assistance during protein folding is schematized in 4 steps: 1. Unfolded polypeptides (black string) are recruited by HSP40 and delivered to HSP70. 2. HSP40 catalyzes the hydrolysis of HSP70-bound ATP into ADP + Pi, which turns HSP70 into a high substrate affinity state due to a conformational change at its C-terminal domain. 3 and 4. Nucleotide exchange factor (NEF) promotes the exchange of ADP to ATP in HSP70, forcing the chaperone into its low-affinity state, and favoring substrate release. Substrate can be fully folded or, if not, can undergo repeated cycles of HSP70-assisted folding.

including *de novo* folding, refolding of misfolded species, translocation or trafficking of proteins into compartments, assembly of oligomeric complexes, and disaggregation (13). The way molecular chaperones assist proteins in folding has been extensively studied over the years and many advances have been made in this regard. The presence of exposed hydrophobic-rich stretches in protein substrates allows chaperones to differentiate between folded and unfolded or partially folded structures. This molecular encounter stabilizes folding intermediates and blocks the formation of aberrant intermolecular interactions (14). HSP90, HSP70 and HSP60 are the main cellular folding machineries, for which an ATP-regulated cycle of substrate binding and release modulates its folding activities by triggering conformational changes (11,13,15). As an example, Figure 2 illustrates the binding mode of HSP70 to substrates. Allosteric modulation controls affinity of HSP70 for substrates depending on the ATP/ADP binding. Extended hydrophobic polypeptides preferentially bind HSP70. A cradle-like structure consisting on a β-rich conformation domain that is located at the C-terminal substrate binding site of the chaperone favors the binding of such peptides with rather low selectivity. Certain peptides bind stronger than others. Structural studies of peptide-HSP70 complexes have allowed the development of prediction models for putative substrates with high accuracy (16). HSP40 promotes the hydrolysis of ATP to ADP at the N-terminal nucleotide binding site. This reaction triggers a conformational change that fixes the substrate into a high affinity state. By exchange to ATP, the substrate is released and transferred to other chaperone systems or re-engaged into HSP70 cycle again if needed (16).

Chaperone selectivity is also attributed to several other factors, among which one can include their mechanism of action, sub-cellular localization, structure of the chaperone itself, and the aid of other chaperones, like HSP40. For instance and in contrast to HSP70, HSP90 does not provide a defined pocket but its substrate-binding surface is rather large and hydrophobic contacts populate an extended area comprising a big part of the protein (17). The ring-like architecture of chaperonins differentiates their folding assistance from other chaperones. Substrate recognition by the eukaryotic chaperonin TRIC depends on a complex set of interactions involving the apical region of the ring. Each of the eight different subunits that form one ring binds to substrates depending on a particular combination of polar and hydrophobic contacts. This combinatorial recognition seems to discriminate between folded and non-folded structures (18).

1.2.2 Degradation machineries and substrate recognition

Autophagic and proteasomal degradation is another part of protein quality control system. During autophagy cellular structures, including entire organelles, protein aggregates, and even infectious agents, are enclosed in a regulated way into double-membrane vesicles called autophagosomes that are ultimately targeted to lysosomes for hydrolysis of the cargo (12). Proteins that fail to fold need to be eliminated. When unsuccessful cycles of folding take place, proteins are normally sent for degradation in order to minimize the damage that their accumulation can pose on the cell. This task is mainly accomplished by the proteolytic activity of the 26S proteasome, a ca. 2 MDa multimolecular complex that unfolds and cleaves substrates into small peptides or single amino acids (19). This task is accomplished with the aid of several factors that impose a strict regulation on this activity. The highly conserved process of protein degradation starts by covalently attaching a 76-amino acid unit called ubiquitin to substrates in a series of coordinated events that involves enzymes E1, E2, and E3. The reaction starts with an ubiquitin-activating enzyme (E1) catalyzing the adenylation of ubiquitin C-terminus end in an ATP-dependent manner. This ubiquitin then binds to the sulfhydryl group of an active E1 cysteine residue via a thioester linkage, with the release of AMP (Figure 3). E2 enzymes catalyze the transfer of ubiquitin to another active cysteine on their own surface. E3 ligases recognize substrates and bring them in close proximity with E2 enzymes (20). Eventually, an isopeptide bond between the C-terminal glycine of ubiquitin and the epsilon amino group of a substrate lysine side chain is formed. Repetitive cycles of this process eventually lead to the polyubiquitylation of proteins (20). Initial experiments showed that polyubiquitylation signals, when linked through ubiquitin K48 trigger a degradation response (21). Only recently it has been found that both ubiquitin chain length and linkage through different ubiquitin lysine residues might induce a diversity of responses (22). The folding activity of molecular chaperones seems to be constantly competing with the catalytic activity of the ubiquitin-proteasome system (23). However, in order to successfully target proteins for degradation, a link between these two must exist. Many investigations have shown that folding and degradation machineries indeed cooperate for the proper sorting of substrates (24). The presence of co-chaperones is crucial to understand how this cross-talk is established. The name co-chaperone is currently assigned to a large number of proteins that modulate the activity of chaperones and thus function as molecular switches in this context. In mammals, the complex formed by HSP70, C-terminal HSP70-interacting protein (CHIP)

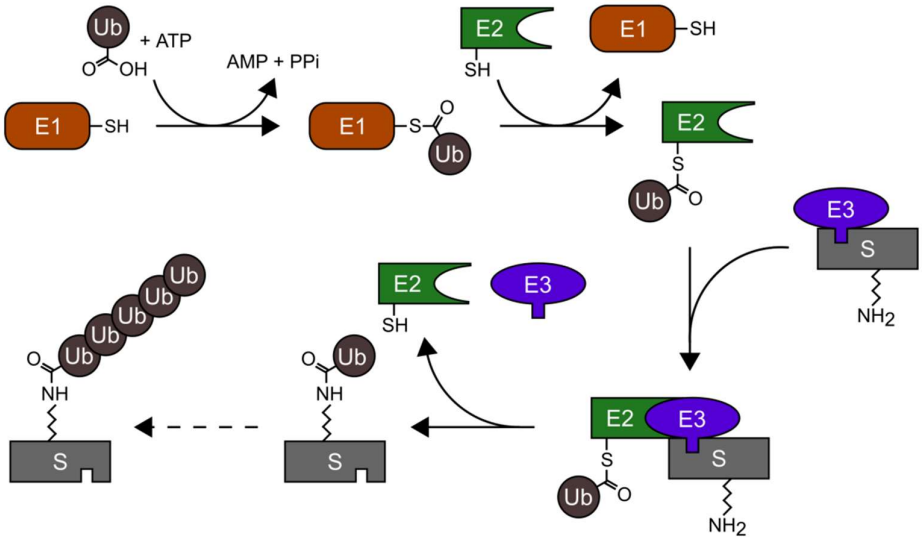

Figure 3. Substrate ubiquitylation reaction. Ubiquitin-activating enzyme (E1) forms a thioester bond between its catalytic cysteine and the C-terminal carboxylic acid of ubiquitin. E1 transfers ubiquitin to the catalytic cysteine of an E2 enzyme. Ubiquitin ligase (E3) brings a substrate (S) to E2, where substrate ubiquitylation occurs on a lysine residue through an amide bond. Repeated cycles of the process can occur to polyubiquitylate substrates.

and BCL2-associated athanogene 1 (BAG-1) is probably one of the best systems found to link chaperones to proteasomal degradation. Discovered as an HSC/HSP70 binding partner, E3 ligase CHIP was found to inhibit the folding activity of the chaperone (25) and stimulate degradation via the 26S proteasome by direct ubiquitylation of chaperone clients (26,27). BAG-1 protein binds both HSP70 and 26S proteasome through its conserved BAG and ubiquitin-like domains, respectively (28). The studies performed on CHIP and BAG-1 give a clear example of how association between chaperones and the proteasome degradation system is modulated. The activity of E3 ligases is fundamental in targeting dysfunctional proteins for degradation through direct or indirect interaction with substrates. In mammals, there are over 600 putative E3 ligases. This large number is thought to reflect the main role of these enzymes in the selectivity of ubiquitin conjugation for substrate degradation (29). Substrate recruitment by E3 ligases occurs by the recognition of specific degradation signals called "degrons". These include N-terminal sequences, post-translational modifications or N-glycosylation, among others. The recognition of hydrophobic patches can also be included in this list, as experiments with CHIP (30,31) and San1 from fission yeast (32) have demonstrated.

The PQC can follow other approaches for the correct identification and handling of proteins.

Compartmentalization is one example. Such is the case of ribosome-associated quality control (RQC), a multi-factor machinery which assists nascent polypeptide chains at the vicinity of ribosomes and promotes the degradation of stalled products (33). Sequestration of ubiquitylated and/or aggregated species in semi-isolated structures is also useful for concentrating resources that improve targeting and degradation of potentially harmful proteins (34). Stress conditions, like exposure to heat shock or oxidative agents, are known to upregulate the expression of several heat shock proteins. Such responses are well characterized in cytosol as well as in the ER and are of particular importance to increase the chaperone capacity of the cell (35). The range of defects that a polypeptide can acquire is extremely large; the same chain can populate several misfolded species, obtain erroneous post-translational modifications, gather point mutations or present different physicochemical lesions (36). This heterogeneity represents another layer of complexity that poses a major challenge for the quality control system, which has to distinguish between damaged species beyond any possible reparation from natural folding intermediates (37). In many cases the differences might be very subtle and hardly distinguishable. Despite the sophisticated strategies that proteostasis machinery has at its disposal, we still do not know how protein "triage" works in detail. The term triage refers to the series of molecular events that eventually help to solve the dichotomy between folding assistance or protein elimination, in accordance with the specific needs of every substrate (38).

Proteome stability lies on a very fragile balance and hence a tight control is needed to ensure it. For this reason, proteostasis network may be considered a double-edge sword. A very stringent selection could result in the degradation of healthy proteins, thus wasting valuable resources. The arrest of the ΔF508-CFTR (cystic fibrosis transmembrane conductance regulator) during its maturation is a classic example of how this occurs. The recognition and degradation of this channel is responsible for the appearance of cystic fibrosis (39), even when evidences have shown that channel activity of the mutant does not differ from that of the wild-type (40). Conversely, a rather lenient or even deficient system might not be able to recognize and recycle faulty proteins, leading to the deleterious accumulation of aggregated species. The correlation observed between the breakdown of quality control system and aging is in agreement with this assumption (41). Overall, a glimpse of the solution to the protein triage enigma probably lies on determining not only the set of binding modes that drive substrate recognition by chaperones and E3 ligases but also on elucidating how multiple

defects may trigger small but yet sufficient changes that push the PQC to make the right move.

1.3 Apoproteins

Cofactor-free proteins (apoproteins) constitute a large group of potentially faulty polypeptides. More than 30% of all proteins require cofactors for their biological activity. Some of them include metal ions, like iron, cooper, and zinc; others need organic cofactors, like coenzyme A, FMN/FAD, and NAD^+, among many others. Several studies have highlighted that the role of cofactors is not only limited to the functional aspect of enzymes but sometimes they are also involved in protein folding and stability (42). Some examples include the copper-containing azurin, which partially loses its thermodynamic stability in the absence of the metal ion (43), and ferredoxin, a protein whose refolding is facilitated by the synthesis and assembly of an iron-sulphur cluster (44). Tryptophan pyrrolase levels are regulated by the amount of the enzyme substrate tryptophan. The presence of the amino acid stabilizes the protein into its holoactive form and inhibits its degradation (45,46). The evidences from these investigations point out towards a cofactor-based stabilization of enzymes that might even regulate their degradation kinetics. In this case, apoproteins can become a problematic burden for the cell if changes in cofactor availability occur due to starvation. If this happens, the system has to deal with increasing amounts of useless molecular machines that are potentially harmful if their stability is indeed compromised. In this context, the question of how protein quality control system treats non-functional and potentially dangerous apoproteins has not yet been addressed in detail.

1.4 Flavoproteins and riboflavin deficiency

The case of flavin-containing proteins is truly remarkable since they comprise a vital group of approximately 100 enzymes that take part in a wide range of biological processes due to their ability to catalyze electron transfer reactions, a fact that turns them especially useful in substrate oxidation and reduction. The two cofactors they need, FMN and FAD (the last more frequently found as a prosthetic group than FMN), cannot be synthesized by humans and need to be obtained from food mostly in the form of vitamin B2 or riboflavin. Riboflavin itself consists on a substituted isoalloxazine ring, whose N-10 atom is bound to a ribityl residue. Once into the system, riboflavin can be enzymatically transform into FMN and FAD again in a two-step process that involves the addition of a phosphate moiety followed by AMP

binding, respectively. The two reactions are carried out by riboflavin kinase and FAD synthase (Figure 4). The reverse transformation can also be performed by the enzymes FAD pyrophosphatase and FMN phosphatase (47). Interestingly, at least for a high fraction of flavoproteins (ca. 60%) mutations are associated with the onset of several diseases, most of which are connected to mitochondrial metabolism and its homeostasis, but also to peroxisomes and endoplasmic reticulum (47). It is noteworthy that very little riboflavin is

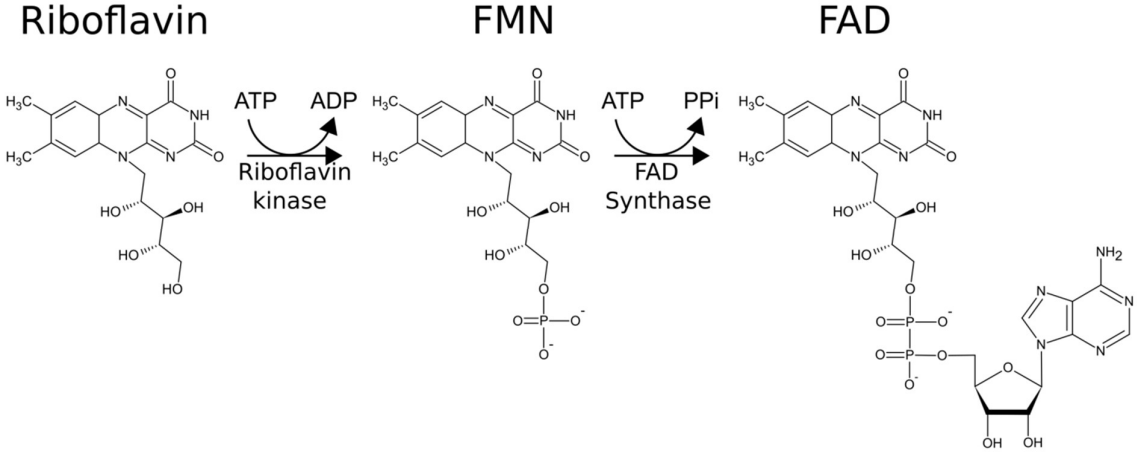

Figure 4. Enzymatic transformation of riboflavin into FMN and FAD. The two-step reaction that transforms riboflavin into FMN and FAD is shown. Phosphorylation and adenylation reactions are carried out by riboflavin kinase and FAD synthase, respectively. In both cases, consumption of ATP is needed.

stored in the human body (48). One report highlighted the finding of a local pool of flavins in the nucleus (49) and another one investigated the accumulation of riboflavin in membranous cytosolic structures of epithelial cancer cells (50). Nevertheless, these seem to be exceptions rather than a general rule. Any excess of FAD and FMN that is not bound to proteins tends to be hydrolyzed very rapidly to FMN and riboflavin, respectively (51). This is also demonstrated by the fact that exacerbated activity of riboflavin kinase and FAD synthase do not result in increased FMN and/or FAD levels (52). As a water-soluble molecule, riboflavin is eliminated in the urine (53) and thus a daily intake of the vitamin is needed to cope with the metabolic necessities of cells (54). Although a wide variety of foods contain considerable amounts of riboflavin, vitamin B2 deficiency is still very common in both developing and industrialized countries, although the former are the most affected ones in this regard (54). Even though cases of severe ariboflavinosis are hardly found, subclinical stages of the deficiency, which can be detected only biochemically even within a few days of dietary deprivation are more widespread (54). The reported consequences derived from riboflavin

low intake comprise developmental abnormalities, anemia, iron absorption and mobilization problems, neurological disorders, sensitivity to cardiovascular diseases and increased risk of cancer onset (55). Furthermore, problems in accessibility to riboflavin might also have different origins besides diet-related. One particular example is the case of hypothyroidism. Analysis of hypothyroid rat livers showed a decrease in the levels of FAD in comparison to normal animals. Addition of thyroxine restored the normal levels of the flavin cofactor (56). Later experiments in liver showed that thyroid hormone directly controls the levels of FAD by modulating the reaction rate of riboflavin kinase, which increases in hyperthyroidism and decreases in cases of hypothyroidism (57,58). In a clinical study with hypothyroid patients, indications of FAD depletion and recovery after thyroxine treatment were obtained by measuring the activity of erythrocyte glutathione reductase (EGR) (59,60). Respiratory infection has also been reported to alter riboflavin metabolism in children. This observation has been verified in mouse models, in which bacterial infection lead to a 5 to 6-fold increase excretion of riboflavin in the urine (61). Another particular alteration in riboflavin metabolism was described in rats under chlorpromazine treatment, a widely used antipsychotic agent. Exacerbated loss of riboflavin was followed by a decrease in FAD levels in liver, heart, and kidney (62). Some mutations can also mimic a situation of riboflavin deficiency even under normal vitamin intake. Such is the case of reported mutations in a group of recently found riboflavin transporters comprising SLC52A1, SLC52A2, and SLC52A3 (63–65). Elderly population is particularly prone to suffer from general malnutrition. Several medical conditions that show a high prevalence within this population are associated with malnutrition; here belong disorders in the respiratory tract, malabsorption, and diabetes, neurological conditions like Parkinson's disease, chest and urinary infections and even physical disability (66).

1.5 Proteostasis machinery and flavoproteins

As explained above, the etiology of riboflavin deficiencies can have diverse causes. Not only diet-based alterations are important but also inborn conditions that mimic some of the vitamin deprivation effects constitute a serious issue for many. Some of these situations can impose a constant degree of metabolic stress on the cell and even on the whole body. Are then cofactor-free flavoproteins detected by the proteostasis machinery at all? Some studies that have focused on describing the effects of riboflavin deprivation on several proteins at the biophysical and biological level gave some hints. The experiments performed by Nagao and

Tanaka (67) were one of the first works in addressing this issue. The consequences of riboflavin deprivation on a series of acyl-CoA dehydrogenases were analyzed in rats. Here it was found that the activity of these enzymes was drastically reduced after exposing the animals to a riboflavin-free diet for 6 weeks. A deeper investigation concluded that partial loss of protein stability and consequent degradation was the main cause behind the decrease in enzymatic activity under vitamin shortage. Multiple acyl-CoA dehydrogenase deficiency (MADD) is a rare disorder that affects oxidative metabolism. The causes of the pathology include defects in the synthesis of flavin cofactors as a consequence of different FLAD1 variants (the gene that encodes FAD synthase) (68). As pointed out before, genetic alterations in riboflavin transporter genes can lead to riboflavin deficiency. The appearance of Brown-Vialetto-Van Laere (BVVL) syndrome has been associated with alterations in two of these genes, namely SLC52A2 and SLC52A3 (63,64). Interestingly, the biochemical and metabolic features that characterize this disease mimic some of those traits observed in MADD patients (69). In most cases though, MADD is caused by inherited defects in one of the two genes that encode for electron transfer flavoprotein (ETF) and ETF: ubiquinone oxidoreductase (ETF:QO). ETF and ETF:QO collect electrons from several dehydrogenases involved in the oxidation of fatty acids and transfer them to the ubiquinone pool in the inner mitochondrial membrane to fuel oxidative phosphorylation. The two enzymes provide a link between fatty acid catabolism and ATP production (70). One of the main characteristics of this condition is the capacity of some patients to positively respond to high doses of riboflavin, a group that has been classified as riboflavin-responsive MADD, or RR-MADD (70). A recent investigation with different mutant variants of ETF:QO showed that not only the activity but also the steady-state levels of some of these mutants, especially the ones that are found in RR-MADD patients, correlate with riboflavin amounts (71). This finding suggests that flavoprotein degradation might depend on the levels of flavin cofactors. The study of one patient with markedly low activities of both short-chain and medium-chain acyl-CoA dehydrogenases (SCAD and MCAD, respectively) showed that protein levels were significantly reduced. Treating this patient with an extra dose of riboflavin resulted in the normalization of SCAD and increase of MCAD activities and the overall improvement of the patient's condition (72). Deregulation of FMN and FAD tissue levels in hypothyroidism cases has been also shown to reduce the activity of some flavoenzymes. Therefore, the presence of FMN and FAD cofactors has been proposed to dictate the accumulation and degradation of

flavoproteins (73,74). These examples indicate that cofactor-free flavoproteins are a suitable target for the protein quality control system, which should be able to select deficient enzymatic forms and send them for degradation if necessary. The results of Saijo and Tanaka (75) agree with this idea. Here, the maturation process of newly synthesized medium-acyl-CoA dehydrogenase (MCAD) was analyzed. It was found that in mitochondria MCAD forms an oligomeric complex with heat shock protein 60 (HSP60). The release of the protein by the chaperone and thus posterior formation of its final tetrameric form is FAD-dependent. This finding provides a relationship between chaperoning function and flavoprotein maturation where FAD is also proposed as a putative folding-promoting agent (76). A recent work that addresses the problem of flavin cofactor delivery to apoproteins agrees with this concept and additionally proposes FAD synthase enzymes (FADS) as a maturation factor that directly interacts with client apoproteins for FAD delivery, probably in coordination with chaperones (77).

How is the selection and triage process of apoproteins efficiently carried out without resulting in the degradation of healthy proteins? Biophysical and structural analyses have shown that secondary and overall tertiary structure of flavin deficient proteins do not significantly differ from fully loaded proteins (78,79). Hence, dealing with cofactor-free flavoenzymes might be considered as a challenge for the proteostasis machinery if no clear determinants are available for the system to discriminate beyond normality. Some exceptions of this include FAD-dependence on complex formation of yeast succinate dehydrogenase (80) and bacterial vanillyl-alcohol oxidase (81). In both cases flavinylation favors the complex assembly process. A riboflavin deficiency in this particular case could be detected by the increase of monomeric forms and thus recognition based on the abnormal concentration of non-oligomerized protein should be operational. However, further analysis of holo- and apoforms of vanillyl-alcohol oxidase enzyme showed that FAD binding has no major repercussions in its monomeric structure (81). Detailed experiments performed on an acyl-CoA dehydrogenase variant showed decreased resistance to urea denaturation, partial loss of packing and tertiary contacts, and higher sensitivity to trypsin proteolysis in the absence of FAD. Although preliminary assays revealed that the apoprotein form still retained its folding capacity and secondary structure, in depth analysis showed that flavinylation might have a defining structural role (82). The effects of flavin cofactors in protein structure are probably very subtle and big conformational changes are not likely to occur. A hint of the mechanism by

which protein quality control could detect flavin-deficient proteins with a high degree of sensitivity is provided by the targeting mechanism of cryptochromes by ubiquitin ligase complex SCF^{FBXL3} (83). The crystal structures of murine CRY2 protein with bound FAD and

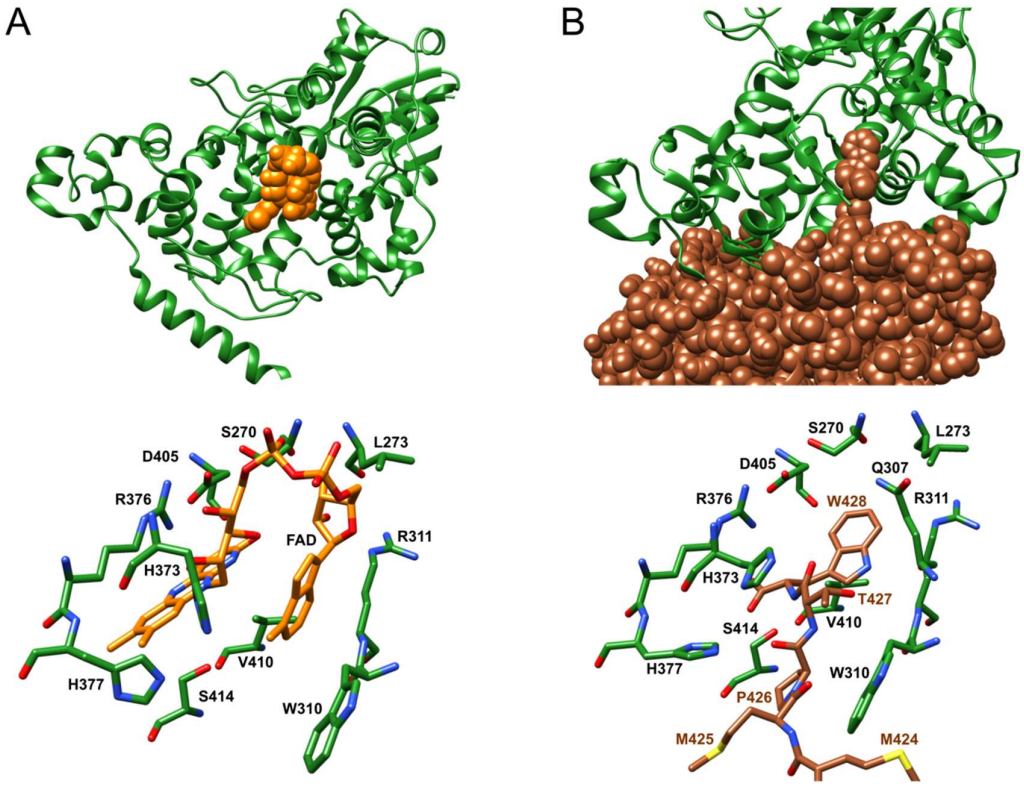

Figure 5. CRY2-FAD vs CRY2-FBXL3 structures(83)**.** (A) CRY2 structure (green) bound to FAD (orange) is shown. FAD-binding site of CRY2 is shown in detail with the residues involved in cofactor binding depicted (bottom). (B) Interaction between CRY2 and FBXL3 (brown spheres) is depicted. In the absence of FAD, the C-terminus of FBXL3 is able to reach the cofactor pocket (FBXL3 domain can be seen as a protuberance that gets inserted into CRY2). In the bottom, atomic details of this region are shown. Interacting amino acids from both CRY2 and FBXL3 are displayed.

in complex with FBXL3 were solved and compared (Figure 5). The dynamics of CRY2 FAD-binding pocket in the absence of the cofactor provides an accessible location for FBXL3 interaction, which inserts the last 5 amino acid of its C-terminal tail into the core of the cofactor-binding site (Figure 5B). Several residues of this terminal region can expand the FAD entrance of CRY2 in the absence of the prosthetic group and establish similar contacts as with the cofactor. In a later study, *in vivo* experiments showed that FAD regulates the levels of CRY1 and CRY2 proteins (84). Despite all the studies that have been mentioned so far, not many investigations have focused on elucidating the relationship between apoproteins and the quality control machinery. The question of how surveillance machinery deals with the

existence of a prominent set of defective enzymes has not been yet addressed in detail. We hypothesized that many flavoproteins can be potentially recognized and degraded by the ubiquitin-proteasome system. We assumed that chaperones as well as E3 ligases should play an important role in the substrate selection process. Biophysical studies suggested that this recognition event might be triggered by small but yet sufficiently evident changes in the structure of apoproteins that are caused by the lack of cofactor in a way that resembles the intramolecular communication process that takes place in allostery (85). These alterations should act as discrimination signals that permit a proper identification of flavin-free proteins without compromising the integrity of cofactor-loaded enzymes. An investigation at molecular level would allow us to test these assumptions and hence understand the basis of the defects associated with riboflavin deficiency by studying flavoproteins in the apostate as well as the role of the proteostasis network in dealing with such defective proteins.

1.6 NQO1 as a model flavoprotein

NAD(P)H:quinone oxidoreductase 1 (NQO1) is a 30 KDa flavoprotein that was first discovered in 1958 in rat liver extracts. The soluble fraction obtained from liver homogenates exhibited a high oxidoreductase activity, which was observed from the reduction measurements of 2,6-dichlorophenolindophenol using NADH or NADPH (86). Unlike other oxidoreductases that catalyze one-electron transfer reactions such as NADPH:cytochrome P450 reductase, NQO1 only catalyzes obligatory two-electron reductions (87). This makes NQO1 a very suitable enzyme for detoxification purposes, especially of quinones, a group of organic compounds that are ubiquitously found in nature. Quinones are usually involved in electron transport processes like cellular respiration and photosynthesis due to their oxidation-reduction properties. However, quinones are also highly reactive oxidants and electrophiles which can be potentially toxic for humans. NQO1 is able to turn quinones into the corresponding hydroquinone or catechol by donating 2 electrons in a single step. This class of reduced compounds are less toxic and can be further metabolized and excreted (88). NQO1 expression is regulated by the NRF2-KEAP1 signaling pathway which controls the response against oxidative stress by upregulating several genes involved in cellular detoxification and drug metabolizing agents (89). Catalytic activity of NQO1 is based on a Ping-Pong mechanism. Here, both the NAD(P)H cofactor and the substrate share the same binding site. Two monomers of NQO1 form an active homodimeric protein which tightly binds two molecules of FAD, each one at the interface between the two monomers, which accepts

electrons from NAD(P)H and donates them to substrates in a sequential manner (90). The FAD moiety lies at the deepest part of NQO1 catalytic pocket while NAD(P)H and substrates bind to the outer or more exposed region (91). NQO1 has also been suggested to protect some proteins against 20S ubiquitin-independent proteasomal degradation. This group includes p53, p73, and c-MYC (92).

Approximately one third of mutations found in single genes results in an increase of the Michaelis-Menten constant (Km), also known as affinity constant of the enzyme towards its cofactor/substrate. For several flavoproteins, a single point mutation leading to an amino acid change has been observed to disrupt the binding of FMN or FAD. The details from seven different enzymes whose cofactor affinity is known to decrease due to one or several single-nucleotide polymorphisms were listed in a work carried out by Ames et al. (93). One of the enzymes in the list is NQO1. The most frequent single-nucleotide polymorphism that has been found in NQO1 coding gene corresponds to a C to T change at the position 609. This nucleotide transition results into the proline 187 replacement by a serine residue, or P187S. The frequency of this mutation highly depends on the ethnic group, and ranges between 4% and 20%, with Asian populations having the highest prevalence (94). Initial genotype-phenotype studies on several mutant NQO1 homozygous cell lines revealed that protein levels of this mutant were almost undetectable and, consequently, its enzymatic activity was reported to be very low (95). Later it was found that this decrease was the result of a rapid degradation both *in vivo* and *in vitro* cellular systems via ubiquitylation and ATP-dependent 26S proteasomal degradation (96). FAD binding experiments showed that mutant NQO1 affinity for the flavin cofactor was much lower than wild-type (97,98). No change in secondary structure has been reported for mutant NQO1. X-ray crystallography experiments did not show any differences between wild-type and mutant proteins, even at the FAD-binding site. On the other side, nuclear magnetic resonance (NMR) analysis suggested that several regions of the enzyme are highly flexible and mobile (97). Different approaches using dynamic light scattering and native PAGE are also in accordance with NMR results (98). The hydrodynamic radius of mutant NQO1 was bigger than wild-type, thus supporting the presence of partially unfolded regions and lack of compactness, which corresponds to a molten globule conformation. The mutant became more sensitive to heat shock, displaying a 7-degree lower melting temperature and higher vulnerability to proteolytic digestion as well, probably as a result of minor changes in folding (98). The presence of FAD *in vitro* was

reported to partially restore the kinetic stability defects of mutant NQO1 (98,99). Nevertheless, addition of both FAD and dicoumarol (a potent inhibitor of NQO1 that

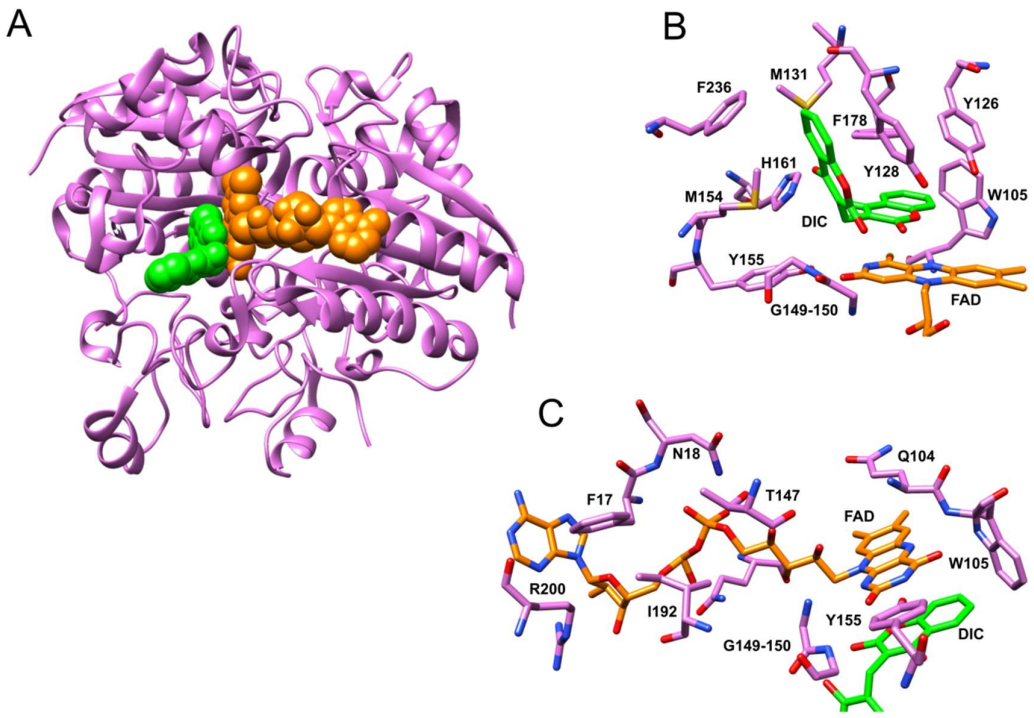

Figure 6. NQO1-FAD-Dicoumarol complex(100)**.** (A) NQO1 dimer (purple) together with FAD (orange) and dicoumarol (green) are depicted. The original NQO1 structure contains a second pair of both cofactor and inhibitor, but those were excluded from this figure. Close-up view of FAD (B) and dicoumarol (C) binding pockets in NQO1 is shown. The main protein residues involved in binding of FAD and dicoumarol are displayed.

competes with NAD(P)H for its binding site) results in some degree of structural correction (99,100). Figure 6 illustrates NQO1 binding to both molecules. In crystallization trials, electron density for the last 50 amino acids of mutant NQO1 were not obtained when cibacron blue (another NQO1 inhibitor targeting NAD(P)H binding pocket) was removed. This tail was rapidly cleaved in proteolysis experiments. For the mutant P187S, interaction between the C-terminus and the core globular domain of the protein is highly disrupted (97). Thus, the addition of both cofactors has a corrective effect on this phenotype, improving thermal denaturation and trypsin sensitivity. Adding FAD alone is not sufficient for restoring wild-type phenotype and only mild effects are observed. E3 ubiquitin ligase C-terminal HSP70-binding protein (CHIP) was found to bind NQO1 directly. This favors its polyubiquitylation and degradation *in vivo*. CHIP binds with high affinity to mutant NQO1, resulting in its rapid degradation (101). The results obtained for this polymorphism prompted researchers to

investigate if wild-type NQO1 was affected in a similar way by the lack of FAD. Wild-type apoNQO1 showed higher charged species as well as a broader distribution of charges compared to the holoprotein in mass spectrometry analysis (the number of charges that proteins can adopt during electrospray ionization is proportional to its surface area) (99). This implies that, in the absence of FAD, wild-type NQO1 contains partially unfolded or extended regions, in a pattern that resembles mutant NQO1. Depletion of FAD rendered wild-type NQO1 very sensitive to trypsin digestion. Proteolysis patterns suggest that C-terminal tail is highly flexible in the absence of cofactor and thus gets cleaved rapidly (102).

1.7 Riboflavin deficiency, proteostasis impairment and disease

Proteostasis relies on a fragile balance between protein folding and misfolding (10). Cells need to ensure that newly synthesized proteins acquire a native and functional conformation by taking care of their complex maturation process. Under normal conditions, cells can accomplish this task. Even under mild stress, like moderate heat shock for instance, cells can still accommodate to the higher load of proteins that require folding assistance. But harsher and prolonged stresses can result in the breakdown of this balance, leading to accumulation of aggregates. The increasing concentration of misfolded and aggregated species, if not cleared out from the system, lead to a toxic gain-of-function and the development of several pathologies (10). It is conceivable that riboflavin deficiency might impose a proteostasis stress on the cell, which suddenly has to deal with an increasing amount of non-functional, non-mature proteins. This situation can become worse if aggregation or abnormal intermolecular binding events occur.

It must be taken into account that the depletion of riboflavin can potentially have additional severe consequences to the cell. The term reactive oxygen species (ROS) refers to a group of highly reactive oxygen-derived molecules that can be produced in cells by means of oxidative metabolism and enzymatic reactions but also by external agents like toxins and radiation. ROS can damage proteins as well as many other cellular structures by oxidation (103). Antioxidant molecules like the glutathione (GSH) tri-peptide efficiently protect cellular structures from ROS by donating electrons to them. As a result, oxidized GSSG dimers form. Repeated cycles of ROS reduction result in the need for GSH regeneration. This regeneration process is usually carried out by glutathione reductase (GR), which utilizes FAD as cofactor to transfer electrons from NADPH back to GSSG (104). Glutathione reductase activity was reduced by 98% in HepG2 cells after 4 days incubation in riboflavin-deficient medium and its

activity became undetectable after 6 days starvation (105). Furthermore, chemical modification of proteins by ROS (especially irreversible carbonylation of some amino acid residues) can lead to misfolding and aggregation (106). Many proteins in the cell follow an ER-dependent secretory pathway. In the ER, an enzyme-based mechanism for thiol oxidation and disulfide bond formation of protein substrates takes place. This protein maturation process is known as oxidative folding and is highly dependent on the presence of FAD since one of the enzymes that participate in the maturation is a flavoprotein (107). Secretion of apolipoprotein B-100 was highly impaired in human liver cells under riboflavin deficiency (108). In this case, nuclear translocation of ATF-6 transcription factor was markedly increased, indicative of a severe ER stress which is known as the unfolded protein response and is triggered when protein folding within the ER is disturbed. The response drives the expression of factors that can buffer exacerbated unfolding and misfolding (109). Thus, riboflavin deficiency could also compromise the antioxidant and ER-oxidative folding capacities of the cell, thus aggravating the damage inflicted on the proteome even further.

1.8 Aim of this work

Except for the exposure of hydrophobic patches, not much is known about the structural elements that allow the proteostasis machinery to recognize defective proteins (36). Under vitamin B2 deficiency many proteins lack the necessary FMN and FAD cofactors to perform their native function. Distinguishing between cofactor-loaded and cofactor-deficient flavoproteins might be a real challenge for the protein quality control in the search for evidence that indicates this deficiency. In this work we wanted to investigate how PQC deals with the flavoproteome upon riboflavin deprivation. Previous studies suggested that the structural integrity of some flavoenzymes as well as their cellular stability and degradation depend on the availability of flavin cofactors (71,82,110). Then, our initial idea was to analyze the mammalian flavoproteome dynamics under riboflavin deficiency by means of mass spectrometry. This would allow us to test on a more global scale whether the PQC is able to engage in the processing and degradation of flavin-free proteins. We hypothesized that protein folding and degradation machineries, i.e. chaperones and E3 ligases, should be involved in this task. Next, we were interested in studying which elements are responsible for the detection of cofactor-deficient flavoproteins and to clarify how PQC distinguishes them from “healthy” cofactor-loaded enzymes. Biophysical and structural data led us to assume that cofactor-free flavoproteins might reveal minor structural changes that function as specific

degradation signals or “dregrons”. The oxidoreductase NQO1 was chosen as a model enzyme in our investigations because of the possibility to compare wild-type and P187S mutant which shows low affinity for FAD. Additionally, mutant NQO1 has been reported to be more visible to the cellular surveillance system, CHIP being one of the key factors and known to couple NQO1 with degradation *in vivo* (101). Biochemical and biophysical data about mutant NQO1 have reported a dynamic behavior of its C-terminal tail, so we set out to test if this recognition event is FAD-dependent and if NQO1 C-terminal tail can function as a degradation signal for CHIP. Because the involvement of HSP70 in the maturation process of NQO1 had been previously reported (111), we wanted to study how cofactor binding influences the interaction of molecular chaperones and NQO1.

Protein conformational changes, even subtle ones, can lead to an increase of aggregation (112). Amyloidogenic and co-aggregation propensity of cofactor-free flavoproteins was a central question of this work. By disrupting the tight balance that controls proteostasis beyond flavoproteome collapse, we hypothesized that cell viability may be at risk. Consequently, the stress caused by vitamin B2 deficiency might favor the appearance of new cellular vulnerability. This work aimed at molecular characterization of this vulnerability, with a goal to manipulate it for therapeutic purposes in the future.

2 MATERIALS AND METHODS

2.1 Materials

2.1.1 Chemicals

Chemical	Company	Catalog number
α-Tocopherol	Sigma-Aldrich	T1539
2-chloroacetamide	Sigma-Aldrich	22790
2-mercaptoethanol	Sigma-Aldrich	M3148
5-Bromo-4-chloro-3-indolyl-β-D-galactopyranoside (X-gal)	Sigma-Aldrich	B9146
8-Anilino-1-naphtalensulfonic acid (ANS)	Sigma-Aldrich	A1028
17-AAG (HSP90 inhibitor)	Enzo Life Sciences	BML-EI308-0001
20S Proteasome	Enzo Life Sciences	BML-PW8720
Acetic acid	Roth	3738.5
Aceton	Roth	9372.1
Acetonitrile (MS grade)	Fisher Scientific	A955-1
Acrylamide/Bisacrylamide (30% ; 37.5 :1)	Roth	3029.1
Agarose	Biozym	840014
Ammoniumperoxodisulfate (APS)	Roth	9592.2
Ampicillin sodium salt	Sigma-Aldrich	A0166
Anti-Flag M2 affinity gel	Sigma-Aldrich	A2220
ATP disodium salt hydrate	Sigma-Aldrich	A26209
Benzonase	Merck	71205-3
Bicine	Sigma-Aldrich	B3876
Bis-Tris	Sigma-Aldrich	14879
Bovine serum albumine (BSA)	Roth	8076.3
Bradford reagent	Sigma-Aldrich	B6916
BrdU (5-Bromo-2'-deoxyuridine)	Merck	19-160
Bromophenol blue	Roth	A512.2
Cycloheximide (CHX)	Sigma-Aldrich	C7698
Citric acid	Fluka	27 490
Coomassie blue G 250	Sigma-Aldrich	9598.2

Chemical	Company	Catalog number
DAPI	Sigma-Aldrich	1246530100
Dicoumarol	Sigma-Aldrich	M1390
Dimethyl sulfoxide (DMSO)	Sigma-Aldrich	D4540
DMF (N,N-dimethylformamide)	Sigma-Aldrich	227056
DMEM (Dulbecco's Modified Eagle Medium)	Sigma-Aldrich	D5671
DNA gel loading dye	New England Biolabs	B7024S
DpnI	New England Biolabs	R0176S
DTT (Dithiothreitol)	Roth	6908.2
EDTA (Ethylendiamintetraacetic acid)	Sigma-Aldrich	E9884
EGTA (Ethylene glycol-bis(2-aminoethylether)-N,N,N',N'-tetraacetic acid)	Roth	3054.3
Ethanol	Sigma-Aldrich	K928.4
Fetal bovine serum (FBS)	Sigma-Aldrich	F0804
Fetal bovine serum (FBS) dialyzed by ultrafiltration	Sigma-Aldrich	F0392
FIN56	Sigma-Aldrich	SML1740
Formaldehyde solution 36.5-38% in water	Sigma-Aldrich	F8775
Formic acid	Fisher chemicals	A117-50
G418 disulfate salt	Sigma-Aldrich	A1720
Glutathione agarose	Jena Bioscience	AC-210-10
Glycerin	Roth	3783.5
Glycin	Roth	3908.3
HEPES (N-2-Hydroxyethyl piperazine-N'-2-ethane sulphonic acid)	Roth	9105.3
Hydrochloric acid 32 %	Roth	P074.1
IGEPAL CA-630	Sigma-Aldrich	56741
Imidazole ($C_3H_4N_2$)	Sigma-Aldrich	56749
Isopropyl alcohol	Sigma-Aldrich	33539
Kanamycin	Sigma-Aldrich	K1377
LB Broth (Lennox)	Roth	X964
LB-agar	Roth	X965
L-Glutamine (Cell culture)	Gibco	25030-024

Chemical	Company	Catalog number
Low fat milk powder	Roth	T145.3
Magnesium acetate tetrahydrate	Roth	0275.1
Magnesium chloride hexahydrate	Roth	A537.4
MEM Non-essential amino acid solution	Gibco	11140-35
Methanol	Roth	CP43.4
Methanol (MS grade)	Fisher Scientific	A456-1
(MTBE) Methyl *tert*-butyl ether	Acros Organics	378720010
MG-132 (Proteasome inhibitor)	Enzo Life Sciences	BML-PI102-0025
NcoI	New England Biolabs	R3193L
NEBbuffer 3.1	New England Biolabs	B7203S
NIAD-4 (2-[[5'(4-hydroxyphenyl)[2,2'-bithiophen]-5-yl]-methylene]-propanedinitrile	Cayman Chemical	18520
Ni-NTA agarose	Jena Bioscience	AC-501-25
NotI-HF	New England Biolabs	R3189L
Opti-MEM	Gibco	31905-062
Paraformaldehyde	Sigma-Aldrich	158127
PBS (Phosphate buffered saline)	Sigma-Aldrich	D6537
Penicillin-Streptomycin	Sigma-Aldrich	P4333
PMSF (Phenylmethylsulfonylfluorid)	Roth	6367.2
Phosphatase inhibitor cocktail 2	Sigma-Aldrich	P5726
Phusion high-fidelity DNA polymerase	New England BioLabs	M0530
Poly-L-Lysine solution	Sigma-Aldrich	P8920
Polyethylenimine, 25 kDa, linear (PEI)	Polysciences Inc.	#23966
Ponceau S	Sigma-Aldrich	B6008
Potassium bromide	Fluka	60093
Potassium hydroxide	Roth	6751.1
Potassium ferricyanide	Sigma-Aldrich	702587
Potassium ferrocyanide	Sigma-Aldrich	P3289
Protein ladder	HighQu	PRL0202
Radicicol	Biozol	R0212
Reprosil-Pur C18 resin	Dr Maisch GmbH	R124.aq
SDS (Sodium dodecyl sulfate)	Roth	CN30.3

Chemical	Company	Catalog number
SigmaFast protease inhibitor tablets	Sigma-Aldrich	S8820
Sodium acetate	Roth	6779.1
Sodium chloride	Roth	3957.2
Sodium hydroxide	Roth	6771.1
Sucrose	Sigma-Aldrich	S0389
SuperSignal west pico PLUS chemiluminescent substrate	Thermo Fisher Scientific	34577
SYBR safe	Thermo Fisher Scientific	S33102
SYPRO orange	Sigma-Aldrich	S5692
Taq DNA polymerase	New England BioLabs	M0273S
TCA (Trichloroacetic acid)	Sigma-Aldrich	T6399
TEMED (Tetramethylethylenediamine)	Roth	2367.3
Tricine	Roth	6977.2
Trifluoroacetic acid	Sigma-Aldrich	299537
Trizma base (2-Amino-2-(hydroxymethyl)-1,3-propanediol)	Sigma-Aldrich	T1503
Triton X-100	Sigma-Aldrich	T8787
Tween 20	Sigma-Aldrich	P1379
Trypan blue solution	Lonza	17-942E
Trypsin-EDTA solution	Sigma-Aldrich	T4049
Trypsin/Lys-C Mix, Mass spec grade	Promega	V5073
Urea (CH_4N_2O)	Roth	2317.4
VER-155008 (HSP70 inhibitor)	Sigma-Aldrich	SML0271
Water (MS grade)	Fisher Scientific	W6-212

2.1.2 Consumables

Consumable	Company	Catalog number
6/12/96-well plates (transparent)	VWR	10062-892/ 10062-894/ 734-2327
10-cm cell culture dishes	VWR	734-2321
96F Nunclon delta black microwell SI	Fisher Scientific	137101
175-cm^2 cell culture flasks	Thermo Fisher Scientific	159920
Cell imaging plate, 24-well	Eppendorf	0030 741005
Cellulose acetate membrane filter	Sartorius Stedim	11107-142

Consumable	Company	Catalog number
Counting chamber	Assistent	40441701
Cuvette (plastic) 1-cm path	VWR	634-0676
Disposable glass pasteur pipettes 230 mm	VWR	612-1702
Eppendorf tubes 1.5 mL	Eppendorf	0030 125.150
Falcon tubes (15 mL/50 ml)	VWR	525-0150/ 525-0156
GenePulser/MicroPulser electroporation cuvettes, 0.4 cm gap	Bio-Rad Laboratories	165-2091
HiLoad 16/600 Superdex 200 pg	GE Healthcare	28989335
HisTrap HP 1 mL	GE Healthcare	17524701
Light-duty tissue wipers	VWR	82003-820
Microcon 30 kDa centrifugal filter (regenerated cellulose)	Merck	MRCF0R030
Microscope cover glass	Paul Marienfeld GmbH	0111520
Microseal 'B' PCR plate sealing film	Bio-Rad Laboratories	MSB1001
Micro slides	Assistent	42406020
Multiplate 96-well PCR plates	Bio-Rad Laboratories	MLL9601
Needle 26G	Braun	465 7683
Nitrile gloves	VWR	112-2373
Nitrocellulose blotting membrane 0.45 µm pore size	GE Healthcare	10600007
PCR tube 0.2 ml	VWR	732-0548
Pipette tips (0.1-20 µL/2-200 µL/100-1000 µL)	VWR	F167012/ F167013/ F167014
Polystyrene round-botton tubes 5 ml (for flow cytometry)	BD Biosciences	352058
Polyvinylfluoride blotting membrane (PVDF) 0.45 µm	GE Healthcare	10600023
ProFlow sort grade 8x sheath fluid (S3 Sorter buffer)	Bio-Rad Laboratories	145-1082
Protein LoBind tubes 1.5 mL	Eppendorf	022431081
Safe-lock tubes 2 ml	Eppendorf	0030 120.094
Serological pipettes (1 ml/5 ml/10 ml)	VWR	612-5504/ 734-1737/ 734-1738
Serological pipettes 25 ml	Corning	4489
Superdex 200 10/300 GL	Sigma-Aldrich	GE17-5175-01

Consumable	Company	Catalog number
Syringe (1 mL)	BD Biosciences	303172
Syringe filters 0.22 µm	Roth	P668.1
Vivaspin 15R 5.000 MWCO HY	Sartorius Stedium	VS15RH12
Wathman cellulose filter paper	GE Healthcare	3030-672

2.1.3 Commercial kits

Kit	Company	Catalog number
Amplex red cholesterol assay kit	Thermo Fisher Scientific	A12216
GeneJET plasmid miniprep kit	Thermo Fisher Scientific	K0503
GenElute HP endotoxin-free plasmid maxiprep kit	Sigma-Aldrich	NA0410-1KT
SuperScript III CellsDirect cDNA synthesis kit	Thermo Fisher Scientific	18080200

2.1.4 Special medium composition

Chemical	Conc. (mg/L)	Company	Catalog number
Inorganic salts			
Calcium chloride dihydrate	264	Carl Roth	T8885.2
Iron(III) nitrate nonahydrate	0.10	Sigma-Aldrich	254223
Potassium chloride	400	Carl Roth	6781.2
Magnesium sulfate heptahydrate	200	Sigma-Aldrich	83266
Sodium chloride	6400	Carl Roth	3967.2
Sodium hydrogen carbonate	3700	PAA Laboratories	PAA G2000.6500
Sodium dihydrogen phosphate	140	Carl Roth	T879.2
D-Glucose hydrate	4900	Carl Roth	6780.1
Amino acids			
L-Alanine	35.6	Sigma-Aldrich	A7627
L-Asparagine	60.0	Sigma-Aldrich	A0884
L-Arginine	84.0	Sigma-Aldrich	A5131
L-Aspartic acid	53.0	Sigma-Aldrich	A9256
L-Cystine	48.0	Sigma-Aldrich	C8755
L-Glutamic acid	59.0	Sigma-Aldrich	G1251

Chemical	Conc. (mg/L)	Company	Catalog number
Amino acids			
L-Glutamine	584.0	Sigma-Aldrich	G3126
L-Glycine	30.0	Sigma-Aldrich	G7126
L-Histidine	42.0	Sigma-Aldrich	H8125
L-Isoleucine	105.0	Sigma-Aldrich	I2752
L-Leucine	105.0	Sigma-Aldrich	L8000
L-Lysine	146.0	Sigma-Aldrich	L5626
L-Methionine	30.0	Sigma-Aldrich	M9625
L-Phenylalanine	66.0	Sigma-Aldrich	P2126
L-Proline	46.0	Sigma-Aldrich	P0380
L-Serine	42.0	Sigma-Aldrich	S4500
L-Threonine	95.0	Sigma-Aldrich	T8625
L-Tryptophane	16.0	Sigma-Aldrich	T0254
L-Tyrosine	72.0	Sigma-Aldrich	T3754
L-Valine	94.0	Sigma-Aldrich	V0500
Vitamins			
Choline chloride	4.0	Sigma-Aldrich	C7017
Folic acid	4.0	Sigma-Aldrich	F8758
Inositol	7.2	Sigma-Aldrich	PHR1351
Niacinamide	4.0	Sigma-Aldrich	PHR1033
Pyridoxal HCl	4.0	Sigma-Aldrich	P9130
Riboflavin	0.4	Sigma-Aldrich	PHR1054
Thiamine	4.0	Sigma-Aldrich	PHR1037

2.1.5 Primary antibodies

Antibody	Company	Catalog number	Dilution
α-synuclein	Santa Cruz Biotechnology	sc-7011-R	1:1000
β-Amyloid, 1-16	BioLegend	80300	1:1000
AKT	Cell Signaling Technology	4691	1:1000
AKT-T308 (phospho)	Cell Signaling Technology	2965	1:1000

Antibody	Company	Catalog number	Dilution
AKT-S473 (phospho)	Cell Signaling Technology	4060	1:1000
AMPK	Cell Signaling Technology	D5A2	1:1000
AMPK-T172 (phospho)	Cell Signaling Technology	40H9	1:1000
BrdU Alexa Fluor 488	Merck	FCMAB101A4	1:200
CDC2	Cell Signaling Technology	E1Z6R	1:1000
CDC2-Y15 (phospho)	Cell Signaling Technology	10A11	1:1000
CHIP	Sigma-Aldrich	C9243	1:1000
CHK1	Cell Signaling Technology	2G1D5	1:1000
CHK1-S345 (phospho)	Cell Signaling Technology	133D3	1:500
FLAG	Sigma-Aldrich	F1804	1:1000
GAPDH	Cell Signaling Technology	14C10	1:1000
GFP	Roche	11814460001	1:1000
HSP70	StressGen	SPA-810	1:1000
NQO1 C-terminal (Goat)	Sigma-Aldrich	N5288	1:1000
NQO1 C-terminal (Rabbit)	Sigma-Aldrich	SAB2500708	1:1000
NQO1 N-terminal	ABGENT	AJ1554a	1:1000
NQO2	Santa Cruz Biotechnology	sc-32942	1:200
p53	Santa Cruz Biotechnology	sc-6243	1:200

2.1.6 Secondary antibodies

Antibody	Company	Catalog number	Dilution
HRP-conjugated anti-Goat IgG	Sigma-Aldrich	A4174	1:5000
HRP-conjugated anti-Mouse IgG	Sigma-Aldrich	A9044	1:5000
HRP-conjugated anti-Rabbit IgG	Cell Signaling Technology	7074	1:5000

2.1.7 Recombinant proteins

Protein	Gene	Uniprot ref. number
Amyloid-beta A4 protein (Aβ)*	APP	P05067
E3 ubiquitin-protein ligase CHIP	STUB1	Q9UNE7
NAD(P)H quinone dehydrogenase 1	NQO1	P15559
Ribosyldihydronicotinamide dehydrogenase 2	NQO2	P16083
Ubiquitin (Bovine)	UBB	P0CG53

Protein	Gene	Uniprot ref. number
Ubiquitin-activating enzyme	UBE1	Q712V1
Ubiquitin-conjugating enzyme E2 D1	UBCH5A***	P51668

*The reference in the table corresponds to the full-length protein. Only a small fragment was used for this work corresponding to a 42 amino acids sequence located C-terminally of the protein (amino acids 671-713).

***Several gene names appear under this reference number in the Uniprot website: UBE2D1, SFT, UBC5A, UBCH5, and UBCH5A.

2.1.8 Chemical compounds used for B16 F0 respirometry assay

Compound	Final concentration	Description
Malate	2 mM	Complex I substrate
Pyruvate	2.5 mM	Complex I substrate
Digitonin*	1.5 µg/mL	Detergent (permeabilizing agent)
ADP	2.5 mM	Substrate for ATP production
Glutamate	10 mM	Complex I substrate
Succinate	10 mM	Complex II substrate
FCCP**	0.5 µM	Uncoupling agent
Rotenone	0.5 µM	Complex I inhibitor
Antimycin A	2.5 µM	Complex III inhibitor

*Digitonin concentration needed for proper permeabilization of B16 F0 cells was empirically determined beforehand. **FCCP was injected in 0.5 µM steps until maximal respiration rate was observed.

2.1.9 Primers

Sequence	Primer (5'→3')
Not1-NQO1-3'	GCGGCCGCTCATTTTCTAGCTTTGATCTGGTTG
Nco1-NQO1-5'	AAACCATGGTCGGCAGAAGAGCACTGATCG
Not1-3'-NQO2	GCGGCCGCTTATTGCCCGAAGTGCCAGTGGGCT
Nco1-5'-NQO2	AAACCATGGCAGGTAAGAAAGTACTCATTG
2xFLAG fw	CATGACGGTGATTATAAAGATCATGACATCGATTACAA GGATGACGACGATAAG
2xFLAG rev	ATAATCACCGTCATGGTCTTTATAGTCCATGGTGGCAA GCTTAAGT
5' NQO1-P187S	GGCTTCCAAGTCTTAGAATCTCAACTGACATAT
3' NQO1-P187S	GCTATATGTCAGTTGAGATTCTAAGACTTGGAA
BRAF-V600E-fw	TTGGTCTAGCTACAGAGAAATCTCGATGGAG
BRAF-V600E-rev	CTCCATCGAGATTTCTCTGTAGCTAGACCAA

Sequence	Primer (5'→3')
1-910 fw	GACCCAAGCTGGCTAGCGCGGCCGCATGAGCAAGGGCGA
1-910 rev	TTGCTCATGCCGGCCGCGGCTAGCCAGCTTGGGTCTCCCTATAGTGAGTCGTATTAATTTCGA
NQO1 Δ50 fw	ACACCACTGTATTTTGCTTGAAGCAGCCTCTTTGACCTA
NQO1 Δ50 rev	TAGGTCAAAGAGGCTGCTTCAAGCAAAATACAGTGGTGT

2.1.10 Plasmids

Plasmid name (number)	Resistance marker	Expression system
pEGFP-F (1-68)	Kanamycin	Mammalian
pUb(h)EΔ (1-383)	Kanamycin	Mammalian
p3XFLAG-CMV-10 (1-483)	Ampicillin	Mammalian
pCHIP (1-813)	Ampicillin	Mammalian
p3F-NQO1 (1-874)	Ampicillin	Mammalian
p3F-NQO2 (1-875)	Ampicillin	Mammalian
pF-NQO1 (1-889)	Ampicillin	Mammalian
pF-NQO2 (1-893)	Ampicillin	Mammalian
pRBS-3xF-BRAF (1-894)	Ampicillin	Mammalian
pRBS-3xF-BRAF-V600E (1-895)	Ampicillin	Mammalian
pVEGF-C-EGFP (1-910)	Ampicillin	Mammalian
p3F-NQO1-Δ50 (1-934)	Ampicillin	Mammalian
p3F-NQO1-P187S-Δ50 (1-935)	Ampicillin	Mammalian
p3F-NQO1-P187S (1-936)	Ampicillin	Mammalian
pcDNA3.1-EGFP (1-949)	Ampicillin	Mammalian
pAβ-EGFP (1-950)	Ampicillin	Mammalian
pSyn (2-75)	Ampicillin	Bacteria
pG-CHIP (2-82)	Ampicillin	Bacteria
pProEX-NQO1 (2-174)	Ampicillin	Bacteria
pProEX-NQO1-P187S (2-175)	Ampicillin	Bacteria
pProEX-NQO2 (2-176)	Ampicillin	Bacteria
pNQO1-Δ50 (2-224)	Ampicillin	Bacteria
pNQO1-P187S-Δ50 (2-225)	Ampicillin	Bacteria

2.1.11 PCR for human NQO1 cDNA amplification

Temperature	Time	Cycle
98ºC	5 min	
98ºC	10 sec	
65ºC	30 sec	25 cycles
72ºC	30 sec	
72ºC	2 min	

2.1.12 PCR for human NQO2 cDNA amplification

Temperature	Time	Cycle
98ºC	5 min	
98ºC	10 sec	
58ºC	30 sec	25 cycles
72ºC	30 sec	
72ºC	2 min	

2.1.13 pFLAG-NQO1 and pFLAG-BRAF PCR amplification with 2xFlag primers

Temperature	Time	Cycle
98ºC	5 min	
98ºC	10 sec	
55ºC	20 sec	25 cycles
72ºC	5 min	
72ºC	10 min	

2.1.14 Site-directed mutagenesis of P187S

Temperature	Time	Cycle
98ºC	5 min	
98ºC	10 sec	
65ºC	30 sec	25 cycles
72ºC	4 min	
72ºC	10 min	

2.1.15 Site-directed mutagenesis of P225 to STOP codon

Temperature	Time	Cycle
98ºC	5 min	
98ºC	10 sec	25 cycles
72ºC	4.5 min	
72ºC	10 min	

2.1.16 Site-directed mutagenesis of V600E

Temperature	Time	Cycle
95ºC	5 min	
95ºC	30 sec	
56ºC	1 min	25 cycles
72ºC	3 min	
72ºC	10 min	

2.1.17 PCR amplification for deletion of mouse VEGF-C 5' IRES region

Temperature	Time	Cycle
98ºC	5 min	
98ºC	30 sec	25 cycles
72ºC	4 min	
72ºC	10 min	

2.2 Methods

2.2.1 Molecular cloning

2.2.1.1 Polymerase chain reaction (PCR)

Polymerase chain reactions were performed using Phusion High-Fidelity DNA Polymerase, except for the site-directed mutagenesis of BRAF V600E, which was performed using Taq DNA Polymerase. PCR reactions were set according to manufacturer's instructions. Shortly, 50 µL PCR reactions were prepared containing 1x Taq or Phusion reaction buffer, 200 µM dNTP, 500 nM of each primer, *ca.* 100 ng DNA template, and 1 Unit of the corresponding polymerase enzyme. PCR were carried out in a PCR thermocycler (Peqlab).

2.2.1.2 Cloning of NQO1 and NQO2 into pPROEX bacterial expression vector

Both N-terminal his-tagged NQO1 and NQO2 human proteins were first cloned into pPROEX HTa plasmid for bacterial expression (Addgene) behind a TRC promoter for high protein expression in fusion with a 6xHis tag. DNA sequences were generated using the primer pair Not1-NQO1-3' and Nco1-NQO-5' for NQO1 and Not1-3'-NQO2 and Nco1-5'-NQO2 for NQO2 (See Materials and Methods 2.1.9). Primer pairs were designed to include a NotI and NcoI restriction sites at 3' and 5' positions, respectively. Single-stranded cDNA library from HeLa cells was used as a template (See Materials and Methods 2.2.1.7 for cDNA library preparation). For the PCR reaction, a total of 2 µL of the cDNA library were used. Both pPROEX HTa plasmid and PCR amplified NQO1/NQO2 products were separately incubated with NotI and NcoI restriction enzymes to create sticky ends. Double Digest Finder online tool from New England BioLabs was used to select the optimal conditions for digestion. 1 µg of DNA was incubated with 1 µL of NcoI and 1µL of NotI enzymes with 1x NEBuffer 3.1 in 50 µL reaction volume. Samples were incubated at 37ºC for 1 h. Reaction mixtures were run in a 1% agarose gel in Tris-Acetate-EDTA (TAE) 1X buffer. A gel fragment containing the amplified product of interest was removed from the agarose gel with a scalpel. GenElute Gel Extraction Kit was used to extract the DNA from the agarose. Using this protocol the extracted DNA is highly pure and in suitable amounts for several downstream applications. In this case, ligation procedure was carried out using T4 DNA Ligase. pPROEX HTa (vector) and NQO1/NQO2 (insert) were added in a 1:3 ratio respectively and pre-incubated for 10 min at room temperature. T4 DNA Ligase was added and samples were incubated at 16ºC overnight. The whole volume of the reaction was transformed into *E.coli* competent cells.

2.2.1.3 Site-directed mutagenesis

Site-directed mutagenesis was used to prepare p3xFLAG-BRAF V600E, p3xFLAG-NQO1 Δ50, p3xFLAG-NQO1 P187S Δ50, pPROEX-NQO1 P187S, pPROEX-NQO1 Δ50, and pPROEX-NQO1 P187S Δ50 expression constructs. For mutagenesis, a pair of complementary primers containing the mutation of interest was designed and used to amplify the protein-coding sequence. The target mutation was introduced within the newly amplified vector through standard PCR reaction. The whole amplified PCR products were treated with 10 Units of DpnI restriction enzyme for 1 h at 37ºC, which differentiates between methylated (bacterial) and non-methylated (PCR) DNA and degrades the first. Samples were then transformed into *E.coli*.

2.2.1.4 Introduction of 2xFLAG sequence into pFLAG-NQO1, pFLAG-NQO2, and pFLAG-BRAF and deletion of VEGF-C sequence from pVEGF-C-EGFP plasmid

2xFLAG tag sequences (DYKDHDGDYKDHDI) were inserted into pFLAG-NQO1 and pFLAG-NQO2 (both from GenScript), as well as into pFLAG-BRAF (Addgene 40775, a gift from Dustin Maly, university of Washington, Seattle) eukaryotic expression vectors by ligation-free cloning. The same protocol was used to obtain pcDNA3.1-EGFP from pVEGF-C-EGFP (ClonTech), a vector containing the murine VEGF-C 5' IRES sequence C-terminally linked to EGFP, in which the former was deleted. Ligation-free cloning was performed as described previously (113). According to this method, inserts were amplified using pairs of primers with 5' overhang sequences (15-18 oligonucleotides in length) that were complementary to the insertion region in the target vector. 10 units of DpnI restriction enzyme were added to the whole PCR reaction product and samples were incubated for 1 h at 37ºC. Samples were then transformed into *E.coli*.

2.2.1.5 Transformation

100 ng of DNA were transform into DH5α *E.coli* cells. DNA was added to 50 µL of bacteria and incubated on ice for 30 min. Heat shock was performed at 42ºC for 30 sec and cells were immediately put back on ice for another 2 min. Sterilized 200 µL LB medium were added and cells were incubated for 1 h at 400 r.p.m at room temperature. A total of 50 µL of bacterial mix were plated on LB-agar 10-cm plates with the corresponding antibiotic (i.e. 100 µg/µL for Ampicillin or 50 µg/µL for Kanamycin). Plates were incubated overnight at 37ºC.

2.2.1.6 Plasmid isolation/purification and DNA concentration determination

For plasmid isolation, either GeneJET Plasmid Miniprep kit or GeneElute HP Plasmid Maxiprep kit were used depending on the amount of DNA needed. A single bacterial colony was picked and growth overnight in 2.5 ml (for Miniprep) or 200 mL (for Maxiprep) LB medium with the corresponding antibiotic. DNA purification from this point was carried out following manufacturer's instructions. DNA concentration was measured at 260 nm using a BioSpectrometer (Eppendorf).

2.2.1.7 Preparation of cDNA library

cDNA library from HeLa cells was prepared using the SuperScript III CellsDirect cDNA Synthesis System. Briefly, a total of 10000 HeLa cells were collected, lysed, and treated with 5 units of DNase I for 10 min at room temperature. 200 units of reverse transcriptase were added and samples were incubated for 50 min at 50ºC to amplify the mRNA from the cell lysates. Reaction was inactivated for 5 min at 85ºC. Samples were stored at -20ºC. The amplified product containing the single-stranded cDNA library was directly used as a template for PCR.

2.2.2 Cell culture, transfection and immunoblotting

B16 F0 cell line (CRL-6322, ATCC) was cultured at 37ºC supplied with 5% CO_2 using freshly prepared DMEM medium supplemented with 10% (v/v) FBS, 2mM L-glutamine, 100 IU/mL penicillin G, 100 µg/mL streptomycin sulfate, and nonessential amino acids. To specifically test the effects of riboflavin deficiency, complete medium lacking riboflavin was prepared. For this purpose, DMEM recipe from Invitrogen (Cat. Num. 10938) was followed. After mixing, pH was adjusted with hydrochloric acid 32% to 7.5. Medium was finally filtered using a 0.22 µm filter and stored in the fridge at 4ºC. Medium was only used within one month after preparation. Before use, 10% (v/v) dialyzed FBS was added as well as 0.4 mg/mL riboflavin supplement for control conditions.

Cells were transfected by means of electroporation at 250 V and 950 µF. For this procedure, $8x10^6$ cells were washed twice in PBS and resuspended in 400 µL intracellular buffer (135 mM KCl, 0.2 mM $CaCl_2$, 2 mM $MgCl_2$, 5 mM EGTA, 10 mM HEPES KOH pH 7.5) freshly supplemented with 25% (v/v) FBS. GenePulser Xcell (Bio-Rad Laboratories) and electroporation cuvettes (0.4 cm gap) were used. Cells were allowed to stay in normal medium for at least 5 to 6 h before riboflavin deprivation. When indicated, cells were transfected using polyethylenimine (PEI). For lipofection, B16 F0 cells were plated on 10 cm dishes and incubated overnight. Next day, cells were transfected with DNA (between 1 and 10 µg) using a DNA:PEI ratio of 1:3 and a 1 mg/ml PEI solution. After 6 h incubation cells were trypsinized and plated again for further treatment.

For immunoblotting, cells were collected by trypsinization and lysed using lysis buffer (20 mM Hepes KOH pH 7.5, 0.5% IGEPAL CA-630, 100 mM KCl, 10 mM $MgCl_2$, and 10% glycerol). The use of different lysis buffers is specified in the corresponding section. Protease inhibitor cocktail was added freshly to the buffer to inhibit the activity of proteases. For

immunoblot experiments of phosphorylated proteins, phosphatase inhibitor cocktail was also additionally added immediately before use. After resuspension in lysis buffer, cells were incubated on ice for 10 min. Either 1 ml syringe with 26 Gauge needle or sonication were used to shear cellular nucleic acids (the method used is indicated in the corresponding sections). Sonication was performed using an MS72 sonotrode for 2 sec at 50% output. Bradford reagent solution was used to determine protein concentration and normalize samples. 5 µL lysate were mixed with 495 µL Bradford reagent and incubated for 5 min at room temperature before measurement. Absorbance values at 595 nm were recorded for each sample. For absolute protein concentration determination, BSA standard curve was prepared. Six different BSA concentrations were used for quantification: 100 µg/mL, 250 µg/mL, 500 µg/mL, 750 µg/mL, 1000 µg/mL, and 1500 µg/mL. After adding reducing SDS sample buffer, normalized probes were heated for 5 min at 95ºC and run using a freshly prepared 10% SDS-PAGE with Mini-PROTEAN Vertical Electrophoresis Cell (Bio-Rad Laboratories). SDS-PAGE gels consisted of a stacking gel (about one fourth of the total gel length) with 4% acrylamide:bisacrylamide on top and 10% resolving gel. Separated samples were transferred onto nitrocellulose membranes using a wet electroblotting system. For western blot, conditions were optimized for each antibody. Either TBS or TBST (with 0.1% Tween20) were used for solution preparation and membrane washing. In general, blocking was performed either with 5% BSA or skim milk solutions. Membranes were incubated with primary antibodies for 24 h to 72 h at 4ºC and washed 3 times 5 min each at room temperature. Membranes were incubated with secondary antibody for 1 h at room temperature. TBST was used to wash membranes afterwards 3 times 5 min each. Pierce ECL Prime Western Blotting Substrate was used for peroxidase reaction. Detection Reagent 1 was mixed with Detection Reagent 2 in a 1:1 ratio. The solution was incubated at room temperature for 5 min and carefully spread throughout the membrane. Images were acquired using ChemiDoc MP imaging system (Bio-Rad Laboratories) with the “band resolution” function activated. Images were analyzed using Image Lab 5.0 software, and the “High saturated pixels” function was used to ensure the linearity of protein signal bands. For coomassie staining, gels were completely soaked in coomassie staining solution (40% methanol, 10% acetic acid, and 1 mg/mL coomassie blue G-250 in water) overnight gently shaking. Gel was then incubated in destaining solution (staining solution without coomassie dye).

Buffer	Reagent
4% SDS-PAGE stacking buffer	4% Acrylamide/Bis-acrylamide (from 30% solution) 125 mM Tris HCl pH 6.8 0.1% SDS 0.1% APS 0.1% TEMED
10% SDS-PAGE resolving buffer	10% Acrylamide/Bis-acrylamide 375 mM Tris HCl pH 8.8 0.1% SDS 0.1% APS 0.1% TEMED
Reducing SDS sample buffer	62.5 mM Tris HCl pH 6.8 2% SDS 10% Glycerol 5% 2-Mercaptoethanol 0.002% Bromophenol blue
Running buffer	25 mM Tris HCl 190mM Glycine 0.1% SDS
Transfer buffer	25 mM Tris HCl 190mM Glycine 20% Methanol
TBS/TBST* (Tris-Borate solution)	50 mM Tris HCl pH 7.6 100 mM NaCl/Tween 20 0.1%*

Table 1. Recipes for immunoblotting buffers

2.2.3 Recombinant protein purification

The protocol described in this section only refers to the first part of recombinant protein purification protocol and it was used for all purifications carried out during this work. The specific details for each individual protein are described in the sections below. Differences in the methodology from this section will be indicated. Purifications were performed at 4ºC unless otherwise indicated. Recombinant proteins were purified from *Escherichia coli* One Shot BL21 (DE3) cells (Thermo Fisher Scientific). A single colony of transformed bacteria growing on LB agar plates was picked, inoculated into 100 mL LB media containing the corresponding antibiotics and cultured O/N at 37ºC at 180 rpm. Next morning 100 mL of bacterial culture were inoculated into 6 L LB (with antibiotic) and incubated at 37ºC at 180 rpm. 0.5 mM IPTG was added for protein expression induction when culture reached 0.4-0.6 absorbance units at 600 nm. Bacterial culture was incubated O/N at 18ºC shaking at the same speed. Overnight grown bacteria were pelleted using 1 L buckets at 7000 g for 10 min in an Avanti J-26 XP centrifuge with a JLA-8.1000 rotor (both from Beckman Coulter). Bacterial pellets were resuspended in the appropriate buffer for next steps.

ProtParam tool (EXPASY) was used to determine molar extinction coefficient of purified proteins based on primary amino acid sequences. Extinction coefficient and 280 nm absorbance value of the final solution were both used to calculate protein concentration using a BioSpectrometer. Protein samples were aliquoted, frozen in liquid nitrogen and stored at -80ºC up to several months.

2.2.3.1 His-NQO1 WT, his-NQO1 P187S, his-NQO1 Δ50 WT, his-NQO1 Δ50 P187S, and his-NQO2 purification

Pelleted bacteria were resuspended in lysis buffer (PBS, 20 mM Imidazole, 1 mM DTT, 1 tablet per 100 mL buffer of protease inhibitor cocktail and 1 mM PMSF protease inhibitor). Cells were lysed using French Press. Lysates were sonicated with a MS72 sonotrode at 90% output for 10 min on ice (90 sec cycles with 60 sec on and 30 sec off). Lysate was centrifuged with Avanti J-26 XP centrifuge and JA25.50 rotor (both from Beckman Coulter) at 45000 g for 30 min. In the meantime HisTrap 1 mL affinity chromatography column (GE Healthcare) was equilibrated with 10 mL washing buffer (lysis buffer without protease inhibitors). Supernatant from lysate was collected and injected into HisTrap 1 mL column at 1 mL/min rate. After injection, column was washed for 10 min. Recombinant protein was eluted by applying a gradient flow from 0 to 100% of elution buffer (PBS, 500 mM Imidazole, and 1 mM DTT) mixed with washing buffer over 20 min at 1 mL/min while 2 mL fractions were collected. Positive fractions were pooled according to 280 nm absorbance trace and concentrated using Vivaspin 15R 5000 MWCO down to 1 mL volume. Concentrated sample was injected into HiLoad Superdex 200 pg size exclusion chromatography column and run at 1 mL/min flow rate. 4 mL fractions were collected and run in 10% SDS-PAGE to assess their purity. Highly pure fractions were pooled and concentrated.

2.2.3.2 His-NQO1 WT APO and his-NQO1 Δ50 WT APO

For apoprotein preparation, a slight modification of the purification protocol described above (section 2.2.3.1) was introduced, according to previous publications (97,114). After injection of supernatant into HisTrap 1 mL affinity chromatography column, 10 mL of denaturation buffer were injected (PBS, 20 mM Imidazole, 2 M Urea, and 2 M KBr) at 1 mL/min rate. Column was equilibrated with 20 mL washing buffer for protein refolding. Elution and further purification were carried out as before.

2.2.3.3 GST-CHIP

Pelleted bacteria were resuspended in lysis buffer (25 mM HEPES KOH pH 7.5, 150 mM KCl, 5 mM $MgCl_2$, 10% Glycerol, 1 mM DTT, and 1 tablet per 100 mL buffer of protease inhibitors cocktail). Cells were lysed using French Press. Lysates were sonicated with a MS72 sonotrode at 90% output for 10 min on ice (90 sec cycles with 60 sec on and 30 sec off). Lysate was centrifuged with Avanti J-26 XP centrifuge and JA25.50 rotor at 45000 g for 30 min. Supernatant was incubated with pre-equilibrated 5 mL 100% Glutathione Sepharose for 2 h at 4ºC. For this equilibration, 10 mL 50% Glutathione Sepharose were previously washed with 40 mL water, centrifuged at 2000 g for 10 min, washed with 30 mL washing buffer (lysis buffer without protease inhibitors cocktail) and centrifuged again. Afterwards, sepharose was separated from the lysate by decantation, washed with 25 mL washing buffer, and drained again using the same method. 4 mL of washing buffer were added to the sepharose together with 500 Units of PreScission Protease for GST-tag removal and incubated O/N at 4ºC while rotating. Supernatant (ca. 5 mL) was collected and Sepharose was additionally washed two times with 5 mL wash buffer each. 15 mL elution were obtained and concentrated using Vivaspin 15 5000 MWCO down to 1 mL volume. This sample was injected into HiLoad Superdex 200 pg size exclusion chromatography column using wash buffer at 1 mL/min flow rate. 4 mL fractions were collected and run in 10% SDS-PAGE to assess their purity. Highly pure fractions were pooled and concentrated.

2.2.3.4 α-Synuclein

Synuclein purification protocol was carried out following a published protocol (115). In this case, only 2 L bacteria culture were used for purification. 0.1 mM IPTG was used for protein induction, which was carried out for 4 h at 37ºC. Pelleted bacteria were resuspended in 200 mL of osmotic shock buffer (30 mM Tris HCl pH 7.2, 2 mM EDTA, and 40% Sucrose) and incubated for 10 min at room temperature. From here, all the steps were done at 4ºC. Bacteria were centrifuged at 9000 g for 20 min, resuspended as fast as possible in 520 mL of ice-cold water with 2 mM $MgCl_2$, incubated for 3 min, and finally centrifuged again as before. The supernatant containing α-synuclein was collected and injected into HiPrep Q Fast Flow anion exchange column previously washed with 20 mL running buffer (20 mM Tris HCl pH 8.0) at 2 mL/min rate. Column was extensively washed with 200 mL running buffer and protein was eluted by applying a gradient flow from 0 to 100% of elution buffer (20 mM Tris HCl pH 8.0, and 500 mM NaCl mixed with washing buffer) over 100 min at 1 mL/min. 10 mL fractions

were collected. Positive fractions were centrifuged with Vivaspin 15R 2000 MWCO down to 1 mL. Sample was injected into HiLoad Superdex 200 pg size exclusion chromatography column at 0.5 mL/min rate in water. α-synuclein containing fractions were pooled, concentrated, heated at 95ºC for 30 min, and centrifuged at 20000 g for 30 min. Supernatant was again injected into the size exclusion chromatography column and run under the same conditions to improve sample purity. Fractions were collected and run in 10% SDS-PAGE. Highly pure fractions were pooled and concentrated.

2.2.4 *In vitro* pull-down assay of NQO1 and NQO2

NQO1 and NQO2 *in vitro* pull-down assays in the presence of synuclein were performed using Ni-NTA agarose. Reaction mixtures containing 50 µM of alpha-synuclein and 20 µM NQO1/NQO2 and were prepared and incubated for 10 min at 37ºC. 0.025% glutaraldehyde was used as a crosslinking agent. Ni-NTA agarose was washed twice with PBS and 10 µL were added to the samples when indicated. 10 µL of agarose were used. Probes were then incubated with the agarose for 1 h at 4ºC. Tubes were gently tapped every 5-10 min for adequate mixing. Micro Bio-Spin Size Exclusion Columns (30 µm pore size) were used for quick removal of unbound proteins. Samples were loaded onto the columns and centrifuged for 1 min at 1000 x g. Columns were then washed two times with PBS. Proteins were eluted after adding 20 µL hot sample buffer and centrifuging for 1 min at 1000 x g. Samples were run in 10% SDS-PAGE and protein bands were revealed by coomassie staining procedure.

2.2.5 Respirometry assay

High resolution respirometry was used to measure *in vivo* mitochondrial respiration rates of B16 F0 cells under normal and riboflavin-deficient conditions using an Oxygraph-2k (Oroboros Instruments). DatLab software 7.1.0.21 (Oroboros Instruments) was used to acquire and analyze respirometry data. B16 F0 cells were plated on 15-cm cell culture dishes and incubated for 3 days under riboflavin-deficient conditions. Cells were harvested by trypsinization and immediately resuspended in MiR05-respiration medium (110 mM Sucrose, 60 mM Potassium lactobionate, 0.5 mM EGTA, 3 mM $MgCl_2$, 20 mM taurine, 10 mM KH_2PO_4, 20 mM Hepes KOH, 2 mg/mL bovine serum albumin, pH 7.1) at a concentration of $0.25x10^6$ cells/mL and $0.5x10^6$ cells/mL for control and starved conditions, respectively. Mitochondrial oxygen consumption was measured in MiR05 buffer simultaneously for both conditions in different chambers. Flux rate was stabilized for ca. 15 min to analyze basal

respiration, followed by the addition of digitonin (for cell permeabilization), substrates, and inhibitors as specified in section 2.1.8. The order of injection corresponds with the list order from top to bottom. Absolute respiration rates were corrected for ROX and normalized to the total number of cells per chamber.

2.2.6 Blue-native gel electrophoresis

To establish Blue-Native Gel Electrophoresis, several published protocols were taken into account (116–120). $8x10^6$ B16 F0 cells were transfected with 15 µg of 3FLAG-NQO1 mammalian expression construct by means of electroporation and plated in 10-cm dishes. After 6 h incubation in DMEM medium, cells were washed twice with PBS, and special medium was added to continue incubation for 24 h under normal or riboflavin-free conditions. During this period, cells were treated with 10 µM MG132 O/N. Next day cells were harvested by trypsinization, resuspended in native lysis buffer (50 mM Bis-Tris HCl pH 7.2, 5 mM NaCl, 10% glycerol, 2 mM $MgCl_2$, 0.1% Triton X-100, and fresh protease cocktail inhibitor), and incubated on ice for 15 min. Lysates were incubated with 100 units of benzonase for 30 min at room temperature and centrifuged for 20 min at 17000 g. Supernatant was collected after centrifugation and protein concentration was normalized to 1.5 µg protein per µL of total solution. 5% coomassie blue G-250 in water was added to each sample to a final concentration of 0.025%. XCell SureLock Mini-Cell electrophoresis System (Thermo Fisher Scientific) and NativePAGE 4-16% Bis-Tris Protein precast gels were used to separate samples. Running buffer (50 mM Bis-Tris HCl pH 6.8, and 50 mM Tricine) with 0.02% coomassie blue G-250 was used during the first running phase (half of the gel) at 150 V. Then, running buffer was exchanged to contain 0.002% coomassie blue G-250. From here samples were run at 250 V until blue dye reached the end of the gel. Before transfer, gel was soaked in 2x Transfer buffer (50 mM Bis-Tris HCl pH 7.2, 50 mM Bicine, and 2 mM EDTA) for 10 min at room temperature. Transfer was done onto PVDF membrane (previously soaked in 100% methanol for 30 sec) for 70 min at 180 V. Both running and transfer were performed at 4ºC. Excess of the stain bound to the membrane was removed incubating in 100% methanol for 3 min while shaking. Membrane was washed with water and finally incubated with 8% acetic acid in water for 15 min at room temperature. Immunoblotting was carried out as described in section 2.2.2. For NQO1 aggregates rescue experiment with FAD/Riboflavin, an additional step was introduced during lysate preparation. After centrifugation, 10 µM FAD/Riboflavin solutions (both prepared in water) were added to the respective supernatant

samples. These probes were incubated for 5 min at room temperature. From here, the rest of the protocol was followed as described above.

2.2.7 Fluorescence-based melting assay

Recombinant proteins at a concentration of 10 µM were mixed with SYPRO Orange dye. Final dye dilution was 1:5000. Fluorescence change was recorded while increasing the temperature from 20ºC to 80ºC in 0.5ºC/15 sec steps using a CFX96 Real-Time PCR cycler (Bio-Rad Laboratories) (excitation at 450-490 nm, emission at 515-530 nm). Sample fluorescence values were subtracted from the background and first derivative of the fluorescence signal with respect to the temperature was calculated. The peak in the derivative versus temperature plot was taken as the apparent melting temperature of the corresponding protein.

2.2.8 CD spectroscopy

J-810 spectropolarimeter (Jasco) was used to record far-UV spectra of recombinant proteins at 37ºC in PBS. 10 µM samples were used and three different repeat scans were obtained for each protein. Absorbance values were subtracted from buffer baseline. Data were collected in a 1 mm path cell from 250 nm to 200 nm in 0.5 nm steps at 50 nm/min.

2.2.9 ANS binding assay

20 µM ANS (8-Anilinonaphtalene-1-Sulfonate) and 10 µM recombinant protein were mixed and incubated for 10 min at room temperature. ANS fluorescence was measured using Infinite M200 Pro Microplate reader (Bio-Rad Laboratories) with excitation at 350 nm and emission scan recorded between 400 nm and 600 nm. The background fluorescence of the buffer was subtracted.

2.2.10 Analytical size exclusion chromatography

100 µg (ca. 30 µM) of purified recombinant protein were injected into a Superdex 200 10/300 GL chromatography column previously equilibrated with PBS for a total of 2 column volumes at 0.5 mL/min and 4ºC. Absorbance at 280 nm were recorded and normalized to the highest value, which was set as 100.

2.2.11 FAD release measurement

Flavin content of purified recombinant proteins was measured *in vitro* by spectrophotometry. 100 µL of 5 µM protein solution was prepared in PBS. SDS was added to the samples to a

final concentration of 0.2% and incubated for 5 min at room temperature. Samples were diluted 10-fold in PBS and fluorescence was measured with M200 Pro Microplate reader (Bio-Rad Laboratories) with excitation at 450 nm and emission scan from 480 nm to 600 nm.

2.2.12 BrdU proliferation assay.

All solutions used in this protocol were prepared in PBS w/o Ca^{2+}/Mg^{2+} unless otherwise indicated. Glass microscope coverslips were first coated with Poly-L-Lysine solution diluted 1:10 in distilled water and incubated 1 h at room temperature while shaking. Cells were plated on 12-well plates (with one Poly-L-Lysine coated glass slide per well) and cultured for 3 days in riboflavin-free medium. On the third day, BrdU pulse was carried out by adding 10 µM BrdU prepared in DMSO and further incubating cells for 5 h. After pulse was finished, media was removed, cells were washed twice with PBS, fixed in 4% paraformaldehyde solution for 45 min at room temperature, washed three times with PBS, and incubated with 0.1% Triton X-100 solution for 20 min at room temperature. 1.5 M hydrochloric acid was used after permeabilization step to denature DNA. Excess of acid was removed by washing cells three times with PBS before blocking in 3% BSA solution for 30 min at room temperature. Cells were incubated with AlexaFluor 488-conjugated anti-BrdU Antibody (1:200 dilution in PBS with 3% BSA) O/N at 4ºC. DAPI solution (1:5000 dilution in PBS) was used to stain cellular DNA for 3 min at room temperature. Cells were washed with PBS three times to wash away unbound DAPI. 5 µL of PBS was pipetted onto a microscope glass slide and coverslips were placed upside down with the cells on the glass slide surface (in contact with the PBS drop). Excess of buffer was removed and coverslips were sealed with nail polish. All samples were analyzed within one week from preparation. Zeiss LSM 780 confocal microscope was used to obtain fluorescent images. Images were analyzed using ImageJ software.

2.2.13 Cell cycle analysis

Cells were plated on 10-cm dishes and incubated under riboflavin starvation conditions for 3 days. Cells were then harvested by trypsinization, washed twice with ice-cold PBS, and fixed using 100% ethanol (from -20ºC). Fixation was carried out adding ethanol drop-wise while softly stirring cell suspension. Fixed cells were incubated for 6 h at 4ºC, washed twice with PBS and resuspended in staining solution (50 µg/mL propidium iodide, and 100 µg/mL RNAse A in PBS) for 30 min at room temperature. Gentle vortexing was carried out every 5 min to avoid sedimentation of cells. Propidium iodide stock solution was prepared in water at

1 mg/mL and stored at 4ºC. S3 flow cytometer (Bio-Rad Laboratories) was used to analyze samples. For each sample approximately 20000 cells were analyzed. The Multi-Cycle DNA tool from FCS Express 5 software (DeNovo) was used for quantification of cell cycle profiles.

2.2.14 MMS/Mitomycin C toxicity assay

Toxicity assay was carried out using either methyl methanesulfonate (MMS) or Mitomycin C. MMS stock was purchased as 99% solution, (i.e. 11.8 M). Due to the high toxicity of this reagent, a 100 mM MMS solution was prepared in water according to (121), and stored at -20ºC for a few weeks. 0.5 mg/mL Mitomycin C stock solution was prepared in water from 2 mg vials. This solution was kept at 4ºC and used within two weeks. Cells were plated in 6-well plates and incubated for 3 days in riboflavin-deficient medium. Both MMS and Mitomycin C treatments were applied separately and cells were incubated for another 24 h. Cells were harvested by trysinization together with media to collect floating cells as well, resuspended in staining buffer solution (complete DMEM media with 30 nM SYTOX Green Dead Cell Stain), and incubated in the dark for 15 min at room temperature. Probes were analyzed by flow cytometry.

2.2.15 Protease sensitivity assay

30 µM purified recombinant protein were incubated with trypsin at 37ºC in PBS to assess the sensitivity of these proteins to limited proteolysis. For this assay, 2 ng/µL of sequencing-grade trypsin (Promega) were used. Reactions were incubated for 10, 20, and 40 min and reactions were stopped by the addition of reducing SDS sample buffer followed by boiling at 95ºC for 5 min.

2.2.16 *In vitro* co-aggregation of NQO1 and Aβ$_{1-42}$ peptide

For co-aggregation assay, NQO1 protein variants and human amyloid β-peptide (Aβ$_{1-42}$) were used. Small aliquots of Aβ$_{1-42}$ at 10 mM were prepared by dissolving peptide powder in DMSO. Sonication was applied for 10 min in a water bath at room temperature to facilitate solubilization. Only when the peptide was properly solubilized, 2 µL aliquots were prepared and frozen at -80ºC for single use. For each assay, 5 µM recombinant protein and 10 µM Aβ$_{1-42}$ were incubated in 100 µL PBS for 1 h at 37ºC at 300 rpm. Wild-type NQO1 was supplemented with 100 µM of FAD to keep the enzyme cofactor-bound during the incubation. 100 µL of 100 mM DTT with 0.1% SDS were added to the samples and incubated for 5 min at room temperature. 50 µL of each solution were applied to a cellulose acetate filter (0.2 µm

pore size; pre-soaked in 0.1% SDS in PBS) placed on top of a Whatman filter paper pre-soaked in water. A 96-well Dot Blot Hybridization Manifold device (Sci-Plas) was used in order to catch the aggregates on the membrane. Bound aggregates were washed five times with 50 µL 0.1% SDS solution in PBS. From here on, membrane blocking and protein detection using corresponding antibodies was done according to section 2.2.2.

2.2.17 Sedimentation assay

B16 F0 cells were transfected with 30 µg Aβ-EGFP expression plasmid by means of electroporation. Cells were cultured in normal medium overnight and medium was exchanged next morning after washing cells extensively with PBS to induce riboflavin deficiency. 5 µM MG132 treatment was also applied at this point. After 24 h, MG132 was washed out and vitamin deficiency treatment was continued for another 2 days, i.e. total starvation was carried out for 3 days in total. Cells were harvested by trypsinization, washed twice with ice-cold PBS, and resuspended in 300 µL lysis buffer (50 mM Tris HCl pH 7.0, 150 mM NaCl, 2.5 mM $MgCl_2$, and 0.5% Triton X-100). Cell lysis was carried out using a 1 mL syringe with a 26 gauge needle attached applying ten up-and-down strokes. Lysates were pre-cleared at 21380 x g for 5 min at 4ºC. Supernatant was taken and fractionated into soluble and pellet fractions by a second-round centrifugation at 53227 x g for 30 min at 4ºC. Supernatant was discarded and pellet was resuspended in 40 µL lysis buffer. SDS reducing sample buffer was added to the samples. The samples were boiled for 5 min at 95ºC.

2.2.18 Microscopy of cellular aggregates

$1.5x10^6$ B16 F0 cells were plated on a 10-cm dish. On the next day, polyethylenimine (PEI) was used to transfect cells with 15 µg of Aβ-EGFP expression vector using a DNA:PEI ratio of 1:3 (PEI stock solution was 1 mg/mL). After 6 h, cells were trypsinized and $1.5x10^5$ cells were re-plated on 12-well plates. Each well contained one poly-L-lysine pre-coated cover glass, which was previously prepared. After 4 h, cells were washed extensively with PBS and medium was changed for riboflavin starvation. 5 µM MG132 were also added to inhibit proteasome degradation. 20 h later, MG132 was washed out and medium was exchanged to continue starvation for extra 2 days. Cells were then fixed at room temperature with 4% paraformaldehyde solution in PBS, treated with 1 µg/mL DAPI for 3 min, and washed three times with PBS. The microscopy cover glasses were mounted as described in section 2.2.12, and fluorescent images were acquired with a Zeiss 780 confocal microscope. At least a total

of 130 EGFP positive cells were counted for every condition. From these pictures, the fraction of cells with aggregates was calculated. The images were analyzed using ImageJ software.

2.2.19 *In vitro* ubiquitylation assay

In vitro ubiquitylation assay was carried out using ubiquitylation buffer (50 mM Tris HCl pH 7.5, 50 mM NaCl, 10 mM $MgCl_2$, 2 mM DTT, and 2 mM ATP). The buffer contained 2.5 µM substrate, i.e. NQO1 or NQO2 enzymes, 100 nM UBE1 (E1 enzyme; Boston Biochem), 2 µM Ubc5 (E2 enzyme), 5 µM CHIP (E3 ligase), and 100 mM Ubiquitin from bovine erythrocytes (Sigma-Aldrich). Reactions were mixed at room temperature and incubated at 37ºC for 1 h. Reducing SDS sample buffer was added to the reactions which were then boiled at 95ºC for 5 min.

2.2.20 Amyloid detection *in vivo*

NIAD-4 was used to assess the presence of amyloids in B16 F0 cells under riboflavin starvation. All solutions of this assay were prepared in PBS. Cells were plated on 10-cm dishes and incubated for 3 days in riboflavin-free medium. Cells were collected by trypsinization, washed with PBS twice and fixed using a 4% formaldehyde solution for 30 min at room temperature. After two additional washes, cells were permeabilized with 0.5% Triton X-100, and 3 mM EDTA pH 8.0 at 4ºC for 30 min and then incubated in the presence of 10 µM NIAD-4 for 30 min at room temperature. Fluorescence intensity of the dye was measured using flow cytometry and data were further analyzed with FCS Express 5 Flow software.

2.2.21 β-galactosidase assay

B16 F0 cells were plated in 6-well plates and incubated for 3 days in riboflavin-deficient medium. Cells were washed twice with PBS and fixed with freshly prepared 3.7% formaldehyde in PBS for 5 min at room temperature. After two more washings, 2 mL/well X-galactosidase staining solution (40 mM citric acid/sodium phosphate pH 4.0, 1 mg/mL Xgal in DMF, 5 mM potassium ferricyanide, 5 mM potassium ferrocyanide, 150 mM NaCl, and 2 mM $MgCl_2$, prepared in water) were added. X-galactosidase staining buffer was prepared fresh before use. Fixed cells were incubated overnight at 37ºC in an incubator with normal concentration of CO_2. Next day, staining solution was removed and replace with water. Images were taken immediately using a Leica MC170 HD camera (Leica Microsystems) attached to an inverted light microscope.

2.2.22 HSP70 inducibility assay

B16 F0 cells were plated in 10-cm dishes and incubated for 2 days in riboflavin-free medium. Dishes were placed at 45ºC for 1 h to induce heat stress. Afterwards, cells were incubated at 37ºC for 5 h, and harvested by trypsinization. Cells were washed twice in PBS and resuspended in 200 µL lysis buffer. Samples were sonicated and normalized to the protein concentration. SDS sample buffer was added and samples were incubated for 5 min at 95ºC.

2.2.23 Translation rate analysis using ubiquitin-EGFP plasmid

B16 F0 cells were transfected with 30 µg of Ubiquitin-EGFP expression plasmid by means of electroporation and plated on 10-cm dishes. After 6 h, riboflavin-deficient medium was added and cells were incubated for 2 days. On the second day, cells were treated with 50 µM MG132 for 5 h. Cells were harvested, washed twice with PBS, and lysed in lysis buffer. After normalization, SDS sample buffer was added to samples which were then incubated for 5 min at 95ºC.

2.2.24 Computational analysis of NQO1 interactome

The Compute pI/MW tool from the ExPASy Web site (https://web.expasy.org/compute_pi/) was used to compute the theoretical pI (isoelectric point) as well as the MW (molecular weight) of the NQO1 interactors found under control and riboflavin-deficient conditions. Boxplotter tool from cleverSuite website (122) was used to analyze individual physicochemical features of the two sets of proteins. Aggregation propensity, disorder propensity, and hydrophobicity were analyzed using the Zyggregator algorithm (123), TOP-IDB (124), and Eisenberg scale (125), respectively. In all cases *M.musculus* Uniprot AC annotation was used as control group. Mann-Whitney test was carried out to analyze the statistical significance of differences between groups.

2.2.25 Cholesterol measurement

B16 F0 cells were cultured for 3 days under riboflavin-deficient conditions. After harvesting, a total of $1.5x10^6$ cells were counted, washed twice with PBS and re-suspended in 50 µL distilled water. Lipid extraction protocol described by Eggers et al. (126) was followed in order to extract cellular lipid fraction. All the steps were performed at room temperature. 270 µL methanol with 3% acetic acid was added to the cell suspension, followed by the addition of 1 ml MTBE (methyl-*tert*-butyl ether). Samples were incubated for 1 h while rotating and phase-separation was then induced by adding 250 µL distilled water. After further incubation

for 5 min, samples were centrifuged for 10 min at 15000g. Approximately 800 µL of the upper organic phase were collected using a glass Pasteur pipette and transferred to another tube. 400 µL re-extraction solution (200 µL MTBE, 6 ml methanol solution with 3% acetic acid, and 5 ml water) were added to the remaining polar fractions to induce a second round of separation. Samples were incubated for 20 min under vigorous shaking (1300 rpm) and centrifuged again for 10 min at 15000 g. The upper phase (ca. 450 µL) was collected and pooled with the fraction from the first extraction. Solvent was completely evaporated under vacuum. The obtained pellet was re-suspended in 60 µL methanol and directly used for cholesterol measurement using the Amplex Red Cholesterol kit. All reactions were carried out in reaction buffer (100 mM KH_2PO_4 pH 7.4, 50 mM NaCl, 5 mM cholic acid, and 0.1% Triton X-100) in a total volume of 100 µL in 96-well black plates. Cholesterol standard curve was prepared with concentrations (ng/mL): 0, 50, 100, 200, 400, and 800. Every reaction contained 150 µM Amplex Red, 1 unit/mL horseradish peroxidase, 1 unit/mL cholesterol oxidase, and 0.1 unit/mL cholesterol esterase. Reactions were incubated for 30 min at 37ºC and fluorescence signal was measured using 560 nm excitation and 590 nm emission. Blank signal from reaction buffer with no cholesterol was subtracted. Fluorescence measurements from three different sample dilutions were obtained for each experiment. Corrected values from three independent starvation experiments were averaged and normalized to values from normal conditions.

2.2.26 Cycloheximide chase

HEK293 cells were transfected with 30 µg NQO1, NQO1 Δ50, or NQO2 expression vectors by means of electroporation. Afterwards, cells were washed extensively with PBS and plated in 6-well plates under riboflavin-starvation conditions. After 4 h incubation, one set of transfected cells were harvested, washed twice in ice-cold PBS, and lysed directly in SDS reducing sample buffer by boiling the mix at 95ºC for 5 min. The other set of cells were treated with 1 mM cycloheximide (CHX) for 4 h in order to stop protein translation. Cells were then collected and lysed in the same conditions as for the previous set. As a control, cells transfected with wild-type NQO1 were left without CHX treatment to observe the increase in protein expression in the absence of any treatment.

2.2.27 *In vitro* 20S proteasome degradation assay

Increasing concentrations of either NQO1 or NQO2 (20, 40, and 80 μM) were mixed with 10 μM α-synuclein together with 50 ng of 20S proteasome in reaction buffer containing 10 mM Tris HCl pH 8.0. Samples were incubated for 1 h at 37ºC and degradation reaction was stopped by adding SDS reducing sample buffer followed by boiling at 95ºC for 5 min. 14% SDS-PAGE was used to separate samples. After separation, polyacrylamide gel was stained using coomassie blue staining protocol.

2.2.28 Preparation of pEGFP-F stable B16 F0 cells

Expression construct with EGFP-F fusion protein (EGFP fused to the C-terminal farnesylation signal of RAS) (127) was used to prepare the modified B16 F0 cell line. Cells were transfected with 30 μg plasmid by means of electroporation. $2x10^6$ cells were plated in a 10-cm dish, and complete DMEM medium was exchanged after 6 h. G418 stock solution was prepared by dissolving G418 into complete DMEM medium without serum and antibiotics at a concentration of 10 mg/mL. Medium pH was adjusted to 7.5 with NaOH, and the stock solution was filtered using a 0.22 μm filter. After 2 days, 1.5 mg/mL G418 was added to transfected cells. Medium was exchanged every 3 days. After 2 weeks, growing cells were trypsinized, washed twice with PBS and sorted using flow cytometry. To select EGFP-positive cells, green fluorescence intensity between 10 and 100-times over negative control values was used as a criterion for selection to improve the purity of the green population. A second round of flow cytometry sorting was carried out after cells grew for another week.

2.2.29 Localization of farnesylated EGFP

Localization of EGFP-F was monitored in the B16 F0 stable cell line. Cells were plated in 24-well black plates with clear film bottom and cultured for 3 days without riboflavin. Living cells were imaged using a Zeiss LSM 780 confocal microscope to track green fluorescence. 63x magnification with immersion oil was used. Images were analyzed using ImageJ.

2.2.30 Mass spectrometry

2.2.30.1 Proteome analysis of B16 F0 cells

2.2.30.1.1 Sample preparation

B16 F0 cells were incubated for 3 days in riboflavin-free medium and lysed in 200 μL lysis buffer (10% SDS, 150 mM NaCl, 100 mM HEPES pH 7.6). Samples were sonicated to shear

the DNA using an MS72 sonotrode at 50% output for 5 sec each sample. Lysates were centrifuged at 16000 g for 3 min and supernatant was collected. Protein concentration was measured and 100 µg of total protein were diluted in buffer containing 4% (w/v) SDS, 100 mM Hepes (pH 7.6), 150 mM NaCl, and 0.1 M DTT and then heated for 5 min at 95ºC. 200 µL buffer (8 M Urea and 50 mM Tris HCl pH 8.5) were added to the lysates and loaded onto spin filters with a 30 kDa cut-off membrane. This step was followed by the filter-aided sample preparation protocol (FASP) described previously (128). Digestion of proteins was carried out overnight using sequencing-grade trypsin. Peptides were acidified (0.1% trifluoroacetic acid final concentration) and desalted using C18 StageTips. Strong cation exchange (SCX) StageTips was used to fractionate the samples. Six fractions were obtained in total and the C18 transelution fraction was mixed with the first of the six SCX fractions. Peptides were dried using a Speec Vaccum and resolved in 1% acetonitrile and 0.1% formic acid.

2.2.30.1.2 LC-MS/MS

LC-MS/MS was carried out using an ultra-high performance liquid chromatography unit (Thermo Scientific Dionex Ultimate 3000) controlled by Chromeleon Express software and a Nanospray Flex Ion Source attached to a Q Exactive Plus mass spectrometer (Thermo Scientific). Peptides were loaded on a C18 reversed-phase precolumn and separated on an in-house packed column (100 µm i.d., 30 cm length, 2.4 µm ReproSil C18 resin) using a gradient with mobile phase A (4% acetonitrile, 0.1% formic acid) to 30% mobile phase B (80% acetonitrile, 0.1% formic acid) for 60 min followed by a second step to 60% B for 30 min, all with a flow rate of 300 nL/min. Data-dependent acquisition mode was used to acquire mass spectrometry data. The 10 most abundant ions were selected (precursor ions) and fragmented using HCD fragmentation. The full mass spectrometry scan range was set to 300-2000 *m/z* with a resolution of 70000. Only ions with a charge ≥2 were selected for tandem MS scan with a resolution of 17500. An isolation window of 2 *m/z* was used and dynamic exclusion of the selected ions was set at 30 s. Data were acquired using the Xcalibur software (Thermo Scientific). The LC unit was controlled by Chromeleon Xpress software.

2.2.30.1.3 Data analysis

Mass spectrometry raw files were analyzed using MaxQuant (version 1.5.2.8) (129). The spectra were compared to UniProtKB mouse FASTA database (downloaded in June 2015;

76086 entries) for protein identification. A false-discovery rate of 1% was used. Unidentified features were matched between runs in a time window of 2 min. Three different categories, i.e. false-positives, identified only by site, and known contaminant hits were excluded from further analysis. For label-free quantification, the minimum ratio count was set to 1. Bioinformatic data analysis was done using Perseus 1.5.2.6. (coxdocs.org/doku.php?id=perseus:start). Label-free quantification (LFQ) intensity ratios between control and riboflavin starvation conditions alone and in combination with MG132 treatment were calculated to quantify changes in protein levels. These ratios were log_2-transformed, and the mean values of at least three valid ratios per group were calculated. In order to analyze the significance of the difference between the medians of the flavoproteome and the rest of the proteome a Mann-Whitney test was performed.

2.2.30.2 Analysis of NQO1 interactors obtained from pull-down experiments

2.2.30.2.1 NQO1 pull-down

B16 F0 cells ($2x10^6$) were plated in the evening on 10-cm dishes. Next morning, cells were transfected with 10 µg of 3xFLAG-NQO1 eukaryotic expression vector using polyethylenimine (PEI) (the ratio of DNA:PEI used was 1:3 using a 1 mg/mL PEI solution). Transfection by lipofection was carried out during 6 h and cells were then trypsinized and plated on 175 cm^2 flasks (one flask per dish) either in normal or riboflavin-deficient conditions. After 24 h 5 µM MG132 treatment was applied and starvation was continued overnight. Cells were collected by trypsinization, washed twice with PBS, and resuspended in ice-cold lysis buffer (50 mM Tris HCl pH 7.4, 150 mM $CaCl_2$, 1 mM EDTA pH 8.0, and 0.1% IGEPAL). Cell suspension was kept on ice for 15 min and sonicated for 3 sec for lysis. Lysates were pre-cleared by centrifugation at 17000 x g for 15 min at 4ºC. In the meantime, ANTI-FLAG M2 affinity gel for pull-down was prepared. In total 5 µL of pure resin were used for each sample. For equilibration procedure, 10 µL original resin (supplied as a 50% suspension in 50% glycerol) were washed twice with PBS and once with lysis buffer. Beads were collected after washing steps by centrifugation at 6000 x g for 30 sec. Absolute protein sample concentration was measured spectrophotometrically by using BSA standard curve as a reference. Samples were then normalized to 2 µg/µL. 250 µL of the normalized lysate (i.e. 500 µg of protein) were mixed with the already pre-washed ANTI-FLAG affinity resin and incubated for 3 h at 4ºC while rotating. After incubation, beads were washed five times with

TBS and then transferred to protein low binding tubes for a final wash with mass spectrometry buffer (20 mM Tric HCl pH 7.4, and 150 mM NaCl).

2.2.30.2.2 Sample preparation

Associated proteins were processed on-beads for LC-MS/MS analysis as follows. Beads were re-suspended in 50 µL of 8 M urea with 50 mM Tris HCl pH 8.5, reduced with 10 mM DTT for 30 min and alkylated with 40 mM chloroacetamide for 20 min at 22ºC. Urea was diluted to a final concentration of 2 M with 25 mM Tris HCl pH 8.5, 10% acetonitrile and proteins were digested using trypsin/lysC mix (mass spec grade, Promega) overnight at 24ºC. Acidified peptides with 0.1% trifluoroacetic acid were desalted and fractionated on combined C18/SCX stage tips into 3 fractions. Peptides were dried and dissolved in 1% acetonitrile and 0.1% formic acid.

2.2.30.2.3 LC-MS/MS

LC-MS/MS was performed on a Q Exactive Plus equipped with an ultra-high pressure liquid chromatography unit (Easy-nLC1000) and a Nanospray Flex Ion-Source (all three from Fisher Scientific). Peptides were separated on an in-house packed column (75 µm inner diameter, 2.4 µm Reprosil-Pur C18 resin using a gradient from mobile phase (4% acetonitrile, 0.1% formic acid) to 30% mobile phase B (80% acetonitrile, 0.1% formic acid) for 60 min followed by a second step to 60% B for 30 min, with a flow rate of 300 nL/min. MS data were recorded in data-dependent mode selecting the 10 most abundant precursor ions for HCD with a normalized collision energy of 27. The full MS scan range was set from 350 to 2000 m/z with a resolution of 70000. Ions with a charge ≥2 were selected for MS/MS scan with resolution of 17500 and an isolation window of 1.6 m/z. The maximum ion injection time for the survey scan and the MS/MS scans was 80 ms, and the ion target values were set to $3x10^6$ and 10^5, respectively. Dynamic exclusion of selected ions was set to 60 sec. Data were acquired using Xcalibur software (Thermo Fisher Scientific).

2.2.30.2.4 Data analysis with MaxQuant

MS raw files from 4 biological replicates were analyzed with MaxQuant (version 1.5.3.30) using default parameters. Enzyme specificity was set to trypsin and lysC, and a maximum of 2 missed cleavages were allowed. A minimal peptide length of 7 amino acids was required. Carbamidomethylcysteine was set as a fixed modification, while N-terminal acetylation and methionine oxidation were set as variable modifications. The spectra were searched against

the UniProtKB mouse FASTA database (downloaded in January 2016, 50189 entries) for protein identification with a false discovery rate of 1%. In the case of identified peptides that were shared between two or more proteins, these were combined and reported in a protein group. Hits in three categories (false positives, only identified by site, and known contaminants) were excluded from further analysis. For label-free quantification, the minimum ratio count was set to 1.

2.2.30.2.5 Data analysis with Perseus

Bioinformatic data analysis was performed using Perseus (version 1.5.2.6). Proteins identified in the pull-down were included in the analysis if they were quantified in all biological replicates in at least one experimental condition. Missing LFQ values were imputed on the basis of normal distribution with a width of 0.3 and a downshift of 1.8. Proteins enriched in the pull-down over background binding for each condition were identified by two-sample t-test at a p-value cut-off of 0.05.

2.2.31 Gene ontology enrichment analysis

GO enrichment analysis was performed using the Gene Ontology (GO) Term Finder (130). Gene Ontology Term Finder was used to analyze the data from both B16 F0 proteomics study and wild-type NQO1 pull-down assay. Either “Function” or “Process” were selected as sorting category and MGI – *M. Musculus* as annotation for the analyses, which were performed using a p-value threshold of 0.01 with Bonferroni correction. B16 F0 proteomics study was also analyzed once using “component” with the same settings.

2.2.32 Statistical analysis

All figures shown in this work were obtained from three biologically independent experiments if not specified differently. Results were visualized and plotted using OriginPro software (version 2018). Data is shown as mean ± SD. T-test was used to evaluate differences in the means between two different groups. To assess the differences for a single variable among more than two groups ANOVA one-factor test was used. Only when alternative hypothesis of ANOVA test was accepted, Tukey’s Post Hoc test was performed to identify specific differences between pairs of means. Statistical differences were considered significant when p-value < 0.05 (* = $p < 0.05$; ** = $p < 0.01$; *** = $p < 0.001$).

In order to analyze changes of proteome upon riboflavin starvation for 3 days in B16 F0 cells, analysis of B16 F0 proteome was performed by filtering those proteins that were quantified in

at least 3 out of 4 biological replicates per group (normal versus starved). Missing LFQ values were imputed on the basis of normal distribution with default parameters. In order to analyze protein changes between conditions, two-sample t-test analysis of at least three average ratios was performed using a false-discovery-rate (FDR) cut-off of 0.001 (0.1%) and s0 = 0.1.

In pull-down experiments, LFQ intensity ratios of identified proteins (3xFLAG-NQO1 over background) were calculated. The log_2-transformed means from at least three different experiments were used to analyze statistical differences using two-sample t-test with a p-value cut-off of 0.05.

3 RESULTS

3.1 Riboflavin deficiency leads to flavoproteome degradation

In order to understand how the protein quality control deals with flavin-deficient apoproteins, we initially decided to perform a mass spectrometry analysis of riboflavin-starved cells to evaluate the changes of flavoproteome levels. The studies performed up to date, especially those that investigate the etiology of multiple acyl-CoA dehydrogenase deficiencies, suggested that flavoprotein stability depends on the cofactor availability. With MS-based quantitative proteomics analysis our purpose was to provide a general view of the cellular flavoproteome. Given that commercial media contains riboflavin, we decided to manually prepare riboflavin-deficient high-glucose DMEM. The list of all components used is provided in section 2.1.4. In normal conditions, 0.4 mg/L riboflavin was added to the medium while it was omitted to induce vitamin deficiency. Murine melanoma B16 F0 cells were incubated for 24 h in riboflavin-free medium and proteomics analysis was performed by means of liquid chromatography followed by tandem mass spectrometry (LC-MS/MS). 6578 proteins together with 68 flavoproteins were identified and quantified. In order to analyze the data, label-free quantification (LFQ) intensity ratios between starved vs control conditions were calculated, $\log_2$ transformed, and plotted (Figure 7A, left). Interestingly, the median abundance of flavoproteins significantly decreased by ca. 13% after 1 day of vitamin starvation compared to normal conditions. The same experiment was performed in the presence of MG132, a strong inhibitor of proteasome activity (131). The results obtained in this experiment revealed that 26S proteasome could be responsible for the selective degradation, since the inhibition rescued 8 out of 10 of the most reduced flavoproteins (Figure 7B, left). To see if the degradation could be stronger, we repeated the proteomics analysis of B16 F0 cells after 3 days starvation. This time, the median abundance of the flavoproteome decreased by ca. 25% in comparison with cells incubated in riboflavin-sufficient medium (Figure 7A, right). NQO1 was identified after 1 and 3 days starvation as one of the 10 most affected flavoproteins (Figure 7B). While NQO1 levels were reduced by ca. 43% after 1 day starvation, only 20% of the protein remained after 3 days. As a control, changes in the levels of enzymes that functionally require vitamins B1 (thiamine), B3 (nicotinamide), or B6 (pyridoxal) were also

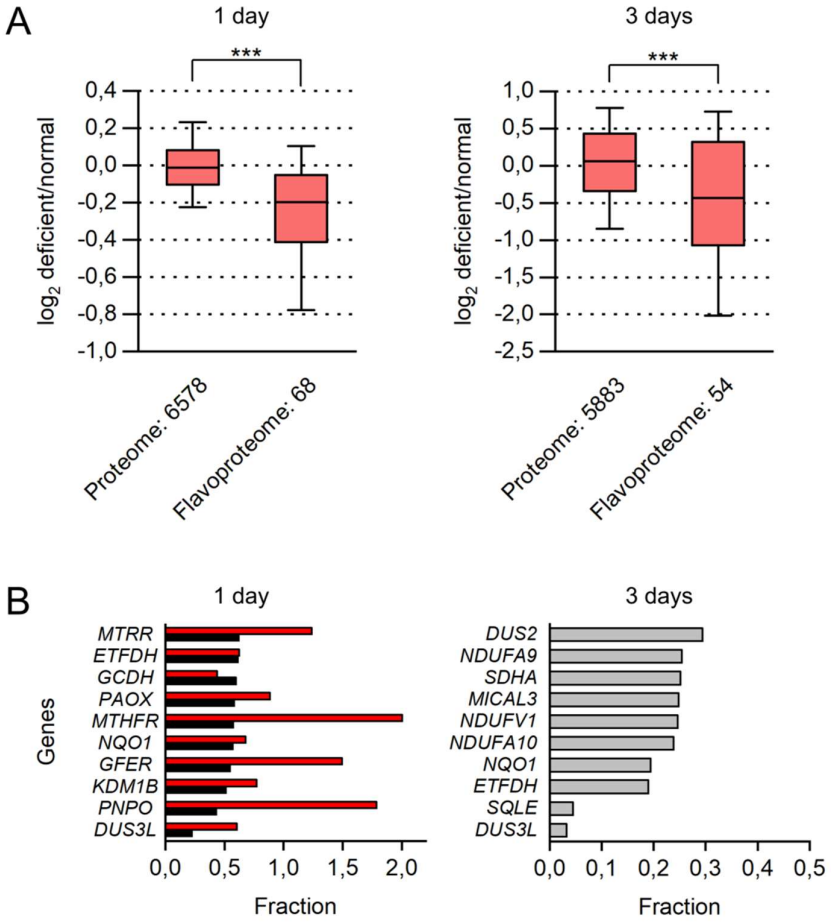

Figure 7. Riboflavin starvation leads to degradation of the flavoproteome. (A) B16 F0 cells were incubated for 1 day (left) or 3 days (right) in riboflavin-deficient conditions and proteome was analyzed by mass spectrometry (n = 4). Intensity ratios between deficient over control conditions were calculated for the quantified proteins. The ratios are shown in boxplots for both experiments. The box corresponds to the 25% and 75% quantiles, and the median line is shown. Whiskers correspond to the 5% and 95% quantiles. Mann-Whitney test was used to compare the medians of the two groups. (B) The lists of the 10 most reduced flavoproteins after 1 day (left) or 3 days (right) of riboflavin starvation are shown. Values obtained under proteasome inhibition treatment for 1 day are plotted (red bars) compared to untreated cells (black bars).

analyzed. However, no changes were observed after 1 day starvation in any of those groups (Figure 8, left). The abundance of proteins relying on thiamine or pyridoxal for their function increased after 3 days starvation (Figure 8, right).

As mentioned above, there are several reasons that make NQO1 a suitable model to test our hypotheses. It belongs to a group of flavoenzymes harboring mutations that negatively affect binding of flavin cofactor (93). A single nucleotide polymorphism was identified for NQO1 (C609T) that translates the proline 187 into a serine residue. This form has been extensively studied and binding affinity (K_d) for cofactor FAD was found to be reduced more than 6-fold

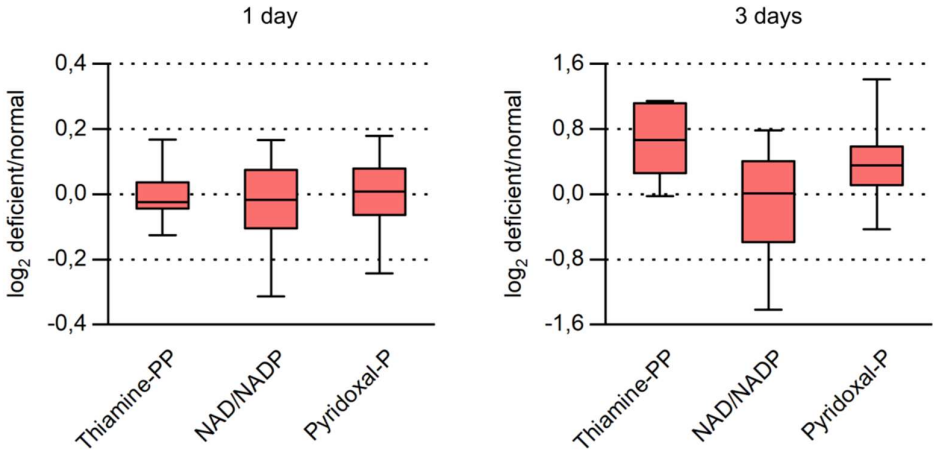

Figure 8. Other groups of proteins are not degraded under riboflavin deprivation. Mass spectrometry analysis of B16 F0 cells was performed after 1 day (left) or 3 days (right) incubation in riboflavin-free medium (n = 4). The ratios between deficient and normal conditions were calculated for proteins belonging to the groups containing the specified cofactors. The box corresponds to the 25% and 75% quantiles, and the median line is shown. Whiskers correspond to the 5% and 95% quantiles.

compared to the wild-type (97). Studies in cellular systems also reported that this mutation leads to an increased destabilization of the enzyme, which is poly-ubiquitylated and degraded by the proteasome (96). We verified the loss of mutant NQO1 stability biochemically. Transient transfection of wild-type and mutant NQO1 proteins was performed in B16 F0 cells

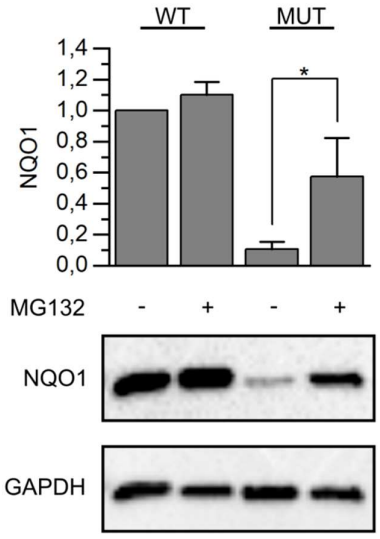

Figure 9. Mutant NQO1 is strongly degraded *in vivo*. Wild-type and mutant NQO1 were transfected separately in B16 F0 cells and protein expression was analyzed after 24 h incubation in normal medium. 5 µM MG132 treatment was applied overnight to inhibit protein degradation. Transfected wild-type NQO1 without MG132 was set as 1. Protein values were normalized to GAPDH (n = 3, mean ± SD). T-test was used to analyze the differences between means.

and protein levels were analyzed by immunoblotting after 24 h. In this experiment, cells were cultured in normal conditions. Compared to the wild-type NQO1, only 10% of mutant protein was remaining (Figure 9). The use of MG132 rescued the protein from degradation, but only partially. Incomplete inhibition of proteasome could explain that degradation was still occurring to some extent.

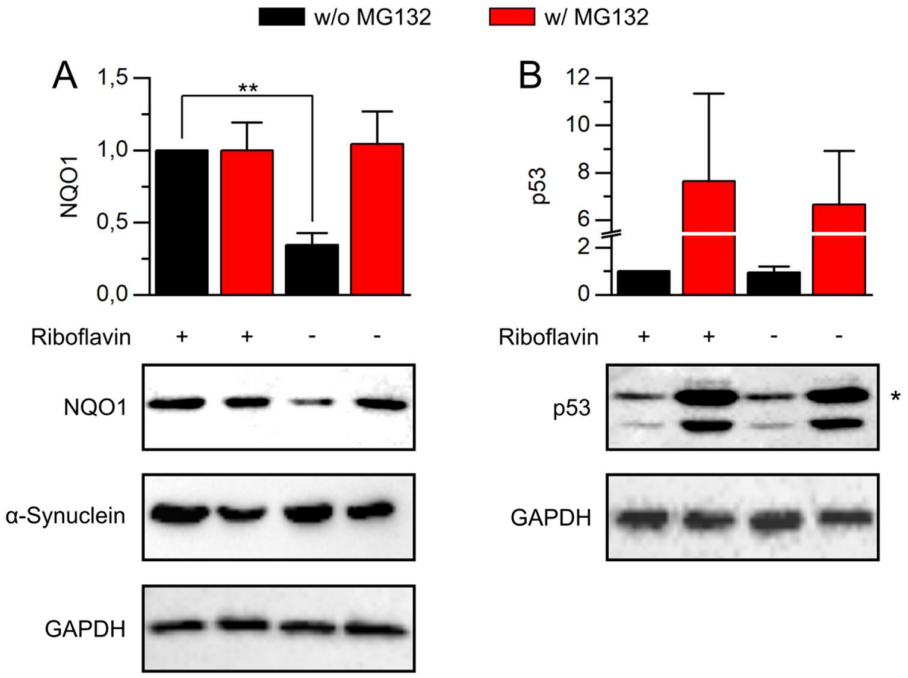

Figure 10. Endogenous wild-type NQO1 is degraded *in vivo* under riboflavin deprivation. (A) B16 F0 cells were incubated for 24 h without riboflavin and wild-type NQO1 protein levels were analyzed by immunoblotting. 5 μM MG132 treatment was applied overnight. NQO1 under normal conditions was set as 1. The values were normalized to GAPDH and plotted (n = 3, mean ± SD. (B). The accumulation of transfected wild-type p53 in B16 F0 was analyzed under the same conditions. The amount of p53 in control sample was set as 1. p53 upper band (*) was used for quantification. The values were normalized to GAPDH and plotted (n = 3, mean ± SD). Significance of the differences between means was assessed by t-test comparing control versus starving conditions.

Next, we analyzed the steady-state levels of endogenous wild-type NQO1 in cells incubated in riboflavin-free medium. We found that the enzyme levels were significantly reduced in B16 F0 cells after 24 h starvation (Figure 10A). MG132 treatment fully rescued NQO1 wild-type from degradation, in contrast to the partial rescue of mutant NQO1 (Figure 9). This result indicates that flavoproteins can be recognized and sent for degradation via the 26S proteasome. Some studies claim that 20S proteasome alone can also degrade proteins without the classical covalent ubiquitin labeling (132). In this case, proteins with some structural disorder like α-synuclein (133) or p53 (134) could directly enter into the catalytic cavity of

the proteasome. NQO1 has been proposed to protect some of these substrates from degradation by direct binding to the proteasome or to the corresponding substrate (99,135,136). We checked the levels of both, endogenous α-synuclein and transiently transfected p53, using the same conditions as in previous experiments. None of the proteins were found to be dependent on the vitamin availability, while NQO1 levels did change (Figure 10).

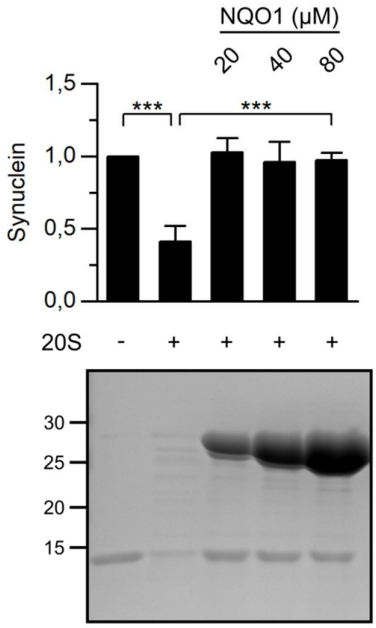

Figure 11. NQO1 protects α-synuclein from 20S proteasome degradation *in vitro*. Alpha-synuclein (10 μM) was incubated with 20S proteasome (50 nM) together with increasing concentrations of NQO1 (20, 40, and 80 μM) for 1 h at 37ºC. After incubation, samples were analyzed in 14% SDS-PAGE. Gel was stained with coomassie blue G-250 to visualize proteins. For quantification, the relative intensity of control sample with α-synuclein alone (lane 1) was set as 1 (n = 3, mean ± SD). ANOVA one-way test was used to analyze the significance of the differences between means.

We also tested in an *in vitro* reconstituted system whether NQO1 has a protective role towards α-synuclein degradation, as previous reports had suggested. Purified α-synuclein and NQO1 were used together with commercial 20S proteasome. Incubation of both proteins with 20S proteasome showed that α-synuclein becomes protected from degradation in the presence of NQO1 (Figure 11). Double molar concentration of NQO1 (20 μM) completely abolished degradation of α-synuclein. Contrary to the results obtained *in vitro*, this effect did not take place in our *in vivo* setting since the partial elimination of NQO1 had no visible consequences for α-synuclein or p53. This could imply that the amount of 20S proteasome in our cellular

system is very low and thus degradation in the absence of NQO1 is negligible or that other factors apart from NQO1 protect both proteins from ubiquitin-independent degradation.

3.2 C-terminal HSP70-interacting protein (CHIP) ubiquitylates cofactor-free NQO1

Next we asked whether the recognition of the mutant and the FAD-free wild-type proteins by the cellular protein quality control system might be taking place in a similar way. Lack of flavin cofactor might represent a defectiveness signal to enhance recognition events. Tsvetkov et al. (101) reported the interaction between mutant NQO1 and C-terminal HSP70 interacting protein (CHIP). They claimed that this binding mediates ubiquitylation and degradation of the enzyme. We hypothesized that CHIP could recognize wild-type NQO1 depending on its cofactor-binding state. To test this hypothesis, we prepared CHIP knockout cell lines by means of CRISPR/Cas9 genome editing (137). *In vivo* degradation of transiently transfected NQO1 was followed under normal and starvation conditions in the presence or absence of

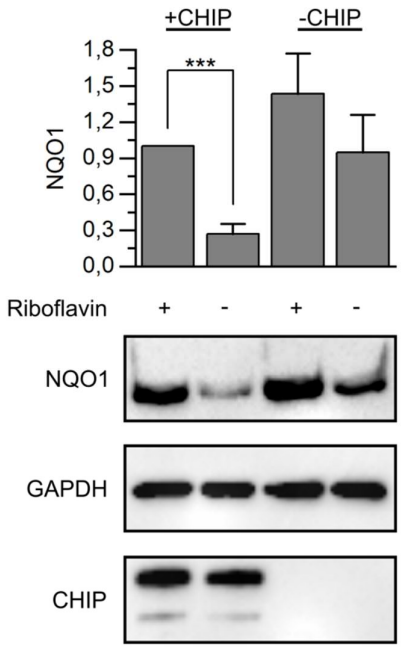

Figure 12. CHIP recognizes and ubiquitylates wild-type apoNQO1 *in vivo*. CHIP was transiently re-introduced by electroporation into CHIP-deficient B16 F0 cells together with wild-type NQO1. Cells were incubated either in normal or riboflavin-deficient medium for 24 h and NQO1 accumulation was analyzed by immunoblotting. The amount of NQO1 in CHIP-transfected cells under normal conditions was set as 1 and values were normalized to GAPDH and plotted (n = 3, mean ± SD). T-test was used to analyze the significance of the differences between means.

CHIP. Wild-type NQO1 was not significantly degraded in the absence of riboflavin in CHIP KO B16 F0 cells. However, reintroduction of the E3 ligase by transient transfection indeed

turned NQO1 much more sensitive to the levels of the vitamin (Figure 12, lanes 1 and 2). Accumulation of NQO1 was slightly more pronounced in the CHIP-free system, in agreement with another publication (101). Riboflavin deficiency still rendered apoNQO1 susceptible for degradation even in CHIP-deficient cells. This observation can be explained by the presence

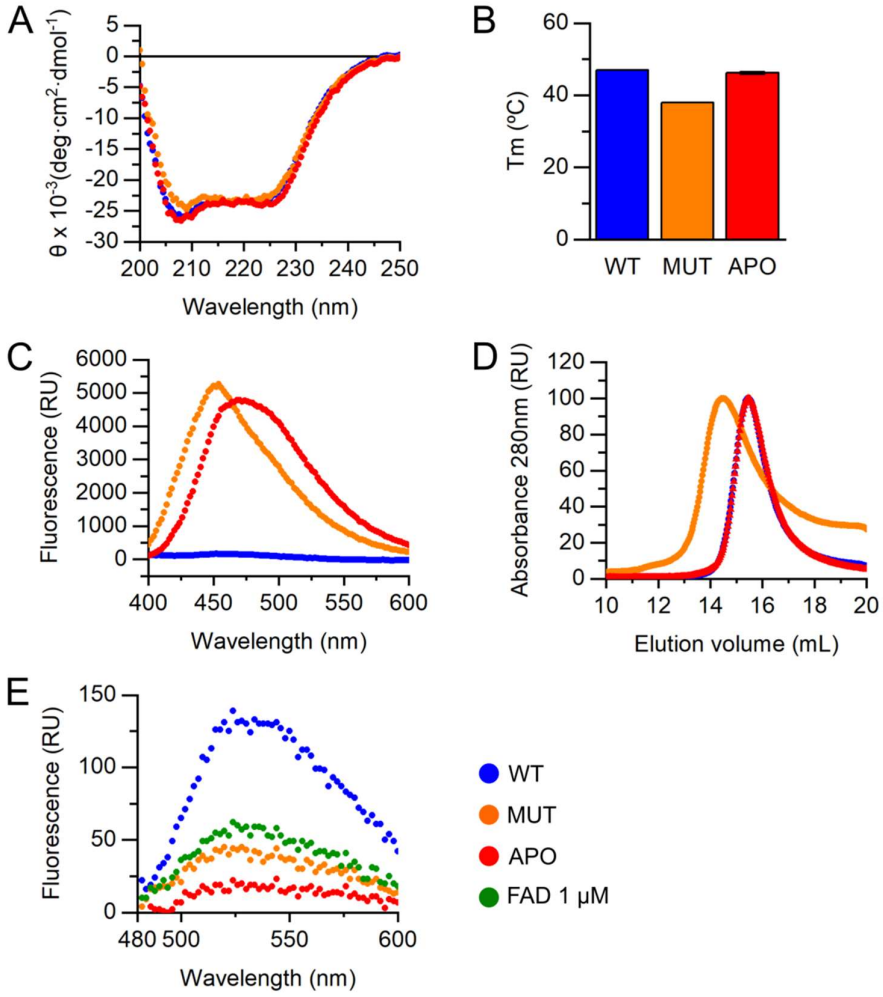

Figure 13. Recombinant mutant NQO1 and wild-type apoNQO1 show no structural changes compared to the wild-type holoprotein. Biophysical characterization of wild-type NQO1 (WT), mutant NQO1 (MUT), and wild-type apoNQO1 (APO) is shown. (A) CD spectroscopy was carried out using 10 µM of proteins. Average values from three independent experiments are plotted. (B) Melting temperature analysis was performed by mixing 10 µM protein with SYPRO orange (1:5000 dilution) and fluorescence was recorded in 0.5ºC-steps between 20ºC and 80ºC (excitation 450-490 nm and emission 515-530 nm). Average melting temperatures (Tm) are shown (n = 3, mean ± SD). (C) Protein solutions (10 µM) were incubated with 20 µM ANS and fluorescence emission was recorded upon excitation at 350 nm. One representative experiment is plotted. (D) Size exclusion chromatography of proteins was performed using Superdex 200 10/300 GL column. The maximum absorbance recorded at 280 nm was set as 100. One representative experiment is shown. (E) Fluorescence of FAD released from proteins was measured. 1 µM FAD was used as a positive control. One representative out of three measurements is plotted.

of other ubiquitin ligases that partially take over CHIP function and recognize its clients.

To further study the apoprotein recognition by CHIP, we decided to reconstitute it *in vitro*. For this purpose, recombinant wild-type and mutant forms of NQO1 were used. The presence of NQO1 during purification can be traced due to the characteristic yellow color that FAD gives to the fractions containing the enzyme. Mutant protein did not show this particular trait, which was expected given the fact that its affinity for the cofactor is lower than the wild-type, as mentioned above (97). Wild-type apoNQO1 protein was obtained according to the apoprotein purification protocols described before (97,138). Briefly, sepharose-bound NQO1 was denatured, washed extensively, and refolded again before elution and next purification steps.

CD spectroscopy revealed that secondary structures of mutant and apoprotein were similar to that of the wild-type protein (Figure 13A). Mutant NQO1 showed a decrease in melting stability of 9ºC (Figure 13B). Its meting temperature dropped from 47ºC to 38ºC. The decrease in apoNQO1 thermal stability was only of 0.5ºC. In gel filtration experiments, NQO1 mutant eluted ca. 2 mL before wild-type protein (Figure 13D, orange), an observation that can be explained by a larger hydrodynamic radius of the former. Lack of the flavin cofactor did not change the elution volume of the wild-type protein (Figure 13D, red). ANS (8-anilino-1-naphtalenesulfonic acid) is a water-soluble aromatic molecule whose fluorescence emission peak shifts and fluorescence intensity increases when the compound changes to hydrophobic environment (139). Fluorescence emission peak of ANS was at 450 nm upon binding to mutant NQO1 (Figure 13C, orange), while no signal for wild-type NQO1 was detected (Figure 13C, blue). Interestingly, wild-type apoNQO1 also showed increased binding of ANS. However, the peak was markedly shifted to the right (max. 470 nm) (Figure 13C, red), probably indicating that binding to the protein took place at a different site. The content of FAD was measured for all three proteins by denaturing them using SDS-containing solution and measuring fluorescence at ex/em of 450/480-600 nm. These measurements confirmed that the apoprotein purification protocol indeed resulted in cofactor depletion of wild-type NQO1 (Figure 13E, red). As expected, the levels of FAD detected in NQO1 mutant sample were very similar to those of the apoprotein (Figure 13E, orange) while wild-type NQO1 FAD content was much higher (Figure 13E, blue). The biophysical characterization of the three NQO1 variants showed minimal difference at the structural level among these proteins. Mutant NQO1 displayed some distinct traits, specifically, the decreased thermal

stability, lower elution volume in size exclusion chromatography and increased ANS binding. For wild-type NQO1, the lack of cofactor had no detrimental effects for protein folding and stability *in vitro*, and the apoprotein seemed to successfully maintain its structural integrity.

To verify the *in vivo* NQO1 stability experiments in CHIP knockout cells, *in vitro* ubiquitylation assay was performed. We wanted to test whether CHIP can directly recognize and ubiquitylate NQO1 depending on the cofactor-loading state of the flavoenzyme. To this end, E2 ubiquitin-conjugating enzyme Ubc5 and E3 ligase CHIP were expressed in bacteria and recombinantly purified. Ubiquitylation reaction was carried out using UBE1 from bovine

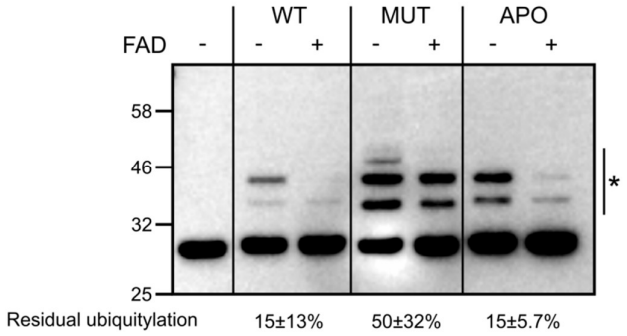

Figure 14. Lack of flavin cofactor enhances NQO1 recognition and ubiquitylation by CHIP. *In vitro* ubiquitylation assay of wild-type holoNQO1, wild-type apoNQO1, and mutant NQO1 in the presence or absence of FAD is shown. FAD (250 µM) was added to the samples as indicated. Reactions were incubated for 1 h at 37ºC. The side bar with the asterisk indicates bands used for quantification. Ubiquitylation without FAD was set as 1 and residual ubiquitylation in the presence of FAD was calculated and is indicated (n = 3, mean ± SD). First lane contains reaction with mutant NQO1 lacking E1 enzyme. One representative image is shown out of three independent experiments.

erythrocytes as ubiquitin activating enzyme, Ubc5 as E2, CHIP as E3, and wild-type holoNQO1, apoNQO1 and mutant NQO1 as substrates. Up to three different protein bands above NQO1 size (28 kDa) appeared on the immunoblotting membranes (Figure 14). Given the size of ubiquitin (8.5 kDa), the signals observed for each bands theoretically correspond to the mono-, di-, and tri-ubiquitylated NQO1. Thus, mutant and wild-type apoNQO1 were directly recognized and ubiquitylated by CHIP. Given the fact that large amounts of wild-type NQO1 are produced during IPTG induction in bacteria, the flavin loading capacity of bacteria might be exhausted (140). Thus, a population still susceptible for ubiquitylation is expected to remain in wild-type NQO1 samples. That is probably why wild-type NQO1 was also slightly ubiquitylated under control conditions (Figure 14, lane 2). FAD was added to the mix to investigate if reloading of the enzymes with the cofactor *in vitro* would have any direct impact on the ubiquitylation reaction. Indeed, the presence of the cofactor significantly reduced the

levels of NQO1 ubiquitylation in all cases. The percentage of ubiquitin-NQO1 signal remaining after FAD loading was calculated. FAD addition rescued wild-type NQO1 in both holo and apo forms to similar extent. The rescuing effect for the mutant at this FAD concentration was not that efficient.

3.3 The C-terminal domain of wild-type NQO1 mediates recognition by CHIP

Given the fact that wild-type apoNQO1 and mutant NQO1 are both recognized by the same ubiquitin ligase, we decided to investigate the possibility that the same structural feature is responsible for the recognition of both proteins. Previous studies found that in mutant NQO1 C-terminal domain possesses higher flexibility and, as a consequence, detaches from the main protein core (97). The intracellular stability of NQO1 mutant has been recently proposed to depend on this highly dynamic tail. Occupation of the NAD(P)H-binding pocket by the potent NQO1 inhibitor dicoumarol seems to be able to correct this structural alteration (100). We speculated that this particular feature might be important for protein quality control recognition. We investigated this possibility by first analyzing the sensitivity of NQO1 to proteolytic cleavage. Wild-type holoNQO1, apoNQO1, and mutant NQO1 were incubated in the presence of trypsin. Samples were collected at different time points. For immunoblotting, NQO1 C-terminus-recognizing antibody was used. This antibody specifically recognizes the last 12 amino acids of NQO1 (SIPTDNQIKARK). These experiments revealed that C-terminus of mutant NQO1 was very rapidly degraded by trypsin. Already after 10 minutes, no signal could be detected (Figure 15, lanes 10, 11, and 12). The rate of the C-terminus

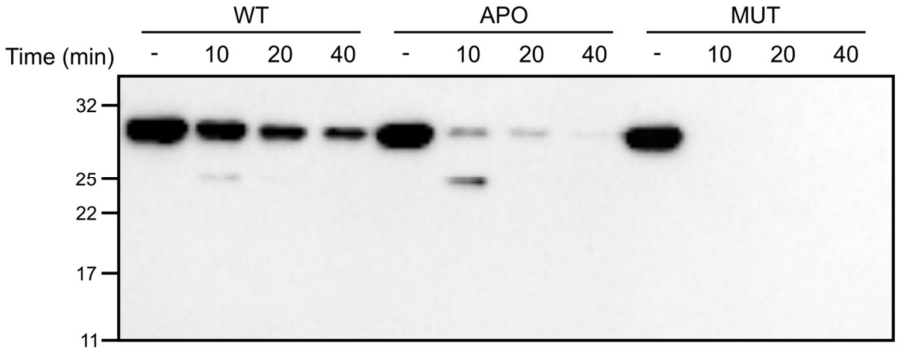

Figure 15. The C-terminus of NQO1 is more available for proteolysis in the absence of FAD. Partial proteolysis experiment of wild-type holo-, apoNQO1, and mutant NQO1 was carried out by incubating enzymes in the presence of sequencing-grade trypsin (2 ng/µL). Anti-NQO1 antibody recognizing the last 12 amino acids of the protein was used to detect and assess the levels of remaining NQO1. One representative experiment out of three is shown.

degradation was higher for wild-type apoNQO1 than for the holoprotein (Figure 15, lanes 1 to 8). Some degradation was still observed for cofactor-loaded wild-type NQO1 (Figure 15, lanes 2, 3, and 4), which probably reflects the dynamic behavior of the C-terminal end of the protein. This region seems to become more flexible when cofactor is not bound, and become highly accessible to the protease. Some reports have highlighted the effect of NQO1 inhibitor dicoumarol on the stability of the protein (97,100), which leads to the accumulation of the mutant protein in cells (100). Binding of dicoumarol, which takes place at the NAD(P)H-binding site in a competitive way with the nicotinamide cofactor, inhibits NQO1 activity but at the same time protects the mutant protein from degradation by overcoming the dynamic

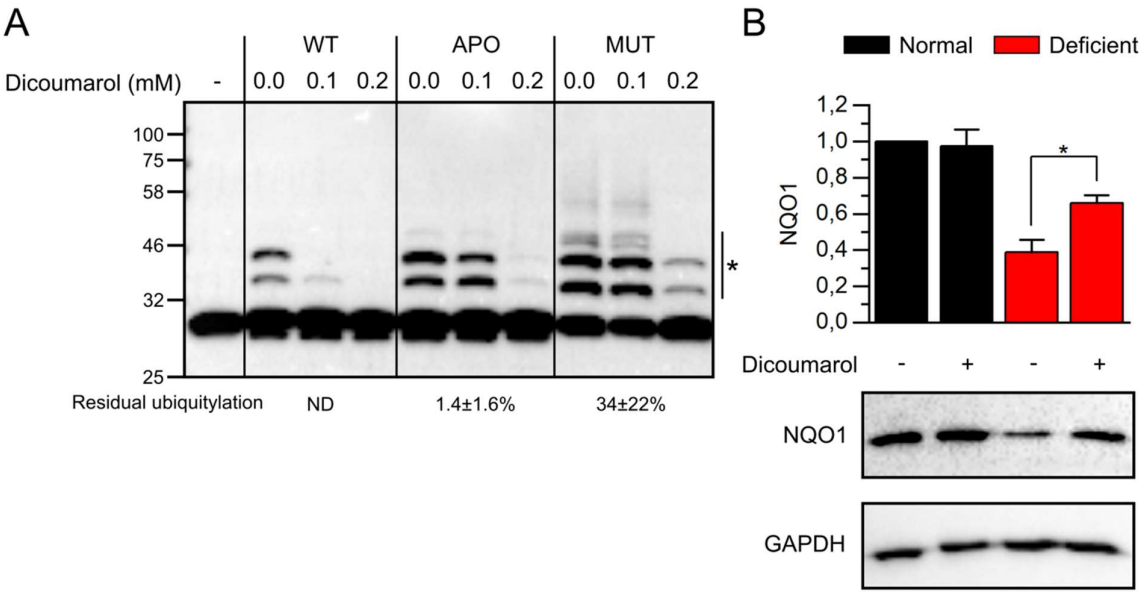

Figure 16. Dicoumarol binding rescues apoNQO1 from degradation. (A) *In vitro* ubiquitylation assay of wild-type holo-, apoNQO1, and mutant NQO1 was performed in the presence of increasing concentrations of dicoumarol (0.1, and 0.2 mM inhibitor). Reactions were incubated for 1 h at 37ºC. The side bar with the asterisk indicates the bands used for quantification. Wild-type NQO1 sample without dicoumarol was set as 1 and residual ubiquitylation was calculated using 0.2 mM dicoumarol values (n = 3, mean ± SD). First lane contains reaction with mutant NQO1 and without E1 enzyme. (B) *In vivo* analysis of wild-type NQO1 stability in B16 F0 cells treated with 100 µM dicoumarol. Cells were incubated for 24 h in riboflavin-free medium and treated with NQO1 inhibitor overnight. NQO1 protein levels under normal conditions were set as 1 and values were normalized to GAPDH (n = 3, mean ± SD). T-test was used to assess the significance of the difference between dicoumarol-treated and non-treated samples. One western blot image is shown as a representative of three independent experiments.

nature that its C-terminus shows (100). *In vitro* ubiquitylation assay using NQO1 as a substrate was performed with increasing concentrations of dicoumarol during the reactions. Ubiquitylation levels were diminished in all cases where dicoumarol was present (Figure

16A). This effect correlated with the amount of the inhibitor used and was very prominent at high doses (Figure 16A, lanes 4, 7, and 10). A low but detectable signal was still observed for wild-type apoNQO1 under 0.2 mM dicoumarol treatment (remaining ubiquitylation was ca. 1.4% compared to untreated sample), meaning almost complete rescue. Interestingly, the rescue was less efficient for mutant NQO1, for which 34% of ubiquitylated species remained (Figure 16A, lane 10). The protective role of dicoumarol towards wild-type apoNQO1 was also tested *in vivo* by analyzing the endogenous levels of NQO1 in melanoma cells cultured in control and riboflavin-deficient conditions. As expected, dicoumarol rescued NQO1 from degradation in the absence of the vitamin, but only partially (Figure 16B). The amount of dicoumarol used in this experiment was 100 μM and no higher concentrations were tested. According to the *in vitro* result shown previously (Figure 16A), the inhibitor should not prevent protein degradation completely at this concentration.

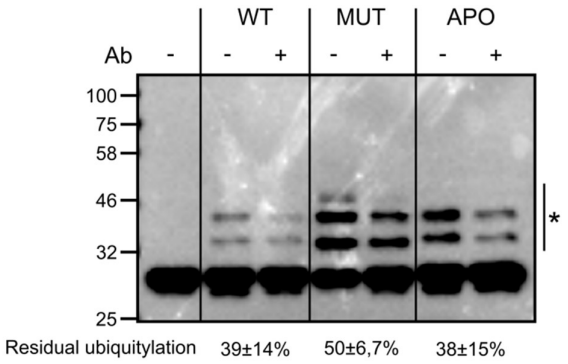

Figure 17. NQO1 ubiquitylation by CHIP is partially blocked in the presence of an antibody recognizing the C-terminus of the substrate. *In vitro* ubiquitylation assay of wild-type holo-, apoNQO1, and mutant NQO1 was performed in the presence of NQO1 C-terminus-recognizing antibody. Reactions were incubated for 1 h at 37ºC. The side bar with the asterisk indicates bands used for quantification. Ubiquitylation without antibody was set as 1 and residual ubiquitylation was calculated (n = 3, mean ± SD). First lane contains reaction with mutant NQO1 without E1 enzyme. One representative image out of three experiments is shown.

To further confirm that CHIP participates in the recognition of the NQO1 C-terminal end, ubiquitylation assay was performed in the presence of an NQO1 C-terminus-recognizing antibody. We expected ubiquitylation reaction to be affected by the blocking effect of the C-terminus-bound antibody. Indeed, the presence of this antibody reduced the levels of ubiquitylated NQO1 in all three cases (Figure 17). The signal for residual ubiquitylation was reduced approximately by half. Together, our results confirmed that loss of FAD increases the dynamic behavior of NQO1 C-terminus and that this region is important during the recognition events mediated by the protein quality control machinery.

3.4 Engineered tail-free NQO1 variants and NQO2 escape recognition by CHIP

To verify the importance of C-terminus for recognition, we engineered NQO1 variants lacking the C-terminal tail. To accomplish this, NQO1 proline 225 was mutated to STOP codon by changing proline codon CCA to TGA. With this method, the last 50 amino acids of both wild-type and mutant NQO1 proteins were removed from the DNA sequence. Variants lacking this part were called NQO1-Δ50. Wild-type NQO1-Δ50 and mutant NQO1-Δ50 were overexpressed in bacteria and purified recombinantly. Purification of wild-type apoNQO1-Δ50 was carried out following the same deflavination and reconstitution procedure explained earlier. Figure 18A shows NQO1 dimer structure with the deleted 50 amino acid tail marked in red and the protein core in grey. Physicochemical analyses were performed to assess if the

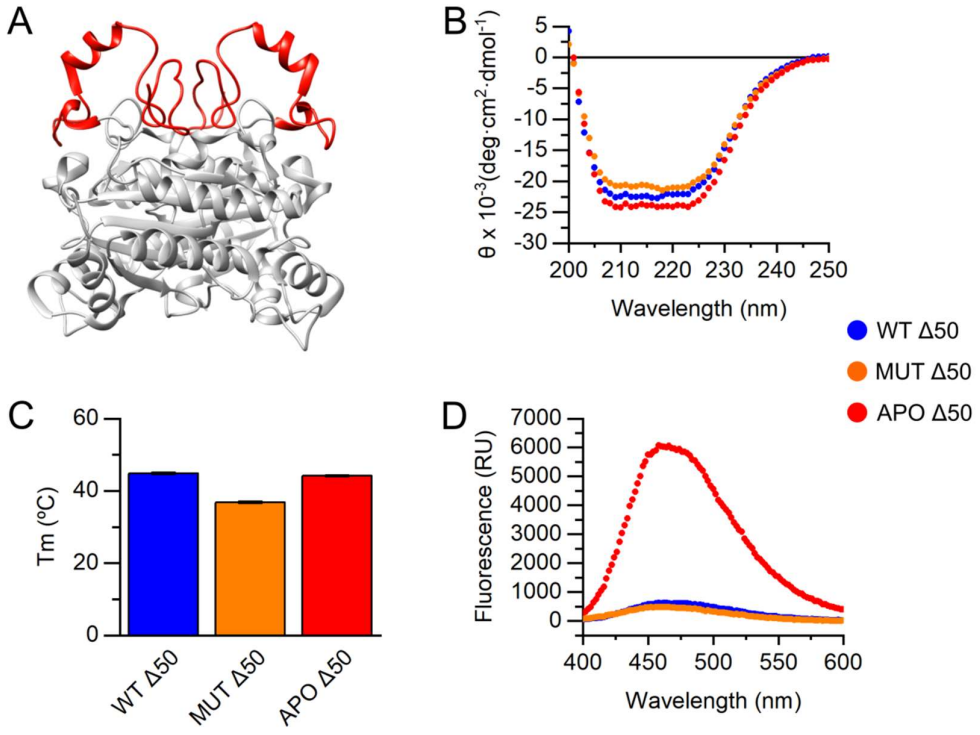

Figure 18. Tail-free NQO1 proteins share similar structural traits. Biophysical characterization of wild-type NQO1 Δ50, mutant NQO1 Δ50 and wild-type apoNQO1 Δ50. (A) X-ray structure of NQO1 dimer (Protein Data Bank ID code 1D4A). C-terminal tail (amino acids P225 - K274) has been marked in red. Stop codon was introduced at P225 to delete this region. (B) CD spectroscopy analysis was performed with 10 µM protein. Average values from three independent experiments are plotted. (C) Melting temperature (Tm) was measured using 10 µM protein mixed with SYPRO orange (1:5000 dilution). Fluorescence was recorded at 0.5ºC-steps between 20ºC and 80ºC (excitation 450-490 nm and emission 515-530 nm). Average melting temperatures are shown (n = 3, mean ± SD). (D) ANS (20 µM) was incubated with 10 µM proteins and binding was measured by recording fluorescence emission between 400-600 nm upon excitation at 350 nm. One representative experiment is plotted.

removal of this region affected the overall structure of the proteins. Truncation of the C-terminal tail did not result in any major secondary structure changes, as CD experiments revealed. Small differences among the traces seemed to appear, especially between wild-type and mutant. This might still reflect minor changes in secondary structure (Figure 18B). On the other side, thermal sensitivity of all NQO1-Δ50 proteins decreased with respect to full-length enzymes (Figure 18C). Melting temperature of both wild-type holoNQO1-Δ50 and apoNQO1-Δ50 was ca. 45ºC, i.e. two degrees lower that the respective full-length variants. An 8 degrees difference in melting temperature was observed between both wild-type holo- and apoNQO1-Δ50 forms and mutant. Interestingly, this difference was independent of the C-terminal end. Testing the binding of ANS to the proteins gave a slightly different result than expected. In previous experiments, NQO1 mutant strongly bound to the fluorescent dye (Figure 13C, orange), but this binding was abolished when the C-terminal tail was depleted (Figure 18C, orange). The result suggests that in the absence of this tail, the fluorescent dye loses the accessibility to non-polar binding stretches present before in the full-length version. A different result was observed for wild-type apoNQO1-Δ50 which still bound to ANS with a maximum emission peak centered at 458 nm. Even with the deleted tail, ANS was binding to the protein in a similar manner as in the case of its full-length homolog. Based on the data presented earlier regarding the NQO1 C-terminus flexibility, we hypothesized that the shorter variants should become invisible to the surveillance capabilities of CHIP. To test this assumption, ubiquitylation assay was performed with NQO1-Δ50 proteins as substrates. Indeed, ubiquitylation was strongly diminished (Figure 19A), although not completely abolished, as one faint band was still present, probably corresponding to the mono-ubiquitylated NQO1-Δ50 (Figure 19A, lanes 2, 3, and 4). Additionally, the sensitivity to CHIP recognition was the same for all three proteins in contrast to the ubiquitylation of full-length forms (Figure 19A). Wild-type NQO1-Δ50 was overexpressed in B16 F0 cells to analyze its stability *in vivo* upon riboflavin deprivation, expecting that the levels of the vitamin will have no effect. The sensitivity of NQO1 to the cofactor deficiency was completely lost in the absence of the C-terminal tail (Figure 19B). Wild-type NQO1 was overexpressed separately as a positive control. In this case, protein degradation seemed less efficient than the effect reported above for endogenous NQO1. Overexpression of NQO1 might overload the targeting capacity of the endogenous degradation machinery (Figure 19B). The accumulation of wild-type NQO1-Δ50 under proteasome inhibition was markedly

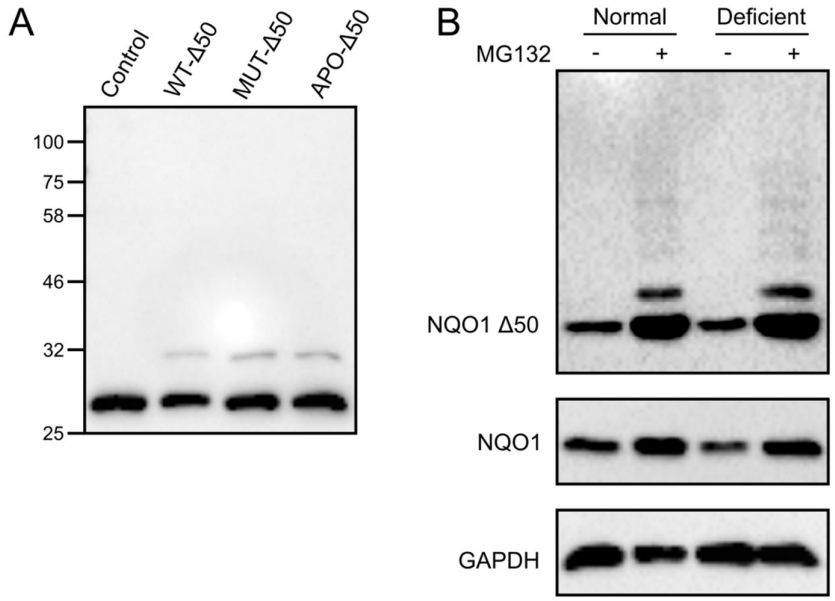

Figure 19. CHIP does not recognize NQO1-Δ50 variants. (A) *In vitro* ubiquitylation of NQO1-Δ50 variants (wild-type NQO1-Δ50, WT-Δ50; mutant NQO1-Δ50, MUT-Δ50; wild-type apoNQO1-Δ50, APO-Δ50) was performed using CHIP and incubating reactions at 37ºC for 1 h. Control lane contains reaction with MUT-Δ50 without E1 enzyme. (B) *In vivo* stability of transfected wild-type NQO1-Δ50 was assessed in B16 F0 cells under riboflavin-deficient conditions for 24 h. Cells were treated with 5 μM MG132 overnight. The steady-state levels of full-length wild-type NQO1 were also analyzed for comparison. GAPDH was used as loading control. One representative experiment is shown.

higher than that of wild-type NQO1. Higher molecular weight protein bands also appeared under proteasome inhibition treatment, most probably corresponding to ubiquitylated species that are not observed when NQO1 full-length is overexpressed. Curiously, an NQO1 paralogue exists and is called NQO2. It belongs to the same family of oxidoreductases (87,141) but has been less studied compared to NQO1. Amino acid sequences of both proteins are highly similar given the 49% identities obtained by protein sequence alignment (87). One of the most remarkable facts that differentiate NQO2 from NQO1 is that the former naturally lacks a C-terminal tail that would correspond to the one found in NQO1 (142). This circumstance led us to hypothesize that CHIP binding to NQO2 should be abrogated, in a similar way as the experiments with tail-deleted versions of NQO1 revealed. As we did previously for NQO1, both wild-type holo- and apoNQO2 recombinant proteins were purified from *E.coli* and FAD depletion was carried out using the same protocol as above. A battery of biophysical assays was carried out to characterize the two forms and investigate if NQO2 structure was compromised in the absence of cofactor. We could verify that FAD had been

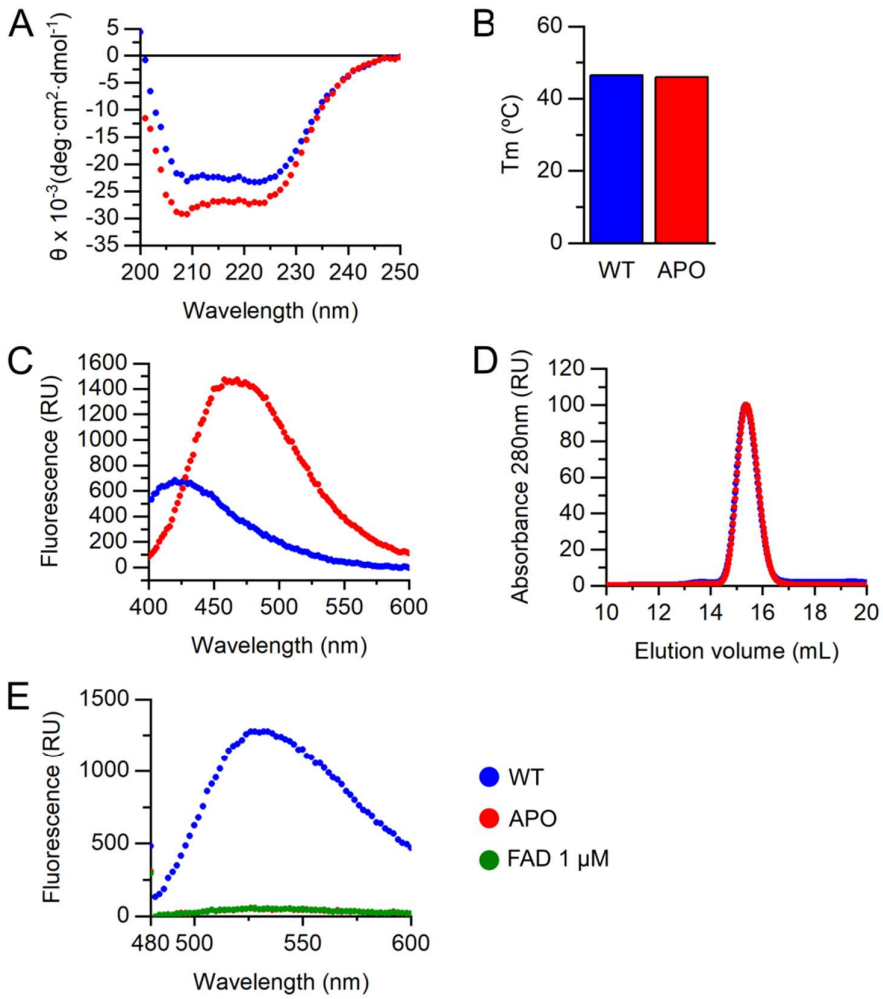

Figure 20. Biophysical comparison of recombinant wild-type holoNQO2 and apoNQO2. (A) CD spectroscopy was carried out using 10 µM protein. Average values from three independent experiments are plotted. (B) Melting temperature was measured by mixing 10 µM protein with SYPRO orange and fluorescence was recorded at 0.5ºC-steps between 20ºC and 80ºC (excitation 450-490 nm and emission 515-530 nm). Average melting temperatures (Tm) are shown (n = 3, mean ± SD). (C) Protein solutions (10 µM) were incubated with 20 µM ANS and fluorescence emission was recorded between 400-600 nm upon excitation at 350 nm. One representative experiment out of three is plotted. (D) Size exclusion chromatography of proteins was performed using Superdex 200 10/300 GL column. The maximum recorded absorbance at 280 nm was set as 100. One representative experiment is shown. (E) Fluorescence of FAD released from proteins was measured. 1 µM FAD was used as a positive control. One representative out of three measurements is plotted.

successfully released from NQO2 (Figure 20E, blue). The levels of FAD released by NQO2 (maximum 1274 fluorescence units) are higher than the values recorded for NQO1 (maximum 132 fluorescence units) (Figure 13E, blue). This means that NQO2 is probably better loaded with FAD during expression in bacteria, which might indicate its higher affinity for FAD. The CD spectra of holo- and apoNQO2 do not overlap completely (Figure 20A). The difference

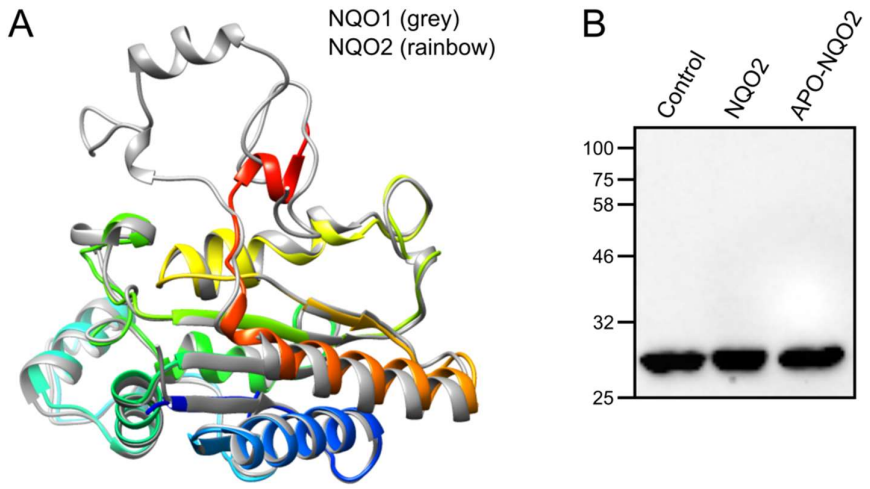

Figure 21. CHIP does not recognize NQO1 paralogue NQO2. (A) Structure superimposition of human NQO1 (Protein Data Bank ID code 1D4A) and human NQO2 (Protein Data Bank ID code 3FW1). (B) *In vitro* ubiquitylation assay of wild-type holo- and apoNQO2 proteins was performed using CHIP as E3 ligase. Reactions were incubated for 1 h at 37ºC. One representative experiment is shown.

indicates that apoNQO2 displays small changes in its secondary structure. Both proteins have a similar thermal denaturation temperature with only 0.5ºC difference, i.e. 46.5ºC for holoNQO2 vs 46ºC for apoNQO2. In the same line with NQO1 measurements, apoNQO2 binding experiment to ANS shows a 458 nm emission peak that is not observed for the holoprotein, indicating that ANS could bind the NQO2 cofactor-binding pocket in the absence of FAD.

Figure 21A shows the high overlap between NQO1 and NQO2 when the structures of both enzymes are superimposed (RMSD of 0.73Å over the shared similarity region of 219 Cα atoms). NQO2 ubiquitylation reaction was carried out using the same experimental setup as described for NQO1. Both wild-type holo- and apoNQO2 forms escaped recognition by CHIP, since no ubiquitylation bands were detected (Figure 21B).

3.4.1 NQO2 binds α-synuclein and prevents its degradation by the 20S proteasome

Given the high resemblance between NQO1 and NQO2 at the structural and sequence level, we wondered whether NQO2 would also protect α-synuclein from proteasomal degradation, similar to the effect exerted by NQO1 (Figure 11). Incubation of NQO2 and α-synuclein together with 20S proteasome *in vitro* revealed that NQO2 can prevent its degradation (Figure 22A). Around 60-70% α-synuclein was degraded in the absence of NQO2. To investigate if this protective effect could be caused by the direct interaction between NQO2 and

α-synuclein, NQO2 *in vitro* pull-down assay was carried out. Ni-NTA agarose was used to bind N-terminal NQO2 histidine tag. After sample incubation in the presence of glutaraldehyde for crosslinking, agarose-bound proteins were washed and eluted. Minimal non-specific binding of α-synuclein to the agarose was observed (Figure 22B, lane 6). In the absence of a crosslinking agent no additional α-synuclein was pulled-down (Figure 22B, lane 4) but when glutaraldehyde was added, a new protein band appeared right below 40 kDa, which is the expected size of the NQO2-α-synuclein heterodimer. The same experiment was repeated using NQO1 instead of NQO2, but no binding could be observed in this case (data not shown).

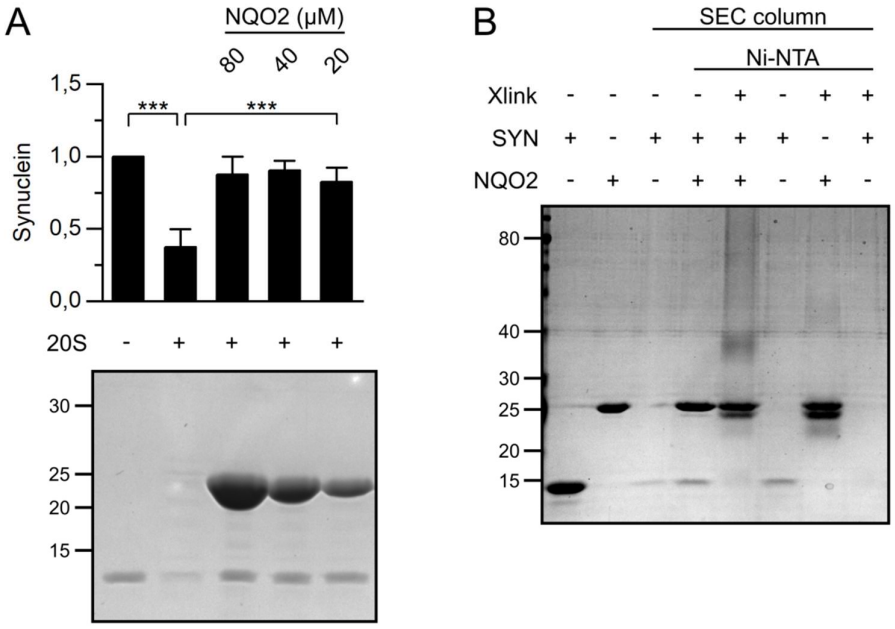

Figure 22. NQO2 directly binds α-synuclein and protects it from degradation by the 20S proteasome. (A) 10 μM α-synuclein was mixed with different concentrations of NQO2 (20, 40, and 80 μM) and 50 nM 20S proteasome. Reactions were incubated for 1 h at 37ºC and SDS-containing reducing buffer was added to stop the reactions. Samples were separated in 14% SDS-PAGE and the gel was stained with coomassie blue G-250 staining solution. Control sample (only α-synuclein) was set as 1 (n = 3, mean ± SD). ANOVA one-way test was used to analyze the significance of the differences between means. (B) *In vitro* NQO2 pull-down experiment is shown. 20 μM NQO2 was mixed with 50 μM α-synuclein and incubated in the presence of Ni-NTA sepharose for 1 h at 4ºC. BioSpin Size Exclusion Column was used to retain agarose-bound proteins, which were then eluted and separated in 10% SDS-PAGE. Gel was stained with coomassie blue G-250.

3.4.2 NQO1 variants and NQO2 have different stability *in vivo*

From the experiments shown until this point, no strict comparison between the stability of NQO1, NQO1-Δ50, and NQO2 could be made. Changes in the protein turnover *in vivo* might result in different protein accumulation. To address this issue, the protein synthesis inhibitor

cycloheximide (CHX) was used to treat HEK293 cells expressing NQO1 and NQO2 proteins transiently. Cells were incubated for 4 h under riboflavin-deficient conditions and protein levels were analyzed after additional 4 h CHX treatment, i.e. 8 h after transfection. The immunoblot revealed that mutant NQO1 and NQO1-Δ50 are degraded faster than wild-type NQO1 (Figure 23). The lack of riboflavin did not increase degradation, probably due to the short starvation period of the experiment. Obviously, a longer starvation is needed to observe protein destabilization. The stability of NQO2 was similar to that of wild-type NQO1 and was not riboflavin-dependent either.

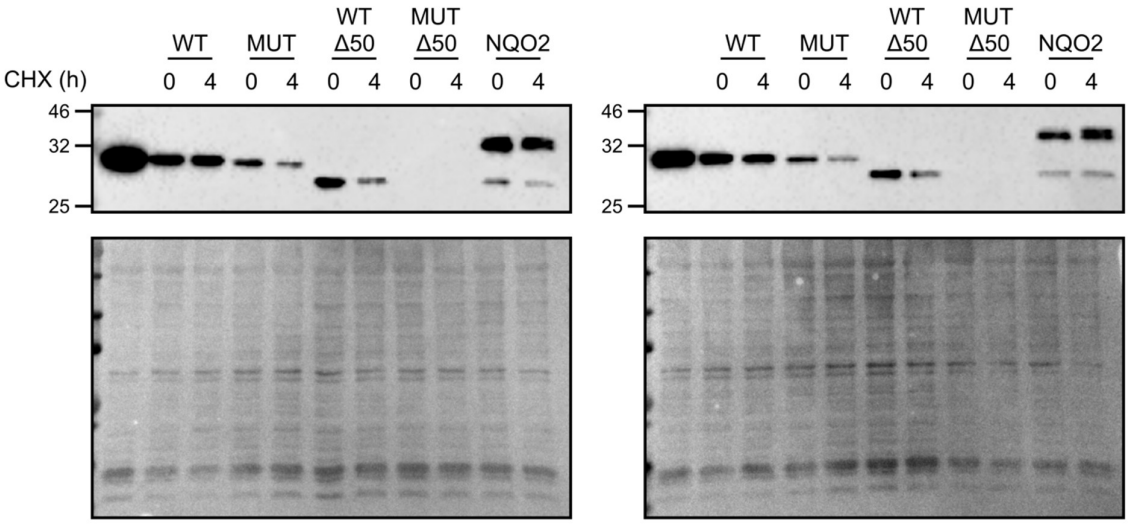

Figure 23. Analysis of protein stability *in vivo*. NQO1 and NQO2 proteins were transfected into B16 F0 cells. These were incubated for 4 h in normal (left) or riboflavin-free medium (right) and then treated with cycloheximide (CHX) for another 4 h. Time point 0 refers to samples collected before adding CHX. The first lane of each blot corresponds to non-treated cells that were collected 8 h after transfection. Ponceau S staining was used to control sample loading.

3.5 Protein co-aggregation and amyloidogenesis is aggravated in the absence of vitamin B2

Proteins can populate alternative structures besides their functional conformation when their stability is compromised and abnormal binding events occur. These structures are known as aggregates (7). Several factors can negatively affect the stability of proteins and give raise to partially unfolded states or loss of compact structure. As a result, this increases the probability of aberrant intermolecular interactions occurring due to an anomalous exposure of hydrophobic regions or patches (2). Aggregation processes might be triggered by increased protein dynamics or small changes in secondary or tertiary structure (143,144). A small

change in structure such as the one described for the C-terminus of NQO1 might contribute to the increased aggregation rate of the protein. The dynamics of this tail can emerge as a potential factor for molecular interactions with other proteins. The Zyggregator algorithm predicts protein aggregation propensity with high accuracy (145). The combination of three different physicochemical properties of amino acid sequences (i.e. hydrophobicity, charge and propensity to acquire either α-helical or β-sheet structure) is fitted into an equation that calculates the aggregation tendency. The CamSol method analyzes the impact of amino acids on the protein solubility (145). As the Zyggregator, the CamSol algorithm assigns the calculated values for each amino acid. Arbitrary values are given to each amino acid of the sequence depending on the physicochemical properties of these residues and experimental data about the effects caused by single substitutions. Both algorithms were used to analyze human wild-type NQO1 sequence (Uniprot P15559) and its C-terminal tail. Aggregation *versus* solubility scores were plotted (Figure 24A). Values higher than 1 (green area) indicate high aggregation and solubility propensities and opposite applies for scores lower than -1 (red area). The traces for aggregation and intrinsic solubility formed a plot whose peaks and valleys do not overlap (Figure 24A). This indicates that a strong negative correlation exists between aggregation and solubility. Although there is a biological connection between the concepts behind the calculations, they differ from the thermodynamics point of view. Solubility refers to the free energy difference between the solution and the aggregated states while Zyggregator method calculates aggregation rates and thus is a measure of the kinetic barrier imposed to a protein in order to reach aggregation (146). Since the information that both algorithms provided about NQO1 seemed to be rather redundant, one additional modification of the CamSol method was used to acquire more insight. This adjustment introduces a structural correction such that intrinsic solubility scores are modified according to the proximity of other amino acids in the three-dimensional conformation and the exposure to the solvent. Thus, areas with low solubility but hidden within the hydrophobic core can be distinguished from those that are more exposed and can certainly trigger aggregation (146,147). The plot that was obtained for NQO1 using this correction was then very revealing. The fragment ranging from residues A94 to M131 shows low solubility, especially in the first section (aa A94 to K113) (Figure 24A, purple). This propensity completely disappeared with the structure correction and the plot trace became flat (Figure 24B, green). The same occurred in the region between V143 and H194, where a low intrinsic solubility profile was observed.

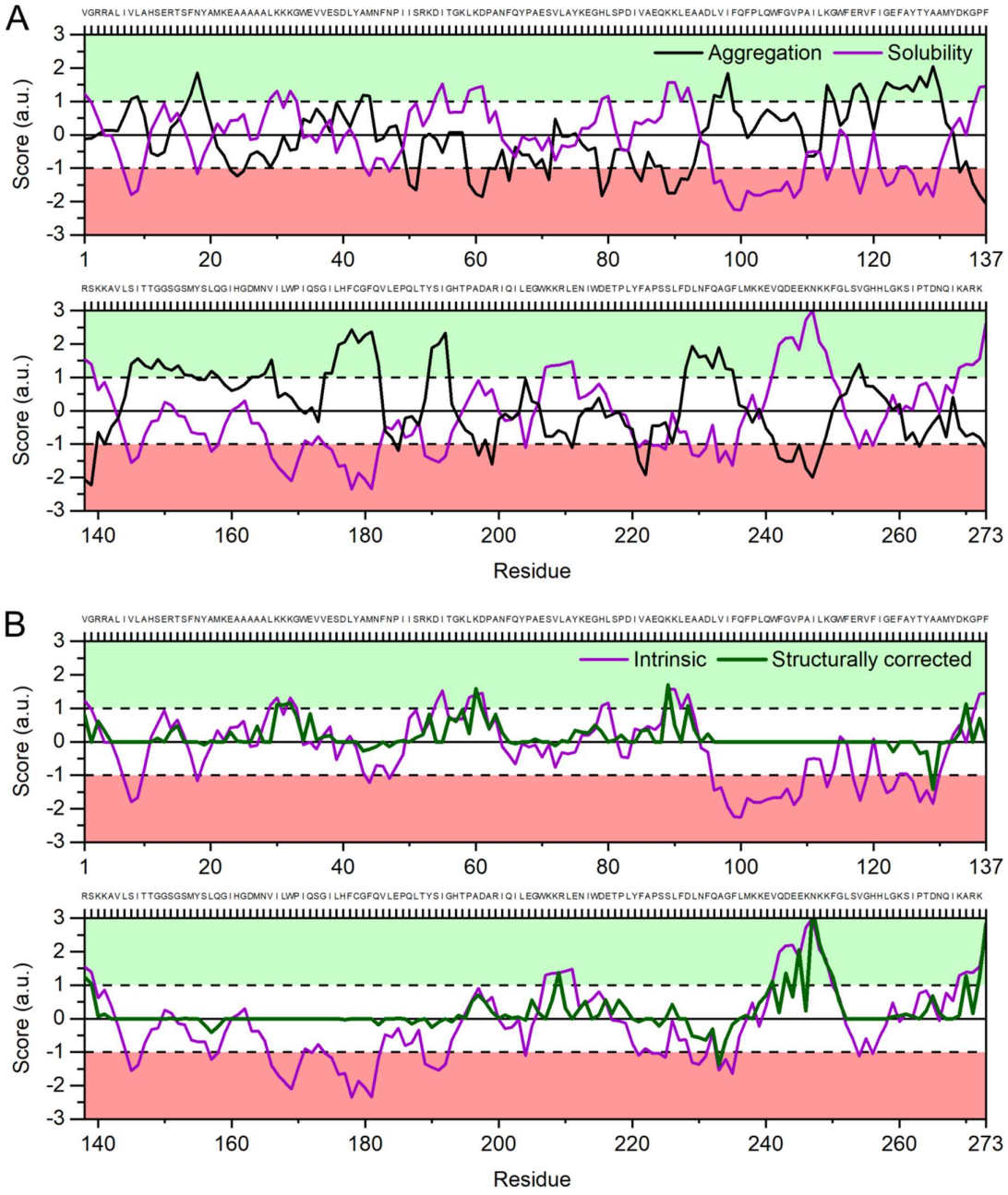

Figure 24. NQO1 C-terminal tail is a potential aggregation-prone structural determinant. Bioinformatics analysis of wild-type NQO1 aggregation and solubility scores is shown. (A) Individual amino acid scores (in arbitrary units) given by the Zyggregator (aggregation) and CamSol (solubility) predictors for each residue are plotted. Individual residues are shown in upper X-axis while residue number is given on the lower X-axis. (B) The same plot is shown using scores predicted by the CamSol. Arbitrary units obtained for the intrinsic amino acid sequence as well as with a structure correction algorithm from the same software were plotted.

Again, the trace drastically went back to 0 when NQO1 structure was taken into account for recalculating the scores. Additionally, these regions showed a high aggregation tendency (Figure 24A, black trace). This data indicates that these particular sequences, albeit highly

aggregation-prone, should not be able to mediate aggregation since they are located within the hydrophobic core of the protein and remain inaccessible to the solvent (147). The area between D229 and G235 prominently stands out among the rest for showing a significant mild to high aggregation propensity and low solubility propensity. Remarkably, structure correction did not completely abolish this proclivity, but just attenuated it. We have previously shown that this fragment, which belongs to the C-terminal end of NQO1, loses the association with the core of the enzyme and becomes highly flexible and accessible for CHIP

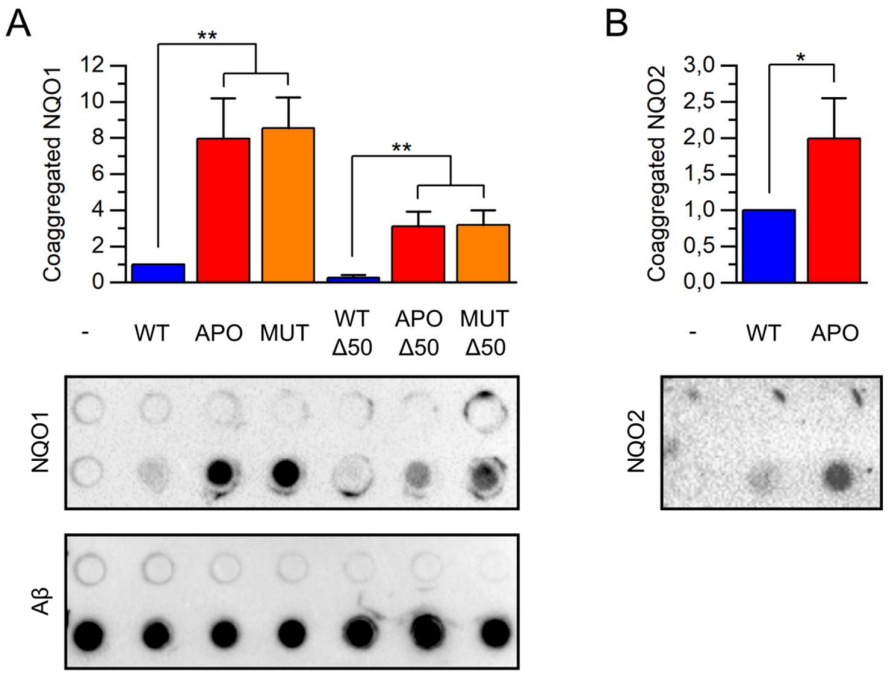

Figure 25. Lack of flavin cofactor aggravates both wild-type apoNQO1 and apoNQO2 co-aggregation with $A\beta_{1-42}$ peptide *in vitro*. (A) *In vitro* co-aggregation assay of wild-type holoNQO1 (WT), apoNQO1 (APO) and mutant NQO1 (MUT) was carried out. NQO1-Δ50 versions were also used in this experiment: wild-type holoNQO1-Δ50 (WT-Δ50), apoNQO1 (APO-Δ50), and mutant NQO1-Δ50 (MUT-Δ50). 5 μM protein was used. In order to trigger aggregation, 10 μM $A\beta_{1-42}$ peptide was used. Samples were incubated for 1 h at 37ºC and trapped onto a cellulose acetate filter using a 96-well dot blot hybridization system. The intensity of wild-type NQO1 signal was set as 1. $A\beta_{1-42}$ immunoblot was used as an aggregation control. One-way ANOVA test was used to assess the significance of differences within groups. (B) *In vitro* co-aggregation of wild-type holoNQO2 (WT) and apoNQO2 (APO) with $A\beta_{1-42}$ was carried out the same way as in (A). The intensity of the wild-type holoNQO2 signal was set as 1. T-test was used to assess the significance of the difference.

recognition in the absence of FAD. Conditions that reduce structural compactness and increase dynamic behavior might substantially shift the equilibrium towards aggregating populations by stimulating intermolecular interactions (148). The local conformational change experienced by wild-type NQO1 when the cofactor is not available could favor NQO1

binding to non-natural partners, according to the increased aggregating propensity of the C-terminal tail observed in computational analysis. To investigate this assumption experimentally, we decided to perform an *in vitro* co-aggregation assay in the absence of flavin cofactor. To this end, we used the amyloid-β peptide ($A\beta_{1-42}$) as a strong aggregating protein which is found in extracellular amyloid plaques of Alzheimer's disease patients (149). Sequential cleavage of amyloid precursor protein (APP) produces several fragments and from these, $A\beta_{1-42}$ shows a strong predisposition for aggregation (150). Amyloid-β peptide was mixed with wild-type NQO1, mutant NQO1, and NQO1-Δ50 enzymes. Aggregates were trapped on a cellulose acetate filter and proteins were detected using conventional immunoblotting procedures. Filter pore size was 0.2 μm, so only amyloid fibrils big enough to be trapped on the filter were detected. Anti-$A\beta_{1-42}$ peptide antibody was used to confirm that aggregation was similar in all samples. As expected, NQO1 in the absence of the $A\beta_{1-42}$ peptide did not aggregate (Figure 25A, upper blot, fist row). Yet when proteins and $A\beta_{1-42}$ peptide were incubated together, NQO1 was detected on the filter. Both wild-type apoNQO1 and mutant NQO1 increasingly bound to amyloids formed by $A\beta_{1-42}$ (Figure 25A). On the other side, the susceptibility for aggregation was reduced in all tail-deficient forms, indicating that the same structural determinant that facilitates recognition by the protein quality control also enhances co-aggregation with amyloidogenic structures. No significant differences in co-aggregation were found between apoNQO1 and mutant proteins (Figure 25A). Wild-type apoNQO2 also showed increased co-aggregation, although only by ca. 2-fold (Figure 25B) when compared to NQO1, indicating that NQO2 does not become as susceptible for co-aggregation as NQO1 when flavin cofactor is missing.

Next, we decided to use $A\beta_{1-42}$ to study co-aggregation of proteins in the context of riboflavin deficiency *in vivo*. For this purpose, eukaryotic expression vector containing $A\beta_{1-42}$ fused C-terminally with EGPF was transfected into B16 F0 cells. The lysates obtained from cells under riboflavin starvation for 3 days were fractionated into soluble and pellet fractions by ultracentrifugation. A significantly higher amount of $A\beta_{1-42}$ was detected in the pellet fraction under starvation conditions according to the ratio between deficient and normal conditions (p-value = 0.037), in comparison to the ratio in the soluble fraction (Figure 26A). NIAD-4 is a soluble molecule that binds to amyloid-like structures with high affinity and upon binding its fluorescence emission signal is dramatically enhanced (151). Cells were incubated for 3 days in riboflavin-deficient medium and stained with NIAD-4 to detect the appearance of

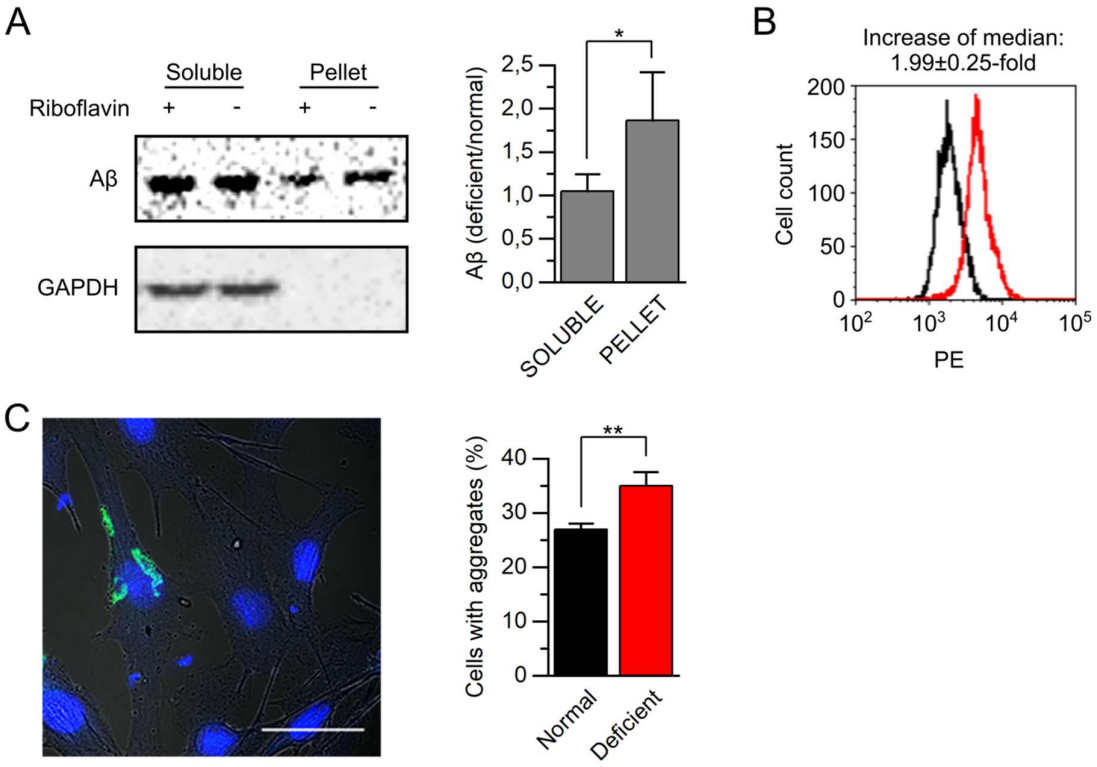

Figure 26. Riboflavin deficiency exacerbates protein aggregation and amyloidogenesis *in vivo*. (A) Aβ-EGFP aggregation in B16 F0 cells was followed using sedimentation assay. Cells overexpressing Aβ-EGFP were incubated for 3 days under riboflavin starvation conditions together with 5 μM MG132 during the first day. Soluble and insoluble fractions of cell lysates were obtained by ultracentrifugation and the content of Aβ-EGFP was analyzed. Aβ-EGFP protein levels in control sample (first lane; soluble) was set as 1. Deficient over normal ratio was calculated for the soluble and pellet fractions and plotted (n = 3, mean ± SD). T-test was used to evaluate the significance of the difference between soluble and pellet ratios. (B) NIAD-4 reagent was used to detect amyloids *in vivo*. B16 F0 cells were cultured for 3 days under riboflavin-deficient conditions. Cells were stained with NIAD-4 and fluorescence was analyzed by flow cytometry (n = 3, mean ± SD). One representative experiment is shown. (C) Quantification of Aβ-EGFP aggregates in B16 F0 cells by means of confocal microscopy. Cells overexpressing Aβ-EGFP were incubated for 3 days under riboflavin starvation conditions together with 5 μM MG132 treatment during the first day. Images were taken with a confocal microscope. An example of aggregates is shown (left) (scale bar: 50 μm). Cells containing aggregates under normal or riboflavin-deficient conditions were quantified (n = 3, mean ± SD). DAPI was used to stain the nucleus (blue). The significance of the difference between the means was estimated by t-test.

amyloid-like structures. Flow cytometry was used to measure red fluorescence in control and starved populations. A marked shift to the right in the PE axis of the histogram plot was measured for the population of cells incubated in the absence of vitamin B2 (Figure 26B, red). The fluorescence intensity increase by ca. 2-fold indicates that, under these conditions, the formation of amyloid structures is favored even when no aggregating protein has been exogenously introduced in the cell. To collect more evidence about the enhanced

amyloidogenesis *in vivo*, $A\beta_{1-42}$ was overexpressed in B16 F0 cells and accumulation of aggregates was detected using confocal microscopy. One typical example of the aggregates found within GFP-positive cells is provided in Figure 26C. The fraction of cells containing green amyloidogenic species was higher under vitamin starvation (Figure 26C), in accordance with the results shown in Figure 26A and 26B.

Since our results revealed that NQO1 can co-aggregate with $A\beta_{1-42}$ largely depending on the availability of the flavin cofactor, we wondered if non-native intermolecular interactions were also occurring with normal endogenous proteins. In order to address this issue biochemically, we chose Blue-Native polyacrylamide gel electrophoresis (BN-PAGE) (152). This method has been used to separate, identify, and characterize oligomeric structures by running them in denaturant-free conditions trying to preserve these assemblies (118). B16 F0 cells were transfected with wild-type NQO1 and incubated for 1 day under riboflavin-deficient conditions. Cell lysates were prepared under native conditions and samples were separated in BN-PAGE. Proteins were transferred from the native gel onto a PVDF membrane using a modified transfer protocol followed by regular antibody probing. The majority of NQO1 was detected as a low molecular weight band. In addition, a smear-like signal ranging from lower to higher molecular weight appeared under riboflavin deprivation (Figure 27A, lane 4). Only upon proteasome inhibition the accumulation of high molecular weight NQO1 species was observed. Under vitamin deprivation and without MG132, NQO1 protein levels decreased. This can be seen both in BN-PAGE and SDS-PAGE (Figure 27A, lane 3) and is in accordance with the results shown above on the cofactor-dependent stability of NQO1 *in vivo* (Figure 10). Importantly, the appearance of higher molecular weight NQO1 species required riboflavin deficiency and proteasomal inhibition alone was not sufficient. It seemed that the mere accumulation of proteins was not enough to trigger aggregation. SDS-PAGE was performed to exclude that aggregation occurred as a result of the different protein expression levels (Figure 27A, middle panel).

Aggregates are highly heterogeneous, not only in composition but also in structure and stability (153). The term “aggregates” can also refer to protein oligomeric species found during initial-mid phases of aggregation, when highly stable β-sheet containing amyloids have not yet been formed. Aggregates can also be amorphous arrangements with no defined structure (112). NQO1 aggregates could still retain some of its tertiary structure and thus

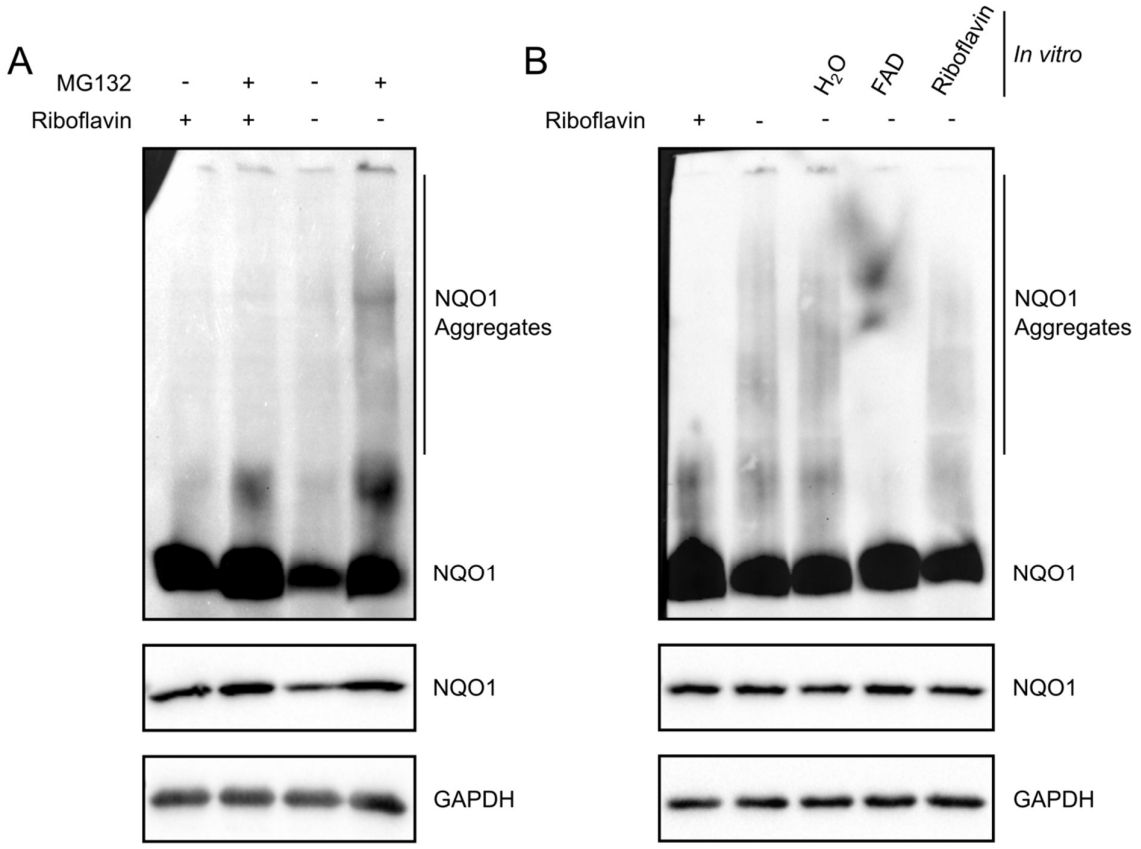

Figure 27. NQO1 becomes susceptible for aggregation under riboflavin-deficient conditions. (A) B16 F0 cells were transfected with wild-type NQO1 and cultured for 1 day in riboflavin-free medium. Cells were treated with 5 μM MG132 overnight where indicated and BN-PAGE was performed with cell lysates. (B) Wild-type NQO1-transfected B16 F0 cells were treated with 5 μM MG132 overnight. H_2O (control), FAD (10 μM), or Riboflavin (10 μM) were added separately to the cell lysates, which were then incubated for 5 min at room temperature and separated in a BN-PAGE. A fraction of protein lysates was used for 10% SDS-PAGE in both experiments. GAPDH immunoblots were used as loading control. Vertical lines at the right of each figure indicate the area considered as NQO1 aggregates. One out of three representative experiments is shown.

undergo disaggregation supported by the presence of an external agent like FAD. To test this, the following experiment was performed. Lysates obtained from B16 F0 cells transiently expressing wild-type NQO1 and cultured for 24 h in riboflavin-free medium were incubated either with FAD or riboflavin (both at 10 μM) for 5 min. Samples were then run in BN-PAGE as before. Riboflavin serves here as a negative control since, as the metabolic precursor of FAD, it is structurally similar to it (77). As expected, NQO1 smear completely disappeared when the lysate was incubated with FAD but not with riboflavin (Figure 27B). It seems that aggregated apoNQO1 remained in such a state that it was partially structured and able to bind

its cofactor. Cofactor binding rescued the protein from aberrant interactions that underlie high molecular complexes.

3.6 Chaperones safeguard cofactor-free NQO1 and prevent aberrant binding

Next, we focused on studying the NQO1 interactome in its holo- and apoforms in order to get a molecular understanding of aggregation involving apoenzymes (Figure 27). B16 F0 cells overexpressing wild-type NQO1 were incubated for 1.5 days under riboflavin-deficient conditions. Cell lysates were mixed with FLAG affinity sepharose to bind 3xFLAG-tagged NQO1 and pull down its interacting partners. Analysis of the pull-down samples was performed by means of mass spectrometry. Individual ratios for NQO1 pull-down over background hits were calculated. The mean values from three different experiments were calculated and statistical analysis was performed to determine the significant changes in each

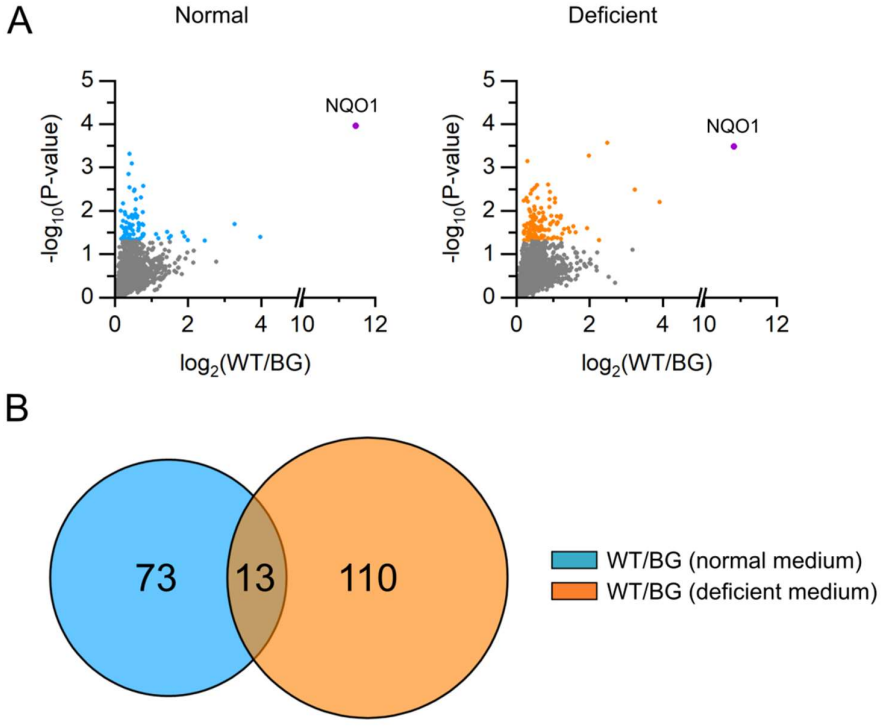

Figure 28. Wild-type apoNQO1 interactome is significantly different from that of holoNQO1. Volcano plots showing wild-type holo- and apoNQO1 interactors are depicted. B16 F0 cells overexpressing wild-type NQO1 were cultured in riboflavin-deficient medium for 24 h and treated with 5 µM MG132 overnight. NQO1 pull-down was carried out with FLAG affinity sepharose. Protein interactors were identified by mass spectrometry. Ratios of NQO1 pull-down over background were calculated and the log_2-transformed means from three different experiments are plotted. Enriched proteins are marked in blue (normal) or orange (deficient) according to $-log_{10}$(p-value < 0.05) obtained by t-test analysis. (B) Venn diagram is shown comparing the identities of NQO1 significant interactors (p-value < 0.05) from normal and riboflavin-deficient cultured cells.

condition (according to p-value < 0.05). From 196 significant interactors, a total of 86 hits belonged to control group while 123 were found under riboflavin-deficient conditions (Figure 28). NQO1 was the most enriched of all hits in both cases, as excepted (Figure 28A). A Venn diagram was prepared in order to visualize the overlap of both sets of interactors. Only 13 proteins were identified under both conditions (Figure 28B). Thus, the availability of the cofactor seems to have an effect on both number and type of proteins that wild-type NQO1 interacts with. Cofactor loss changed the selectivity of NQO1, most probably favoring the interaction with non-native partners that are not involved in the normal function of NQO1 or with components from the protein quality control system that are capable to take care of faulty

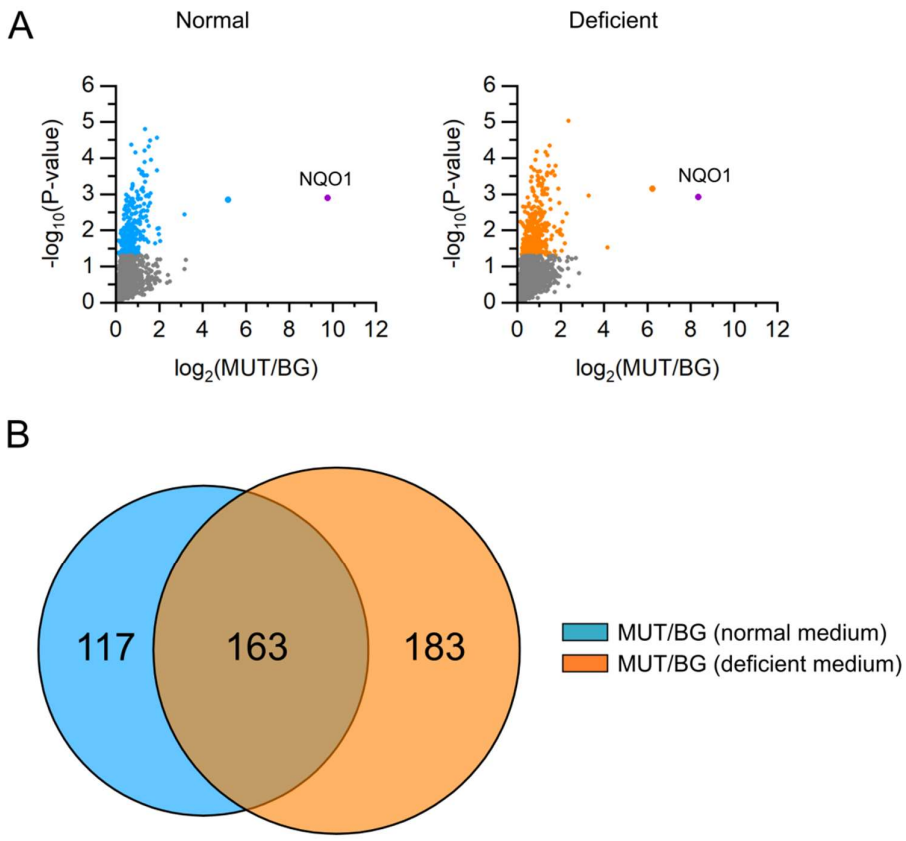

Figure 29. Mutant NQO1 interactome shows few changes under normal and starvation conditions. (A) Volcano plots showing mutant NQO1 interactors under normal and starvation conditions are depicted. B16 F0 cells overexpressing mutant NQO1 were cultured in riboflavin-deficient medium for 24 h and treated with 5 μM MG132 overnight. NQO1 pull-down was carried out with FLAG affinity sepharose. Protein interactors were identified by mass spectrometry. Ratios of NQO1 pull-down over background were calculated and the $\log_2$-transformed means from three different experiments are plotted. Enriched proteins are marked in blue (normal) or orange (deficient) according to $-\log_{10}$(p-value < 0.05) obtained by t-test analysis. (B) Venn diagram is shown comparing the identities of NQO1 significant interactors (p-value < 0.05) from normal and riboflavin-deficient cultured cells.

apoproteins. The same pull-down experiment followed by mass spectrometry analysis was performed using mutant NQO1 as bait. We expected to observe differences between the two experiments, given the unstable nature of the mutant form. Ratios between protein and background pull-downs as well as statistical analysis were carried out the same way as before. A total of 463 significant interactors (p-value < 0.05) were quantified and NQO1 was again the most enriched protein in the pull-down (Figure 29A). Venn diagram showed that the overlap between the two interactomes (normal and deficient) was much higher for the mutant protein than for wild-type, 163 vs 13 proteins, respectively (Figure 29B). The overlap corresponds to 6.6% of the total number of proteins detected under both conditions for wild-type versus 35.2% for mutant. Compared to wild-type NQO1, riboflavin deprivation does not change the binding nature of the mutant variant much, thus rendering it less sensitive to the availability of vitamin B2. The accumulation of this unstable variant, however, promotes aggregation with bystander proteins even in the presence of sufficient riboflavin. Comparison of wild-type and mutant NQO1 interactors in a Venn diagram revealed a higher percentage of identities under riboflavin-free conditions (18.8%) when compared to control samples (9.5%), a result that indicates the presence of similar structural determinants that favor certain interactions in the cofactor-free form of the enzyme (Figure 30).

Computational analysis of wild-type holo- and apoNQO1 interactomes was performed for a better understanding of the proteomics results presented in Figure 28. The CleverSuite tool was used for this purpose (122). Wild-type NQO1 interactors obtained under control and

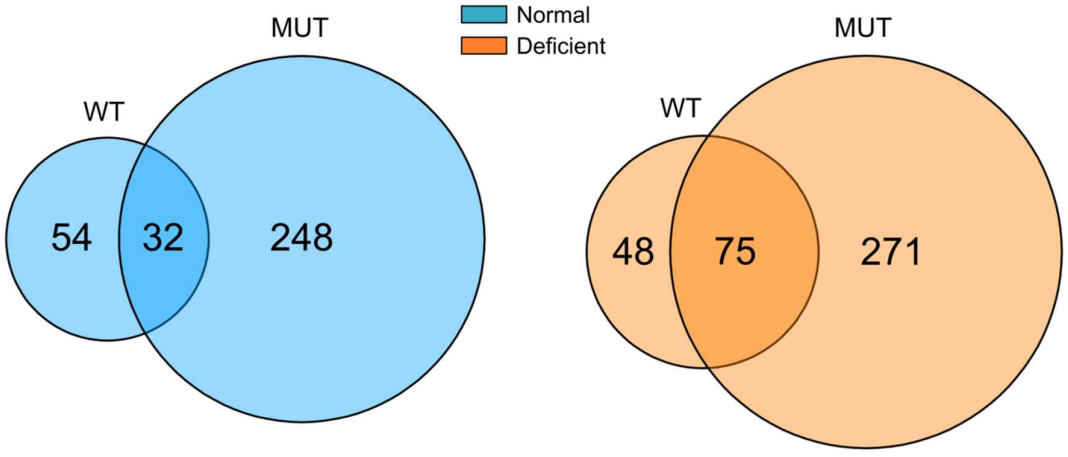

Figure 30. Wild-type and mutant NQO1 interactors show high overlap under riboflavin-deficient conditions. Wild-type and mutant NQO1 interactors obtained by mass spectrometry analysis were compared according to the cell culture conditions. The number of non-overlapping and overlapping hits is shown.

riboflavin-starvation conditions were compared looking for differences in isoelectric point (pI), molecular weight (MW), aggregation propensity, intrinsically disordered regions, and hydrophobicity. Statistical analyses with a p-value cut-off of 0.05 revealed no differences for any of the physicochemical traits analyzed (Figure 51). A Gene Ontology (GO) enrichment analysis was then performed using GO Term Finder classification system (130). Function was selected as the category for the analysis with a 0.01 p-value cut-off. GO terms involved

Gene	Protein
	Folding
AIP	Aryl hydrocarbon receptor interacting protein
CCT5	T-complex protein 1 subunit epsilon
CCT7	T-complex protein 1 subunit eta
DNAJA1	Dnaj homolog subfamily A member 1
DNAJA2	Dnaj homolog subfamily A member 2
HSPA8	Heat shock cognate 71 kDa protein
HSP90AB1	Heat shock protein HSP90-beta
PFDN1	Prefoldin subunit 1
TMX1	Thioredoxin-related transmembrane protein 1
TOR1A	Torsin-1A
	Degradation
BAG6	BCL2-associated anathogene 6
RCHY1	RING finger and CHY zinc finger domain-containing protein
RLIM	E3 ubiquitin protein ligase RLIM
SDF2L1	Stromal cell-derived factor 2-like protein 1
SGTA	Small glutamine-rich tetratricopeptide repeat-containing protein alpha
UBE2J1	Ubiquitin-conjugating enzyme E2 J1
UBXN4	UBX domain-containing protein 4
UBXN8	UBX domain-containing protein 8

Table 2. Chaperones and degradation machinery among NQO1 interactors. Wild-type apoNQO1 interactome obtained in NQO1 pull-down experiments was analyzed. Proteins involved in folding and degradation that were significantly enriched in wild-type apoNQO1 pull-down in comparison to the interactome of the holoform and are shown.

in protein quality control activities appeared significantly enriched in apoNQO1 but not in holoNQO1 interactors set. Several chaperones and degradation factors were found to be more enriched under starvation conditions (Table 2). Curiously, TRIC chaperonin subunits were

ubiquitously identified in both conditions. From the eight different subunits that form this cytosolic chaperone complex (154), TCP1, CCT2, CCT4, CCT6, and CCT8 were enriched under both conditions, but only CCT5 and CCT7 interacted with apoNQO1. Association with chaperones HSPA8 and HSP90AB1 as well as co-chaperones DNAJA1 and DNAJA2 (all cytosolic) increased under starvation. HSPA8 is more commonly known as heat shock cognate 70 kDa protein (HSP70) and is expressed constitutively. HSP90AB1 is the main form of HSP90 in mammals and is also constitutively expressed (155). DNAJA1 and DNAJA2 are two of the most well-studied cytosolic HSP40 co-chaperones in mammals, which are mainly involved in protein folding together with HSP70 (156). Other important factors that are listed include the HSP90 co-chaperone AIP (also called FKBP37) and one subunit of the heterohexameric chaperone complex prefoldin (PFDN1). Two ER quality control-related proteins also appeared in the pull-down, namely TMX1 and TOR1A. A small subset of proteins involved in degradation was markedly enriched in apoNQO1 pull-down. Both ER co-chaperone SDF2L1 and ER membrane-bound E2 ubiquitin-conjugating enzyme UBE2J1 were found among the enriched partners in addition to another two transmembrane proteins involved in ERAD that act in coordination with the ATPase CDC48/p97, i.e. UBX domain proteins 4 and 8 (157). The co-chaperone SGTA binds to HSP70 and HSP90 and promotes the stabilization of substrates, especially androgen receptor (AR) (158). BAG6 protein is part of a heterotrimeric complex that protects mislocalized proteins from aggregation in the cytosol and takes care of their recycling process either by facilitating the transport into the ER or by promoting ubiquitin-dependent degradation (159,160) and it was also present in the pull-down. The results from this analysis provide a link between protein quality control and proteasomal degradation machinery in the context of NQO1 turnover under vitamin B2 deficiency where some of the most essential factors for protein folding and maturation are recruited to NQO1. The differences found in the pull-down experiment provide the first hint of how the protein quality control machinery deals with flavoproteins in the absence of the flavin cofactor *in vivo*.

The activity of the HSP70-HSP40 chaperone machinery, in coordination with HSP110, has been observed to be actively involved in the clearance of cellular aggregates in bacteria and eukaryotes (161,162). Thus, in the light of our pull-down results, we hypothesized that blocking the chaperone function of HSP70 would leave apoNQO1 in an “unguarded” state. Consequently, we expected the protein to bind other structures more avidly given the absence

of a holding agent. To investigate this, we used the HSP70 inhibitor VER-155008, which selectively binds to the chaperone nucleotide binding site (NBS) and acts as an ATP-competitor, impairing the chaperoning cycle (163). In order to test the effect of the HSP70 inhibitor on apoNQO1 aggregation, wild-type NQO1 was transfected into B16 F0 cells. After 24 h incubation in riboflavin-free medium and overnight treatment with MG132 and VER-155008, lysates were analyzed in BN-PAGE. As observed in previous experiments, a fraction of NQO1 moves slower within the native gel under deficient conditions (Figure 31, lane 3), an indication of protein binding to other structures and formation of high molecular complexes. These complexes were not present in the control sample (Figure 31, lane 1). The NQO1 smear did not appear under normal conditions when HSP70 inhibitor was added, but a significant increase in the high molecular weight fraction was displayed in samples treated with the

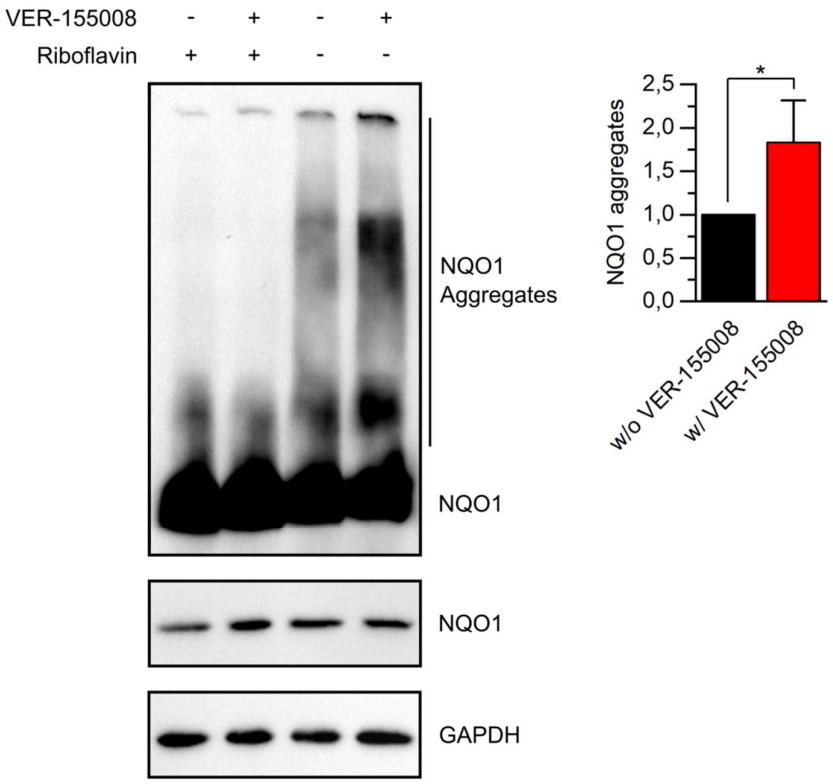

Figure 31. Inhibition of HSC70/HSP70 enhances aberrant interaction of NQO1 under riboflavin-deficient conditions. B16 F0 cells were transfected with wild-type NQO1 and cultured for 1 day under riboflavin-deficient conditions. 5 µM MG132 treatment was used throughout while 10 µM VER-155008 was only used when indicated. Both drugs were applied overnight. Lysates were obtained under native conditions and were used to perform BN-PAGE. The side bar of the immunoblot indicates the fraction of aggregated NQO1 used for quantification. A fraction of samples were used to run 10% SDS-PAGE (middle and lower panels). GAPDH levels were analyzed as loading control. Values were normalized to GAPDH and potted (n = 3, mean ± SD). T-test was used to assess the significance of the differences.

inhibitor compared to non-treated ones, both under starvation conditions (Figure 31, lanes 3 and 4). Again, from the SDS-PAGE, we could see that differences in aggregation did not occur as a consequence of protein expression variance.

3.6.1 Heat shock response is partially impaired in riboflavin-starved cells

An increase in the cellular AMP/ATP ratio triggers AMPK activation, a master regulator of metabolism whose activity is crucial to restore ATP levels and control its expenditure. The work carried out by Dai et al. (164) reveals a close relationship between metabolic and proteotoxic stress responses in NIH3T3 cells. The activation of AMPK either by metformin treatment or by glucose/amino acid deprivation triggers a metabolic stress response that inhibits HSF1 and, consequently, heat shock response in those cells. Conversely, proteotoxic stress diminishes metabolic response by reducing phosphorylation of AMPK at T172. As a vitamin, riboflavin is a key nutrient for the cell since it plays a central role in several biochemical processes. The functionality of many energy-related metabolic enzymes depends on riboflavin-derived cofactors FMN and FAD. Several flavoenzymes belong to the electron transport chain, a multicomplex domain located at the inner mitochondrial membrane which is the main source of ATP production in the cell. The destabilization effects we have previously observed at the proteome level in the absence of riboflavin might have an impact on the metabolic status of the cell, possibly by hampering ATP production. Hence, we reasoned that AMPK, as a master signaling molecule, could play a significant role in the cellular response to a stressful situation like riboflavin starvation. To assess this, melanoma cells were incubated for 1 and 3 days in riboflavin-free medium and the phosphorylation levels of AMPK were analyzed by western blot. No changes in phosphorylation were observed after 1 day incubation in riboflavin-deficient medium (Figure 32). Nevertheless, the levels of AMPK T172 increased by ca. 1.5-fold after 3 days starvation (Figure 32) while the levels of non-phosphorylated AMPK and GAPDH remained unaltered. The increase in AMPK phosphorylation by approximately 50% suggests that energy metabolism and therefore ATP production might be compromised due to vitamin starvation. The phosphorylation increase, however, was rather weak and delayed, suggesting that either metabolic stress is not strong enough or that the cell compensates the deficiency somehow. This result led us to assume that, in line with the work mentioned earlier (164), heat shock response in riboflavin-starved cells might be hindered. To test this, we decided to track the levels of heat shock protein 70

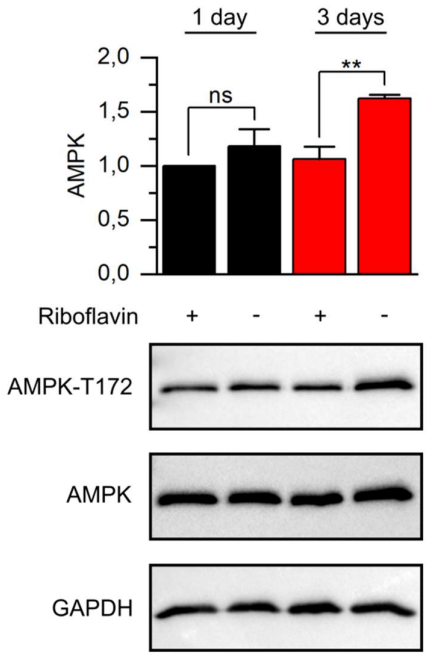

Figure 32. Riboflavin starvation activates AMPK. B16 F0 cells were incubated without riboflavin for 1 day (black bars) or 3 days (red bars). Lysates were run in 10% SDS-PAGE and the levels of total AMPK and phospho AMPK T172 were analyzed. Non-phosphorylated AMPK signal after 1 day starvation was set as 1. Protein values were normalized to GAPDH levels (n = 3, mean ± SD). T-test was performed to analyze the differences between normal and starvation conditions.

(HSP70), a well-known molecular chaperone that is highly induced upon protein-damaging stress due to HSF-1 transcriptional activation (165). B16 F0 cells were incubated for 2 days under riboflavin deficiency and then heat shock was applied for 1 h at 45ºC. Kinetics studies showed that proteotoxic stress response in mammalian cells is quite fast since maximal expression of key proteostasis-related genes peaks within a few hours after stress (166). Taking this into account, cells were incubated at 37ºC for 5 h post-heat shock and harvested to analyze changes in HSP70 protein expression levels. As expected, HSP70 protein was not detected in non-stressed cells. Surprisingly, chaperone induction showed a strong dependency on the presence of riboflavin. The absence of the vitamin affected the response to the stress given the ca. 5-fold decrease in HSP70 expression compared to normal conditions (Figure 33A). By boosting catabolic pathways while inhibiting anabolic ones, cells improve survival upon starvation. Due to the high energetic cost that it entails, protein translation is usually blocked through different mechanisms, for instance via AMPK activation (167). If so, the changes in expression levels found previously (Figure 33A) cannot be directly attributed to a defect in the heat shock response. Therefore, a proper control that evaluates translation under

riboflavin-free conditions was needed. To this end, an ubiquitin-EGFP reporter expression plasmid was used (Figure 33B, upper scheme). A single ubiquitin molecule is linked to EGFP through its C-terminal end. The glycine at position 76 (the last amino acid of ubiquitin) was

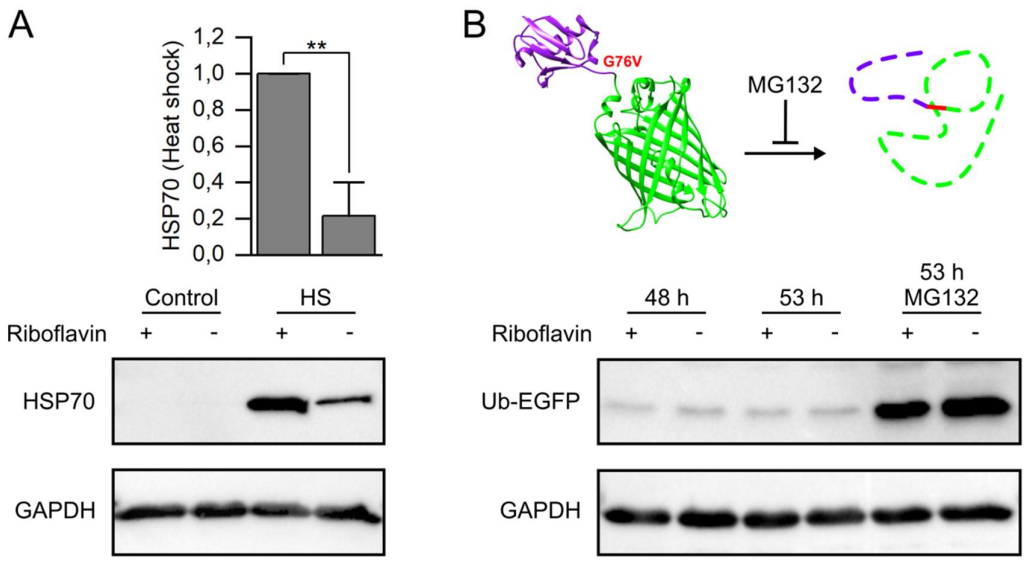

Figure 33. Riboflavin deficiency impairs heat shock response. (A) B16 F0 cells were incubated for 2 days in the absence of riboflavin. On the second day, 45ºC heat shock (HS) was applied for 1h. Afterwards, cells were incubated in normal conditions (37ºC) for 5 h and HSP70 expression was analyzed. HSP70 induction after heat shock under normal conditions was set as 1. Values were normalized to GAPDH. (B) Ubiquitin-EGFP fusion construct was used to evaluate translation rate in riboflavin-starved cells. Upon translation, EGFP is immediately degraded due to the irreversibly bound ubiquitin located at its N-terminus (upper scheme). Upon proteasome inhibition the fusion protein can accumulate. B16 F0 cells were transfected with this construct and incubated 2 days in riboflavin-depleted medium. 50 µM MG132 treatment was applied for 5 h and GFP accumulation was analyzed by immunoblot.

changed to valine. This substitution renders ubiquitin non-cleavable. Consequently, the fusion protein is degraded by the 26S proteasome shortly after synthesis. B16 F0 cell were transfected with this construct and incubated for 2 days in riboflavin-free medium. Proteasome inhibitor MG132 was added and incubation was prolonged for 5 h. Ubiquitin-EGFP accumulation can only occur when protein degradation is stopped and thus translation rates can be analyzed by the extent of this accumulation. GFP western blot revealed that very few of the protein is present without the inhibitor. The thick bands that appeared upon MG132 addition revealed a strong accumulation of the protein when proteasome activity is blocked (Figure 33B). EGFP accumulation did not change under vitamin starvation, arguing for an equal translation rate in both conditions. Since protein synthesis seemed to be active, we

concluded that the impaired proteotoxic stress response can be attributed to the riboflavin starvation and not to different protein translation rates in both conditions.

3.7 Riboflavin deficiency affects cellular response to HSP90 inhibitors and alkylating agents

Some drugs that are commonly used in the clinics have little or no toxicity in their original form and hence need to be first metabolized by the cellular enzymatic machinery (168). As an oxidoreductase, NQO1 is one of the most important enzymes that catalyzes the reduction of several quinone and benzoquinone-derived compounds, transforming them into more active derivatives (169). 17-AAG belongs to a benzoquinone family of HSP90 inhibitors that has been extensively investigated over the recent years because of the anti-tumoral capacity they show. The anticancer activity of 17-AGG directly depends on the two-electron reduction by NQO1 (170). The activity of HSP90 is especially important in the context of signal transduction, since it participates in the folding of many kinases and protects them from proteasomal degradation (171). Our experimental data suggests that changes in NQO1 protein

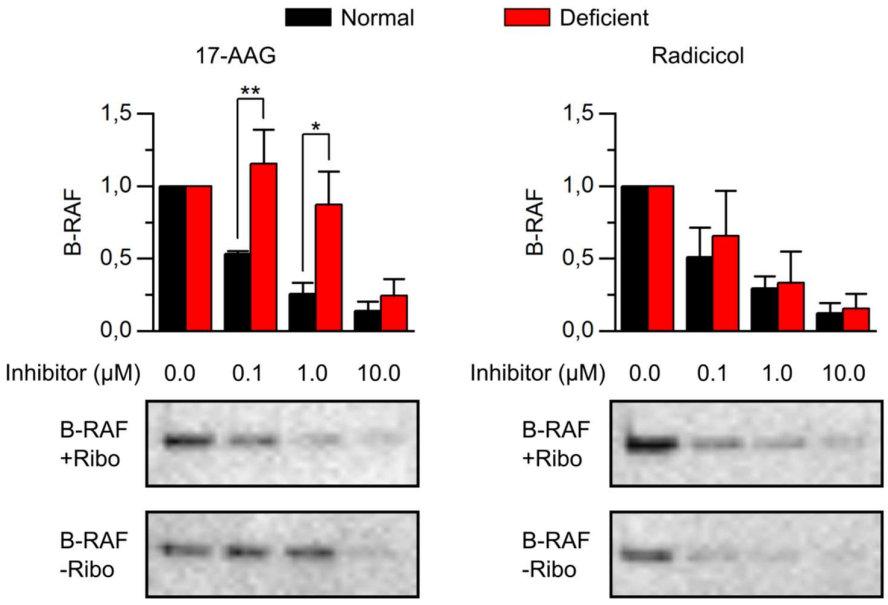

Figure 34. Cellular sensitivity to the HSP90 inhibitor 17-AAG is controlled by NQO1 activity and depends on riboflavin levels. B16 F0 cells were transfected with B-RAF V600E and cultured in riboflavin-deficient medium for 34 h. Increasing concentrations of either 17-AAG (left) or Radicicol (right) were added for 14 h to assess the efficiency of HSP90 inhibition. This was done by measuring the levels of the HSP90 client kinase B-RAF V600E by immunoblot (n = 3, mean ± SD). The signal for B-RAF protein in untreated cells was set as 1 in both experiments. T-test was used to analyze the significance of the differences between control and starved cells.

levels due to variations in the cofactor availability should affect the sensitivity of cells to 17-AAG treatment. Under starvation conditions cells should become insensitive to the inhibitor. To test this assumption we decided to monitor the degradation of the B-RAF oncogenic mutant V600E, a known HSP90 substrate that is degraded upon chaperone inhibition (172). Melanoma cells were transfected with B-RAF V600E, cultured for 34 h under riboflavin-deficient conditions and treated with increasing concentrations of 17-AAG for another 14 h. As a control, the same experiment was repeated using radicicol, an HSP90 inhibitor that is structurally different from 17-AAG and that does not require biotransformation by NQO1 (170). B-RAF V600E protein levels decreased in the presence of both HSP90 inhibitors in a concentration-dependent manner under normal conditions. However, the deleterious effect of 17-AAG on the mutant stability was clearly weakened in riboflavin-starved cells (Figure 34, left). For the lowest and intermediate concentrations of 17-AAG, no changes in B-RAF V600E levels were observed compared to non-treated cells. A high concentration of 17-AAG was needed to trigger degradation of the oncogenic kinase (Figure 34, left). In this case, the high amount of inhibitor is probably overloading the metabolic capacity of NQO1. Using radicicol as HSP90 inhibitor showed no differences between normal and vitamin-deficient conditions (Figure 34, right). The decrease in B-RAF stability was the same for all the

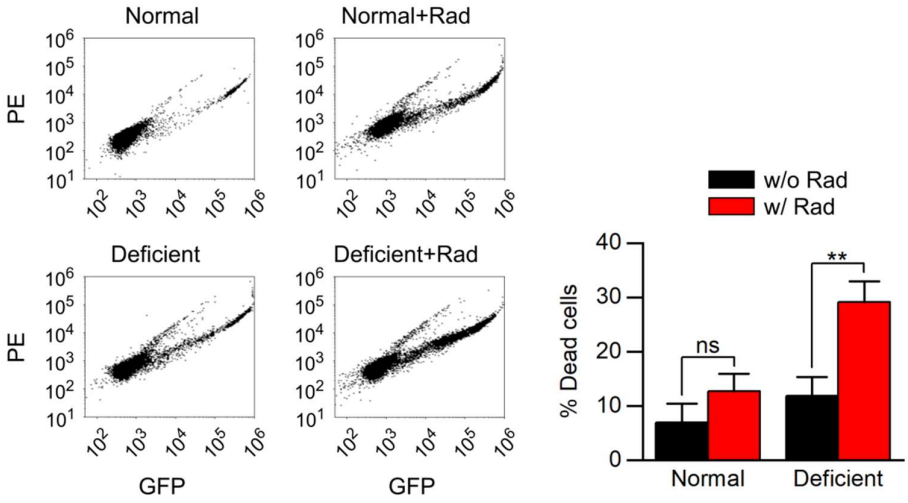

Figure 35. Riboflavin-starved cells treated with radicicol show reduced viability. B16 F0 cells were cultured for 2 days in medium depleted of riboflavin. 5 µM radicicol was added and incubation was continued under the same conditions for 36 h. Both supernatant and cells were collected and stained with SYTOX green (30 nM). Flow cytometry was used to analyze and quantify cell death. PE vs GFP 2D graphs are shown with the conditions used for each sample specified. The data were analyzed using the FCS Express 5 software. Percentages of dead cells are plotted (n = 3, mean ± SD). T-test was used to analyze the significance of the differences.

concentrations tested, independently of the cell culture conditions used. The differences observed between both inhibitors reflect the functional consequences associated with riboflavin deprivation.

Cellular proteostasis is at a constant balance. Stressful situations can be counteracted by specific cellular responses that aim at diminishing possible detrimental effects (10). According to our proteomics data, riboflavin deficiency is associated with the destabilization

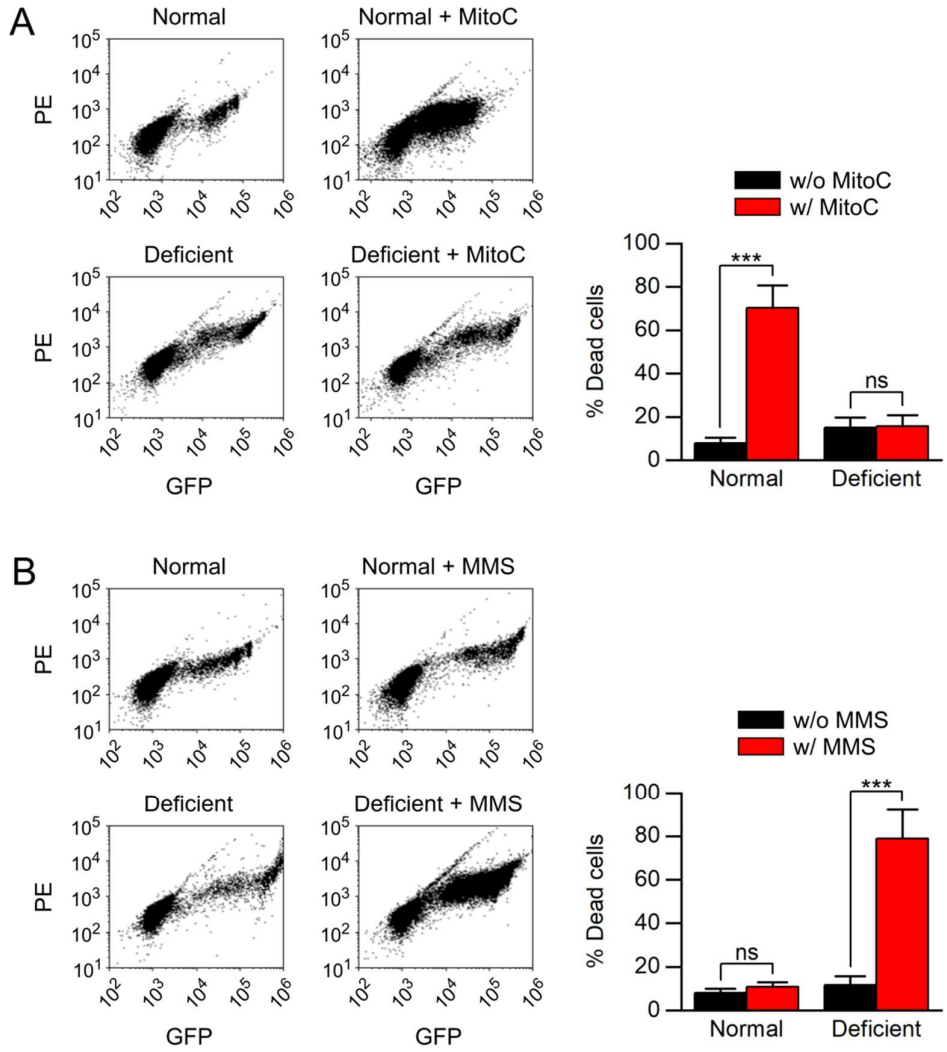

Figure 36. Cells lacking riboflavin show decreased sensitivity to Mitomycin C and increased sensitivity to MMS. B16 F0 cells were cultured for 3 days in medium without riboflavin. Either 100 µM Mitomycin C (A) or 500 µM MMS (B) were applied for 24 h. Both supernatant and cells were collected and stained with SYTOX green (30 nM). Flow cytometry was used to determine the percentage of dead cells. PE vs GFP 2D graphs are shown with the conditions used for each sample specified. The data were analyzed using the FCS Express 5 software. Percentages of dead cell populations are plotted (n = 3, mean ± SD). T-test was used to analyze the significance of the differences.

and degradation of flavoproteins. Actually, this situation might pose a large burden on the protein quality control system, which is in charge of detecting and eliminating non-functional proteins to avoid proteome damage in form of aggregation. We hypothesized that chaperone inhibition would disrupt this balance and thus have a negative impact on the cell viability under riboflavin-free conditions. B16 F0 cells were incubated for 2 days without riboflavin and radicicol treatment was applied for additional 36 h. SYTOX green staining was used to identify dead cells, which were quantified by flow cytometry. The effect of HSP90 inhibitor radicicol was stronger in riboflavin-starved cells, in which a 2.5-fold toxicity increase was observed. For non-starved cells, differences were not significant (Figure 35).

Mitomycin C is a quinone-derived molecule well-known for its anti-tumoral properties. The investigations performed by Ross et al. (173) showed that NQO1 reduces and activates Mitomycin C, which then binds covalently to DNA and has cytotoxic effects in cells. Similarly as for the HSP90 inhibitors above, cell sensitivity to Mitomycin C was investigated after 3 days starvation, expecting to find differences in toxicity compared to normal conditions. The activation-independent alkylating agent MMS was used in parallel as a negative control. Cells were treated for 24 h with Mitomycin C or MMS and dead cells were quantified using SYTOX green staining. As predicted, the toxic effect exerted by Mitomycin C was much higher (ca. 10-fold higher) in cells cultured under normal conditions in comparison to vitamin B2-free conditions (Figure 36A). Vitamin depletion rendered cells completely insensitive towards the drug, since lack of NQO1 activity prevented activation of Mitomycin C. Unexpectedly, the use of MMS had an unpredicted result. While cells incubated under normal conditions were not killed in the presence of MMS, cells incubated under starvation conditions displayed increase sensitivity. The increment of the dead population reached ca. 5 to 6-fold levels in comparison to non-treated cells (Figure 36B). Both Mitomycin C and MMS reaction mechanisms are shown in Figures 52 and 53, respectively.

3.8 Riboflavin starvation causes metabolic reprogramming in B16 F0 cells

The metabolic response that was observed upon AMPK activation (Figure 32), even if weak, suggests that cells reacted to the starvation. We wanted to investigate how adaptation to starvation occurred in melanoma cells and which proteome rearrangements were at the center of this process. This could provide a valuable insight for two reasons: first, it would help us to better understand why riboflavin-starved cells show an increased sensitivity towards MMS;

secondly, additional liabilities for novel therapeutic approaches under these conditions could be elucidated. Adjusting protein expression levels is useful for cellular adaptation to a challenging environment. Thus, we decided to carry out an exhaustive re-analysis of the mass spectrometry data presented before (Figures 7 and 8) looking for functional cluster variations. Initially, we compared the stability of the flavoproteome versus the rest of the proteome by quantifying expression changes in cells incubated in normal and riboflavin-free medium. Ratios between normal and deficient conditions were calculated from mass spectrometry

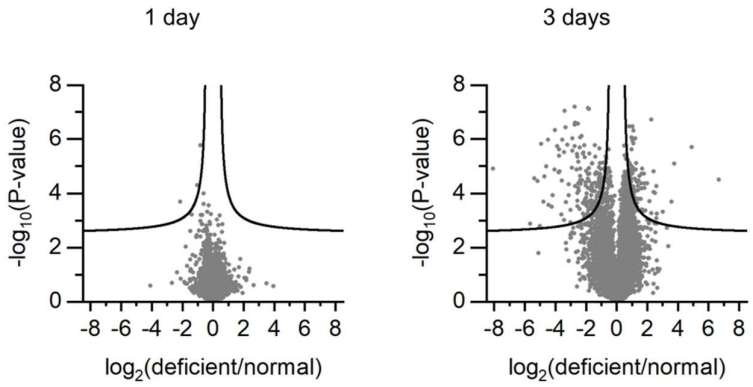

Figure 37. Riboflavin starvation for 3 days changes B16 F0 proteome. B16 F0 cells were cultured for 1 day (left) or 3 days (right) in riboflavin-deficient medium. Proteomics analysis by means of mass spectrometry was performed. Deficient over control intensity ratios were calculated for each quantified protein and log_2-transformed. Means of at least three different valid ratios were calculated and plotted. T-test was performed to evaluate significant changes of the means obtained for each hit by setting a false-discovery-rate (FDR) cut-off of 0.001 (0.1%).

quantification analysis. Compared to 1 day incubation without riboflavin, when expression changes are mostly negligible, a total of 88 proteins were found to be significantly enriched and 162 reduced after 3 days starvation according to a false discovery rate threshold of 0.1% (Figure 37). GO enrichment analyses were performed for enriched and reduced sets using "process" as the sorting category. From the group of enriched proteins, pyruvate metabolic cluster was especially increased. This group contained 10 hits corresponding to enzymes that are involved in the catabolism of glucose (Figure 38, upper left). From those, 7 enzymes participate in glycolysis, the metabolic pathway that transforms glucose into two three-carbon pyruvate molecules. Pyruvate dehydrogenase kinase isozymes 1 and 3 (PDK1/3) as well as lactate dehydrogenase A (LDHA) were also changed. The first two enzymes phosphorylate pyruvate dehydrogenase complex, leading to its inhibition, while the latter catalyzes the transformation of pyruvic acid into lactic acid at the expense of reducing power in the form of NADH. GO enrichment analysis of the depleted hits revealed that riboflavin deficiency had a

severe effect on three main groups of proteins, namely electron transport chain, sterol biosynthesis, and cell cycle (Figure 38, upper right and bottom).

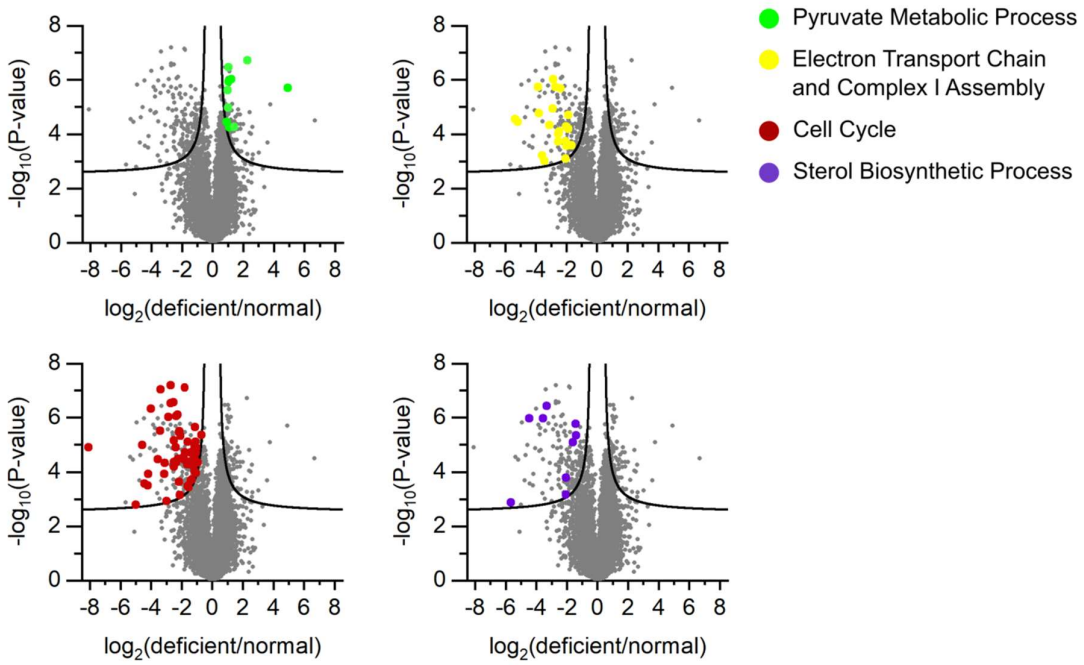

Figure 38. Expression of proteins involved in anaerobic catabolism is increased in melanoma cells after 3 days of riboflavin starvation, while proteins involved in aerobic catabolism, sterol biosynthesis and cell cycle are reduced. B16 F0 cells were cultured for 3 days under riboflavin-deficient conditions. Proteomics analysis by means of mass spectrometry was performed. Deficient over control intensity ratios were calculated for each quantified protein and $\log_2$-transformed. Means of at least three different valid ratios were calculated and plotted. T-test was performed to evaluate significant changes of the means obtained for each hit by setting a false-discovery-rate (FDR) cut-off of 0.001 (0.1%). GO terms are indicated and color-coded.

A closer look at the oxidative phosphorylation group showed that 16 proteins were markedly reduced; 13 proteins are directly involved in ATP production through oxidative

	Gene ontology term	Cluster frequency
Enriched (88)	Pyruvate metabolism	11.4% (10/88)
Depleted (162)	Electron transport chain	9.8% (16/162)
	NADH dehydrogenase complex assembly	8.0% (13/162)
	Cell cycle	38.8% (63/162)
	Sterol biosynthesis	5.5% (9/162)

Table 3. GO enrichment analysis of cell proteome under riboflavin starvation. Significantly reduced and increased hits obtained from proteome analysis of riboflavin-starved cells were used for GO enrichment analysis using GO Term Finder tool (Princeton University) and a p-value threshold of 0.01. GO category "process" was used. The hits found are listed in table 4 (See appendix section 6.4).

phosphorylation; 11 of them belong to the multi-subunit protein complex I of the respiratory chain, also known as NADH:ubiquinone oxidoreductase (174). NADH dehydrogenase complex assembly cluster was also very prominently reduced; 6 hits from this group belong to the electron transport chain group as well. However, they were originally classified separately as indicated in Table 3. In this work they are referred to as electron transport chain group for simplicity reasons and in Figure 38 they are grouped. Mammalian NADH:ubiquinone oxidoreductase (electron transport chain complex I) is a 45 subunit complex that is located on the inner mitochondrial membrane (174). The complex contains 14 core subunits, seven of which are encoded by the mitochondrial DNA (ND1 to ND6 and NDL4) and form a hydrophobic structure embedded in the inner mitochondrial membrane. The rest (NDUFS1, 2, 7, and 8 together with NDUFV1, and 2) are encoded by the nuclear DNA and form a hydrophilic arrangement facing the matrix of the mitochondria. The remaining 31 proteins are known as supernumerary or supplementary subunits (175). In our analysis, 13 supplementary subunits (NDUFB8, NDUFA8, NDUFA10, NDUFS4, NDUFS6, NDUFB3, NDUFA7, NDUFA11, NDUFB7, NDUFA9, NDUFA2, NDUFA13, and NDUFS5) plus 5 from hydrophilic core (NDUFS1, NDUFV1, NDUFV2, NDUFS7, and NDUFS8) were found to be reduced. NDUFV1 is a key subunit, as it holds the FMN cofactor within the complex that mediates electron transfer to the ubiquinone pool of mitochondrial membrane. Additional 3 members from complex I hydrophobic core were found in mass spectrometry analysis too, but had not been initially identified by the GO software analysis. They comprise subunits ND5, ND6, and ND4L. Nevertheless we also include them in this group given their importance in the assembly, structure, and functionality of NADH dehydrogenase complex (174). *ETFDH* gene encoding the electron transfer flavoprotein: ubiquinone oxidoreductase (ETF:QO) was partially depleted as well. This inner mitochondrial membrane protein mediates the transfer of electrons coming from β-oxidation of fatty acids to the ubiquinone (also known as coenzyme Q10) of the electron transfer chain and thus is a key member of the oxidative phosphorylation machinery that links fat degradation with energy production (176). The two hydrophilic and catalytic subunits of the electron transport chain complex II, namely SDHA and SDHB also decreased under riboflavin starvation. As the complex II oxidizes succinate to fumarate, it links the respiratory chain and TCA cycle (177).

Surprisingly, more than 60 different proteins out of 162 depleted ones (ca. 40%) are involved in cell cycle regulation. From the GO analysis we could observe that this cluster was very

heterogeneous. Several subgroups were merged into the one set that is shown in Figure 38 and Table 3 with the name “Cell cycle”. Within this group, a plethora of factors integrating signaling activities, DNA replication, DNA repair and chromosome organization were markedly depleted. These proteins regulate cell cycle progression through diverse mechanisms. Some examples include the G2/M regulator CDK1/Cyclin B1 complex, the G1 to S phase promoter CDK2, CDK-regulatory factor CSK2, and UHRF1, an expression regulator of several mitotic genes. The expression of two subunits of the anaphase promoting complex (APC), namely APC2 and APC7, also went down. The function of APC in targeting cell cycle proteins for degradation is vital in the transition from metaphase to anaphase (178). UBE2S, the E2 enzyme that enhances the degradation of APC substrates, was also in this group. The levels of the catalytic subunit of DNA polymerase alpha (POLA1) and cofactor subunit of DNA polymerase delta (PCNA) as well as two DNA helicases (HELLS and SMARCAD1) were reduced. DNA repairing machinery seemed to be affected as well. HELLS, SMARCAD1, and PCNA are also involved in DNA damage repair. Other factors include FANCD2, NOP53, LIG1, CDK2, and ATAD5. Several proteins involved in chromosome condensation, integrity, and segregation were significantly depleted as well. Among them, 2 histone acetyltransferases (NAA40, and HAT1), 4 members of the structural maintenance chromosome complex (SMC1A, SMC2, SMC3, and SMC4) and two factors of chromosome condensation complexes (NCAPD3, an NCAPG) were depleted. The levels of MIS12, DSN1, CEP55, HAUS1, and AURKA, all members of the mitotic spindle as well as histone assembly factor CHAF1B were also reduced under riboflavin starvation.

The last group of depleted proteins that is indicated in Table 3 encompasses 9 enzymes from the sterol biosynthetic pathway. From these, 6 are directly involved in the mevalonate pathway, a multi-step process that produces cholesterol and other isoprenoids. Apolipoprotein E (APOE) and cytochrome P450 reductase (POR) were also enriched but are not directly involved in this anabolic pathway. Cytochrome P450 reductase works as the obligate electron donor for microsomal cytochrome P450 enzymes (179), one of which is responsible for demethylating lanosterol during its enzymatic conversion into cholesterol (180).

Finally, a different GO enrichment analysis was performed using “component” as sorting category instead of “process”. Genes associated with lysosomal function, especially lysosomal hydrolases, were found to be upregulated (p-value of the GO term = 2.24×10^{-8}). Some enzymes (NAGA, GM2A, GUSB, and MAN2B2) are involved in the degradation of

complex sugar molecules like gangliosides, glycosaminoglycans, D-mannosides but also of glycoproteins and glycolipids. Some petidases (CTSD, CTSA, and DPP7) were upregulated as well. Interestingly, senescence-related β-galactosidase protein (GLB1 gene) increased by ca. 2-fold (p-value = $1.82x10^{-5}$) under riboflavin deprivation compared to normal conditions.
The extensive proteome analysis we carried out revealed the multiplicity of changes at the expression level in B16 F0 cells under riboflavin starvation and thus provides a new platform for the search of novel cell liabilities. Next, we decided to perform a series of biochemical experiments to verify the differences found in mass spectrometry.

3.8.1 Cell cycle arrest

Strikingly, many proteins involved in cell cycle progression were found to be depleted under starvation in comparison to normal conditions. This prompted us to investigate the proliferation capacity of B16 F0 cells. Given our previous observations, we expected vitamin B2 deficiency to have a severe impact on cellular proliferation. To test this, B16 F0 cells were incubated for 3 days without riboflavin and a 5 h bromodeoxyuridine pulse was carried out to label newly synthesized DNA. The incorporation of BrdU into the replicating DNA was detected using an anti-BrdU antibody conjugated with Alexa Fluor 488. Fluorescent images revealed that the incorporation of the thymidine analog was greatly diminished in starved cells (Figure 39A). DAPI staining was also performed in order to have a positive control for nucleus integrity. DIC images were taken to exclude confluence-derived artifacts. To study this phenomenon in more detail, cell cycle analysis was carried out. Riboflavin-starved cells for 3 days were fixed in ethanol and stained with propidium iodide (PI). The binding of this dye is proportional to the amount of DNA present in the cell and hence makes PI staining a suitable technique for cell cycle analysis. Flow cytometry analysis of PI fluorescence showed typical cell cycle profiles (Figure 39B, right). The two peaks correspond to G1 and G2/M phases (from lower to higher intensity of PI signal, respectively). The region in the middle is normally assigned to the DNA replication or S phase. The percentage values for each of the three cell populations were obtained. Significant differences were observed for phase periods of the cell cycle between normal and starvation conditions. The number of G1 and G2/M cells increased by 20% and 55%, respectively. On the contrary, cells undergoing DNA replication dramatically decreased (Figure 39B, left). This result shows a clear accumulation of non-proliferative cells and reduction of proliferative ones. Cyclin-dependent kinase 1 (CDK1) promotes cell progression by targeting key factors, especially during G2/M phase (181). The

protein levels of this master regulator were reduced by ca. 7-fold according to mass spectrometry. Hence, we wanted to verify this effect biochemically. The protein levels of

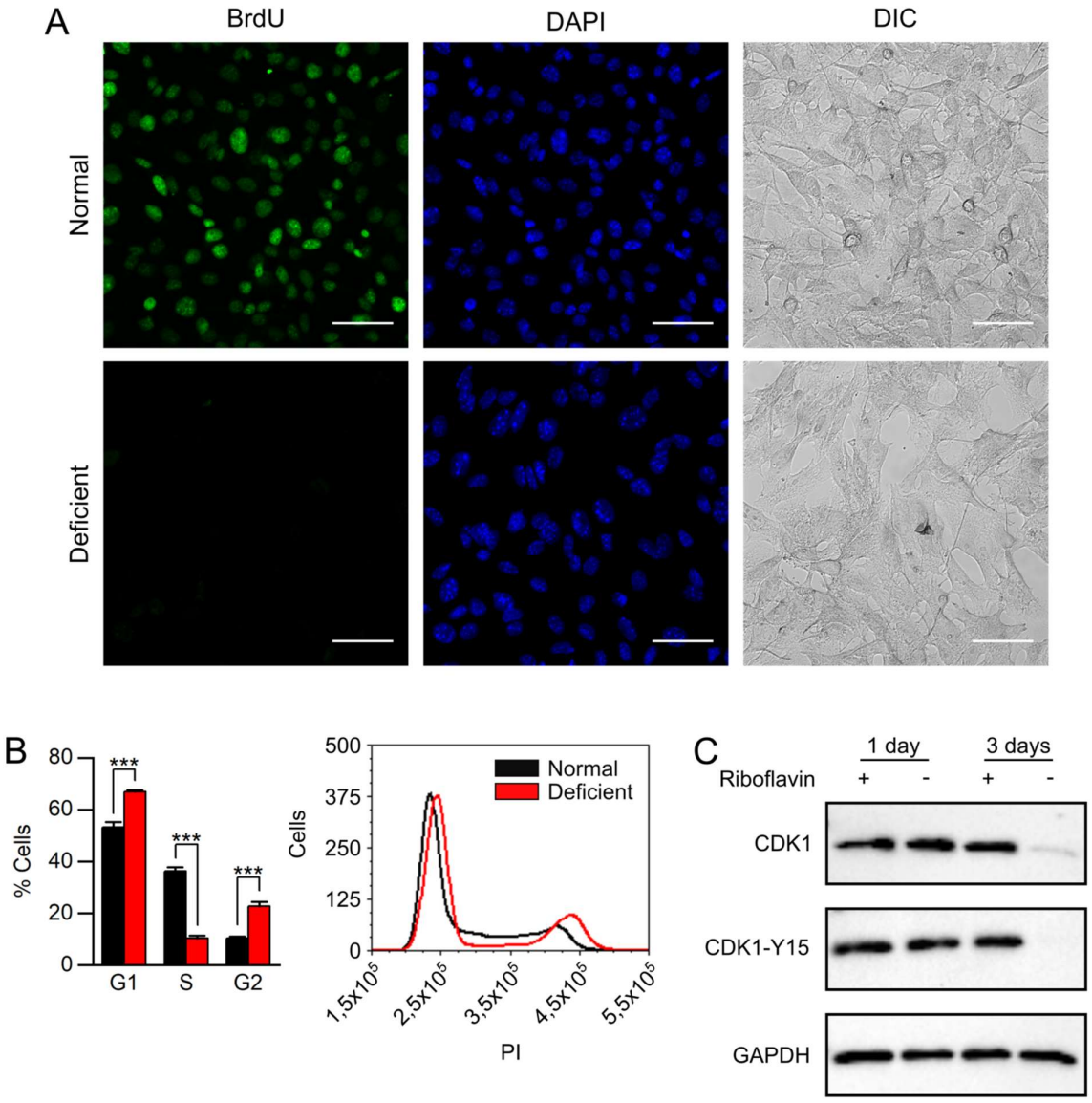

Figure 39. Riboflavin deficiency inhibits proliferation in B16 F0 cells. (A) B16 F0 cells were cultured under riboflavin-deficient conditions for 3 days. 5 h BrdU pulse was carried out and anti-BrdU Alexa Fluor 488 antibody was used to detect incorporated BrdU. Fluorescence signal was detected using a Zeiss LSM 780 confocal microscope (scale bar: 50 µm). DAPI and DIC images are also shown. ImageJ was used to analyze the images. (B) Cell cycle analysis of B16 F0 cells was performed after incubating cells for 3 days without riboflavin. Propidium iodide (PI) was used to stain DNA. Cell cycle profiles were analyzed using the Multi-Cycle DNA tool from FCS Express 5 software. The percentage values for each population (G1, S, and G2) were averaged and plotted (left) (n = 3, mean ± SD). T-test was used to analyze the significance of the differences between means. One representative cell cycle profile is shown (right). (C) The protein levels of cyclin-dependent kinase 1 (CDK1) and CDK1 phosphorylated at tyrosine 15 (Y15) were analyzed in B16 F0 cells after 1 day or 3 days starvation by immunoblot. GAPDH was used as a loading control. One representative experiment is shown.

CDK1 and its inactive phosphorylated form CDK1-Y15 were analyzed in cells after 1 or 3 days incubation without riboflavin. Immunoblotting results showed a drastic reduction in both non-phosphorylated and phosphorylated kinase after 3 days of riboflavin deprivation (Figure 39C). No changes in CDK1 were observed after shorter starvation (1 day) in agreement with cell cycle results as well.

Checkpoint kinase 1 (CHK1) controls the correct activation of the cell cycle-associated checkpoint response. This protein is mainly activated by phosphorylation upon DNA damage, which then prevents a premature entry of cells into mitosis by regulating the number of replication origins and the rate of fork progression. CHK1 function is also necessary for the correct replication of DNA in non-stressed cells (182,183). While the levels of this protein remained unchanged after a short-term starvation (1 day), it could not be detected by mass spectrometry analysis after 3 days starvation. Fork elongation machinery was affected

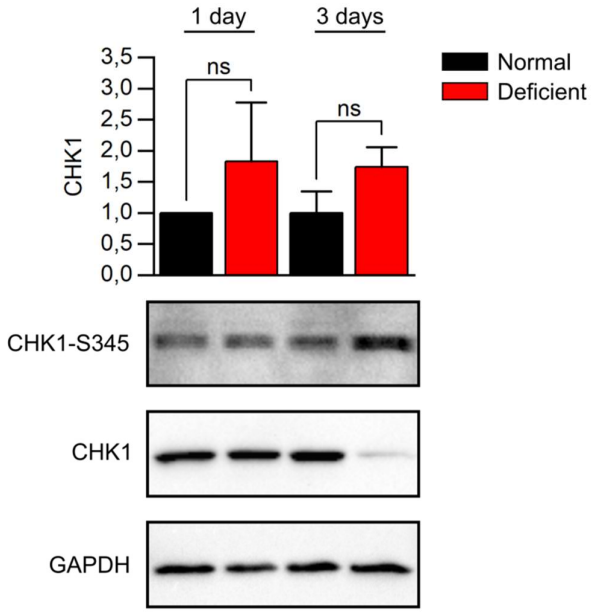

Figure 40. CHK1 levels are strongly reduced but its total phosphorylation is not affected under riboflavin starvation. The levels of checkpoint kinase 1 (CHK1) were analyzed in B16 F0 cells that had been cultured for 1 or 3 days in riboflavin-depleted medium. Lysates were analyzed by immunoblot. CHK1 (phospho S345) levels under control conditions (1 day) were set as 1. Protein values were normalized to GAPDH levels (n = 3, mean ± SD). T-test was performed to analyze differences between means.

according to proteomics analysis and thus we carried out an immunoblot assay to evaluate the levels of the enzyme and its active phosphorylated form (phospho S345). The western blot revealed a very strong reduction of CHK1 in B16 F0 cells after 3 days starvation. Unexpectedly, the levels of CHK1 (phospho S345) were slightly higher in starved cells

compared to normal conditions for the two times analyzed, although not statistically significant (Figure 40, lanes 2 and 4). The overall CHK1 activation did not differ from normal conditions. However, it must be taken into account that the total pool of non-phosphorylated kinase remained much lower under longer starvation (Figure 40, lane 4).

3.8.2 Gain of MMS sensitivity in serum-starved cells

We wondered whether the effect observed upon MMS treatment was specific for riboflavin deficiency or was related to cell cycle stop. By inducing a proliferation stop of B16 F0 cells by different means, we aimed to answer this question. Melanoma cells were incubated in serum-free medium. By removing growth factors from culture medium, cells reduced their proliferation rate, which was confirmed by cell cycle analysis (Figure 55). However, the cell cycle profile was not identical to the one observed after vitamin B2 starvation. Serum withdrawal resulted in the accumulation of cells in G1 and in the reduction of the DNA-replicating population. The percentage of G2/M cells did not change after 1 day and even

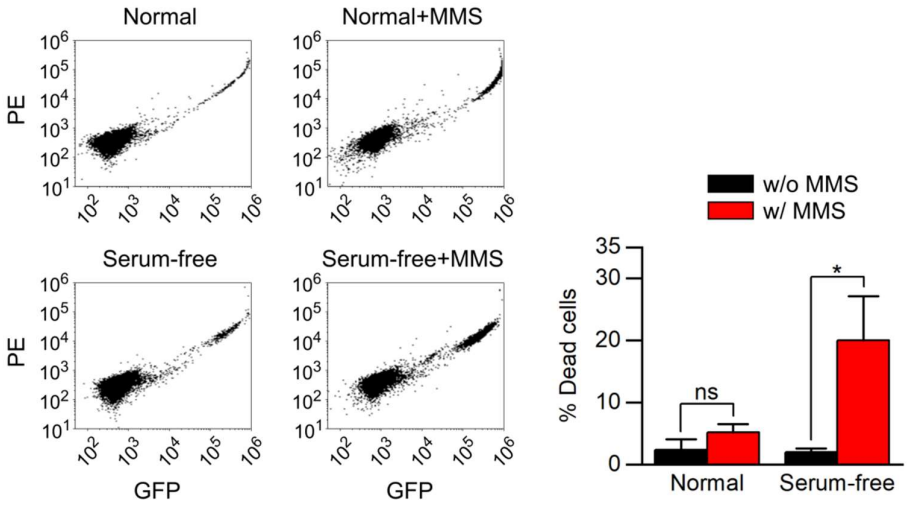

Figure 41. Serum-starvation increases MMS sensitivity in B16 F0 cells. B16 F0 cells were incubated for 1 day in serum-free medium and treated with 500 µM MMS for 24 h. Cells were harvested and stained using SYTOX green solution (30 nM). Cell viability was analyzed and quantified by flow cytometry. Data were analyzed using the FCS Express 5 software. PE vs GFP 2D graphs are shown with the conditions used for each sample indicated. Percentages of dead cells are plotted (n = 3, mean ± SD). T-test was used to analyze the significance of the differences.

decreased after 2 days, opposite to the significant increase in G2/M population under riboflavin deficiency. Next, serum-starved B16 F0 cells for 1 day were treated for additional 24 h with 500 µM MMS while continuing the serum starvation. Interestingly, sensitivity to the alkylating agent increased by ca. 10-fold in the absence of serum (Figure 41). This effect

indicated that MMS sensitivity could be induced by inhibiting cell proliferation using another strategy than vitamin B2 deprivation.

3.8.3 Impairment of oxidative phosphorylation

Vitamin B2 deficiency resulted in the decreased expression of more than 20 electron transport chain proteins according to mass spectrometry data (Figure 38). The lack of ETF:QO and several subunits from complex I and complex II led us to assume that cell respiration should be highly compromised as a consequence of vitamin B2 starvation. To test this assumption biochemically, high resolution respirometry assays were performed. Cells were starved for 3 days in medium lacking riboflavin and oxygen consumption rates were measured using oxygraph-2k. Remarkable differences were observed between basal respiration rates in control and starvation conditions. Oxygen consumption was 2.56-fold higher under normal conditions (Figure 42B). It is known that oxygen consumption rate correlates with the ATP/ADP ratio within the cell. The levels of ADP regulate the electron flow through the electron transport chain and control the synthesis of ATP according to the demands of the cell (184). Respiration levels became similar when cells were permeabilized with digitonin (leak) due to the absence of sufficient ADP in the chamber. Addition of non-limiting amounts of ADP together with complex I substrates malate, pyruvate, and glutamate triggered a remarkable increment of the oxygen consumption rate in control cells only while no increase was observed in starved cells (Figure 42A). Addition of complex II substrate succinate increased respiration in both conditions. Uncoupling agents are compounds that possess protonophoric activity, i.e. the ability to transport protons across proton-impermeable membranes. Consequently, the use of these compounds disrupts the mitochondrial membrane potential whose proton-motive force drives ATP production in cells (185). The protonophore treatment renders respirometry rates insensitive to ADP levels. Hence, the use of uncoupling agents in respirometry assays is useful to assess the maximum electron flux capacity that electron transport chain can sustain (ETS). The uncoupling agent FCCP was used after succinate addition, and substantial increments in respiration were observed after repeated injections of the compound in cell chambers. The same treatment showed only a milder increase in maximal respiration in starved cells (Figure 42A and B, ETS). The ratio between control and starved conditions for leak, CI, CI+CII, and ETS values was calculated. This ratio allowed us to compare at which step changes between control and vitamin-deficient conditions are more pronounced. Figure 42C shows that a major increase in respiration exists

between leak and complex I measurements, indicating that complex I activity is highly compromised under vitamin deprivation. No such increase was observed when comparing the ratios of CI+CII and ETS to CI.

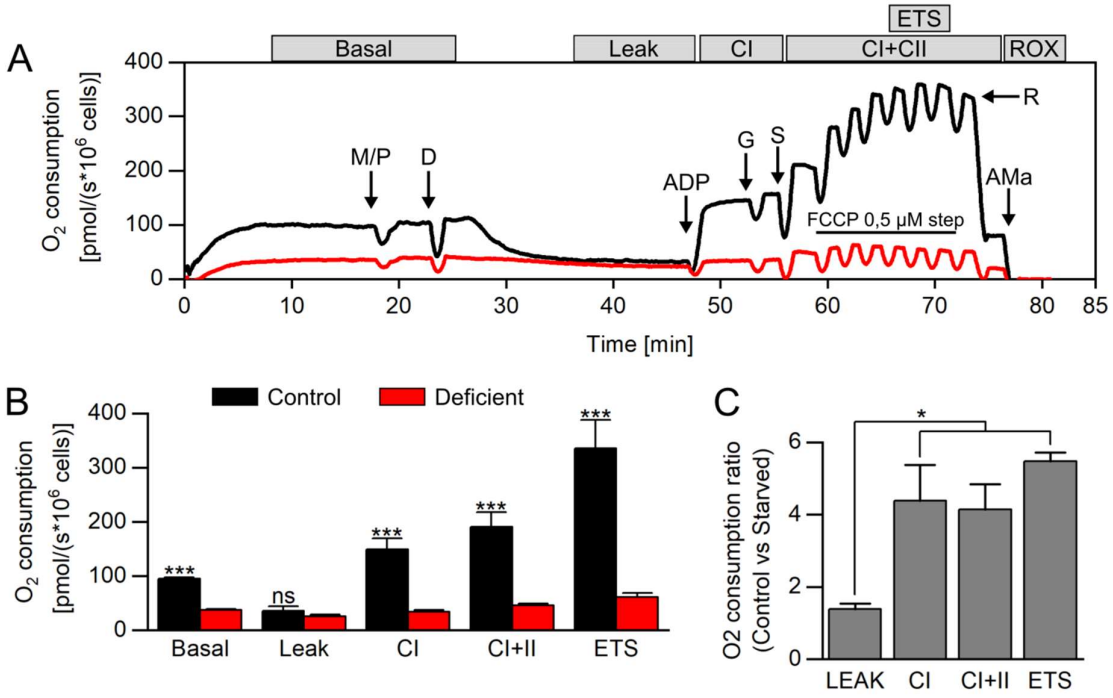

Figure 42. The functionality of the electron transport chain in riboflavin-starved B16 F0 cells is impaired. (A) B16 F0 cells were incubated for 3 days in riboflavin-deficient medium and high resolution respirometry experiments were performed. Oxygen consumption rates were measured in Oxygraph-2k and normalized to the number of cells. Oxygen consumption traces were allowed to stabilize for ca. 10 min in the absence of any treatment (basal respiration). Treatments were then applied sequentially: 2 mM malate (M); 2.5 mM pyruvate (P), 1.5 µg/ml digitonin (D), 2.5 mM ADP, 10 mM glutamate (G), 10 mM succinate (S), 0.5 µM steps FCCP, 0.5 µM rotenone (R), and 2.5 µM antimycin A (AMa). ROX stands for residual oxygen consumption. (B) Rates for basal, leak, complex I (CI), complex I and complex II (CI+CII), and electron transport system (ETS) were calculated using values obtained from stable readings of (A) and plotted (n = 3, mean ± SD). (C) The ratio between control and starved conditions for leak, CI, CI+CII, and ETS respiration was calculated (mean ± SD). T-test was used to analyze the significance of the differences in (B), while ANOVA test was used in (C).

3.8.4 Decrease of cholesterol levels

Mass spectrometry revealed that cholesterol synthesis pathway was highly suppressed in the absence of riboflavin, since several enzymes of the mevalonate pathway were partially depleted. HMG-CoA reductase was the most depleted enzyme within this group. Reduction reached a factor of 50 [$\log_2$ (deficient/normal) = -5.66] in comparison to control conditions. HMG-CoA reductase is the rate-limiting enzyme of the mevalonate pathway and cholesterol accumulation is known to induce the degradation of this enzyme as a negative feedback

mechanism (186). Hence, our mass spectrometry results could have reflected an increase in cholesterol levels, due to the regulatory mechanism exerted over HMG-CoA reductase. In order to clarify this possibility, cholesterol levels were analyzed in B16 F0 cells after 3 days incubation without riboflavin. Cellular lipid content was purified and cholesterol was measured using a fluorescence-based assay. The total cholesterol content was reduced by ca. 30% in riboflavin-deficient cells (Figure 43, left). For normalization, cholesterol amounts were adjusted by a factor of 2.2. This value was obtained from a previous lipidomics analysis in which starved cells showed a 2.2-fold increase in total lipid content in comparison with control cells (data not shown) and reflected the fact that starved cells become bigger in size (Figure 43, right). Geometric calculation predicts a 2.5-fold increase of sphere surface according to the 1.6-fold cell radius increase and thus supports the need for normalization.

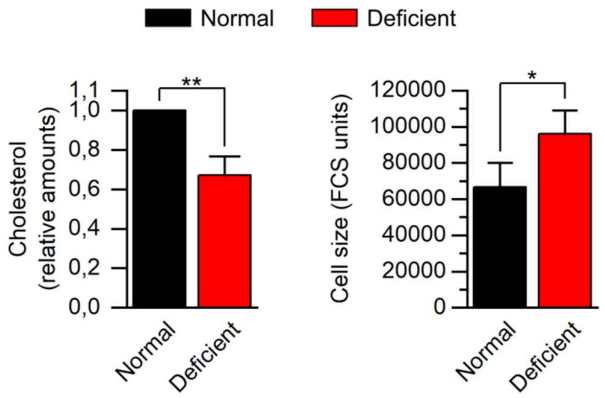

Figure 43. Riboflavin deficiency results in the decrease of cholesterol levels. (Left) Lipid fraction was isolated from B16 F0 cells after 3 days incubation in riboflavin-free medium. $1.5x10^6$ cells were used for the measurement. The Amplex Red Cholesterol Kit was used to determine cholesterol levels. Reaction buffer without lipid fraction was used as blank and the signal was subtracted from all the other values. Measurements were done in triplicates. Subtracted values from three different experiments were averaged. Normal condition was set as 1 and values were plotted (n = 3, mean ± SD). T-test was used to evaluate the significance of the differences. (Right) Cell size of B16 F0 cells was measured after 3 days starvation using flow cytometry (FCS units are shown). Normal condition was set as 1 (n = 3, mean ± SD). T-test was used to compare the means.

Prenylation is a post-translational modification that involves attaching isoprenoid molecules of either 15 (farnesyl) or 20 (geranyl) carbons in length to cysteine residues of proteins. This modification allows proteins to directly interact with membranes and thus regulates their localization and function (187). Two intermediates from the mevalonate pathway, namely farnesyl and geranyl, are substrates of protein lipidation. Inhibition of the mevalonate pathway might affect prenylation and, as a consequence, impair the correct membrane localization of proteins. To test this, EGFP protein fused to the C-terminal 20 amino acids

from HRAS was used. This region of HRAS is known to be farnesylated. Stably transfected B16 F0 cells expressing this protein were incubated for 3 days in the absence of vitamin B2. GFP localization signal was then analyzed microscopically, but no mislocalization of farnesylated EGFP was observed under starvation conditions (Figure 44).

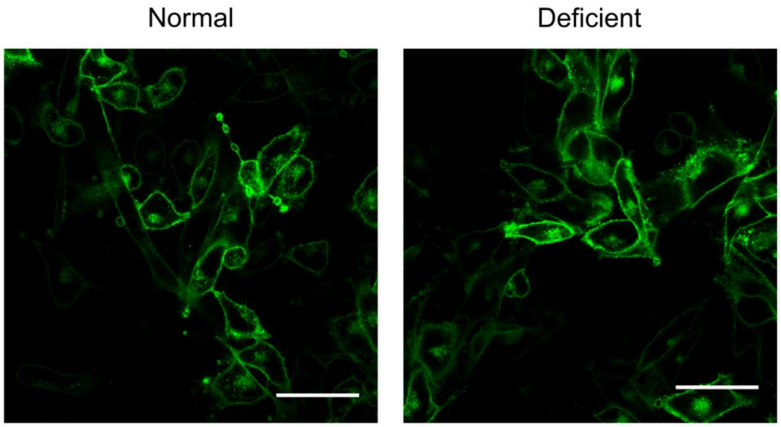

Figure 44. EGFP-F is not mislocalized under riboflavin-deficient conditions. B16 F0 cells stably expressing EGFP-F were incubated for 3 days in riboflavin-free medium. A Zeiss LSM 780 confocal microscope was used to image cells (scale bar: 50 µm). Representative pictures of one out of three independent experiments are shown.

3.8.5 β-galactosidase activity increase

β-galactosidase is one of the many hydrolytic enzymes found within lysosomes and it is responsible for cleaving galactopyranosides, especially lactose (188). β-galactosidase activity can be assessed in cells by using a substrate called X-Gal. This colourless compound is

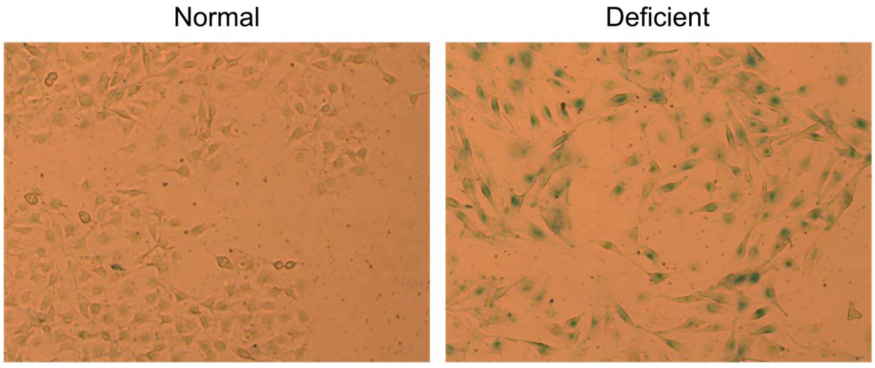

Figure 45. Riboflavin deficiency increases β-galactosidase expression in B16 F0 cells. B16 F0 cells were cultured in riboflavin-deficient medium for 3 days. Detection of β-galactosidase enzymatic activity was carried out using X-gal colorimetric assay. Cells were incubated at 37ºC for 24 h with X-gal staining solution. Images were taken using a Leica MC170 HD camera with an inverted light microscope. Representative pictures of one out of three independent experiments are shown.

cleaved by the enzyme to produce an indole molecule. The released indole dimerizes and yields an insoluble blue derivative which accumulates in the cell and can be observed by light microscopy (188). Proteome analysis revealed that the expression of β-galactosidase enzyme increased ca. 2-fold under starvation conditions. To verify this finding biochemically, X-gal assay was carried out using B16 F0 cells that had been incubated for 3 days in medium lacking riboflavin. After 24 h staining with X-gal solution, cells were imaged. As expected, a blue precipitate appeared within cells under vitamin deprivation while control cells remained mostly transparent (Figure 45).

3.8.6 Reduction of AKT-kinase activity

AKT is one of the most important anti-apoptotic serine threonine kinases in the cell. Active AKT induces several changes at the molecular and physiological level by targeting a plethora of downstream effectors. Among others, AKT promotes cell survival and proliferation, but it has also been implicated in metabolism, migration, and differentiation (189). This signaling pathway is especially relevant in the context of cancer and tumor resistance to chemotherapeutic agents (190). AKT pathway activation depends on the upstream stimulation of several proteins including receptor tyrosine kinases, G-protein-coupled receptors and PI3K by growth factors. AKT activity at the plasma membrane depends on two phosphorylation

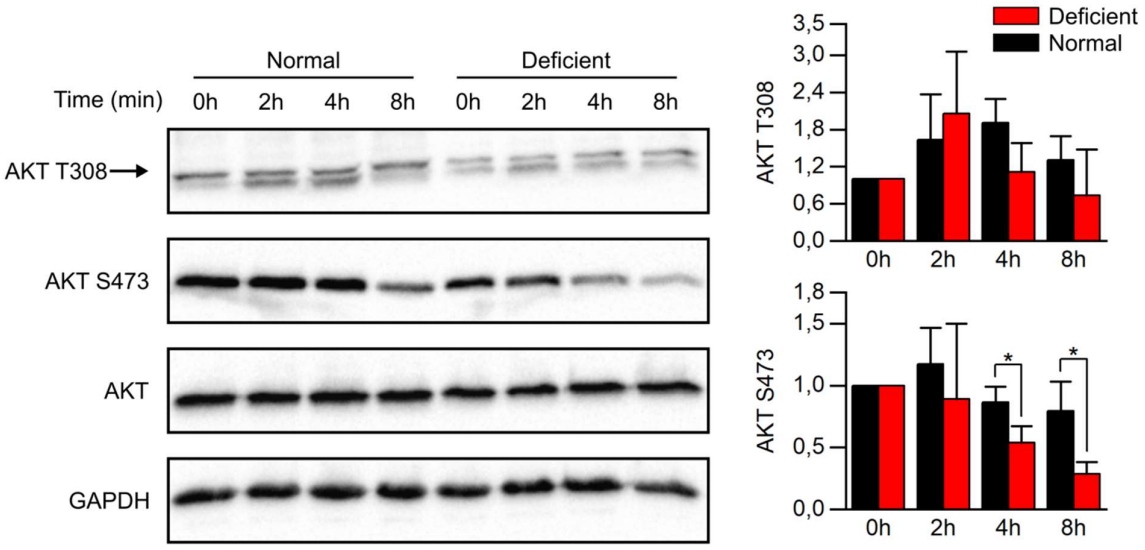

Figure 46. AKT activation is partially impaired in riboflavin-starved B16 F0 cells under MMS treatment. B16 F0 cells were cultured for 3 days under riboflavin-deficient conditions and treated with 500 µM MMS. Cells were harvested at different time points after MMS treatment (0, 2, 4, and 8 h) and phosphorylation levels of AKT T308 and S473 were analyzed by immunoblot. Phosphorylation levels at 0-time point for both conditions were set as 1. Values were normalized to GAPDH (n = 3, mean ± SD). Means were compared using a t-test.

sites, namely T308 and S473. Modification of both residues is needed to reach maximal activity. Mevalonate pathway impairment might result in alterations of plasma membrane under riboflavin starvation. Due to its central role in cell survival and taking into account the importance of the plasma membrane in AKT activation, we wondered whether AKT signaling pathway was functional in MMS-treated cells. B16 F0 cells were incubated for 3 days in medium lacking riboflavin. AKT T308 and S473 phosphorylation levels were analyzed at different time points after addition of MMS. A slight increase in AKT T308 phosphorylation occurred early after treatment, although this change was not significant (Figure 46). Under normal conditions, phosphorylation at S473 remained stable for the analyzed period but markedly decreased after 4 and 8 hours treatment under starvation conditions (Figure 46). The levels of the non-phosphorylated form of AKT did not change throughout the experiment. Thus, attenuation of AKT signaling occurs at a faster rate in cells lacking vitamin B2 and might contribute to the decreased survival of cells during chemotherapy.

4 DISCUSSION

4.1 Flavin-deficient proteins are engaged by the protein quality control machinery and degraded via the ubiquitin proteasome pathway

As the precursor of two cofactors, FMN and FAD, riboflavin/vitamin B2 is essential for the proper functioning of ca. 100 enzymes in mammalian cells (47). It remains unknown what cellular strategies are used to deal with cofactor-deficient enzymes at the molecular level. The major body of this work has focused on understanding the turnover of flavoproteins in their cofactor-free form within the cellular environment to elucidate the mechanisms that the protein quality control system applies to deal with them. Up to date, only a few studies have explored the direct effects that riboflavin availability has on flavoproteins (71,82,110). We hypothesized that the stability of flavin enzymes is linked to riboflavin levels. We also proposed that cofactor binding might define the engagement of the proteostasis machinery with flavoenzymes, leading to their degradation. First, in order to evaluate the significance of riboflavin deficiency on the stability of flavin-containing proteins, we decided to measure the levels of this specific proteome subset by using a mass spectrometry approach under riboflavin-free conditions. Quantitative proteomics was chosen for this purpose based on its powerful capacity in a wide range of biological setups (191).

Indeed the levels of flavin enzymes were reduced in the absence of vitamin B2. One study reported a slight inhibition of protein synthesis during riboflavin starvation (110). However, our experiments suggested that overall translation might not be suppressed in B16 F0 cells under riboflavin starvation (Figure 33B). Analysis of the 10 most reduced flavoproteins revealed that 8 were rescued by proteasomal inhibition (Figure 7B). The degree of accumulation under MG132 treatment was different for each protein and even higher than under normal conditions for 4 of them. This may be attributed to different protein turnover rates. It is important to mention that flavoproteome degradation most probably affects newly synthesized polypeptides and not holoproteins. This assumption is based on the binding strength of flavin cofactors to their corresponding enzymes. A small percentage of flavoproteins bind FMN or FAD covalently through Y, H, or C linkage to the 8α-methyl or the C6 atom of the isoalloxazine ring (192). The rest binds to the cofactor non-covalently with relatively strong affinity, showing dissociation constants that range between 10^{-7} and 10^{-10} M

(193). The high affinity implies that loaded flavoproteins are not likely to lose FMN or FAD. Accordingly, proteins with low turnover rates should be less susceptible to short deprivation periods, while more degradation should be observed for proteins with a high turnover rate.

NQO1 stability was severely affected according to proteomics analysis. This finding prompted us to validate NQO1 stability biochemically. Indeed, FAD levels were able to modulate the degradation of NQO1, which became unstable in its apoform (Figure 10A). One of the goals of this work was to investigate how the protein quality control system participates in the selection and triaging of flavoproteins. NQO1 degradation was dependent on the ubiquitin-proteasome pathway since inhibition of 26S proteasome rescued the enzyme. Ubiquitin ligases are responsible for binding substrates and targeting them for proteasomal degradation. Previous reports claimed that ubiquitin ligase CHIP binds and ubiquitylates mutant NQO1 (101). The premise we held at this point was that NQO1 recognition by CHIP relied on the cofactor-loading status of the enzyme. Both *in vivo* and *in vitro* results confirmed this hypothesis. Interestingly, NQO1 seemed to be partially degraded even in the absence of CHIP (Figure 12). Two reasons can provide an explanation of this. First, a different ubiquitin ligase might be able to target apoNQO1 for degradation, thus compensating the absence of CHIP since it is known that one particular substrate can bind to different E3 ligases. Second, the 20S proteasome might be responsible for the residual degradation under starvation conditions (99). Addition of FAD protected all NQO1 forms, i.e. wild-type holo-, apoNQO1, and mutant NQO1 from CHIP ubiquitylation (Figure 14), implying that NQO1, even when folded, can bind FAD. Nevertheless, even a high concentration was not able to completely protect NQO1 from ubiquitylation. The concentration of FAD we used during the experiment is much higher than the intracellular one (ca. 60 nM) and hence it means that *in vitro* flavinylation process is probably not as efficient as *in vivo*, where it has been proposed to follow an active process that involves FAD synthase (FADS) and FAD delivery in the maturation of flavoproteins (77). The small fraction of apparently holoNQO1 that was still recognized and ubiquitylated by CHIP could represent a small percentage of protein that was not properly loaded with the cofactor during purification.

The differences between wild-type holo- and apoNQO1 in pull-down experiments revealed how proteostasis machinery deals with flavoproteins under riboflavin deprivation (Figure 28). Cofactor-free NQO1 recruits cytosolic and constitutively expressed HSC70 and HSP90 proteins as well as two key HSP40 co-chaperones, namely DNAJA1 and DNAJA2. This

result is highly significant given the importance of these chaperones in folding and maturation of proteins in the cytosol (194). The constitutively expressed HSC70 protein is involved in many housekeeping tasks including folding during translation (195), protein translocation across membranes (196), chaperone-mediated autophagy (197), and disassembly of clathrin-coated vesicles (198). While HSC70 interacts with a wide variety of unfolded proteins, the action of HSP90 focuses on the maturation of more defined subsets of proteins, most prominently kinases and steroid hormone receptors (199). Some studies supported a role of HSP90 in promoting ligand binding to proteins by maintaining the apoproteins in an open conformation, as in the case of heme binding to guanylyl cyclase during its maturation (200). The HSP40/DNAJ family comprises 41 members in mammals. Most of them share a typical J domain through which binding to HSP70 proteins occurs (201). HSP40 can modulate the activity of HSP70 by stimulating ATP hydrolysis on HSP70 N-terminal domain (202). Thus, HSP40 participates in the regulation of the ATP-dependent cycle of HSP70 proteins by regulating the interconversion between its high and low substrate affinity states (202). HSP40s are also able to bind directly to substrates through their C-terminal domain and participate actively in substrate delivery to HSP70. Actually, it is though that HSP40s provide most of the substrate specificity, which is in accordance with higher number of HSP40s than HSP70s (194,203). Finally, our analysis indicates that chaperonin TRIC can be involved in NQO1 maturation under normal and starvation conditions. Binding of wild-type NQO1 to HSP90 or TRIC was not reported before (111). Wild-type NQO1 binding to chaperones might occur during the initial stages after polypeptide synthesis. When sufficient amounts of cofactor are present, folding equilibrium is probably pushed towards the NQO1 native conformation. On the other side, half-life of NQO1 in complex with chaperones increases in the absence of FAD. The enrichment of several chaperones in the pull-down experiments represents a hallmark of riboflavin deficiency. A distinct “chaperome” complex forms around apoNQO1, probably to prevent aggregation. Initial steps might involve the recognition of newly synthesized unfolded NQO1 by HSP40s and its delivery to HSP70 and HSP90, which can couple ATP-driven force with the folding process. HSP70 and HSP90 might work as holdases too, keeping NQO1 in an open FAD-binding conformation while preventing non-native interactions with other molecules. Pull-down results agree with our previous proteomics and biochemical data *in vivo*, where we showed that NQO1 was targeted for degradation in the absence of FAD. Several degradation factors were enriched in apoNQO1

pull-down, which means that failure to attain a native structure in the absence of cofactor targets the protein for degradation.

By comparing wild-type holo- and apoNQO1 interacting partners we found that FAD highly modifies the capacity of NQO1 to form aberrant interactions. The same was not observed in mutant NQO1 pull-down, where similar proteins were enriched under normal and starvation conditions (Figure 29). In this case, folding and ubiquitin-proteasome degradation factors were more abundant than for apoNQO1, which indicates higher degree of destabilization of mutant form. At the same time, the high overlap between wild-type apo- and mutant NQO1 interactomes underscores similar mechanisms of association (Figure 30). Further biochemical assays will be necessary to clarify the mass spectrometry results we have presented here for both wild-type and mutant NQO1.

4.2 The C-terminal tail of apoNQO1 is involved in recognition by the ubiquitin ligase CHIP

The *in vitro* characterization of NQO1 and NQO2 variants has given us a better understanding of the biophysical properties of apoproteins and how they behave in the absence of the cofactor. Information about secondary structure can be obtained from the CD spectroscopy data. In this case, no differences were observed among NQO1 protein variants (Figure 13A). More noticeable changes in secondary structure were detected between holo- and apoNQO2 (Figure 20A). Secondary structure from NQO2 is more prone to be affected due to the presence of two cofactors, namely FAD and zinc. In our apoprotein preparation zinc is also probably lost due to the harsh denaturing conditions that we applied.

The fluorescence peak shift upon ANS binding to wild-type apoNQO1 in comparison with that of the mutant suggests that the dye interaction is specific for each protein (Figure 13C). Previous reports have investigated the interaction between ANS and hemin-containing proteins in the presence and absence of the cofactor (204,205). Fluorescent dye bound with high affinity to the cofactor binding site. The increase in ANS fluorescence emission yield when incubated with apoNQO1 could be explained by ANS binding to the empty cofactor site. However, we cannot exclude that other regions become available for ANS binding given the difference between mutant and apoNQO1 spectra. ANS seemed to bind more avidly to the C-terminus of mutant NQO1, since its deletion completely abrogated the fluorescence emission signal (Figure 18D). The same was not observed for wild-type apoNQO1-Δ50, for which ANS binding still occurred. On the other side, the fluorescence observed upon ANS

binding to apoNQO2 indicates that binding might also take place in the cofactor pocket (Figure 20C). Native mass spectrometry showed that wild-type NQO1 can accommodate a higher number of charges on its surface after electrospray ionization in the absence of FAD, an indication of a more extended surface (99). Molecular dynamics simulations demonstrated that certain regions of the protein become more flexible in the apostate (100). Our analyses did not provide such deep information about the structural status of NQO1 variants and no substantial differences were found, except for a higher apoenzyme affinity for ANS. The analysis performed on both hFADS and cholesterol oxidase supports our conclusions because folding and secondary structure were not affected in the absence of FAD for both proteins (78,79). In the case of cholesterol oxidase mutant H69A, only small changes in the enzyme tertiary structure were reported, such as higher exposure of hydrophobic surfaces as well as enhanced sensitivity to limited proteolysis (78).

The biophysical analyses of mutant NQO1 suggest that this polymorphism presents more pronounced changes. It seems that mutant protein populates a native-like structure but lacks some of the wild-type packed conformation at the same time. Size exclusion chromatography and ANS binding strongly support this. Loss of compactness is most likely the cause of its ca. 8 degrees lower thermal stability. Our experimental characterization of mutant NQO1 is in accordance with previous studies that analyzed the consequences of the polymorphism at the biophysical level, like the experiments using x-ray crystallography and NMR spectroscopy (97), which also support the conclusion of a globular native-like protein that exists in a more disordered state.

Reconstitution experiments of cholesterol oxidase with excess of FAD decreased the enzyme sensitivity to heat denaturation and proteolytic cleavage (78). Our proteolytic digestion assays revealed similar stabilization of NQO1. The destabilization without FAD was most pronounced for the mutant, followed by wild-type apoNQO1 and the holoenzyme (Figure 15). It is important to notice that the digestion process is time-dependent and also affected loaded NQO1, as it has been observed before (97). Cofactor binding probably reduces the rate at which the C-terminal tail of NQO1 dissociates from the core domain of the protein. Obviously, this conformational change still occurs in the presence of FAD, but at a much lower rate. Similar proteolysis experiments performed with increasing concentrations of urea demonstrated that cleavage occurs through a local fluctuation event and not due to partial unfolding of the whole protein (100). By physically blocking the access of CHIP to the

C-terminal end of the enzyme with a specific antibody ubiquitylation levels decreased, indicating that binding through this region is important for the reaction to occur (Figure 17). Finally, the use of the NQO1 inhibitor dicoumarol was based on recent investigations that showed that inhibitor binding together with FAD can stabilize flexible regions of NQO1 mutant protein, especially the C-terminal domain. Treatment of cells with dicoumarol prevented mutant NQO1 degradation *in vivo*. A similar but less strong accumulation was also observed for the wild-type protein in a previous study (100). This stabilization probably relies on Van der Waals interactions between the inhibitor and phenylalanine236 (on the C-terminal tail of NQO1), as the crystal structure of NQO1 in complex with dicoumarol revealed (206). A slight but significant accumulation of apoNQO1 was also observed upon dicoumarol treatment in B16 F0 cells (Figure 16B). Recognition of mutant NQO1 by CHIP *in vitro* was only mildly inhibited in the presence of high concentrations of dicoumarol (Figure 16A), probably because FAD was not present in the ubiquitylation reaction and both ligands might be needed for protein stabilization.

Using tail-deleted NQO1 variants reinforced the previous conclusions we obtained in experiments with full-length proteins. All NQO1-Δ50 proteins turned out to be hardly detectable for CHIP (Figure 19A). NQO1-Δ50 recognition through domains other than the C-terminus can account for the remaining band appearing in ubiquitylation experiments. The direct interaction between NQO1 and HSP70 was analyzed by others (111). The researchers identified an N-terminal putative HSP70-binding sequence in NQO1 ($R_4R_5A_6L_7I_8V_9L_{10}A_{11}H_{12}$). Replacing isoleucine 8 by aspartic acid disrupted the interaction with HSP70 and as a consequence NQO1 was degraded by the ubiquitin-proteasome system (111). Apart from the C-terminal region, a thermolysin cutting site was found between S72-V73 of NQO1 N-terminal site. Molecular dynamics simulation confirmed that the flexibility of this domain also depends on FAD, which is not exposed to the solvent under normal conditions (100). This domain might as well function as a degradation signal in starvation conditions, but additional experiments are needed to investigate this possibility. The levels of FAD did not affect the stability of wild-type NQO1-Δ50, meaning that conformational dynamics of the C-terminal domain are important for *in vivo* recognition of apoNQO1 (Figure 19B). Nevertheless, NQO1-Δ50 variants were unstable and degradation rate was higher compared to full-length proteins *in vivo* according to CHX-chase experiments (Figure 23).

This entails that other factors of the proteostasis machinery can recognize NQO1 regions outside the C-terminus in a cofactor-independent manner.

Like NQO1, NQO2 is an oxidoreductase whose activity depends on the presence of FAD. The role of NQO2 in metabolism as well as its specificity towards different substrates are less understood (207). Despite the many similarities that both paralogs have, some of the most particular aspects that characterizes NQO2 is its low affinity for NAD(P)H and its preferential use of nicotinamide riboside (NRH) instead, a much less common cofactor (207), as well as the lack of C-terminal tail like the one in NQO1. NQO2 is 43 amino acids shorter than NQO1 (142). The flexibility and sensitivity to certain proteases that characterizes this region in NQO1 is not present in NQO2 (102). This led us to assume that NQO2 would remain invisible to CHIP and indeed our experiments proved this assumption (Figure 21B).

Our data established the NQO1 C-terminal tail as a structural determinant that protein quality control recognizes when flavin cofactor is missing. Noticeably, the ubiquitin ligase CHIP binds the C-terminal tails of HSC70/HSP70 and HSP90 chaperones through its TPR domain (208). Later it was found that CHIP could function in a chaperone-independent manner by directly binding to substrate proteins, such as SMAD1/5 via their C-terminal tails (209). Thus, CHIP is an E3 ligase that has evolved to recognize protruding and misfolded structures and thus appears to be a good candidate for NQO1 C-terminus recognition. We assume that TRP domain of CHIP should mediate the interaction with NQO1 C-terminal tail, although further experiments will be needed to prove it.

NQO1 has been proposed to protect several proteins like p53, p73 and α-synuclein from 20S proteasomal degradation (99,135,136). These proteins contain highly flexible structural regions lacking a defined structure. Structural disorder is thought to turn them vulnerable for ubiquitin-independent degradation by the 20S proteasome. *In vitro* experiments validated the work from others that claim a protective role for NQO1 (Figure 11). Nevertheless, the protection could not be reproduced *in vivo*, where the degradation of NQO1 under riboflavin deficiency had no effect on p53 and α-synuclein levels. The mechanism by which these proteins are degraded *in vivo* has not been fully elucidated yet and many questions about the regulation of ubiquitin-independent degradation mechanisms still need to be answered. We also found out that degradation of α-synuclein *in vitro* was blocked by the presence of NQO2 (Figure 22A). Pull-down experiments showed direct binding between NQO2 and α-synuclein (Figure 22B), while the same result was not observed for NQO1 under the experimental

conditions we used. This could indicate that the protection mechanism is different for each enzyme. NQO1 might block degradation by binding to the 20S proteasome, as has been reported before (99), and not through direct binding to the corresponding protein.

4.3 Cofactor-free flavoproteins are engaged in co-aggregation

Chemical and structural modifications of proteins, especially those that affect folding and cause a partial or total loss of the native conformation, can lead to aberrant intermolecular interactions and eventually cause aggregation. Although initial investigations suggested that substantial destabilization is needed for aggregation, it is now believed that small conformational changes can be sufficient. This is the case of folding intermediates and proteins with highly flexible regions and unstructured domains (112). The folding of proteins is defined in many cases by the formation and stability of intermediate species (210). Fyn SH3 domain mutants that mimic a folding intermediate state of the protein aggregate spontaneously as a consequence of its C-terminus destabilization (211). The case of β-2-microglobuin is especially impressive because aggregation and fibril formation correlates with a single isomerization reaction of a proline residue between the *trans* and *cis* states (212). Exposure of hydrophobic surfaces as it might happen in folding intermediates is a well-known property that governs aggregation (213). This encouraged us to investigate the potential aggregation propensity of cofactor-free flavoproteins. Computational analysis with the Zyggregator and CamSol predictors showed that NQO1 C-terminal domain between residues Y221 and G235 contains a sequence window with intrinsic low solubility scores (Figure 24). NQO1 C-terminus becomes highly dynamic in the absence of cofactor, losing its association with the core of the protein. This fact, in combination with the computational analysis result led us to think that this sequence might promote NQO1 aggregation. The assumption was tested biochemically in an *in vitro* experiment where co-aggregation of NQO1 with $A\beta_{1-42}$ peptide was investigated. The $A\beta_{1-42}$ peptide was used as an aggregation scaffold for its well-known amyloidogenic behavior. Amyloidogenic proteins have been reported to interact with metastable proteins (214,215). We found that NQO1 binding to $A\beta_{1-42}$ peptide depended on the loading state of NQO1, because fully-loaded wild-type NQO1 barely showed any co-aggregation. Interestingly, co-aggregation levels of wild-type apo- and mutant NQO1 were similar (Figure 25A). As expected, deleting the C-terminal domain had an inhibitory effect on $A\beta_{1-42}$ peptide binding to NQO1. Computational analysis revealed several regions with low solubility scores besides C-terminus. However, these patches are located

within the hydrophobic core of the protein and thus are not exposed to the solvent under normal conditions. Therefore, they should not be expected to participate in intermolecular binding events that trigger aggregation. Further analysis will be needed in order to determine whether other NQO1 regions can engage in aberrant interactions and promote aggregation.

Native gels revealed apoNQO1 populating high molecular weight species in comparison to the cofactor-loaded enzyme (Figure 27A). This observation indicates that NQO1 binds to other structures more readily when the enzyme lacks FAD, in agreement with the pull-down results. Proteasome inhibition was needed to promote NQO1 accumulation and trigger this effect. Surprisingly, we found that these aberrant interactions can be corrected by the addition of FAD to cell lysate. The recovery effect was very fast, since cofactor was incubated in the presence of the deflavinated lysate for 5 min only (Figure 27B). The effect was specific because the addition of riboflavin did not reduce the amount of NQO1 oligomers. It seems that, even under these circumstances, NQO1 still retains its conformation needed to bind FAD. To further assess the recovery effect, enzyme activity should be measured to ensure that functionality is also corrected. This finding is important in the context of disaggregation and stress recovery. Subcellular localization of aggregated species is commonly observed in different cells types upon stress. This phenomenon is thought to fulfill a double role: first, the protection of the cellular environment from aggregate-derived toxicity, and second, the concentration of refolding and degradation factors to facilitate the recovery phase. Disaggregation is carried out by a bi-chaperone system consisting on Hsp70-Hsp40 and Hsp104. This arrangement was first discovered in yeast, but a similar system has been observed in bacteria, plants, and in mitochondria and chloroplasts of unicellular and multicellular organisms (216). Disaggregation activity is crucial for cellular adaptation to heat-shock stress. More recent investigations have revealed that in eukaryotic cells HSP70 and HSP40 are also highly involved in the clearance of cellular aggregates in combination with HSP110 family members acting as nucleotide exchange factors (217). Actually, HSP70 directly prevented the accumulation of NQO1 aggregates (Figure 31). This result is connected with one of the initial motivations of this study, i.e. to understand the role of PQC in apoprotein maturation and turnover. The correct function of chaperones seems to be needed to suppress apoprotein non-native interactions and thus, inhibit aggregation. In the absence of such activity, homeostasis can be affected. The role of prosthetic groups as disaggregation

factors have not been studied before. For the first time, we have demonstrated that cofactors might influence protein disaggregation in mammalian lysates.

We used $A\beta_{1-42}$ peptide-EGFP fusion protein to study aggregation *in vivo*, expecting to intensify $A\beta_{1-42}$ amyloidogenesis under riboflavin-deficient conditions. Indeed, we observed that lack of riboflavin resulted in increased aggregation of Aβ-EGFP in B16 F0 cells. Even in the absence of this highly-aggregating peptide, a significant increase in the formation of amyloids was observed, indicating that proteome stability decreases in the absence of vitamin B2 (Figure 26B). Proteomics experiments need to be done in order to elucidate which fraction of the proteome succumbs to aggregation when riboflavin is missing. The experiments performed *in vivo* with $A\beta_{1-42}$ did not clarify this point, but it seems plausible that flavoproteome destabilization is responsible for the exacerbated aggregation.

Different pathologic conditions are linked to aggregation, but neurotoxic aggregation in the nervous system has gathered most of the attention up to date, as it gives raise to neurodegenerative disorders that entail an increasing health problem (8). Our findings revealed that modification of riboflavin levels might promote the development of amyloid-related diseases. Age is the most characteristic trait that associates with protein aggregation diseases, especially in the case of Alzheimer's and Parkinson's diseases. Actually, the threshold at which accumulation of polyQ-YFP fusion proteins occurred in *C.elegans* was found to be age-dependent (218). The role of the proteostasis machinery in age-dependent aggregation-related events has been investigated. Both heat shock and unfolded protein responses were severely diminished in adult worms compared to young ones (219,220). In the same line, impairment in aggregates clearance mechanisms has also been related to ageing and is thought to aggravate aberrant accumulation of proteins (221). This indicates that neurological pathologies could arise due to a decline of the proteostasis network activity in aging cells and tissues. As it was mentioned in the introductory part of this work, elderly population is specifically susceptible to suffer from malnutrition (66). Our results suggest that flavoproteome destabilization under riboflavin deficiency because of malnutrition might trigger aggregation and boost the toxicity of already pre-existing aggregates. This positive feedback loop could potentially cause further proteome destabilization and accelerate pathogenesis. Therefore, vitamin B2 deficiency might be considered as an additional risk factor in the etiology of aggregation diseases.

4.4 Alkylating chemotherapy is more efficient in riboflavin-starved cells

Proteostasis machinery is able to detect and degrade damaged proteins whose accumulation can constitute a threat for the homeostasis of the cell. In a normal situation, proteotoxic damage can be counteracted by the combined work of chaperones and both degradation systems, namely ubiquitin-proteasome system and autophagy (10). However, the proteostasis network can be altered, e.g. during aging or due to mutations of quality control machinery, which would lead to increased protein aggregation and eventually to cell death (10). The way aggregates and misfolded species become toxic and put at risk cellular homeostasis is not yet fully understood. Some studies suggested that it is by sequestration and targeting of pivotal components of the protein quality control system how normal household becomes disturbed (222,223) (Figure 47). Co-expression of HSP40 together with HSP110 in *Drosophila* models of Huntington disease had a protective effect towards polyQ-aggregation toxicity, a result that supports this notion (224). Other studies have reported that ubiquitin-proteasome system is inhibited by the presence of different aggregating species (225). This scenario is schematized

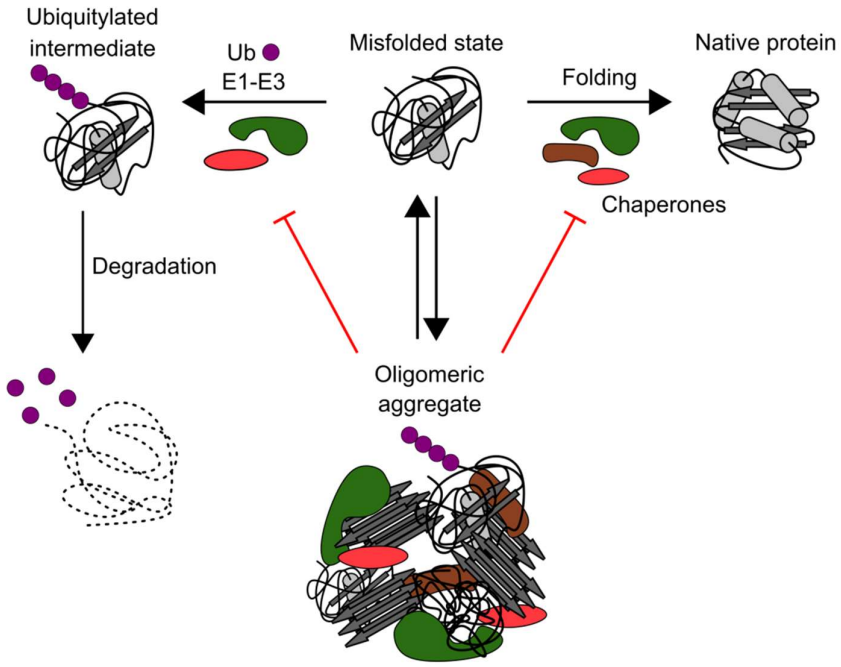

Figure 47. Proteostasis machinery is sequestered by aggregates. Misfolded or damaged proteins can either get refolded or be targeted for degradation. In both cases the protein quality control machinery is involved. Under certain conditions potentially toxic aggregates might form. Abnormal accumulation of these species might hijack too many resources from the quality control system and block its crucial household activities. If the aggregated species cannot be cleared out, the situation can become chronic and lead to cellular toxicity and disease.

in Figure 47 as well and relies on the similar sequestration principle indicated above. Another possible mechanism to explain the toxicity induced by aggregated species could be their capacity to affect metastable proteins through aberrant interactions (214,215). Mutant variants with higher sensitivity to temperature stress (215) as well as proteins that show high structural flexibility and have disordered regions (214) are prone to bind pre-existing aggregates and amyloidogenic species. These interactions can inactivate crucial cellular functions and accelerate aggregation, acting as a positive feedback mechanism that further disrupts cellular homeostasis. In general, aggregation and misfolding-related diseases seem to be the best examples of the pathological consequences that overcharging of the proteostasis machinery might have. However, neither previous reports nor our own experiments have shown reduced cellular viability due to riboflavin starvation, probably indicating that the chaperone capacity of the system can buffer the proteostasis stress that vitamin B2 deficiency imposes, at least at the time points analyzed (226). Since tumorigenic cells rely on an enhanced protein degradation capacity in order to survive and sustain their malignancy (227), we expected that a further perturbation of proteostasis would compromise their viability. Rewardingly, inhibiting HSP90 (one of the specific chaperones that were pulled-down together with apoNQO1) by radicicol had a toxic effect only in riboflavin-starved cells (Figure 35). This observation confirmed that chaperone inhibition might indeed break proteostasis balance and cause cell death. A pre-conditioned sensitivity towards the inhibitor might arise as a result of the proteostatic burden that apoproteins become for cells under these conditions. In order to survive, cells have to deal with flavoproteome destabilization. Inhibiting HSP90 seemed to enlarge this burden, finally leading to a cellular collapse. A mechanistic link between two types of cellular stresses, namely the nutrient-related and the proteotoxic stress was observed in B16 F0 cells in this work. Proteotoxic response, measured by the induction of HSP70, was strongly inhibited during vitamin B2 deficiency (Figure 33A). This finding underlines the proteostasis vulnerability that starved cells experience and opens new possibilities to study the consequences of proteostasis impairment due to nutritional restriction.

Mitomycin C, an antineoplastic quinone-like compound, was first shown to have antibacterial and later anti-tumoral capacities (228). *In vitro* and *in vivo* experiments using recombinant rat NQO1 protein and HT-29 human colon cells showed that oxidoreductase activity of NQO1 is necessary to metabolize Mitomycin C (229). The two-electron reduction of Mitomycin C by NQO1 transforms it into an electrophilic molecule that easily reacts with DNA and forms

DNA crosslinks (230), leading to an increase in cell toxicity, an effect that has been observed in human tumor cell lines upon NQO1 induction (231,232). Our experiments revealed that, under riboflavin-deficient conditions, Mitomycin C lost its cytotoxicity (Figure 36A). NQO1 is one of the most degraded flavoenzymes in the absence of riboflavin, which would explain the loss of Mitomycin C effect under these conditions. On the other side, we cannot exclude that other enzymes are responsible for the activation of the drug in cells. Cytochrome P450 reductase, xanthine oxidase, cytochrome b_5 reductase, or xanthine dehydrogenase are possible candidates, as *in vitro* assays suggest (233). A few years after Mitomycin C was discovered and isolated, it became increasingly used as a single agent or in combination with other anti-tumoral drugs to treat several cancers, especially those occurring at the bladder, breast, cervix, stomach, head and neck, lung, and pancreas (234). Hence, its use in the clinics has been substantial over the years and the studies concerning the sensitivity towards Mitomycin C-based treatments attracted much interest. We have exposed the potential therapeutic consequences that riboflavin deprivation has in tumor cells, as their resistance towards the drug increases. Maintaining the levels of riboflavin in cell appears to be of practical importance in the context of tumor therapy. A surprising result was found when cells were treated with methyl methanesulfonate (MMS), another alkylating agent (235). Without the need for an enzyme-dependent activation, MMS is a purine methylating compound that was

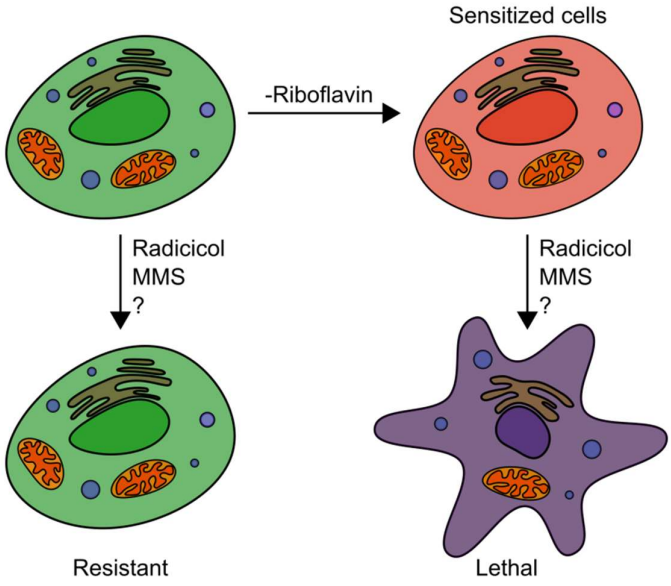

Figure 48. Cellular sensitization by riboflavin depletion. Under normal conditions (green), cells are resistant to radicicol and MMS treatment. Toxicity (lethal/purple) can be induced by introducing an additional step, in which cells are sensitized to the treatments by incubating them in riboflavin-free medium for 3 days (red).

used in Mitomycin C cytotoxicity assays as a negative control. Unexpectedly, the toxicity of MMS was markedly higher in starved cells (Figure 36B). An indirect and complex molecular mechanism can be anticipated as a reason for the increased cellular sensitivity towards MMS under riboflavin depletion. Overall, the treatments that we have performed with radicicol as well as with MMS on melanoma cells indicate that vitamin B2 deprivation induces a remarkable vulnerability and underscores the therapeutic potential of riboflavin starvation (Figure 48).

4.5 Rearrangement of energy metabolism and cell cycle inhibition are hallmarks of riboflavin deficiency

Given the increased sensitization and metabolic AMPK response, we were interested in understanding how B16 F0 adapted to starvation at proteome level. We reasoned that deep proteome analysis might uncover new liabilities of starved cells and provide a mechanistic understanding for the toxic responses we already reported. We observed significant changes in the expression pattern of four functional groups of proteins, namely those of pyruvate metabolism, oxidative phosphorylation, sterol biosynthesis and cell cycle. The first subset increased its expression levels while the other three were reduced (Figure 38).

Our respirometry assays showed that cell respiration capacity is highly affected under starvation conditions. The analysis specifically pointed towards a severe deficiency in complex I electron transfer capacity (Figure 42). This experimental fact is in accordance with proteomics data which showed a reduction of 21 subunits from complex I of the electron transport chain. Activity of complex II was not so severely undermined, although complex II subunits SDHA and SDHB were decreased in mass spectrometry experiments. As a counterpart to oxidative phosphorylation impairment, the only group that was found to be significantly overexpressed encompasses several enzymes involved in glucose catabolism. Additionally, lysosomal activity also increased, thus reinforcing the catalytic flux into glycolysis. This clearly indicates a shift in energy metabolism from oxidative phosphorylation to aerobic glycolysis in which glucose is transformed into lactic acid as a final product. Interestingly this kind of metabolic behavior was already described approximately 90 years ago by Otto Warburg, who reported a remarkable increase in the glucose consumption rate and lactate secretion in tumor cells (236). The phenomenon, mainly characterized by an increase in glucose fermentation under aerobic conditions, is known as the “Warburg effect”. Initially, it was proposed that the increase glycolytic flux occurred as a result of defective

oxidative metabolism. Later it was found that this is not the case since cellular respiration in most tumors is not impaired. Although it has been extensively studied over the years, the reasons that drive cancer cells to adopt this particular metabolic program have not been yet clarified. It is probable that by following this strategy cancer cells can invest more resources in the form of intermediate metabolites needed for biosynthetic pathways fuelling and reducing power generation. This adaptation could in principle support the high proliferating rate characteristic for tumor cells (237). Our case is apparently contradictory. Riboflavin-

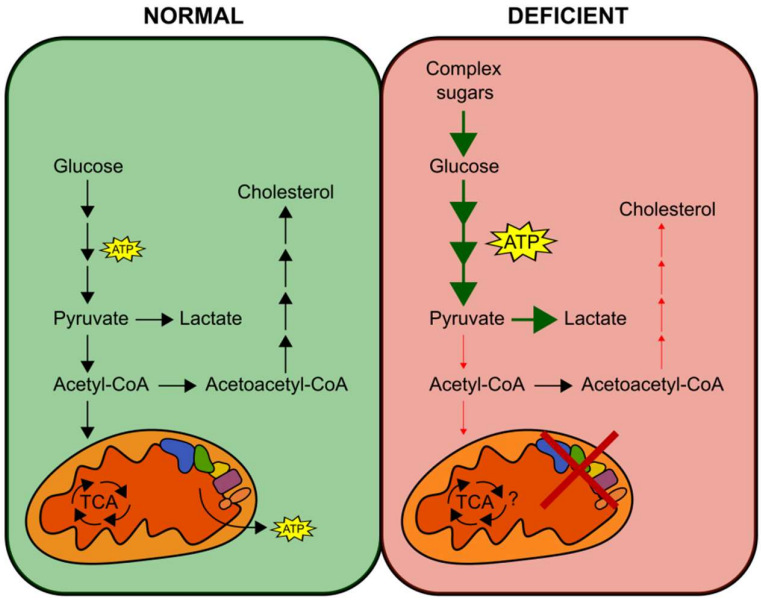

Figure 49. Metabolic rearrangement of melanoma cells under riboflavin starvation. Under normal conditions, cells obtain energy from their two main energetic pathways, i.e. glycolysis and oxidative phosphorylation. In glycolysis, glucose is transformed into pyruvate and acetyl-CoA, thus producing ATP. A fraction of acetyl-CoA is used as fuel for the TCA cycle and the production of more ATP through the electron transport chain. Some acetyl-CoA is also used as substrate for cholesterol synthesis through the mevalonate pathway. Under riboflavin starvation, glycolytic pathway is strongly increased. Production of lactate from pyruvate is favored while formation of acetyl-CoA is not. Oxidative phosphorylation and mevalonate pathway are both highly impaired under riboflavin starvation and cells are forced to rely on glucose fermentation to produce energy.

starved melanoma cells showed a metabolic profile similar to the one described by Otto Warburg but at the same time cell proliferation was extremely reduced. We believe that aerobic glycolysis increased as a result of a deficient cell respiration, as the respirometry assays clearly revealed. That is why the metabolic reprogramming under riboflavin starvation cannot be classified as a classical Warburg effect despite some similarities. Hence, blocking

ATP production by means of electron transport chain failure might force the cell to rely on fermentation-based mechanisms to survive (Figure 49).

A senescent-like phenotype defines B16 F0 cells that suffer from vitamin B2 starvation. One of the main hallmarks of senescence is growth arrest. In contrast to other situations where proliferation is also impaired, like apoptosis or quiescence, senescent cells show a strong metabolic activity, which is reflected by their increase in size. Electron transport chain inhibition and increased glycolytic flux has also been described as typical features of a senescent metabolism. Other studies point out towards an autophagy increase as well (238). The most remarkable biochemical evidence of a riboflavin-associated senescence phenotype that we found was the increased expression of β-galactosidase, a well established marker of this condition. On the other hand, the expression of CDK inhibitors p16 and p21 rises during senescence, but their levels did not changed under riboflavin starvation according to mass spectrometry data (239). In summary, our results indicate that riboflavin deficiency could induce a senescence-like state in starved melanoma cells. Investigating other factors involved in senescence induction should provide a better understanding of the connection between these two processes.

Sterol biosynthesis cluster was also affected by riboflavin deficiency. From this subset of proteins, 6 out of 9 are directly involved in the mevalonate pathway, an anabolic multi-step process that mediates the synthesis of cholesterol as well as other non-sterol isoprenoid molecules like ubiquinone, hemeA, and dolichol by using acetyl-CoA and acetoacetyl-CoA as substrates (240). This result is quite surprising because only two enzymes of this pathway are flavoproteins, namely squalene monooxygenase (SQLE) and delta(24)-sterol reductase (DHCR24). A strong negative feedback control is exerted on HMG-CoA reductase (186), which was actually the most reduced enzyme of the group. This fact required excluding that cholesterol accumulation was responsible for the mevalonate pathway impairment under riboflavin deprivation. Measurement of cholesterol cell content showed that cholesterol levels decreased by ca. 30% under riboflavin starvation (Figure 43).

Cholesterol is known to modulate the physical properties of cell membranes. The degree of stiffness and packing capacity it provides to membranes is crucial for the formation of lipid rafts (241). Additionally, a role of cholesterol in protecting lipids from chemical damage, for instance in cases of oxidative stress, has also been reported (242). A study with lymphocytic leukemia cells revealed a correlation between chemotherapeutic treatment with DNA-

damaging agents, increase of mtDNA mutations and exacerbated production of reactive oxygen species (243). Hence, oxidative damage of membranes can also be induced by antineoplastic drugs. Actually, this effect has been shown in patients undergoing chemotherapy (244). Extensive oxidative damage of lipids has been reported to trigger a regulated form of cell death called ferroptosis (245). We considered the possibility that chemical damage of lipids by MMS could be exacerbated in riboflavin-deficient cells due to the reduced protective effect from cholesterol and also as a consequence of increased ROS generation. An experiment was performed in order to investigate if cholesterol reduction was related to the exacerbated sensitivity of starved cells towards MMS. As a control, FIN56 was used for ferroptosis induction. Alpha-tocopherol (vitamin E) is known to protect cells from lipid oxidation-damaging effects (246). Alpha-tocopherol treatment was applied in combination with MMS and FIN56 due to its antioxidant capacity. If the gain of MMS sensitivity were based on increased lipid peroxidation, as it is the case for FIN56 toxicity, antioxidant treatment should reverse the toxic effects of the alkylating agent. Preliminary results indicated that MMS toxicity in starved B16 F0 cells does not involve lipid peroxidation (Figure 56). Cell toxicity decreased by 20% in FIN56-treated cells which were also treated with alpha-tocopherol in parallel. Antioxidant addition had no such effect during MMS treatment.

To our surprise, the levels of several cell cycle-regulating elements decreased under riboflavin-free conditions. The depletion of two of the main factors that drive cell cycle, namely CDK1 and CDK2, as well as several chromosome integrity-related factors and replication machinery proteins suggested that cell division should be blocked, as it was verified later experimentally. BrdU labeling and cell cycle analysis proved that cells undergo cell cycle arrest after vitamin B2 deprivation for 3 days (Figure 39A and B). Cell accumulation occurred at both G1 and G2/M phases. The levels of cyclin-dependent kinase 2 (CDK2) were reduced by ca. 2.21-fold in cells cultured without riboflavin according to mass spectrometry measurements. CDK2, together with cyclins A and E, regulates DNA replication start and promotes S phase progression (247). Therefore CDK2 reduction might explain G1/S transition blockade observed under riboflavin starvation. The degradation of CDK1 implies that cells fail to enter mitosis after DNA replication (Figure 39C), since non-phosphorylated CDK1 is needed to surpass this checkpoint. Inactivation of CDK1 by phosphorylation at Y15 is needed for exiting mitosis (248). Even when CDK1-Y15 levels are also reduced under the

same conditions, this result is not contradictory and can be explained by the lack of non-phosphorylated CDK1 in the first place. The accumulation of cells in G2/M phase agrees with CDK1 immunoblotting results since it indicates that mitosis is inhibited and cell division cannot be accomplished. Similar to CDK1, the reduction of AURORA kinase A in our proteomics analysis indicates a delay in mitotic entry and G2/M checkpoint blockade (249). The proliferation and cell cycle analysis results are in agreement with a previous work that showed cell cycle arrest in HepG2 cells under partial riboflavin deprivation (250). However, our starvation experiments revealed more severe effects, specifically at S and G2/M phases. This could be attributed to the fact that for HepG2 cells low concentration of vitamin B2 was still present in the starvation medium.

Induction of cell cycle arrest by serum starvation turned cells sensitive to MMS (Figure 41). Both serum and riboflavin-starved cells showed a similar increase in sensitivity, indicating that MMS toxicity was not specifically dependent on riboflavin starvation, but appeared as a consequence of proliferation impairment.

We aimed to understand the adaptation response of B16 F0 cells to riboflavin starvation. It seems that cells accommodate to this stress through a complex metabolic reorganization. Proteomics and biochemical data provided an overview of this cellular response. However, the exact mechanisms responsible for such adaptation remain unclear. Most of the depleted proteins that we identified do not contain a flavin cofactor, which means that their stability should remain unaffected. Changes at the transcriptional or translational levels could provide a rationale for the changes. Transcriptome analysis would help to understand the events behind the metabolic adaptation better. Usually, cells counteract severe nutrient starvation conditions by inducing autophagy, which regulates the degradation process of cellular structures to maintain the nutrient levels and delay apoptosis (251). The response to specific nutrient deprivation like glucose (252) and amino acids (253) has been studied and the molecular mechanisms by which starvation signaling is transduced are understood to some extent. Vitamin deficiency is a much less explored field, including the case of vitamin B2. More investigations are needed to elucidate how metabolic reprogramming occurs and which are the molecular events and the specific factors behind it. Our results provide a starting point for those investigations. AMP-activated protein kinase (AMPK) is one of the central metabolic regulators in the cell. The increase in AMP and ADP during energetic stress activates AMPK, which then orchestrates a whole metabolic adaptation by turning off

anabolic pathways and promoting catabolic metabolism to restore the levels of ATP (254). Long-term riboflavin starvation (3 days) activated AMPK by increasing phosphorylation at T172 (Figure 32). AMPK activation can explain some of the metabolic features that starved cells present. Energetic stress might appear as a result of oxidative phosphorylation impairment. It is plausible that AMPK activation occurs as a response to cope with electron transport chain failure under riboflavin depletion. The metabolic shift observed during senescence, which resembles the riboflavin-deficient phenotype has not been yet fully elucidated. Curiously, AMPK has been proposed to mediate this response (238). In our experimental system, the weakness of AMPK activation signal might implicate that glycolysis is able to compensate the absence of oxygen-dependent energy production. Additionally, the activity of AMPK is biochemically in contrast to the metabolic effects of AKT. In several models, activation of AKT prevents phosphorylation-dependent activation of AMPK and vice versa (255). The overall phosphorylation levels of AKT seemed to remain lower under riboflavin deficiency and its response to MMS treatment is partially deficient. This might ultimately have severe consequences for anti-apoptotic signaling and cell survival. The role of cholesterol decrease in membrane-dependent signaling events is also an interesting possibility that needs to be addressed. Finally, activation of AMPK shuts down protein synthesis. Yet, an experiment using ubiquitin-EGFP reporter plasmid indicates that incubation in riboflavin-free medium does not affect overall translation rate in melanoma cells. Experiments with this reporter were carried out after starvation for 2 days and thus additional time points should be tested in order to strengthen this argument.

4.6 Therapeutic implications

We have discussed the potential consequences of riboflavin deficiency in the context of protein quality control and aggregation. Partial loss of protein stability might arise in cofactor-deficient conditions. The absence of riboflavin seems to turn flavoproteins into a subset of metastable species that can participate in aggregation processes or perhaps even function as aggregation drivers themselves, especially under long-term starvation periods. The concept of pharmacologic chaperones (PC) refers to the capacity of certain small molecules to bind proteins and stabilize intermediate conformations that eventually favor the transition to the native state. The use of PC has recently gathered attention as a potential therapeutic approach for some disorders that can benefit from their capacity to correct mutant proteins (256). One example of PCs application is their use for lysosomal storage disorders (LSDs). This

heterogeneous group of more than 50 diseases shares a common trait, namely the malfunctioning of different lysosomal mutant proteins that are needed for correct lysosomal function. The use of PCs has been proven to ameliorate disease progression by increasing the stability and activity of these mutant forms (257). In analogy, we propose the use of riboflavin as well as flavin analogs as a possible strategy for the treatment of metabolic diseases that originate from inborn flavoproteins defects. Actually, treatment with high doses of vitamins results in the improvement of up to 50 different human diseases in which enzymes with polymorphisms are involved (93). The use of high doses of riboflavin in the diet as a treatment in riboflavin-responsive multiple acyl-CoA dehydrogenase deficiency (RR-MADD) has been demonstrated to successfully increase the activity of mutant acyl-CoA dehydrogenases, ETF, and ETF:QO proteins (70,71). This fact, together with the results presented in this work can be seen as a proof of concept of the beneficial capacity of PCs in general and of the potential to apply flavin-like molecules as folding agents in particular.

Furthermore, proteomics analysis together with the chemotherapy experiments we have carried out revealed the potential of riboflavin deficiency as a powerful therapeutic approach in the cancer field. Under starvation conditions, proliferation inhibition seems to increase alkylating agent sensitivity. The evidences indicated that loss of resistance is common to all non-proliferating cells. This generalization, however, needs to be proven by further investigation. Even if the effect is not riboflavin-specific, we think that riboflavin deprivation still constitutes a promising therapeutic option. The study of CHK1 phosphorylation levels supports this assumption. CHK1 is a multifunctional kinase that responds to DNA damage and DNA replication stalling by triggering a cell cycle checkpoint that controls replication fork progression and promotes cell survival. Previous experiments have shown that loss of CHK1 activity causes mitotic catastrophe, a form of apoptosis that occurs during mitosis failure (183). CHK1 was still phosphorylated up to normal levels under riboflavin starvation (Figure 40). However, the remaining pool of non-phosphorylated CHK1 was highly reduced. By reducing the non-phosphorylated CHK1 kinase pool, cells might lose their ability to escape death upon DNA damage. According to mass spectrometry data, deficiency of the DNA repair machinery is a hallmark of riboflavin deficiency as well. Thus, vitamin B2 deprivation might facilitate the accumulation of chemical modifications in DNA.

In addition to alkylating agents, many other compounds have been used over the years to treat patients with different types of cancer. Anti-mitotic compounds comprise a group of drugs

that specifically target microtubules and have been proven as anticancer therapy. The occurrence of side effects and resistance during the treatment, however, limits their use (258). Other compounds that interfere with mitotic events, like chromatid segregation, spindle assembly, or kinetochore formation have been designed to reduce the negative effects of classical anti-mitotic agents (259). Proteins involved in spindle formation and chromosome organization, stability, and segregation were reduced under riboflavin starvation conditions. These results indicate that riboflavin withdrawal can enhance mitotic drug responses that seek to interfere with cancer proliferation in a classical anti-mitotic therapy. DNA damage-based approaches like the one we used are likely to improve their efficacy under such conditions.

A recent work studied the possibility of treating melanoma cells by inducing senescence. A CRISPR/Cas9-based approach identified SMARCB1 as a potent suppressor of senescence. The following treatment with a BCL2 family inhibitor killed the senescent cancer cells with high specificity (260). This approach can also be potentially used in order to kill riboflavin-starved melanoma cells, given the similarities with the senescent phenotype that cells develop.

Tumorigenesis depends on the accumulation of genetic errors whose combination can sustain a proliferative and aggressive cellular phenotype. Some of these mutations are crucial for malignancy progression and thus have been pharmaceutically targeted with the hope of eliminating affected cells exclusively. The dependency of some cancers on single key factors that highly support tumorigenic behavior is known as oncogene addiction. Signaling factors like RAS or MYC, which are in control of many cellular pro-survival processes, are just examples of oncogene addiction. It has also been observed that tumor cells often suffer from several stresses, like increase proteotoxic burden, ROS production, DNA damage and mitotic collapse, among others. Tumors counteract stress by intensively investing into respective resistance mechanisms. Non-oncogenic addiction refers to the necessity for these protective pathways that do not encompass oncogenic drivers *per se*, but together with oncogenes provide a unique advantage to maintain the tumorigenic phenotype (261,262). We believe that melanoma cells might be addicted to the flavoproteome function in a similar way. The lack of riboflavin storing systems in mammalian cells can be seen as a possibility to control the cellular riboflavin supply together with other drugs to induce anti-cancer toxicity. Flavin cofactor analogs might induce riboflavin deficiency-like conditions that mimic the effects we have described in this work. We propose that such approaches could increase the efficiency of cancer therapy. A comprehensive study of riboflavin deficiency comparing transformed

versus non-transformed cell lines would be needed in the future. First, it would extend our knowledge on the multivalent consequences of riboflavin deprivation in a different cellular context and, second, it would provide more detailed understanding of the potential of riboflavin starvation as a novel therapeutic approach in oncology.

4.7 Conclusions

Proteomics and biochemical analysis have revealed that flavin cofactors play an important role for the intracellular stability of flavoproteins. Vitamin B2 deficiency not only compromised the functionality of flavoenzymes but their structural fitness as well, turning them susceptible for degradation under starvation conditions. The case of NQO1 has proven to be a good model of this destabilization. Loss of FAD endangers the kinetic stability of NQO1 C-terminal domain, which dissociates from the core region of the protein when FAD is lacking. The protein quality control system is able to recognize and degrade faulty polypeptides (36). The flexibility of the C-terminal tail is interpreted as a defectiveness signal by the quality surveillance machinery. Molecular chaperones bind apoNQO1, probably in the initial phases of its maturation to support its folding. Communication between chaperones and degradation factors is also likely to occur during this process. Absence of FAD in NQO1 determines the binding of CHIP to the enzyme and, consequently, its ubiquitylation and degradation. We have found that NQO1 and other cofactor-free flavoproteins constitute a metastable subset of aggregation-prone polypeptides. The imbalance between folding and aggregation favors the onset of protein misfolding diseases (10). We suggest that riboflavin deficiency might be associated with the development of neurodegeneration, especially in cases of long-term and severe vitamin B2 deficiency. A model based on NQO1 aggregation is provided in Figure 50.

This work has shed new light on how the proteostasis machinery deals with apoenzymes. It has revealed the therapeutic potential that apoenzyme destabilization might offer. Two different approaches have been discussed. The first includes the use of flavin cofactors as pharmacological chaperones to correct protein structural deficits. This application has already been proved to be successful to correct destabilization of mutant flavoproteins (93). Secondly, riboflavin starvation was shown here to induce several metabolic changes in melanoma cells, which can be summarized as a transition from oxidative phosphorylation to glycolysis. Proliferation and cholesterol production were severely impaired as well. The metabolic

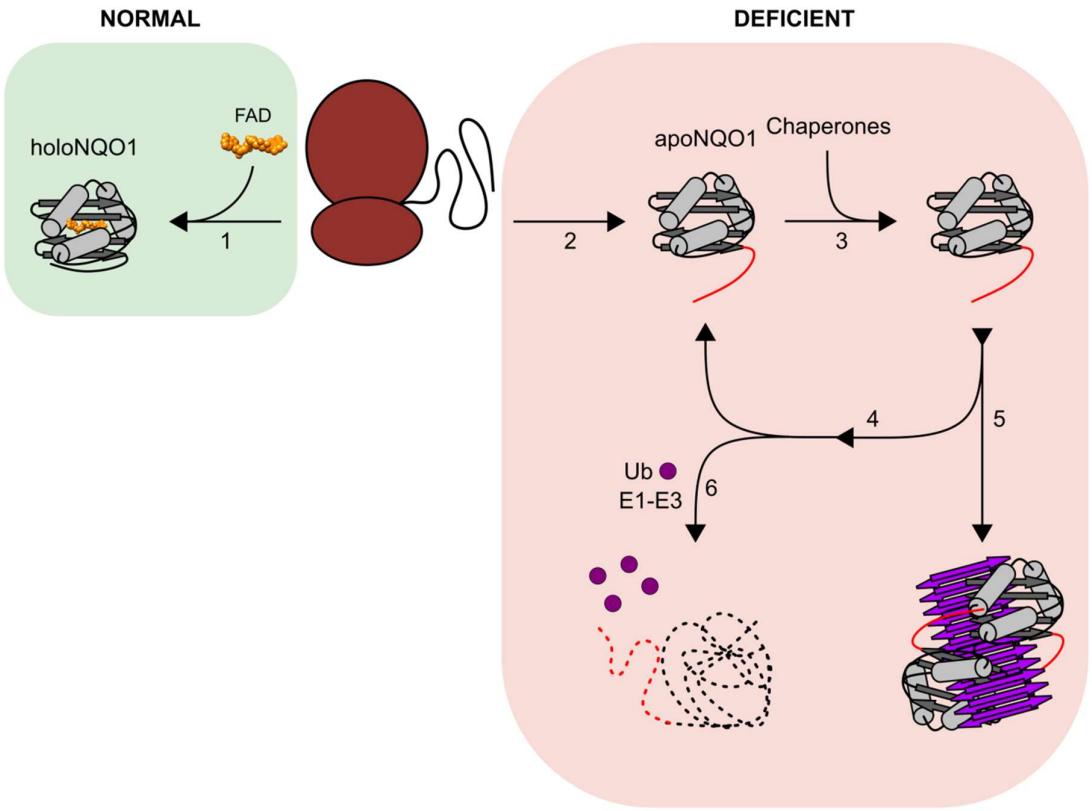

Figure 50. NQO1 aggregation. (1) Under normal conditions, binding of FAD favors the correct folding of NQO1, which can reach its functional conformation. (2) In the absence of riboflavin, NQO1 C-terminal tail becomes highly flexible. (3) Chaperones bind to apoNQO1 and promote its folding. (4) Several chaperone cycles can take place if the maturation process is not successful. (6) At any point, degradation machinery can recognize NQO1 as a defective protein that needs to be degraded. (5) Apoprotein accumulation or proteostasis machinery impairment might promote aggregation of apoNQO1.

reprogramming can come at a fitness cost that eventually might increase tumor vulnerability to chemotherapy. The sensitization of cancer cells is known as the "one-two punch" approach. Here, a first-round treatment induces sensitivity in the cancer, which is later exploited with a different therapy to cause a major effect (260,263). We tested this model in our experimental system and found that cells become more sensitive to alkylating chemotherapy under riboflavin starvation. The strong dependency of melanoma cells on the flavoproteome functionality can be considered as a non-oncogene addiction, which we suggest to call "flavoaddiction". The cellular stress imposed by vitamin B2 deficiency should be exploited therapeutically in the future.

5 REFERENCES

1. Dill KA, Ozkan SB, Shell MS, Weikl TR. The Protein Folding Problem. Annu Rev Biophys. 2008 May 7;37(1):289–316.

2. Jahn TR, Radford SE. Folding versus aggregation: Polypeptide conformations on competing pathways. Highlight Issue Protein Fold. 2008 Jan 1;469(1):100–17.

3. Rambaran RN, Serpell LC. Amyloid fibrils. Prion. 2008 Jul 1;2(3):112–7.

4. Tartaglia GG, Vendruscolo M. Proteome-Level Interplay between Folding and Aggregation Propensities of Proteins. J Mol Biol. 2010;402(5):919–28.

5. Vendruscolo M. Proteome folding and aggregation. Curr Opin Struct Biol. 2012;22(2):138–43.

6. Amm I, Sommer T, Wolf DH. Protein quality control and elimination of protein waste: The role of the ubiquitin–proteasome system. Biochim Biophys Acta BBA - Mol Cell Res. 2014;1843(1):182–96.

7. Chiti F, Dobson CM. Protein Misfolding, Amyloid Formation, and Human Disease: A Summary of Progress Over the Last Decade. Annu Rev Biochem. 2017 Jun 20;86(1):27–68.

8. Aguzzi A, O'Connor T. Protein aggregation diseases: pathogenicity and therapeutic perspectives. Nat Rev Drug Discov. 2010 Mar 1;9:237.

9. Finka A, Goloubinoff P. Proteomic data from human cell cultures refine mechanisms of chaperone-mediated protein homeostasis. Cell Stress Chaperones. 2013 Sep 1;18(5):591–605.

10. Hipp MS, Park S-H, Hartl FU. Proteostasis impairment in protein-misfolding and -aggregation diseases. Trends Cell Biol. 2014 Sep;24(9):506–14.

11. Hartl FU, Bracher A, Hayer-Hartl M. Molecular chaperones in protein folding and proteostasis. Nature. 2011 Jul 21;475(7356):324–32.

12. Bento CF, Renna M, Ghislat G, Puri C, Ashkenazi A, Vicinanza M, Menzies FM, Rubinsztein DC. Mammalian Autophagy: How Does It Work? Annu Rev Biochem. 2016 Jun 2;85(1):685–713.

13. Kim YE, Hipp MS, Bracher A, Hayer-Hartl M, Ulrich Hartl F. Molecular Chaperone Functions in Protein Folding and Proteostasis. Annu Rev Biochem. 2013 Jun 2;82(1):323–55.

14. Hoffmann A, Bukau B, Kramer G. Structure and function of the molecular chaperone Trigger Factor. Biochim Biophys Acta BBA - Mol Cell Res. 2010;1803(6):650–61.

15. Clare Daniel K., Saibil Helen R. ATP-driven molecular chaperone machines. Biopolymers. 2013;99(11):846–59.

16. Clerico EM, Tilitsky JM, Meng W, Gierasch LM. How Hsp70 Molecular Machines Interact with Their Substrates to Mediate Diverse Physiological Functions. J Mol Biol. 2015;427(7):1575–88.

17. Karagöz GE, Rüdiger SGD. Hsp90 interaction with clients. Trends Biochem Sci. 2015 Feb 1;40(2):117–25.

18. Joachimiak LA, Walzthoeni T, Liu CW, Aebersold R, Frydman J. The Structural Basis of Substrate Recognition by the Eukaryotic Chaperonin TRiC/CCT. Cell. 2014 Nov 20;159(5):1042–55.

19. Bard JAM, Goodall EA, Greene ER, Jonsson E, Dong KC, Martin A. Structure and Function of the 26S Proteasome. Annu Rev Biochem. 2018 Jun 20;87(1):697–724.

20. Buetow L, Huang DT. Structural insights into the catalysis and regulation of E3 ubiquitin ligases. Nat Rev Mol Cell Biol. 2016 Oct;17(10):626–42.

21. Pickart CM. Ubiquitin in chains. Trends Biochem Sci. 2000 Nov 1;25(11):544–8.

22. Woelk T, Sigismund S, Penengo L, Polo S. The ubiquitination code: a signalling problem. Cell Div. 2007 Mar 13;2(1):11.

23. Marques C, Guo W, Pereira P, Taylor A, Patterson C, Evans PC, Shang F. The triage of damaged proteins: degradation by the ubiquitin-proteasome pathway or repair by molecular chaperones. FASEB J. 2006 Feb 9;20(6):741–3.

24. Esser C, Alberti S, Höhfeld J. Cooperation of molecular chaperones with the ubiquitin/proteasome system. Biochim Biophys Acta BBA - Mol Cell Res. 2004;1695(1):171–88.

25. Ballinger CA, Connel P, Wu Y, Hu Z, Thompson LJ, Yin L-Y, Patterson C. Identification of CHIP, a Novel Tetratricopeptide Repeat-Containing Protein That Interacts with Heat Shock Proteins and Negatively Regulates Chaperone Functions. Mol Cell Biol. 1999;19(6):4535–45.

26. Connell P, Ballinger CA, Jiang J, Wu Y, Thompson LJ, Höhfeld J, Patterson C. The co-chaperone CHIP regulates protein triage decisions mediated by heat-shock proteins. Nat Cell Biol. 2000 Dec 8;3:93.

27. Meacham GC, Patterson C, Zhang W, Younger JM, Cyr DM. The Hsc70 co-chaperone CHIP targets immature CFTR for proteasomal degradation. Nat Cell Biol. 2000 Dec 8;3:100.

28. Lüders J, Demand J, Höhfeld J. The Ubiquitin-related BAG-1 Provides a Link between the Molecular Chaperones Hsc70/Hsp70 and the Proteasome. J Biol Chem. 2000 Feb 18;275(7):4613–7.

29. Kriegenburg Franziska, Ellgaard Lars, Hartmann-Petersen Rasmus. Molecular chaperones in targeting misfolded proteins for ubiquitin-dependent degradation. FEBS J. 2012;279(4):532–42.

30. Rosser MFN, Washburn E, Muchowski PJ, Patterson C, Cyr DM. Chaperone Functions of the E3 Ubiquitin Ligase CHIP. J Biol Chem. 2007 Aug 3;282(31):22267–77.

31. Murata S, Minami Y, Minami M, Chiba T, Tanaka K. CHIP is a chaperone-dependent E3 ligase that ubiquitylates unfolded protein. EMBO Rep. 2001 Dec 1;2(12):1133.

32. Fredrickson EK, Rosenbaum JC, Locke MN, Milac TI, Gardner RG, Brodsky JL. Exposed hydrophobicity is a key determinant of nuclear quality control degradation. Mol Biol Cell. 2011 May 5;22(13):2384–95.

33. Zlotorynski E. Ubiquitylation mediates quality control. Nat Rev Mol Cell Biol. 2017 Jan 24;18:71.

34. Sontag EM FJ. Sorting out the trash: the spatial nature of eukaryotic protein quality control. Curr Opin Cell Biol. 2014 Feb;26:139–46.

35. Klaips CL, Jayaraj GG, Hartl FU. Pathways of cellular proteostasis in aging and disease. J Cell Biol. 2018 Jan 2;217(1):51.

36. Shao S, Hegde RS. Target Selection during Protein Quality Control. Trends Biochem Sci. 2016 Feb 1;41(2):124–37.

37. Finley D. Misfolded proteins driven to destruction by Hul5. Nat Cell Biol. 2011 Oct 9;13:1290.

38. Lanneau D, Wettstein G, Bonniaud P, Garrido C. Heat Shock Proteins: Cell Protection through Protein Triage. ScientificWorldJournal. 2010;10:1543–52.

39. Ward CL, Omura S, Kopito RR. Degradation of CFTR by the ubiquitin-proteasome pathway. Cell. 1995 Oct 6;83(1):121–7.

40. Li C, Ramjeesingh M, Reyes E, Jensen T, Chang X, Rommens JM, Bear CE. The cystic fibrosis mutation (ΔF508) does not influence the chloride channel activity of CFTR. Nat Genet. 1993 Apr 1;3:311.

41. Higuchi-Sanabria R, Frankino PA, Paul JW, Tronnes SU, Dillin A. A Futile Battle? Protein Quality Control and the Stress of Aging. Dev Cell. 2018 Jan 22;44(2):139–63.

42. Wittung-Stafshede P. Role of Cofactors in Protein Folding. Acc Chem Res. 2002 Apr 1;35(4):201–8.

43. Leckner J, Bonander N, Wittung-Stafshede P, Malmström BG, Karlsson BG. The effect of the metal ion on the folding energetics of azurin: a comparison of the native, zinc and apoprotein. Biochim Biophys Acta BBA - Protein Struct Mol Enzymol. 1997 Sep 1;1342(1):19–27.

44. Pagani S, Vecchio G, Iametti S, Bianchi R, Bonomi F. On the role of the 2Fe-2S cluster in the formation of the structure of spinach ferredoxin. Biochim Biophys Acta BBA - Protein Struct Mol Enzymol. 1986;870(3):538–44.

45. Feigelson P, Greengard O. Regulation of Liver Tryptophan Pyrrolase Activity. J Biol Chem. 1962 Jun 1;237(6):1908–13.

46. Schimke RT, Sweeney EW, Berlin CM. The Roles of Synthesis and Degradation in the Control of Rat Liver Tryptophan Pyrrolase. J Biol Chem. 1965 Jan 1;240(1):322–31.

47. Lienhart W-D, Gudipati V, Macheroux P. The human flavoproteome. Arch Biochem Biophys. 2013 Jul 15;535(2):150–62.

48. Barile M, Giancaspero TA, Leone P, Galluccio M, Indiveri C. Riboflavin transport and metabolism in humans. J Inherit Metab Dis. 2016;39(4):545–57.

49. Giancaspero TA, Busco G, Panebianco C, Carmone C, Miccolis A, Liuzzi GM, Colella M, Barile M. FAD Synthesis and Degradation in the Nucleus Create a Local Flavin Cofactor Pool. J Biol Chem. 2013 Oct 4;288(40):29069–80.

50. Miranda-Lorenzo I, Dorado J, Lonardo E, Alcala S, Serrano AG, Clausell-Tormos J, Cioffi M, Megias D, Zagorac S, Balic A, Hidalgo M, Erkan M, Kleeff J, Scarpa A, Sainz Jr B, Heeschen C. Intracellular autofluorescence: a biomarker for epithelial cancer stem cells. Nat Meth. 2014 Nov;11(11):1161–9.

51. McCormick DB. Two interconnected B vitamins: riboflavin and pyridoxine. Physiol Rev. 1989 Oct 1;69(4):1170–98.

52. RIVLIN RS, LANGDON RG. Effects of Thyroxine Upon Biosynthesis of Flavin Mononucleotide and Flavin Adenine Dinucleotide. Endocrinology. 1969 Mar 1;84(3):584–8.

53. Chastain JL, McCormick DB. Flavin catabolites: identification and quantitation in human urine. Am J Clin Nutr. 1987 Nov 1;46(5):830–4.

54. Thakur K, Tomar SK, Singh AK, Mandal S, Arora S. Riboflavin and health: A review of recent human research. Crit Rev Food Sci Nutr. 2017 Nov 22;57(17):3650–60.

55. Powers HJ. Riboflavin (vitamin B-2) and health. Am J Clin Nutr. 2003 Jun 1;77(6):1352–60.

56. Domján G, Kókai K. The flavin adenine dinucleotide (FAD) content of the rat's liver in hypothyroid state and in the liver of hypothyroid animals after in vivo thyroxine treatment. Acta Biol Acad Sci Hung. 1966;16(3):237–41.

57. Lee S-S, McCormick DB. Thyroid hormone regulation of flavocoenzyme biosynthesis. Arch Biochem Biophys. 1985 Feb 15;237(1):197–201.

58. Rivlin RS, Langdon RG. Regulation of hepatic fad levels by thyroid hormone. Adv Enzyme Regul. 1966 Jan 1;4:45–58.

59. Tillotson JA, Baker EM. An enzymatic measurement of the riboflavin status in man. Am J Clin Nutr. 1972 Apr 1;25(4):425–31.

60. Cimino JA, Jhangiani S, Schwartz E, Cooperman JM. Riboflavin Metabolism in the Hypothyroid Human Adult. Proc Soc Exp Biol Med. 1987 Feb 1;184(2):151–3.

61. Brijlal S, Lakshmi AV, Bamji MS, Suresh P. Flavin metabolism during respiratory infection in mice. Br J Nutr. 1996;76(3):453–62.

62. Pelliccione N, Pinto J, Yee Ping Huang, Rivlin RS. Accelerated development of riboflavin deficiency by treatment with chlorpromazine. Biochem Pharmacol. 1983 Oct 1;32(19):2949–53.

63. Bosch AM, Abeling NGGM, IJlst L, Knoester H, van der Pol WL, Stroomer AEM, Wanders RJ, Visser G, Wijburg FA, Duran M, Waterham HR. Brown-Vialetto-Van Laere and Fazio Londe syndrome is associated with a riboflavin transporter defect mimicking mild MADD: a new inborn error of metabolism with potential treatment. J Inherit Metab Dis. 2011 Feb 1;34(1):159–64.

64. Haack TB, Makowski C, Yao Y, Graf E, Hempel M, Wieland T, Tauer U, Ahting U, Mayr JA, Freisinger P, Yoshimatsu H, Inui K, Strom TM, Meitinger T, Yonezawa A, Prokisch H. Impaired riboflavin transport due to missense mutations in SLC52A2 causes Brown-Vialetto-Van Laere syndrome. J Inherit Metab Dis. 2012 Nov 1;35(6):943–8.

65. Ho G, Yonezawa A, Masuda S, Inui K, Sim KG, Carpenter K, Olsen RKJ, Mitchell JJ, Rhead WJ, Peters G, Christodoulou J. Maternal riboflavin deficiency, resulting in transient neonatal-onset glutaric aciduria Type 2, is caused by a microdeletion in the riboflavin transporter gene GPR172B. Hum Mutat. 2010 Nov 18;32(1):E1976–84.

66. Hickson M. Malnutrition and ageing. Postgrad Med J. 2006 Jan 1;82(963):2.

67. Kay Tanaka MN. FAD_dependent Regulation of Transcription, Translation, Post-translational Processing, and Post-processing stability of Various Mithchondrial Acyl-Coa Dehydrogenases and of Electron Transfer Flavoprotein and the Site of Holoenzyme Formation. J Biol Chem. 1992 Sep 5;267:17925–32.

68. Olsen RKJ, Koňaříková E, Giancaspero TA, Mosegaard S, Boczonadi V, Mataković L, Veauville-Merllié A, Terrile C, Schwarzmayr T, Haack TB, Auranen M, Leone P, Galluccio M, Imbard A, Gutierrez-Rios P, Palmfeldt J, Graf E, Vianey-Saban C, Oppenheim M, Schiff M, Pichard S, Rigal O, Pyle A, Chinnery PF, Konstantopoulou V, Möslinger D, Feichtinger RG, Talim B, Topaloglu H, Coskun T, Gucer S, Botta A, Pegoraro E, Malena A, Vergani L, Mazzà D, Zollino M, Ghezzi D, Acquaviva C, Tyni T, Boneh A, Meitinger T, Strom TM, Gregersen N, Mayr JA, Horvath R, Barile M, Prokisch H. Riboflavin-Responsive and -Non-responsive Mutations in FAD Synthase Cause Multiple Acyl-CoA Dehydrogenase and Combined Respiratory-Chain Deficiency. Am J Hum Genet. 2016 Jun 2;98(6):1130–45.

69. Bennett MJ. Brown-Vialetto-Van Laere and Fazio Londe syndromes: defects of riboflavin transport with biochemical similarities to multiple acyl-CoA dehydrogenation defects (MADD). J Inherit Metab Dis. 2012 Nov 1;35(6):941–2.

70. Olsen RKJ, Olpin SE, Andresen BS, Miedzybrodzka ZH, Pourfarzam M, Merinero B, Frerman FE, Beresford MW, Dean JCS, Cornelius N, Andersen O, Oldfors A, Holme E, Gregersen N, Turnbull DM, Morris AAM. ETFDH mutations as a major cause of riboflavin-responsive multiple acyl-CoA dehydrogenation deficiency. Brain. 2007 Aug 1;130(8):2045–54.

71. Cornelius N, Frerman FE, Corydon TJ, Palmfeldt J, Bross P, Gregersen N, Olsen RKJ. Molecular mechanisms of riboflavin responsiveness in patients with ETF-QO variations and multiple acyl-CoA dehydrogenation deficiency. Hum Mol Genet. 2012 Aug 1;21(15):3435–48.

72. Didonato S, Gellera C, Peluchetti D, Uziel G, Antonelli A, Lus G, Rimoldi M. Normalization of short-chain acylcoenzyme a dehydrogenase after riboflavin treatment in a girl with multiple acylcoenzyme a dehydrogenase—deficient myopathy. Ann Neurol. 1989 May;25(5):479–84.

73. Rivlin RS. Regulation of flavoprotein enzymes in hypothyroidism and in riboflavin deficiency. Adv Enzyme Regul. 1970 Jan 1;8:239–50.

74. Burch HB, Lowry OH, Padilla AM, Combs AM. EFFECTS OF RIBOFLAVIN DEFICIENCY AND REALIMENTATION ON FLAVIN ENZYMES OF TISSUES. J Biol Chem. 1956 Nov 1;223(1):29–45.

75. Saijo T, Welch WJ, Tanaka K. Intramitochondrial folding and assembly of medium-chain acyl-CoA dehydrogenase (MCAD). Demonstration of impaired transfer of K304E-variant MCAD from its complex with hsp60 to the native tetramer. J Biol Chem. 1994 Feb 11;269(6):4401–8.

76. Saijo T, Tanaka K. Isoalloxazine Ring of FAD Is Required for the Formation of the Core in the Hsp60-assisted Folding of Medium Chain Acyl-CoA Dehydrogenase Subunit into the Assembly Competent Conformation in Mitochondria. J Biol Chem. 1995 Jan 27;270(4):1899–907.

77. Giancaspero TA, Colella M, Brizio C, Difonzo G, Fiorino GM, Leone P, Brandsch R, Bonomi F, Iametti S, Barile M. Remaining challenges in cellular flavin cofactor homeostasis and flavoprotein biogenesis. Front Chem. 2015;3:30.

78. Caldinelli L, Iametti S, Barbiroli A, Fessas D, Bonomi F, Piubelli L, Molla G, Pollegioni L. Relevance of the flavin binding to the stability and folding of engineered cholesterol oxidase containing noncovalently bound FAD. Protein Sci. 2008 Mar 1;17(3):409–19.

79. Torchetti EM, Bonomi F, Galluccio M, Gianazza E, Giancaspero TA, Iametti S, Indiveri C, Barile M. Human FAD synthase (isoform 2): a component of the machinery that delivers FAD to apo-flavoproteins. FEBS J. 2011 Nov 1;278(22):4434–49.

80. Kim HJ, Jeong M-Y, Na U, Winge DR. Flavinylation and Assembly of Succinate Dehydrogenase Are Dependent on the C-terminal Tail of the Flavoprotein Subunit. J Biol Chem. 2012 Nov 23;287(48):40670–9.

81. Tahallah N, van den Heuvel RHH, van den Berg WAM, Maier CS, van Berkel WJH, Heck AJR. Cofactor-dependent Assembly of the Flavoenzyme Vanillyl-alcohol Oxidase. J Biol Chem. 2002 Sep 27;277(39):36425–32.

82. Henriques BJ, Rodrigues JV, Olsen RK, Bross P, Gomes CM. Role of Flavinylation in a Mild Variant of Multiple Acyl-CoA Dehydrogenation Deficiency: A MOLECULAR RATIONALE FOR THE EFFECTS OF RIBOFLAVIN SUPPLEMENTATION. J Biol Chem. 2009 Feb 13;284(7):4222–9.

83. Xing W, Busino L, Hinds TR, Marionni ST, Saifee NH, Bush MF, Pagano M, Zheng N. SCFFBXL3 ubiquitin ligase targets cryptochromes at their cofactor pocket. Nature. 2013 Apr 4;496(7443):64–8.

84. Hirano A, Braas D, Fu Y-H, Ptáček LJ. FAD Regulates CRYPTOCHROME Protein Stability and Circadian Clock in Mice. Cell Rep. 2017 Apr 11;19(2):255–66.

85. Motlagh HN, Wrabl JO, Li J, Hilser VJ. The ensemble nature of allostery. Nature. 2014 Apr 16;508:331.

86. Franco Navazio LE. Soluble Diaphorase in Animal Tissues. Acta Chem Scand. 1958 Mar 8;12:595.

87. Chen S, Wu K, Knox R. Structure-function studies of DT-diaphorase (NQO1) and NRH:quinone oxidoreductase (NQO2)11This article is dedicated to the memory of Dr. Lars Ernster, who recently passed away. Free Radic Biol Med. 2000 Aug 1;29(3):276–84.

88. Monks TJ, Jones DC. The Metabolism and Toxicity of Quinones, Quinonimines, Quinone Methides, and Quinone-Thioethers. Curr Drug Metab. 2002;3(4):425–38.

89. Kansanen E, Kuosmanen SM, Leinonen H, Levonen A-L. The Keap1-Nrf2 pathway: Mechanisms of activation and dysregulation in cancer. Redox Biol. 2013;1(1):45–9.

90. Pidugu LSM, Mbimba JCE, Ahmad M, Pozharski E, Sausville EA, Emadi A, Toth EA. A direct interaction between NQO1 and a chemotherapeutic dimeric naphthoquinone. BMC Struct Biol. 2016 Jan 28;16(1):1.

91. Quinones and Quinone Enzymes. Elsevier; 2004. 611 p.

92. Asher G, Lotem J, Cohen B, Sachs L, Shaul Y. Regulation of p53 stability and p53-dependent apoptosis by NADH quinone oxidoreductase 1. Proc Natl Acad Sci. 2001 Jan 30;98(3):1188–93.

93. Ames BN, Elson-Schwab I, Silver EA. High-dose vitamin therapy stimulates variant enzymes with decreased coenzyme binding affinity (increased Km): relevance to genetic disease and polymorphisms. Am J Clin Nutr. 2002 Apr 1;75(4):616–58.

94. Kelsey KT, Ross D, Traver RD, Christiani DC, Zuo ZF, Spitz MR, Wang M, Xu X, Lee BK, Schwartz BS, Wiencke JK. Ethnic variation in the prevalence of a common NAD(P)H quinone oxidoreductase polymorphism and its implications for anti-cancer chemotherapy. Br J Cancer. 1997;76(7):852–4.

95. Siegel D, McGuiness S, Winski S, Ross D. Genotype-Phenotype relationships in studies of a polymorphism in NAD(P)H:quinone oxidoreductase 1. Pharmacogenetics. 1999;9(1):113–21.

96. Siegel D, Anwar A, Winski SL, Kepa JK, Zolman KL, Ross D. Rapid Polyubiquitination and Proteasomal Degradation of a Mutant Form of NAD(P)H:Quinone Oxidoreductase 1. Mol Pharmacol. 2001 Feb 1;59(2):263.

97. Lienhart W-D, Gudipati V, Uhl MK, Binter A, Pulido SA, Saf R, Zangger K, Gruber K, Macheroux P. Collapse of the native structure caused by a single amino acid exchange in human NAD(P)H:quinone oxidoreductase1. FEBS J. 2014 Oct 1;281(20):4691–704.

98. Pey AL, Megarity CF, Timson DJ. FAD binding overcomes defects in activity and stability displayed by cancer-associated variants of human NQO1. Biochim Biophys Acta BBA - Mol Basis Dis. 2014 Nov;1842(11):2163–73.

99. Moscovitz O, Tsvetkov P, Hazan N, Michaelevski I, Keisar H, Ben-Nissan G, Shaul Y, Sharon M. A Mutually Inhibitory Feedback Loop between the 20S Proteasome and Its Regulator, NQO1. Mol Cell. 2012 Jul 13;47(1):76–86.

100. Medina-Carmona E, Palomino-Morales RJ, Fuchs JE, Padín-Gonzalez E, Mesa-Torres N, Salido E, Timson DJ, Pey AL. Conformational dynamics is key to understanding loss-of-function of NQO1 cancer-associated polymorphisms and its correction by pharmacological ligands. Sci Rep. 2016 Feb 3;6:20331.

101. Tsvetkov P, Adamovich Y, Elliott E, Shaul Y. E3 Ligase STUB1/CHIP Regulates NAD(P)H:Quinone Oxidoreductase 1 (NQO1) Accumulation in Aged Brain, a Process Impaired in Certain Alzheimer Disease Patients. J Biol Chem. 2011 Mar 18;286(11):8839–45.

102. Chen S, Deng PSK, Bailey JM, Swiderek KM. A two-domain structure for the two subunits of NAD(P)H:quinone acceptor oxidoreductase. Protein Sci. 1994 Jan 1;3(1):51–7.

103. Korovila I, Hugo M, Castro JP, Weber D, Höhn A, Grune T, Jung T. Proteostasis, oxidative stress and aging. Redox Biol. 2017 Oct 1;13:550–67.

104. Espinosa-Diez C, Miguel V, Mennerich D, Kietzmann T, Sánchez-Pérez P, Cadenas S, Lamas S. Antioxidant responses and cellular adjustments to oxidative stress. Redox Biol. 2015 Dec 1;6:183–97.

105. Werner R, Manthey KC, Griffin JB, Zempleni J. HepG2 cells develop signs of riboflavin deficiency within 4 days of culture in riboflavin-deficient medium. J Nutr Biochem. 2005 Oct 1;16(10):617–24.

106. Nyström T. Role of oxidative carbonylation in protein quality control and senescence. EMBO J. 2005 Apr 6;24(7):1311.

107. Tu BP, Weissman JS. Oxidative protein folding in eukaryotes. J Cell Biol. 2004 Feb 2;164(3):341.

108. Manthey KC, Chew YC, Zempleni J. Riboflavin Deficiency Impairs Oxidative Folding and Secretion of Apolipoprotein B-100 in HepG2 Cells, Triggering Stress Response Systems. J Nutr. 2005 May 1;135(5):978–82.

109. Hetz C. The unfolded protein response: controlling cell fate decisions under ER stress and beyond. Nat Rev Mol Cell Biol. 2012 Jan 18;13:89.

110. Nagao M, Tanaka K. FAD-dependent regulation of transcription, translation, post-translational processing, and post-processing stability of various mitochondrial acyl-CoA dehydrogenases and of electron transfer flavoprotein and the site of holoenzyme formation. J Biol Chem. 1992 Sep 5;267(25):17925–32.

111. Anwar A, Siegel D, Kepa JK, Ross D. Interaction of the Molecular Chaperone Hsp70 with Human NAD(P)H:Quinone Oxidoreductase 1. J Biol Chem. 2002 Apr 19;277(16):14060–7.

112. Fink AL. Protein aggregation: folding aggregates, inclusion bodies and amyloid. Fold Des. 1998 Feb 1;3(1):R9–23.

113. Li C, Wen A, Shen B, Lu J, Huang Y, Chang Y. FastCloning: a highly simplified, purification-free, sequence- and ligation-independent PCR cloning method. BMC Biotechnol. 2011 Oct 12;11(1):92.

114. Hefti MH, Vervoort J, van Berkel WJH. Deflavination and reconstitution of flavoproteins. Eur J Biochem. 2003 Nov 1;270(21):4227–42.

115. Huang C, Ren G, Zhou H, Wang C. A new method for purification of recombinant human α-synuclein in Escherichia coli. Protein Expr Purif. 2005 Jul 1;42(1):173–7.

116. Fiala GJ, Schamel WWA, Blumenthal B. Blue Native Polyacrylamide Gel Electrophoresis (BN-PAGE) for Analysis of Multiprotein Complexes from Cellular Lysates. J Vis Exp. 2011 Feb 24;(48):e2164.

117. Swamy M, Siegers GM, Minguet S, Wollscheid B, Schamel WWA. Blue Native Polyacrylamide Gel Electrophoresis (BN-PAGE) for the Identification and Analysis of Multiprotein Complexes. Sci STKE. 2006 Jul 25;2006(345):pl4.

118. Wittig I, Schägger H. Native electrophoretic techniques to identify protein–protein interactions. PROTEOMICS. 2009 Dec 1;9(23):5214–23.

119. Wittig I, Braun H-P, Schagger H. Blue native PAGE. Nat Protoc. 2006 Jun;1(1):418–28.

120. Wolfgang W. A. Schamel MMC-C. Two-dimensional Blue Native/SDS Gel Electrophoresis of Multi-Protein Complexes from Whole Cellular Lysates. Mol Cell Proteomics. 2004 Feb;176–82.

121. Nikolova T, Ensminger M, Löbrich M, Kaina B. Homologous recombination protects mammalian cells from replication-associated DNA double-strand breaks arising in response to methyl methanesulfonate. DNA Repair. 2010 Oct 5;9(10):1050–63.

122. Klus P, Bolognesi B, Agostini F, Marchese D, Zanzoni A, Tartaglia GG. The cleverSuite approach for protein characterization: predictions of structural properties, solubility, chaperone requirements and RNA-binding abilities. Bioinformatics. 2014 Jun 1;30(11):1601–8.

123. Tartaglia GG, Vendruscolo M. Proteome-Level Interplay between Folding and Aggregation Propensities of Proteins. J Mol Biol. 2010 Oct 8;402(5):919–28.

124. Campen A, Williams RM, Brown CJ, Meng J, Uversky VN, Dunker AK. TOP-IDP-Scale: A New Amino Acid Scale Measuring Propensity for Intrinsic Disorder. Protein Pept Lett. 2008;15(9):956–63.

125. Eisenberg D, Schwarz E, Komaromy M, Wall R. Analysis of membrane and surface protein sequences with the hydrophobic moment plot. J Mol Biol. 1984 Oct 15;179(1):125–42.

126. Eggers LF, Schwudke D. Shotgun Lipidomics Approach for Clinical Samples. Methods Mol Biol. 2018;(1730):163–74.

127. Jiang W, Hunter T. Analysis of cell-cycle profiles in transfected cells using a membrane-targeted GFP. Biotechniques. 1998;24(3):349–50.

128. Wisniewski JR, Zougman A, Nagaraj N, Mann M. Universal sample preparation method for proteome analysis. Nat Meth. 2009 May;6(5):359–62.

129. Cox J, Mann M. MaxQuant enables high peptide identification rates, individualized p.p.b.-range mass accuracies and proteome-wide protein quantification. Nat Biotech. 2008 Dec;26(12):1367–72.

130. Boyle EI, Weng S, Gollub J, Jin H, Botstein D, Cherry JM, Sherlock G. GO::TermFinder—open source software for accessing Gene Ontology information and finding significantly enriched Gene Ontology terms associated with a list of genes. Bioinformatics. 2004 Dec 12;20(18):3710–5.

131. Goldberg AL. Development of proteasome inhibitors as research tools and cancer drugs. J Cell Biol. 2012 Nov 12;199(4):583.

132. Jariel-Encontre I, Bossis G, Piechaczyk M. Ubiquitin-independent degradation of proteins by the proteasome. Biochim Biophys Acta BBA - Rev Cancer. 2008 Dec;1786(2):153–77.

133. Förster A, Hill CP. Proteasome degradation: enter the substrate. Trends Cell Biol. 2003 Nov 1;13(11):550–3.

134. Tsvetkov P, Reuven N, Shaul Y. Ubiquitin-independent p53 proteasomal degradation. Cell Death Differ. 2009 Jun 26;17:103.

135. Asher G, Lotem J, Sachs L, Kahana C, Shaul Y. Mdm-2 and ubiquitin-independent p53 proteasomal degradation regulated by NQO1. Proc Natl Acad Sci. 2002 Oct 1;99(20):13125.

136. Asher G, Tsvetkov P, Kahana C, Shaul Y. A mechanism of ubiquitin-independent proteasomal degradation of the tumor suppressors p53 and p73. Genes Dev. 2005 Feb 1;19(3):316–21.

137. Ran FA, Hsu PD, Wright J, Agarwala V, Scott DA, Zhang F. Genome engineering using the CRISPR-Cas9 system. Nat Protoc. 2013 Oct 24;8:2281.

138. Hefti MH, Milder FJ, Boeren S, Vervoort J, van Berkel WJ. A His-tag based immobilization method for the preparation and reconstitution of apoflavoproteins. Biochim Biophys Acta BBA - Gen Subj. 2003 Jan 20;1619(2):139–43.

139. Málnási-Csizmadia András, Hegyi György, Tölgyesi Ferenc, Szent-Györgyi Andrew G., Nyitray László. Fluorescence measurements detect changes in scallop myosin regulatory domain. Eur J Biochem. 2001 Dec 25;261(2):452–8.

140. Zheng C, Zhao Z, Li Y, Wang L, Su Z. Effect of IPTG amount on apo- and holo- forms of glycerophosphate oxidase expressed in Escherichia coli. Protein Expr Purif. 2011 Feb 1;75(2):133–7.

141. Jaiswal AK. Human NAD(P)H:quinone oxidoreductase2. Gene structure, activity, and tissue-specific expression. J Biol Chem. 1994 May 20;269(20):14502–8.

142. Wu K, Knox R, Sun XZ, Joseph P, Jaiswal AK, Zhang D, Deng PS-K, Chen S. Catalytic Properties of NAD(P)H:Quinone Oxidoreductase-2 (NQO2), a Dihydronicotinamide Riboside Dependent Oxidoreductase. Arch Biochem Biophys. 1997 Nov 15;347(2):221–8.

143. Rodriguez Camargo DC, Tripsianes K, Buday K, Franko A, Göbl C, Hartlmüller C, Sarkar R, Aichler M, Mettenleiter G, Schulz M, Böddrich A, Erck C, Martens H, Walch AK, Madl T, Wanker EE, Conrad M, de Angelis MH, Reif B. The redox environment triggers conformational changes and aggregation of hIAPP in Type II Diabetes. Sci Rep. 2017 Mar 13;7:44041.

144. Srivastava KR, Lapidus LJ. Prion protein dynamics before aggregation. Proc Natl Acad Sci. 2017 Apr 4;114(14):3572.

145. Tartaglia GG, Vendruscolo M. The Zyggregator method for predicting protein aggregation propensities. Chem Soc Rev. 2008;37(7):1395–401.

146. Sormanni P, Aprile FA, Vendruscolo M. The CamSol Method of Rational Design of Protein Mutants with Enhanced Solubility. J Mol Biol. 2015 Jan 30;427(2):478–90.

147. Gianni S, Camilloni C, Giri R, Toto A, Bonetti D, Morrone A, Sormanni P, Brunori M, Vendruscolo M. Understanding the frustration arising from the competition between function, misfolding, and aggregation in a globular protein. Proc Natl Acad Sci. 2014;111(39):14141–14146.

148. Lu Y, Lim L, Song J. NMR studies reveal that protein dynamics critically mediate aggregation of the well-folded and very soluble E. coli S1 ribosomal protein. bioRxiv. 2017 Aug 19;178459.

149. Goedert M. Alzheimer's and Parkinson's diseases: The prion concept in relation to assembled Aβ, tau, and α-synuclein. Science. 2015 Aug 7;349(6248):1255555.

150. Meisl G, Yang X, Hellstrand E, Frohm B, Kirkegaard JB, Cohen SIA, Dobson CM, Linse S, Knowles TPJ. Differences in nucleation behavior underlie the contrasting aggregation kinetics of the Aβ40 and Aβ42 peptides. Proc Natl Acad Sci. 2014 Jul 1;111(26):9384.

151. Nesterov Evgueni E., Skoch Jesse, Hyman Bradley T., Klunk William E., Bacskai Brian J., Swager Timothy M. In Vivo Optical Imaging of Amyloid Aggregates in Brain: Design of Fluorescent Markers. Angew Chem Int Ed. 2005 Aug 22;44(34):5452–6.

152. Wittig Ilka, Schägger Hermann. Features and applications of blue-native and clear-native electrophoresis. PROTEOMICS. 2008 Sep 24;8(19):3974–90.

153. Tiiman A, Jarvet J, Gräslund A, Vukojević V. Heterogeneity and Turnover of Intermediates during Amyloid-β (Aβ) Peptide Aggregation Studied by Fluorescence Correlation Spectroscopy. Biochemistry. 2015 Dec 15;54(49):7203–11.

154. Leitner A, Joachimiak LA, Bracher A, Mönkemeyer L, Walzthoeni T, Chen B, Pechmann S, Holmes S, Cong Y, Ma B, Ludtke S, Chiu W, Hartl FU, Aebersold R, Frydman J. The Molecular Architecture of the Eukaryotic Chaperonin TRiC/CCT. Structure. 2012 May 9;20(5):814–25.

155. Chen B, Piel WH, Gui L, Bruford E, Monteiro A. The HSP90 family of genes in the human genome: Insights into their divergence and evolution. Genomics. 2005 Dec 1;86(6):627–37.

156. Young JC. The role of the cytosolic HSP70 chaperone system in diseases caused by misfolding and aberrant trafficking of ion channels. Dis Models Amp Mech. 2014 Mar 1;7(3):319.

157. Schuberth C, Buchberger A. UBX domain proteins: major regulators of the AAA ATPase Cdc48/p97. Cell Mol Life Sci. 2008 Aug 1;65(15):2360–71.

158. Roberts JD, Thapaliya A, Martínez-Lumbreras S, Krysztofinska EM, Isaacson RL. Structural and Functional Insights into Small, Glutamine-Rich, Tetratricopeptide Repeat Protein Alpha. Front Mol Biosci. 2015;2:71.

159. Hessa T, Sharma A, Mariappan M, Eshleman HD, Gutierrez E, Hegde RS. Protein targeting and degradation are coupled for elimination of mislocalized proteins. Nature. 2011 Jul 10;475:394.

160. Minami R, Hayakawa A, Kagawa H, Yanagi Y, Yokosawa H, Kawahara H. BAG-6 is essential for selective elimination of defective proteasomal substrates. J Cell Biol. 2010 Aug 23;190(4):637.

161. Priya S, Sharma SK, Goloubinoff P. Molecular chaperones as enzymes that catalytically unfold misfolded polypeptides. FEBS Lett. 2013 Jun 27;587(13):1981–7.

162. Shorter J. The Mammalian Disaggregase Machinery: Hsp110 Synergizes with Hsp70 and Hsp40 to Catalyze Protein Disaggregation and Reactivation in a Cell-Free System. PLOS ONE. 2011 Oct 14;6(10):e26319.

163. Schlecht R, Scholz SR, Dahmen H, Wegener A, Sirrenberg C, Musil D, Bomke J, Eggenweiler H-M, Mayer MP, Bukau B. Functional Analysis of Hsp70 Inhibitors. PLOS ONE. 2013;8(11):1–12.

164. Dai S, Tang Z, Cao J, Zhou W, Li H, Sampson S, Dai C. Suppression of the HSF1-mediated proteotoxic stress response by the metabolic stress sensor AMPK. EMBO J. 2015 Feb 3;34(3):275.

165. Vihervaara A, Sistonen L. HSF1 at a glance. J Cell Sci. 2014 Jan 15;127(2):261.

166. Wang S, Diller KR, Aggarwal SJ. Kinetics Study of Endogenous Heat Shock Protein 70 Expression. J Biomech Eng. 2004 Jan 9;125(6):794–7.

167. Manning BD. Adaptation to Starvation: Translating a Matter of Life or Death. Cancer Cell. 2013 Jun 10;23(6):713–5.

168. Aghi M, Hochberg F, Breakefield XO. Prodrug activation enzymes in cancer gene therapy. J Gene Med. 2000 May 24;2(3):148–64.

169. Rooseboom M, Commandeur JNM, Vermeulen NPE. Enzyme-Catalyzed Activation of Anticancer Prodrugs. Pharmacol Rev. 2004 Mar 1;56(1):53.

170. Paul Workman LRK. DT-Diaphorase Expression and Tumor Cell Sensitivity to 17-Allylamino,17-demethoxygeldanamycin, an Inhibitor of Heat Shock Protein 90. J Natl Cancer Insitute. 1999 Nov 17;91(22):1940–9.

171. Travers J, Sharp S, Workman P. HSP90 inhibition: two-pronged exploitation of cancer dependencies. Spec Issue Cancer Dev. 2012 Mar 1;17(5):242–52.

172. da Rocha Dias S, Friedlos F, Light Y, Springer C, Workman P, Marais R. Activated B-RAF Is an Hsp90 Client Protein That Is Targeted by the Anticancer Drug 17-Allylamino-17-Demethoxygeldanamycin. Cancer Res. 2005 Dec 1;65(23):10686.

173. Siegel D, Beall H, Senekowitsch C, Kasai M, Arai H, Gibson NW, Ross D. Bioreductive activation of mitomycin C by DT-diaphorase. Biochemistry. 1992 Sep 1;31(34):7879–85.

174. Guerrero-Castillo S, Baertling F, Kownatzki D, Wessels HJ, Arnold S, Brandt U, Nijtmans L. The Assembly Pathway of Mitochondrial Respiratory Chain Complex I. Cell Metab. 2017 Jan 10;25(1):128–39.

175. Hirst J. Mitochondrial Complex I. Annu Rev Biochem. 2013 Jun 2;82(1):551–75.

176. Watmough NJ, Frerman FE. The electron transfer flavoprotein: Ubiquinone oxidoreductases. Quinone Bind Catal. 2010 Dec 1;1797(12):1910–6.

177. Signes A, Fernandez-Vizarra E. Assembly of mammalian oxidative phosphorylation complexes I–V and supercomplexes. Essays Biochem. 2018 Jul 20;62(3):255.

178. Castro A, Bernis C, Vigneron S, Labbé J-C, Lorca T. The anaphase-promoting complex: a key factor in the regulation of cell cycle. Oncogene. 2005 Jan 13;24:314.

179. Schmidt K, Hughes C, Chudek JA, Goodyear SR, Aspden RM, Talbot R, Gundersen TE, Blomhoff R, Henderson C, Wolf CR, Tickle C. Cholesterol Metabolism: the Main Pathway Acting Downstream of Cytochrome P450 Oxidoreductase in Skeletal Development of the Limb. Mol Cell Biol. 2009 May 15;29(10):2716.

180. Gibbons GF. The role of cytochrome P450 in the regulation of cholesterol biosynthesis. Lipids. 2002 Dec 1;37(12):1163–70.

181. Nurse P. Universal control mechanism regulating onset of M-phase. Nature. 1990 Apr 5;344:503.

182. Petermann E, Woodcock M, Helleday T. Chk1 promotes replication fork progression by controlling replication initiation. Proc Natl Acad Sci. 2010 Sep 14;107(37):16090.

183. Niida H, Katsuno Y, Banerjee B, Hande MP, Nakanishi M. Specific Role of Chk1 Phosphorylations in Cell Survival and Checkpoint Activation. Mol Cell Biol. 2007 Apr 1;27(7):2572.

184. Jacobus WE, Moreadith RW, Vandegaer KM. Mitochondrial respiratory control. Evidence against the regulation of respiration by extramitochondrial phosphorylation potentials or by [ATP]/[ADP] ratios. J Biol Chem. 1982 Mar 10;257(5):2397–402.

185. Terada H. Uncouplers of oxidative phosphorylation. Environ Health Perspect. 1990 Jul 1;87:213–8.

186. Cerqueira NMFSA, Oliveira EF, Gesto DS, Santos-Martins D, Moreira C, Moorthy HN, Ramos MJ, Fernandes PA. Cholesterol Biosynthesis: A Mechanistic Overview. Biochemistry. 2016 Oct 4;55(39):5483–506.

187. Wang M, Casey PJ. Protein prenylation: unique fats make their mark on biology. Nat Rev Mol Cell Biol. 2016 Jan 21;17:110.

188. Juers DH, Matthews BW, Huber RE. LacZ β-galactosidase: Structure and function of an enzyme of historical and molecular biological importance. Protein Sci. 2012 Sep 25;21(12):1792–807.

189. Manning BD, Toker A. AKT/PKB Signaling: Navigating the Network. Cell. 2017 Apr 20;169(3):381–405.

190. Cassinelli G, Zuco V, Gatti L, Lanzi C, Zaffaroni N, Colombo D, Perego P. Targeting the Akt Kinase to Modulate Survival, Invasiveness and Drug Resistance of Cancer Cells. Curr Med Chem. 2013;20(15):1923–45.

191. Wang M, You J, Bemis KG, Tegeler TJ, Brown DPG. Label-free mass spectrometry-based protein quantification technologies in proteomic analysis. Brief Funct Genomics. 2008 Sep 1;7(5):329–39.

192. Mewies Martin, McIntire William S., Scrutton Nigel S. Covalent attachment of flavin adenine dinucleotide (FAD) and flavin mononucleotide (FMN) to enzymes: The current state of affairs. Protein Sci. 2008 Dec 31;7(1):7–20.

193. Husain M, Massey V. Reversible resolution of flavoproteins into apoproteins and free flavins. Methods in Enzymology. 1978;53:429–37.

194. Young JC. Mechanisms of the Hsp70 chaperone system. Biochem Cell Biol. 2010 Mar 18;88(2):291–300.

195. Balchin D, Hayer-Hartl M, Hartl FU. In vivo aspects of protein folding and quality control. Science. 2016 Jul 1;353(6294):aac4354.

196. Craig EA. Hsp70 at the membrane: driving protein translocation. BMC Biol. 2018 Jan 17;16(1):11.

197. Kaushik S, Bandyopadhyay U, Sridhar S, Kiffin R, Martinez-Vicente M, Kon M, Orenstein SJ, Wong E, Cuervo AM. Chaperone-mediated autophagy at a glance. J Cell Sci. 2011 Feb 15;124(4):495.

198. Braell WA, Schlossman DM, Schmid SL, Rothman JE. Dissociation of clathrin coats coupled to the hydrolysis of ATP: role of an uncoating ATPase. J Cell Biol. 1984 Aug 1;99(2):734.

199. Schopf FH, Biebl MM, Buchner J. The HSP90 chaperone machinery. Nat Rev Mol Cell Biol. 2017 Apr 21;18:345.

200. Ghosh A, Stuehr DJ. Soluble guanylyl cyclase requires heat shock protein 90 for heme insertion during maturation of the NO-active enzyme. Proc Natl Acad Sci. 2012 Aug 7;109(32):12998.

201. Qiu X-B, Shao Y-M, Miao S, Wang L. The diversity of the DnaJ/Hsp40 family, the crucial partners for Hsp70 chaperones. Cell Mol Life Sci CMLS. 2006 Nov 1;63(22):2560–70.

202. Laufen T, Mayer MP, Beisel C, Klostermeier D, Mogk A, Reinstein J, Bukau B. Mechanism of regulation of Hsp70 chaperones by DnaJ cochaperones. Proc Natl Acad Sci. 1999 May 11;96(10):5452.

203. Alderson TR, Kim JH, Markley JL. Dynamical Structures of Hsp70 and Hsp70-Hsp40 Complexes. Structure. 2016;24(7):1014–30.

204. Rosén C-G. Binding of fluorescent probe, 1-anilino-8-naphthalene sulfonate, to apo-horseradish peroxidase. FEBS Lett. 1970 Feb 16;6(3):158–60.

205. Stryer L. The interaction of a naphthalene dye with apomyoglobin and apohemoglobin: A fluorescent probe of non-polar binding sites. J Mol Biol. 1965 Sep 1;13(2):482–95.

206. Asher G, Dym O, Tsvetkov P, Adler J, Shaul Y. The Crystal Structure of NAD(P)H Quinone Oxidoreductase 1 in Complex with Its Potent Inhibitor Dicoumarol. Biochemistry. 2006 May 1;45(20):6372–8.

207. Leung KKK, Litchfield DW, Shilton BH. Flavin adenine dinucleotide content of quinone reductase 2: Analysis and optimization for structure–function studies. Anal Biochem. 2012 Jan 1;420(1):84–9.

208. Zhang H, Amick J, Chakravarti R, Santarriaga S, Schlanger S, McGlone C, Dare M, Nix JC, Scaglione KM, Stuehr DJ, Misra S, Page RC. A Bipartite Interaction between Hsp70 and CHIP Regulates Ubiquitination of Chaperoned Client Proteins. Structure. 2015;23(3):472–82.

209. Wang L, Liu Y-T, Hao R, Chen L, Chang Z, Wang H-R, Wang Z-X, Wu J-W. Molecular Mechanism of the Negative Regulation of Smad1/5 Protein by Carboxyl Terminus of Hsc70-interacting Protein (CHIP). J Biol Chem. 2011 May 6;286(18):15883–94.

210. Fawzi NL, Chubukov V, Clark LA, Brown S, Head-Gordon T. Influence of denatured and intermediate states of folding on protein aggregation. Protein Sci. 2009 Jan 1;14(4):993–1003.

211. Neudecker P, Robustelli P, Cavalli A, Walsh P, Lundström P, Zarrine-Afsar A, Sharpe S, Vendruscolo M, Kay LE. Structure of an Intermediate State in Protein Folding and Aggregation. Science. 2012 Apr 20;336(6079):362.

212. Jahn TR, Parker MJ, Homans SW, Radford SE. Amyloid formation under physiological conditions proceeds via a native-like folding intermediate. Nat Struct Amp Mol Biol. 2006 Feb 19;13:195.

213. Münch C, Bertolotti A. Exposure of Hydrophobic Surfaces Initiates Aggregation of Diverse ALS-Causing Superoxide Dismutase-1 Mutants. J Mol Biol. 2010 Jun 11;399(3):512–25.

214. Olzscha H, Schermann SM, Woerner AC, Pinkert S, Hecht MH, Tartaglia GG, Vendruscolo M, Hayer-Hartl M, Hartl FU, Vabulas RM. Amyloid-like Aggregates Sequester Numerous Metastable Proteins with Essential Cellular Functions. Cell. 2011 Jan 7;144(1):67–78.

215. Gidalevitz T, Ben-Zvi A, Ho KH, Brignull HR, Morimoto RI. Progressive Disruption of Cellular Protein Folding in Models of Polyglutamine Diseases. Science. 2006 Mar 10;311(5766):1471.

216. Tyedmers J, Mogk A, Bukau B. Cellular strategies for controlling protein aggregation. Nat Rev Mol Cell Biol. 2010 Oct 14;11:777.

217. Nillegoda NB, Wentink AS, Bukau B. Protein Disaggregation in Multicellular Organisms. Trends Biochem Sci. 2018 Apr 1;43(4):285–300.

218. Morley JF, Brignull HR, Weyers JJ, Morimoto RI. The threshold for polyglutamine-expansion protein aggregation and cellular toxicity is dynamic and influenced by aging in *Caenorhabditis elegans*. Proc Natl Acad Sci. 2002 Aug 6;99(16):10417.

219. Ben-Zvi A, Miller EA, Morimoto RI. Collapse of proteostasis represents an early molecular event in *Caenorhabditis elegans* aging. Proc Natl Acad Sci. 2009 Sep 1;106(35):14914.

220. David DC, Ollikainen N, Trinidad JC, Cary MP, Burlingame AL, Kenyon C. Widespread Protein Aggregation as an Inherent Part of Aging in C. elegans. PLOS Biol. 2010;8(8):1–23.

221. Vilchez D, Saez I, Dillin A. The role of protein clearance mechanisms in organismal ageing and age-related diseases. Nat Commun. 2014 Dec 8;5:5659.

222. Park S-H, Kukushkin Y, Gupta R, Chen T, Konagai A, Hipp MS, Hayer-Hartl M, Hartl FU. PolyQ Proteins Interfere with Nuclear Degradation of Cytosolic Proteins by Sequestering the Sis1p Chaperone. Cell. 2013 Jul 3;154(1):134–45.

223. Wang J, Farr GW, Zeiss CJ, Rodriguez-Gil DJ, Wilson JH, Furtak K, Rutkowski DT, Kaufman RJ, Ruse CI, Yates JR, Perrin S, Feany MB, Horwich AL. Progressive aggregation despite chaperone associations of a mutant SOD1-YFP in transgenic mice that develop ALS. Proc Natl Acad Sci. 2009 Feb 3;106(5):1392.

224. Kuo Y, Ren S, Lao U, Edgar BA, Wang T. Suppression of polyglutamine protein toxicity by co-expression of a heat-shock protein 40 and a heat-shock protein 110. Cell Death Amp Dis. 2013 Oct 3;4:e833.

225. Bence NF, Sampat RM, Kopito RR. Impairment of the Ubiquitin-Proteasome System by Protein Aggregation. Science. 2001 May 25;292(5521):1552.

226. Richard I Morimoto. Proteotoxic stress and inducible chaperone networks in neurodegenerative disease and aging. Genes Dev. 2008;22:1427–38.

227. Chen L, Brewer MD, Guo L, Wang R, Jiang P, Yang X. Enhanced Degradation of Misfolded Proteins Promotes Tumorigenesis. Cell Rep. 2017 Mar 28;18(13):3143–54.

228. SHIBA S, TERAWAKI A, TAGUCHI T, KAWAMATA J. Selective Inhibition of Formation of Deoxyribonucleic Acid in Escherichia coli by Mitomycin C. Nature. 1959 Apr 11;183:1056.

229. Siegel D, Gibson NW, Preusch PC, Ross D. Metabolism of Mitomycin C by DT-Diaphorase: Role in Mitomycin C-induced DNA Damage and Cytotoxicity in Human Colon Carcinoma Cells. Cancer Res. 1990 Dec 1;50(23):7483.

230. David Ross DS. Bioreductive Activation of MitomycinC by DT-Diaphorase. Biochemistry. 1992;31:7879–85.

231. Begleiter A, Leith MK, Thliveris JA, Digby T. Dietary induction of NQO1 increases the antitumour activity of mitomycin C in human colon tumours in vivo. Br J Cancer. 2004 Oct 5;91:1624.

232. Wang X, Doherty GP, Leith MK, Curphey TJ, Begleiter A. Enhanced cytotoxicity of mitomycin C in human tumour cells with inducers of DT-diaphorase. Br J Cancer. 1999 May 28;80:1223.

233. Cummings J, Spanswick V, Tomasz M, Smyth J. Enzymology of mitomycin C metabolic activation in tumour tissue: implications for enzyme-directed bioreductive drug development. Biochem Pharmacol. 1998 Aug;56(4):405–14.

234. Bradner WT. Mitomycin C: a clinical update. Cancer Treat Rev. 2001 Feb 1;27(1):35–50.

235. Hu C-W, Chen C-M, Ho HH, Chao M-R. Simultaneous quantification of methylated purines in DNA by isotope dilution LC-MS/MS coupled with automated solid-phase extraction. Anal Bioanal Chem. 2012 Jan 1;402(3):1199–208.

236. Warburg O. Über den Stoffwechsel der Carcinomzelle. Naturwissenschaften. 1924;12(50):1131–7.

237. DeBerardinis RJ, Lum JJ, Hatzivassiliou G, Thompson CB. The Biology of Cancer: Metabolic Reprogramming Fuels Cell Growth and Proliferation. Cell Metab. 2008;7(1):11–20.

238. Wiley CD, Campisi J. From Ancient Pathways to Aging Cells—Connecting Metabolism and Cellular Senescence. Cell Metab. 2016 Jun 14;23(6):1013–21.

239. Fridman AL, Tainsky MA. Critical pathways in cellular senescence and immortalization revealed by gene expression profiling. Oncogene. 2008 Aug 18;27:5975.

240. Buhaescu I, Izzedine H. Mevalonate pathway: A review of clinical and therapeutical implications. Clin Biochem. 2007 Jun 1;40(9):575–84.

241. Simons K, Ikonen E. How Cells Handle Cholesterol. Science. 2000 Dec 1;290(5497):1721.

242. Zhang X, Barraza KM, Beauchamp JL. Cholesterol provides nonsacrificial protection of membrane lipids from chemical damage at air–water interface. Proc Natl Acad Sci. 2018 Mar 27;115(13):3255.

243. Carew JS, Zhou Y, Albitar M, Carew JD, Keating MJ, Huang P. Mitochondrial DNA mutations in primary leukemia cells after chemotherapy: clinical significance and therapeutic implications. Leukemia. 2003 Jul 29;17:1437.

244. Conklin KA. Chemotherapy-Associated Oxidative Stress: Impact on Chemotherapeutic Effectiveness. Integr Cancer Ther. 2004 Dec 1;3(4):294–300.

245. Dixon SJ, Lemberg KM, Lamprecht MR, Skouta R, Zaitsev EM, Gleason CE, Patel DN, Bauer AJ, Cantley AM, Yang WS, Morrison B, Stockwell BR. Ferroptosis: An Iron-Dependent Form of Nonapoptotic Cell Death. Cell. 2012 May 25;149(5):1060–72.

246. Shimada K, Skouta R, Kaplan A, Yang WS, Hayano M, Dixon SJ, Brown LM, Valenzuela CA, Wolpaw AJ, Stockwell BR. Global survey of cell death mechanisms reveals metabolic regulation of ferroptosis. Nat Chem Biol. 2016 May 9;12:497.

247. Pagano M, Pepperkok R, Lukas J, Baldin V, Ansorge W, Bartek J, Draetta G. Regulation of the cell cycle by the cdk2 protein kinase in cultured human fibroblasts. J Cell Biol. 1993 Apr 1;121(1):101.

248. Potapova TA, Daum JR, Byrd KS, Gorbsky GJ, Cohen-Fix O. Fine Tuning the Cell Cycle: Activation of the Cdk1 Inhibitory Phosphorylation Pathway during Mitotic Exit. Mol Biol Cell. 2009 Jan 21;20(6):1737–48.

249. Fu J, Bian M, Jiang Q, Zhang C. Roles of Aurora Kinases in Mitosis and Tumorigenesis. Mol Cancer Res. 2007 Jan 1;5(1):1.

250. Manthey KC, Rodriguez-Melendez R, Hoi JT, Zempleni J. Riboflavin deficiency causes protein and DNA damage in HepG2 cells, triggering arrest in G1 phase of the cell cycle. J Nutr Biochem. 2006 Apr;17(4):250–6.

251. Shang L, Chen S, Du F, Li S, Zhao L, Wang X. Nutrient starvation elicits an acute autophagic response mediated by Ulk1 dephosphorylation and its subsequent dissociation from AMPK. Proc Natl Acad Sci. 2011 Mar 22;108(12):4788.

252. Graham NA, Tahmasian M, Kohli B, Komisopoulou E, Zhu M, Vivanco I, Teitell MA, Wu H, Ribas A, Lo RS, Mellinghoff IK, Mischel PS, Graeber TG. Glucose deprivation activates a metabolic and signaling amplification loop leading to cell death. Mol Syst Biol. 2012 Jan 1;8(1):589.

253. Demetriades C, Doumpas N, Teleman AA. Regulation of TORC1 in Response to Amino Acid Starvation via Lysosomal Recruitment of TSC2. Cell. 2014 Feb 13;156(4):786–99.

254. Hardie DG, Ross FA, Hawley SA. AMPK: a nutrient and energy sensor that maintains energy homeostasis. Nat Rev Mol Cell Biol. 2012 Apr;13(4):251–62.

255. Zhao Y, Hu X, Liu Y, Dong S, Wen Z, He W, Zhang S, Huang Q, Shi M. ROS signaling under metabolic stress: cross-talk between AMPK and AKT pathway. Mol Cancer. 2017 Apr 13;16(1):79.

256. William E. Balch ETP. Biological and Chemical Approaches to Diseases of Proteostasis Deficiency. Annu Rev Biochem. 2009 Jul 7;78:959–91.

257. Parenti G, Andria G, Valenzano KJ. Pharmacological Chaperone Therapy: Preclinical Development, Clinical Translation, and Prospects for the Treatment of Lysosomal Storage Disorders. Mol Ther. 2015 Jul 1;23(7):1138–48.

258. Haschka M, Karbon G, Fava LL, Villunger A. Perturbing mitosis for anti-cancer therapy: is cell death the only answer? EMBO Rep. 2018 Mar 1;19(3):e45440.

259. Chan K-S, Koh C-G, Li H-Y. Mitosis-targeted anti-cancer therapies: where they stand. Cell Death Amp Dis. 2012 Oct 18;3:e411.

260. Wang L, Oliveira RL de, Wang C, Neto JMF, Mainardi S, Evers B, Lieftink C, Morris B, Jochems F, Willemsen L, Beijersbergen RL, Bernards R. High-Throughput Functional Genetic and Compound Screens Identify Targets for Senescence Induction in Cancer. Cell Rep. 2017;21(3):773–83.

261. Nagel R, Semenova EA, Berns A. Drugging the addict: non-oncogene addiction as a target for cancer therapy. EMBO Rep. 2016 Nov 1;17(11):1516.

262. Luo J, Solimini NL, Elledge SJ. Principles of Cancer Therapy: Oncogene and Non-oncogene Addiction. Cell. 2009 Mar 6;136(5):823–37.

263. Wang L, Oliveira RL de, Huijberts S, Bosdriesz E, Pencheva N, Brunen D, Bosma A, Song J-Y, Zevenhoven J, Vries GTL, Horlings H, Nuijen B, Beijnen JH, Schellens JHM, Bernards R. An Acquired Vulnerability of Drug-Resistant Melanoma with Therapeutic Potential. Cell. 2018;173(6):1413-1425.e14.

6 APPENDIX

6.1 Physicochemical analysis of wild-type NQO1 protein interactors under normal and riboflavin-deficient conditions

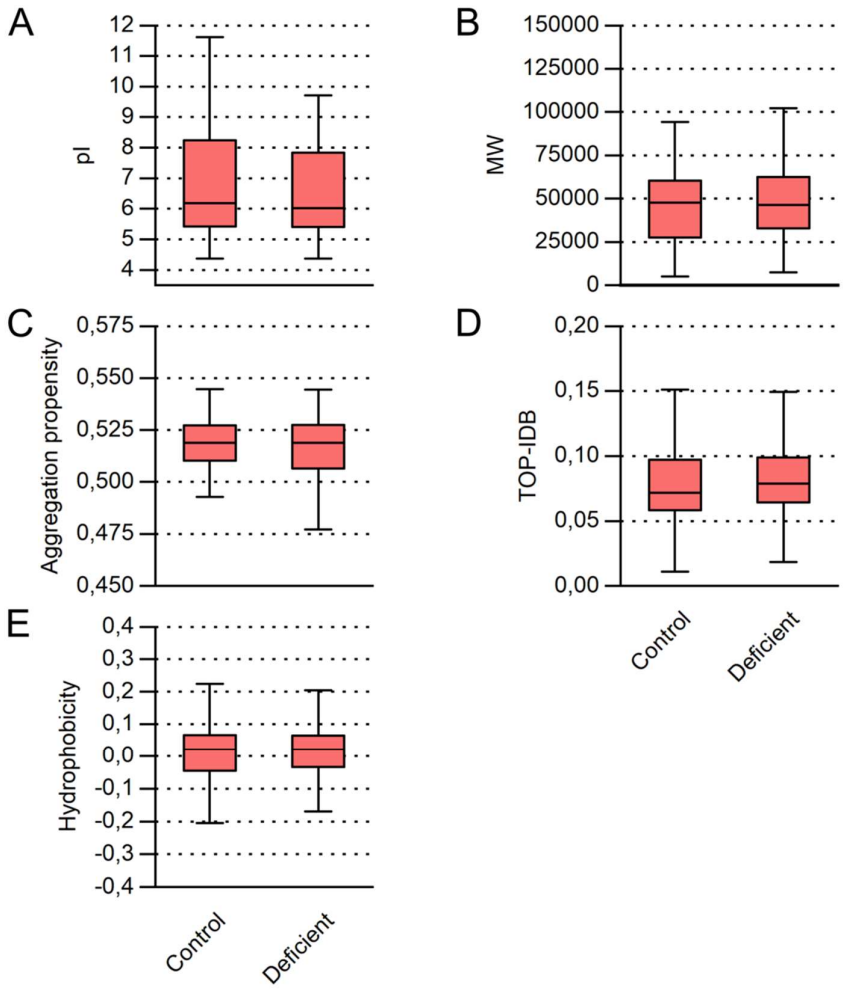

Figure 51. Wild-type holo- and apoNQO1 interactomes show no biophysical differences. B16 F0 cells overexpressing wild-type NQO1 were cultured in riboflavin-deficient medium for 24 h and treated with 5 μM MG132 overnight. NQO1 pull-down was carried out and its interactome was analyzed under both conditions by mass spectrometry. Holo- and apoNQO1-binding proteins were compared biophysically by using the CleverSuite online tool (122). Isoelectric point (pI), molecular weight (MW), aggregation propensities, disorder propensity (TOP-IDB), and hydrophobicity were computed for both NQO1 interactome sets. The values obtained are plotted in box plots. The box corresponds to the 25% and 75% quantiles, together with the median line. Whiskers correspond to the 5% and 95% quantiles. Mann-Whitney test was used to compare the medians between the two groups using a p-value threshold of 0.05.

6.2 Mechanism of guanine base methylation by methyl methanesulfonate (MMS)

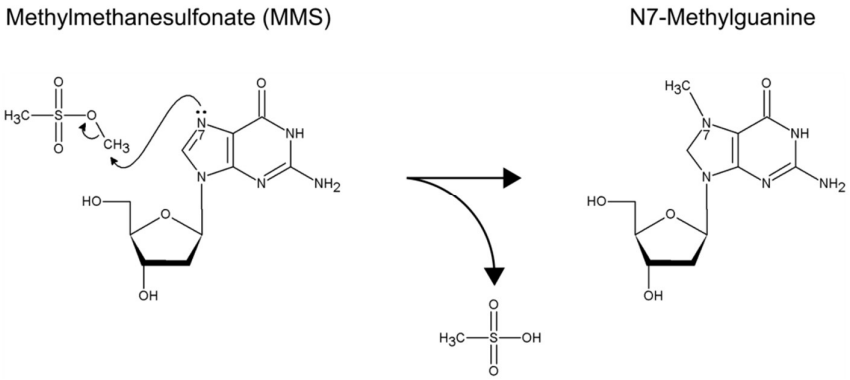

Figure 52. Schematic representation of methyl methanesulfonate (MMS) methylation reaction with N7 from guanosine. N7 from guanine base carries out a nucleophilic attack on the methyl group from the MMS molecule (left) forming methylguanine (right).

6.3 Mechanism of Mytomycin C activation and crosslinking with guanine base

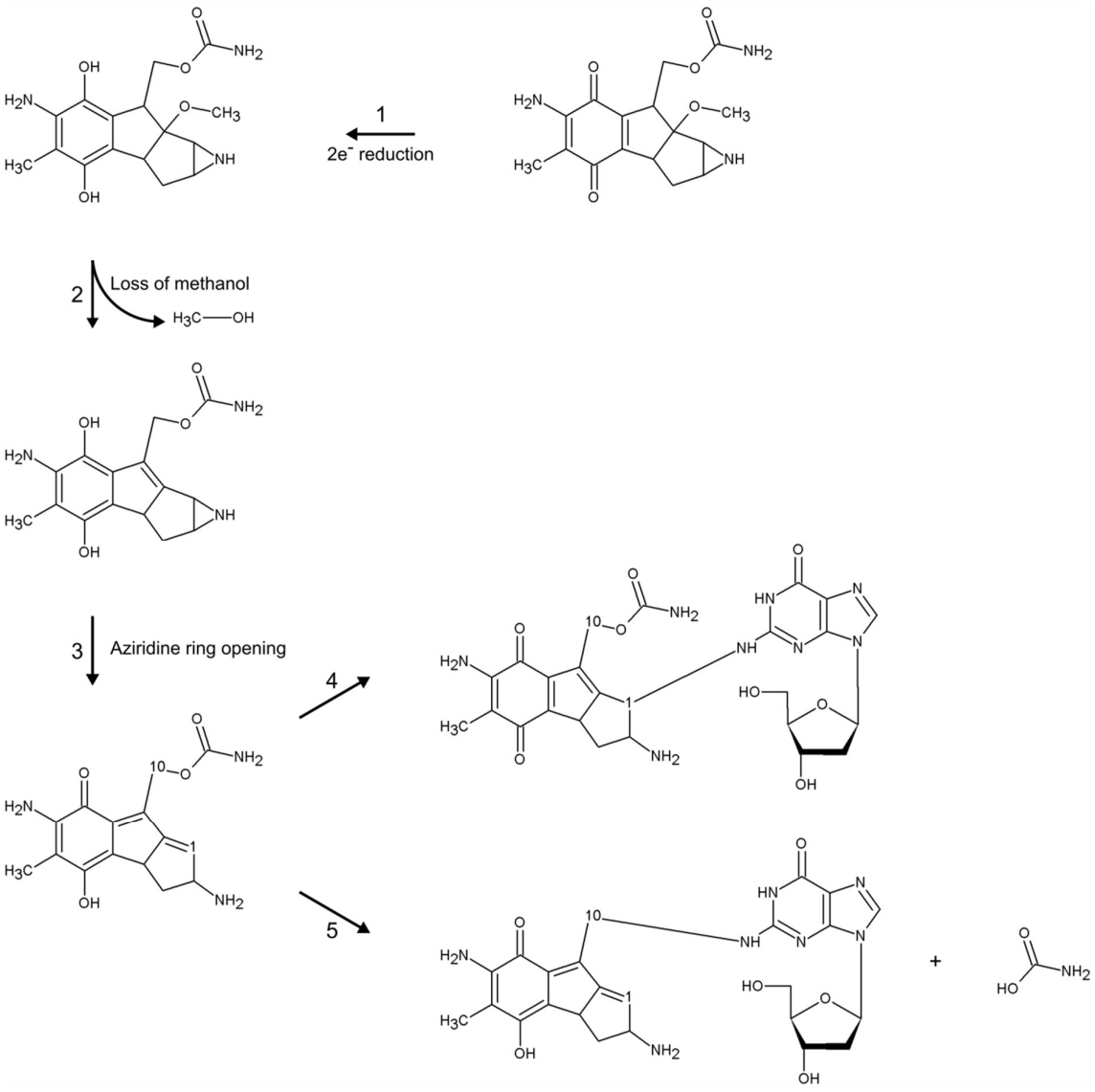

Figure 53. Schematic representation of the reduction-dependent activation of Mitomycin C followed by crosslinking reaction with guanosine. (1) Activation of Mitomycin C takes place via a 2-electron reduction, (2) followed by the release of a methanol molecule. (3) Once the aziridine ring opens, (4) carbon 1 can react with an amine group from guanine base. (5) The same amine group can also react with carbon 10 from Mitomycin C. A molecule of carbamic acid (CNH_2OOH) is lost in this process.

6.4 Proteome changes during riboflavin starvation

Gene ontology cluster	Genes
Pyruvate metabolism (Process)	*PDK1, PDK3, TPI1, PFKP, PFKL, HK1, PGK1, ALDOC, LDHA, PGM1*
Electron transport chain (Process)	*SDHA, NDUFS1, NDUFV1, NDUFB8, NDUFA8, SDHB, NDUFA10, CCNB1, NDUFS4, ETFDH, CDK1, NDUFV2, NDUFS6, NDUFB3, NDUFA7, NDUFS8*
NADH dehydrogenase complex assembly (Process)	*NDUFA11, NDUFS7, NDUFB8, NDUFA8, NDUFB7, NDUFA10, NDUFS4, NDUFA9, NDUFA2, NDUFA13, NDUFB3, NDUFS8, NDUFS5*
Cell cycle (Process)	*UBE2S, CEP55, CKS2, SMC3, SMC1A, ANAPC2, MCM6, ANAPC7, SMARCAD1, MKI67, KIF2C, FANCD2, IQGAP3, CUL7, CCNB1, HELLS, CDK2, NOP53, PLK1, KIF4, MIS12, LIG1, ASNS, EPS8, MELK, UHRF1, ERCC61, DSN1, CDK1, SYDE1, SMC4, PBK, HAUS1, CHAF1B, AURKA, SMC2, NCAPD3, NCAPG, ARHGEF2, SDE2, RBL1, PCNA, ATAD5, RACGAP1, MAD2L1, POLA1, RCF2, GINS3, PRIM2, RRM2, POLD1, RRM1, PRIM1, RCF3, RBBP7, TK1, NUDT16L1, RAD51AP1, HAT1, HIST1H1T, WHSC1, DNMT1, NAA40*
Sterol biosynthesis (Process)	*FDPS, APOE, HMGCR, DHCR24, FDFT1, SQLE, HMGCS1, POR, IDI1*
Lysosome (Component)	*ATP13A2, NAGA, GM2A, CTSD, GUSB, AR18A, TECPR1, MAN2B2, GLB1, PLBD2, CTSA, DPP7*

Table 4. GO enrichment analysis of riboflavin-starved B16 F0 cells (genes). B16 F0 cells were incubated for 3 days in riboflavin-deficient medium and proteome was analyzed by mass spectrometry. Intensity ratios between deficient and control conditions were calculated for each protein and were $\log_2$-transformed. Hits that were significantly enriched or depleted according to a FDR cut-off of 0.001 (0.1%) were analyzed with the GO Term Finder tool (https://go.princeton.edu/cgi-bin/GOTermFinder). The main clusters are indicated together with the sorting category used for the analyses in brackets.

6.5 Riboflavin starvation effects on glycolysis and sterol biosynthetic pathways

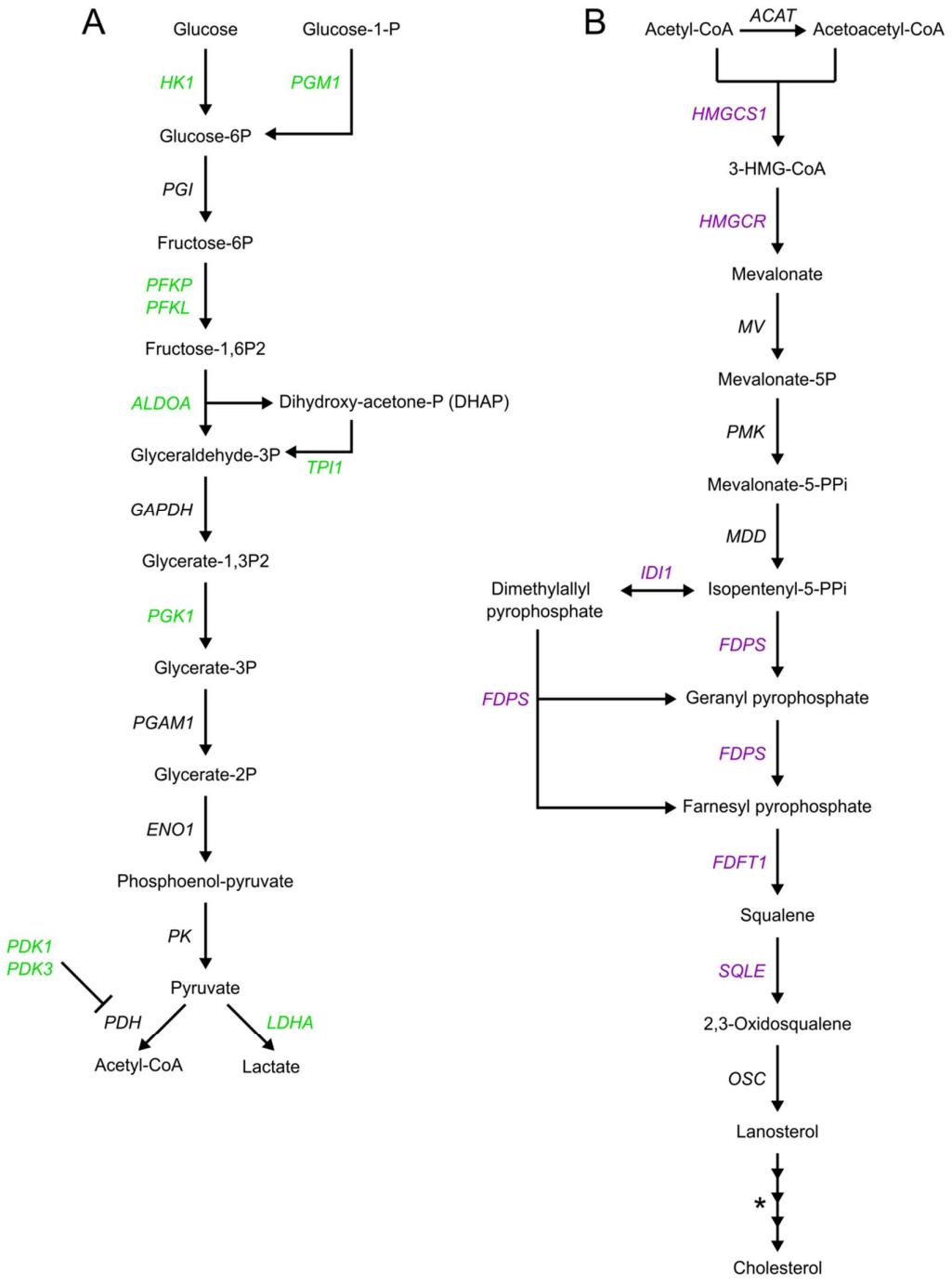

Figure 54. Schematic representation of glycolysis and sterol biosynthesis enzymatic pathways. Glycolysis (A) and mevalonate (B) pathways are shown. Increased (green) and reduced (purple) genes are indicated in each case. *Conversion of lanosterol into cholesterol is a multistep process and is not detailed in this scheme.

6.6 Cell cycle analysis of serum-starved melanoma cells

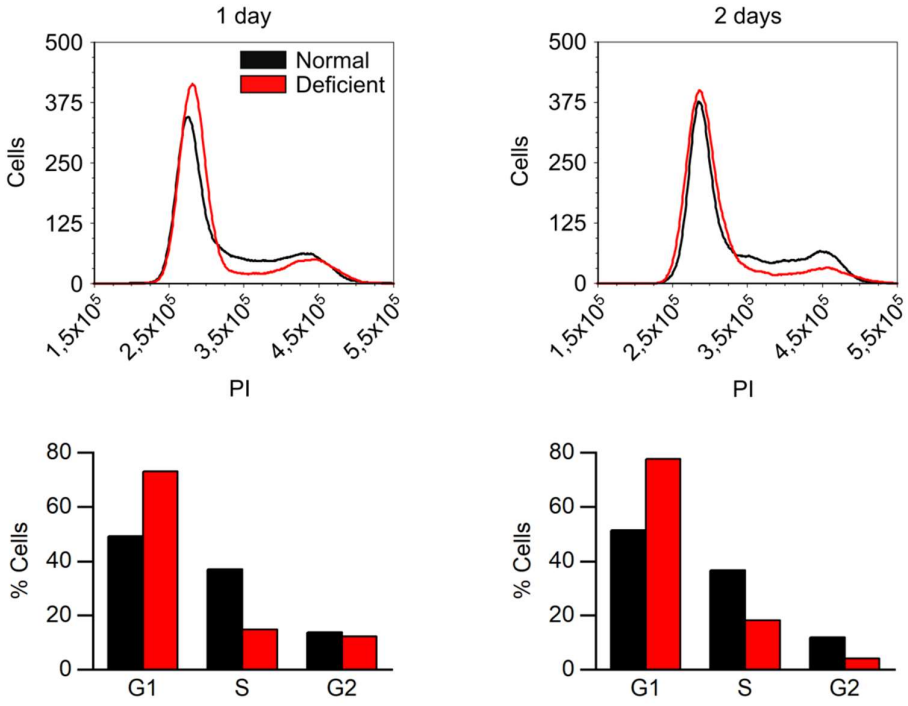

Figure 55. Serum starvation inhibits cell proliferation. B16 F0 cells were incubated in DMEM without serum for 1 or 2 days. Cell DNA was stained with PI and cell cycle analysis was performed using flow cytometry. The data were analyzed using the Multi-Cycle DNA tool from the FCS Express 5 software. The percentage values for each population (G1, S, and G2) were obtained and plotted.

6.7 Analysis of cell death mechanism triggered by MMS

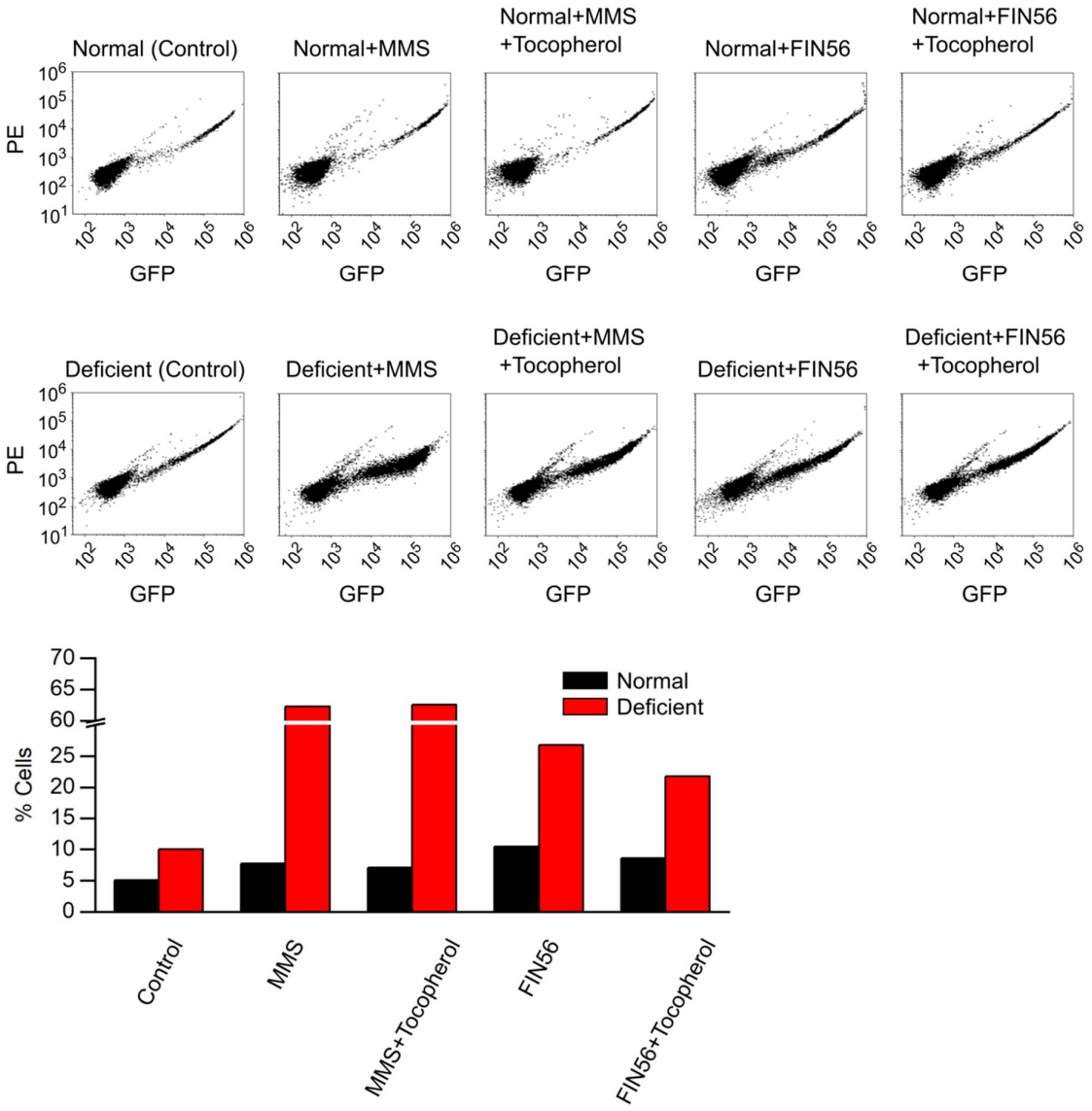

Figure 56. Tocopherol does not protect B16 F0 cells from MMS-induced cell death. B16 F0 cells were incubated for 3 days in riboflavin-deficient medium and MMS (500 µM), or FIN56 (15 µM) treatments in the absence or presence of tocopherol/vitamin E (100 µM) were applied for 24 h. Cells were incubated in DMEM with 30 nM SYTOX green for 15 min. Flow cytometry was used to analyze cell death. PE vs GFP 2D graphs are shown and the conditions used for each sample are specified. FCS Express 5 software was used to analyze the data.

7 STATEMENT OF CONTRIBUTIONS

Dr. Giulia Calloni performed sample preparation and mass spectrometry experiments presented in this work. In these experiments, I prepared, treated, and lysed cells.

Marion Alriquet carried out experiments from Figure 26C (section 3.5), and Figure 34 (section 3.7).

Wei-Han Lang prepared B16 F0 CHIP knockout cell line by means of CRISPR/Cas9 technique.